TITLE PAGE

Report Title: LOW-ENGINE-FRICTION TECHNOLOGY FOR ADVANCED NATURAL-GAS RECIPROCATING ENGINES

Final Technical Report

Reporting Period: April 1, 2002 – November 30, 2006

for

DoE Cooperative Agreement No. DE-FC26-02NT41339

Submitted by

Victor Wong, Tian Tian, G. Smedley, L. Moughon, Rosalind Takata, J. Jocsak

Massachusetts Institute of Technology
Room 31-155, 77 Massachusetts Avenue
Cambridge, MA 02139

and

Rudy Stanglmaier, Ted Bestor, Morgan Defoort, Kris Quillen, Kirk Evans

Sub-Contract University
Colorado State University
Fort Collins, CO 80523

February 28, 2007

Submitted to:
NETL AAD Document Control Building 921
Department of Energy
National Energy Technology Laboratory
P.O. Box 10940
Pittsburgh, PA 15236-0940

DISCLAIMER

ABSTRACT

This program aims at improving the efficiency of advanced natural-gas reciprocating engines (ANGRE) by reducing piston and piston ring assembly friction without major adverse effects on engine performance, such as increased oil consumption and wear. An iterative process of simulation, experimentation and analysis has been followed towards achieving the goal of demonstrating a complete optimized low-friction engine system. In this program, a detailed set of piston and piston-ring dynamic and friction models have been adapted and applied that illustrate the fundamental relationships among mechanical, surface/material and lubricant design parameters and friction losses. Demonstration of low-friction ring-pack designs in the Waukesha VGF 18GL engine confirmed ring-pack friction reduction of 30-40%, which translates to total engine FEMP (friction mean effective pressure) reduction of 7-10% from the baseline configuration without significantly increasing oil consumption or blow-by flow. The study on surface textures, including roughness characteristics, cross hatch patterns, dimples and grooves have shown that even relatively small-scale changes can have a large effect on ring/liner friction, in some cases reducing FMEP by as much as 30% from a smooth surface case. The measured FMEP reductions were in good agreement with the model predictions.

The combined analysis of lubricant and surface design indicates that low-viscosity lubricants can be very effective in reducing friction, subject to component wear for extremely thin oils, which can be mitigated with further lubricant formulation and/or engineered surfaces. Hence a combined approach of lubricant design and appropriate wear reduction offers improved potential for minimum engine friction loss. Testing of low-friction lubricants showed that total engine FMEP reduced by up to ~16.5% from the commercial reference oil without significantly increasing oil consumption or blow-by flow. Piston friction studies indicate that a flatter piston with a more flexible skirt, together with optimizing the waviness and film thickness on the piston skirt offer significant friction reduction. Combined with low-friction ring-pack, material and lubricant parameters, a total power cylinder friction reduction of 30-50% is expected, translating to an engine efficiency increase of two percentage points from its current baseline towards the goal of 50% ARES engine efficiency.

The design strategies developed in this study have promising potential for application in all modern reciprocating engines as they represent simple, low-cost methods to extract significant fuel savings. The current program has possible spinoffs and applications in other industries as well, including transportation, CHP, and diesel power generation. The progress made in this program has wide engine efficiency implications, and potential deployment of low-friction engine components or lubricants in the near term is quite possible.

TABLE OF CONTENTS

LIST OF FIGURES

LIST OF TABLES

LOW-ENGINE-FRICTION TECHNOLOGY FOR ADVANCED NATURAL-GAS RECIPROCATING ENGINES

Final Technical Report
Massachusetts Institute of Technology
DoE Cooperative Agreement No. DE-FC26-02NT41339

EXECUTIVE SUMMARY

This program aims at improving the efficiency of advanced natural-gas reciprocating engines (ANGRE) by reducing piston and piston ring assembly friction without major adverse effects on engine performance, such as increased oil consumption and wear. The approach is to apply or adapt existing computer models to evaluate the friction reduction potential of power-cylinder component design, surface treatment, and lubrication concepts. The promising low-friction candidate design concepts are validated experimentally on a full-size large-bore natural-gas engine at Colorado State University (CSU). Waukesha Engine Dresser, Inc. provides the engine, parts, and engineering support for the program.

The program has five major tasks, as shown in the Milestones chart, summarized as follows. Task (1): Assess opportunities for friction reduction by performing preliminary analyses and evaluating existing empirical data; Task (2): Modify or adapt existing engine friction and lubrication models to ANGRE engines and to develop friction reduction concepts and recommendations; Task (3): Assess friction reduction opportunities, develop and recommend friction-reducing designs. Task (4): Test and demonstrate recommended concepts in a full-scale ARES Waukesha engine; (5) Analyze test results and iterate on initial recommendations. Task (5) is a concurrent task to Tasks 3 and 4. All major tasks have been completed. In Task (4), demonstration of low-friction ring-packs and low-friction lubricants have been completed and results are promising. However, further studies in combining lubricant and material technology for further efficiency gains are recommended, along with further validation experiments to be conducted using low-friction pistons and surface treatments. Major findings are summarized below.

Specifically, from Task (3), the detailed analysis recommended a low-friction ring-pack to consist of a top piston ring with a "skewed-barrel" profile (geometry of ring profile), a reduced-tension oil-control ring, together with a second (scraper) ring with a negative twist (torsional preload). The study also recommended that a flexible (less rigid) piston skirt with a generally flatter piston-skirt geometric profile is preferred to minimize metal-metal contact during piston-liner impact and lubrication. Honing or groove patterns on the piston/rings or liner that are oriented more perpendicular to the piston motion generally reduce friction and wear. The study on surface textures, including roughness characteristics, cross hatch patterns, dimples and grooves have shown that even relatively small-scale changes can have a large effect on ring/liner friction, in some cases reducing FMEP by as much as 30% from a smooth surface case. The analysis also considered optimal depths and widths of dimples and grooves. For lubricants, the study considered the effects of changing lubricant viscosity either uniformly throughout, or preferentially at various parts, of the engine cycle. It is recommended that reducing the level of viscosity everywhere in the cycle is more effective

than lowering it only at mid-stroke but increasing it preferentially at top (or bottom) dead centers to reduce metal-metal contact friction. Friction modifiers are effective in reducing asperity contact friction but may have other practical implementation concerns. The study recommended that a combined application of lubricant and material technology be pursued to simultaneously reduce friction, wear and oil consumption.

From Task (4), actual demonstration of low-friction ring-pack designs in a Waukesha VGF 18GL engine confirmed ring-pack friction reduction of 30-40%, which translates to total engine FEMP (friction mean effective pressure) reduction of 7-10% from the baseline configuration without significantly increasing oil consumption or blow-by flow. The measured FMEP reductions were in good agreement with the model predictions. Most of this benefit was achieved via adjusting oil-control ring tension and the geometric profile of the running surface of the top piston ring. Testing of low-friction lubricants showed that total engine FMEP reduced by up to ~16.5% from the commercial reference oil without significantly increasing oil consumption or blow-by flow. The measured FMEP reductions displayed good agreement with predictions.

Task (5) provides careful review of the results and, through team discussions, determines the proper combination and schedule of additional analysis and experimentation. It appears that testing of material/surface design should be implemented synergistically in conjunction with further lubricant experiments. Results indicate that piston and lubricants offer as much friction reduction benefit as the ring-pack. Expanded studies in these areas beyond the current program would therefore be appropriate and are recommended.

During this program, the project team participated in each of the three ARES-ARICE ASME-ICED Technical Conferences organized by active ARES researchers. In addition to participation in ARES Roundtables held periodically, we organized and held Industry-University Workshop on Low-Engine Friction was at MIT and Purdue, in which all major manufacturers of ARES engines participated with strongly supporting feedback to continue the informal technical consortium. An ASME-ICED ARES Workshop was also conducted in the 2003 ASME Annual Conference in Washington D.C. to inform the public of our studies. Eight (8) technical papers have been peer-reviewed and published at various technical conferences, and the program trained and graduated eight graduate students at MIT and CSU combined. MIT, CSU, Waukesha and our lubricant partner established working relationships that will continue even beyond the current program. We interacted productively with industry, other universities and national laboratories in the ARES/ARICE community and look forward to continued opportunities in the future after the current program ends.

The design strategies developed in this study have promising potential for application in all modern reciprocating engines as they represent simple, low-cost methods to extract significant fuel savings and to reduce harmful environmental effects, without compromising engine performance. The current program has possible spinoffs and applications in other industries as well, including transportation, CHP, and diesel power generation. Discussions with various government agencies and University-Industry workshops will be continued to ensure that the full potential for friction reduction in these areas will be fully explored and areas for further investigation identified. Potential deployment of low-friction engine components or lubricants in the near term is quite possible if future continued funding permits.

LOW-ENGINE-FRICTION TECHNOLOGY FOR ADVANCED NATURAL-GAS RECIPROCATING ENGINES
Final Technical Report
(Reporting Period: April 1, 2002 – November 30, 2006)
DoE Cooperative Agreement No. DE-FC26-02NT41339

I. INTRODUCTION

A. Objectives

The objectives of this program aim at reducing parasitic losses in advanced natural gas reciprocating engines (ANGRE) through lowering friction in the power cylinder (piston and ring-pack). Computer models have been applied to assess the opportunities of piston and piston ring-pack design, surface finish, and lubrication strategies aimed at friction minimization. We have investigated fundamental design parameters and performance relationships to reduce friction without causing adverse effects such as increased wear and oil consumption. The main concepts developed from these analyses have been validated experimentally in a full size ANGRE engine. The various steps towards meeting the program objectives included developing and applying the computer models, analyses of various low-friction strategies, using recommendations of promising low-friction piston/ring-pack/lubricant options, systematic analysis of the experimental data sets, and actual testing and demonstration in an ANGRE engine.

B. Scope of Work

A combined analytical and experimental program has been undertaken. The scope of work includes evaluating the performance and designs of current large-bore natural gas engine and power cylinder components, and modifying or adapting existing analytical tools for ANGRE applications. Computer modeling and analysis have been used to understand and to optimize friction reduction concepts. Concept validation has been conducted experimentally on a Waukesha VGF engine; concurrent computer parametric studies on design parameters have been performed and validated by engine tests. Testing was done at Colorado State University.

C. Tasks Performed

The program has five major tasks, see Table I-1, Project Milestone Plan. (1) Work Planning: organizing the work plan and project team and defining the overall strategy and approaches; (2) Assessing opportunities for friction reduction by performing preliminary analyses and evaluating existing empirical data; (3) Modification or adaptation of existing engine friction and lubrication models to ANGRE engines and developing friction reduction concepts and recommendations; (4) Testing and demonstration of these concepts in an actual engine experimentally; (5) Analysis of test results and iterating the designs for an optimal low-friction system. Task (1) and (2) have been completed during the first year. Task (3)

included analysis of friction reduction strategies in three main technology areas: (a) mechanical design of piston-rings and engine piston design, (b) use of advanced materials and surface technologies, such as cross hatch patterns, roughness and skewness of surface features, dimples and grooves, and (c) lubricant technology. Analyses in all these areas have been fully accomplished and recommendations made. In Task (4), we have tested piston rings with low-friction designs and low-friction lubricants in a multi-cylinder Waukesha natural gas engine. Good progress in planning to procure and implement low-friction piston and dimpled or structured surfaces were made, but these were never tested. We have tested several low-friction lubricants with good results, however. Task (5) involved a continuous process of interactions among design and experimentation, and working very closely with our industrial partners and suppliers.

D. Major Accomplishments

In this program, the major accomplishments include the following:

- Demonstration of low-friction ring-pack designs confirmed ring-pack friction reduction of 30-40%, which translates to total engine FEMP (friction mean effective pressure) reduction of 7-10% from the baseline configuration without significantly increasing oil consumption or blow-by flow. The measured FMEP reductions were in good agreement with the model predictions. Most of this benefit was achieved via adjusting oil-control ring tension and the geometric profile of the running surface of the top piston ring.
- Piston analysis showed possible piston friction reductions of 50% or more, with control of piston profile and other piston parameters. Hence, friction reduction via piston design is comparable and likely to be additive to that achievable via changes in the ring-pack.
- The study on surface textures, including roughness characteristics, cross hatch patterns, dimples and grooves have shown that even relatively small-scale changes can have a large effect on ring/liner friction, in some cases reducing FMEP by as much as 30% from a smooth surface case. Also, it may be possible to combine the effects of lubricant viscosity and surface texturing to reduce friction even further, while mitigating unwanted side-effects such as wear and oil consumption.
- Testing of low-friction lubricants showed that total engine FMEP reduced by up to ~16.5% from the commercial reference oil without significantly increasing oil consumption or blow-by flow. The measured FMEP reductions displayed good agreement with the model predictions.
- The combined analysis of lubricant and surface design indicates that low-viscosity lubricants can be very effective in reducing friction, subject to component wear considerations for extremely thin oils. Engineered surfaces can reduce wear. Hence a combined approach of lubricant design and appropriate wear reduction offers improved potential for minimum engine friction losses.

E. Report Outline

This report contains comprehensive technical discussions of the analytical models, the detailed analysis of friction reduction strategies in three main areas: (a) Ring-pack friction analyses as well as piston analyses , including considerations of design parameters such as

piston ovality and geometric designs, (b) surface texture studies of designs via roughness, cross hatch patterns, dimples and surface grooves, and (c) the third section on lubricants. Experimental testing results are presented at the end, with work done at and reported by Colorado State University. Major conclusions are summarized and discussed, and recommendations made at the end. An Executive Summary appears at the front of the Report.

TABLE I-1: PROJECT MILESTONE PLAN DoE Form 4600.3

(Low Engine Friction Technology for Advanced Natural Gas Reciprocating Engines)

Milestone Plan Period: April 1, 2002 – November 30, 2006

#	MAJOR TASKS	CY 2002			CY 2003				CY 2004				CY 2005				CY 2006			
		2Q	3Q	4Q	1Q	2Q	3Q	4Q	1Q	2Q	3Q	4Q	1Q	2Q	3Q	4Q	1Q	2Q	3Q	4Q
1	Develop Program Plan																			
2	Assess Opportunities based on Prel Observations																			
3	Design & Performance Analysis																			
3.1	(a) Piston analyses for improved piston friction reduction																			
3.2	(b) Perform parametric and system analyses to include effects of material, surface characteristics such as roughness, wear trends, and lubricant																			
3.3	(c) Recommend low-friction design options for ring/piston, material, and lubricant systems.																			
4	**Demonstrate Optimal Design Concepts**																			
4.1	Establish Baseline Tests (Done)																			
4.2	Validate effects of individual component design parameter changes to include piston, material, &																			
4.3	Demonstrate complete low-friction engine system with aggregate improvements																			
5	**Analyze Test Results of Additional System Parameters (Piston, Material, & Lube); Iterate**																			
6	**Manage Reporting & Education**																			
6.1	Prepare periodic reviews and reports																			
6.1.1	- Monthly team telephone conferences	*	*	*	*	*	*	*	*	*	*	*	*	*	*	*	*	*	*	*	*	*	*	*
6.1.2	- Deliver annual reports																			
6.1.3	- Deliver final report																			

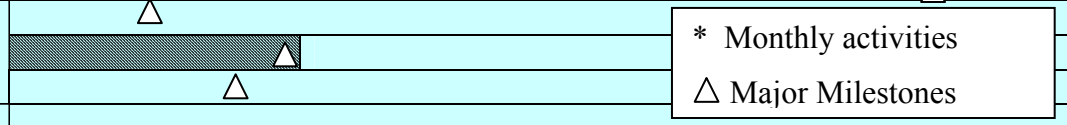

II. RESULTS AND DISCUSSION

(A) DESIGN AND PERFORMANCE ANALYSIS OF RING-PACK FRICTION

1. Introduction to the Model Concepts

1.1. Overview

MIT's computer models [1-4] have been applied to target the most important contributors to friction in the piston-cylinder assembly of the engine. The specific models used to analyze the behavior of the piston and piston rings are described in some detail in the following sections in this Report. Initial studies focused on changing the mechanical design, viz. piston-ring geometry, to reduce ring friction [5,6]. Subsequently, the models have been used for parametric studies on lubricant and surface parameters for the rings, as well as for piston design parameters. Strategies for design changes to reduce friction contributions from these sources have been suggested.

1.2. Objectives and Approach used in the Present Study

The goal of the present study is to develop mechanical designs of piston and rings, surface finishes, and lubricants to reduce piston and piston ring friction, without increasing oil consumption, blow-by, and wear. In the current research, the computer models have been used to develop optimized mechanical designs, surface finishes and lubricants with a comprehensive analysis for both pistons and rings, and lubricants

1. Piston-ring models have been developed/adapted, modified, and applied to investigate the fundamental behavior of piston rings, lubricant, and surface texture. Both hydrodynamic and boundary lubrication for piston-rings have been studied, as well as the interaction between rings, lubricant, and surface finish.
2. Piston models have been modified and applied to investigate the behavior of the piston, and the effects of several parameters including piston profile, lubricant availability, and lubricant viscosity.
3. Results from the parametric studies on the piston and rings have been used to make recommendations for friction reduction in the Waukesha engine power cylinder.
4. We have collaborated with a lubricant supplier to study lubricant effects analytically and experimentally. We worked with ring and piston manufacturers to furnish prototype component designs.
5. We teamed up with Colorado State University and Waukesha Engine Dresser Inc. in testing and validating the low-friction ring and lubricant designs on an 18-liter Waukesha VGF engine. Results are promising.

An experimental evaluation of the designs has been conducted to validate the model predictions and to evaluate certain effects that could not be predicted quantitatively by the model. The use of this combined approach with the goal of developing an optimized piston and

ring pack is what distinguishes this work from many of the previous studies that have been conducted in this area.

Specifically for the low-friction ring pack, we considered ring geometry and tension and these have been tested in full-scale engine conditions. Parametric studies have been conducted considering various surface finish and lubricant parameters, and piston designs. Advanced surface finishing techniques, such as dimpling, was also evaluated. A cooperative partnership with a lubricant manufacturer has been formed for lubricant testing of low-friction oils. These oils have been tested and results are encouraging.

1.3. Sources of Friction in Modern Internal Combustion Engines

Only about one third of the fuel energy consumed in an internal combustion engine is delivered as mechanical work, with approximate one-third to the coolant, and one-third to the engine exhaust. For large advanced reciprocating engine systems (ARES), such as those for power generation, this percentage of fuel energy delivered as work is higher, over 40%. The multi-year ARES goal is to increase this engine efficiency from approximately 40% to a target of 50%, a ten percentage point (10%) increase from current production engines. Every method and concept is used towards achieving that goal, incrementally year by year. However, mechanical losses alone, due to friction, already account for up to 15% of the total energy consumed [7]. About 40-55% of those total mechanical losses occur in the power cylinder of an engine [8], and approximately half of the power cylinder friction losses come from friction generated by the piston rings, and half from the piston (with only a small fraction of the losses due to the connecting pin) [7-9]. As a result, reducing both piston and piston ring friction has the potential to improve engine efficiency, lower fuel consumption and reduce emissions. These are important objectives for today's engine manufacturers, who are striving to improve engine performance while trying to meet increasingly stringent emissions standards.

1.4. Overview of the Ring-Liner System

1.4.1. Description of the Piston Ring-Liner System

The piston ring pack in an internal combustion engine typically consists of three rings located in grooves in the piston, as shown in Figure 1-1. The primary purpose of the ring pack is to prevent high-pressure gases from leaking out of the combustion chamber, which would result in power losses. The rings must also prevent excessive leakage of oil from the crank case to the combustion chamber, while themselves remaining sufficiently lubricated. A third function of the piston rings, particularly for the top ring, is the dissipation of heat from the piston to the cylinder liner. The rings should perform all of these functions without introducing excessive frictional losses into the system, and while keeping wear of both the rings and the cylinder liner to a minimum.

The system achieves these three objectives by using three specialized piston rings, each with a specific function. The top ring seals the ring-liner interface in order to prevent high-pressure gas from escaping from the cylinder into the lower parts of the ring pack. The top ring also dissipates heat from the piston to the cylinder liner. The oil control ring controls the amount

of oil that flows towards the combustion chamber to lubricate the upper rings, regulating both the lubrication of the top two rings and oil consumption. The second ring scrapes down any excessive oil that passes the oil control ring, further controlling oil consumption while maintaining adequate lubrication. In some cases the second ring is deemed unnecessary (as in racing engines, where light weight is more important than oil consumption), while in others extra scraper rings are added, as in large diesel engines with long life and low oil consumption requirements.

1.4.2. Typical Piston Ring Designs

The designs of the three piston rings reflect their different purposes. The top ring, both far from the lubricant supply and exposed to harsh conditions, is designed to retain, and use to maximum effect, any available oil. The second ring, also called the scraper ring, is designed to scrape excess oil down the liner (towards the crank case) on down-strokes, but not transport oil back up the liner, which can increase oil consumption. The oil control ring must conform to the liner, so that excessive leakage does not occur, and adequately control the oil supply to the top two rings under all engine conditions.

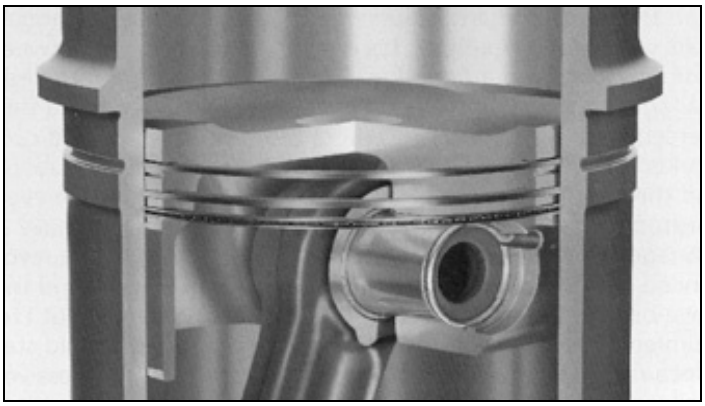

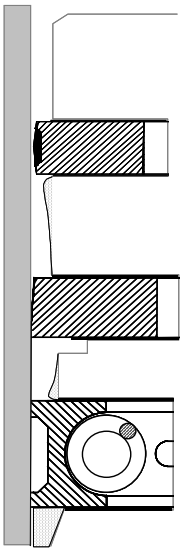

Figure 1-1: The Piston Ring Pack **Cross-Sectional View:**

The top ring is the closest to the combustion chamber, so that it is exposed to very harsh conditions and rapidly changing loads. High combustion chamber gas pressures, in particular, can put high radial loads on the top ring, causing the ring to push into the liner at high force. When lubrication is insufficient, this high contact force can lead to high friction and wear. Ring/liner friction increases the mechanical loss of the engine, while wear results in the increase of the ring gap over time, increasing leakage of combustion chamber gases and further reducing engine efficiency. The barrel-shaped face profile of the top ring has been shown to be most

effective for lubrication [10], and thus reduces this friction and wear to a minimum.

The second ring has a tapered face that very effectively accumulates oil on its lower edge, for downward scraping, but it cannot accumulate oil on its upper edge to scrape upward towards the combustion chamber. This allows the second ring to reduce oil consumption and provide as a secondary control on oil flow. The scraper ring's unidirectional scraping profile is illustrated below in Figure 1-2.

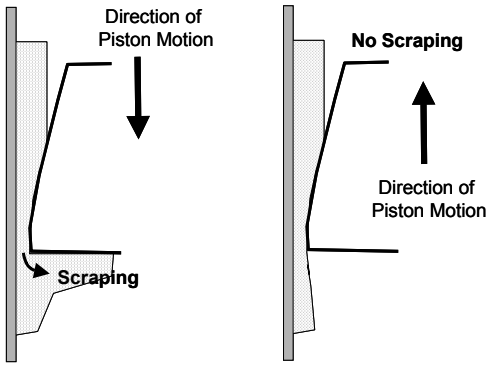

Figure 1-2: Effect of Taper Face Profile on Oil Transport

The oil control ring's purpose is to control the supply of oil traveling to the top two rings, making conformability to the liner a key design criterion. Several different oil control ring designs are in use, for different engine types. The focus of this study was the twin-land oil control ring (TLOCR), which is typically used in large diesel engines. The TLOCR consists of a spring mounted inside two rails, where the circumferential length of the spring determines the ring tension. The high ring tension provided by the spring produces adequate ring-liner conformability, accommodating the thermal and mechanical deformation of the cylinder bore that occurs during engine operation. The two lands effectively control oil flow by exerting a high pressure on the oil film, where the high ring tension can create a very high pressure on the oil film because of the thinness of the lands. A single land may be sufficient to control oil flow if it always conforms well, but oil ring tilt can cause one land to tilt away from the liner. Two lands are used because it is believed that at least one of the lands will control oil at any given time in the engine cycle, depending on the relative angle between the ring and the liner.

The rings are manufactured in different materials depending on the type of engine in which they are to be installed. In larger diesel engines, the rings are typically made of ductile cast iron, whose high thermal stability makes it desirable in the high operating temperatures in these engines. Cast iron ring faces are typically coated with a chrome layer for wear reduction, and considerable research is currently being devoted to the identification and development of other materials and face coatings for reduced friction and wear. Steel is the more popular material for rings to be used in smaller gasoline engines because it is stronger than cast iron, and, therefore, the size of the rings can be reduced and conformability improved without a reduction in ring life. Some studies have been conducted in which steel rings were investigated for larger diesel engines. These rings showed promise for use in larger engines, except for temperature limitations and some significant wear observed with certain steel materials used in articulated pistons.

1.4.3. Dynamic Phenomena in the Piston Ring-Liner System

The external conditions operating on the rings (temperatures, pressures, etc.) change throughout the engine cycle, causing the rings to displace and twist relative to their ring grooves. The small (order of 100 microns) clearances between the rings and their grooves can allow significant gas flow, so that pressure balances across the rings change throughout the cycle. This dynamic movement of the rings significantly affects the performance of the rings, including oil flow, ring/liner and ring/groove friction and blow-by (gas leakage). Integral to addressing the general criteria discussed above, the piston rings must perform well dynamically, throughout the engine cycle.

Several other factors also affect ring-liner lubrication as well as the ability of the rings to seal the ring-liner interface. Bore distortion occurs because of mechanical stresses and thermal expansion due to the temperature gradient along the liner in the direction of piston motion. This overall bore distortion is comprised of radial expansion and circumferential out-of-roundness, and it is therefore a complex 3-D phenomenon that can significantly affect the conformability of the piston rings to the liner. Ring-liner lubrication is also significantly affected by the asymmetric geometry of the crank and connecting rod. As a result of this asymmetry and the various forces encountered during the engine cycle, the piston will tend to tilt about the axis of the piston pin throughout the engine cycle, which will affect angle between the ring and the liner.

The dynamics that arise due to the clearances between the ring and the grooves, combined with bore distortion and piston tilt, ultimately determine the ring-liner relative angle. This angle significantly affects the lubrication between the ring and the liner, and the friction generated by their interaction. The link between these dynamic phenomena and piston ring friction and lubrication is discussed in more detail in Section 2.

1.5. Overview of the Piston/Liner System

1.5.1. Description of the Piston/Liner System

The main function of the piston is to transmit the combustion gas pressures in the combustion cylinder to the crankshaft. The oscillating motion of the connecting rod causes an oscillating side force, between the piston and liner, to be generated as the piston moves through the engine cycle. The piston must support this force, while sliding, with a minimum of friction generation. Other considerations for the piston include noise and vibration generation – sufficient oil must be present to cushion the piston "slap" as it moves from one side of the liner to the other – and wear.

1.5.2. Typical Piston Designs

In general, the piston consists of an upper region, containing grooves for the piston rings, and a lower region known as the "skirt". The skirt supports the piston/liner contact pressures,

and is the site of friction generation and wear. Thus, this is the main region of interest in this study. Skirt friction and wear are affected by three design characteristics, the skirt profile, the waviness, and the surface roughness. The skirt profile is of the largest scale, and describes the large-scale variation in piston radius in the axial direction. The waviness results from the piston machining process and results in circumferential surface grooves on the scale of 10μ. The roughness is on yet a smaller scale, on the order of 1μ or less, and is controlled by the skirt material and the surface finishing techniques used. All of these piston characteristics affect friction, although the amount and the manner in which they affect friction depend on several other factors, including lubricant formulation and the extent of piston wear.

Pistons are produced with many different profiles, including tapered, barrel, and others, each offering advantages and disadvantages. This study focuses on barrel-profile pistons, such as the one shown schematically in Figure 1-3. The barrel shape of the skirt maintains a small piston diameter near the upper land, which allows for thermal expansion, while maintaining a relatively large wetted skirt area, which helps to reduce wear. The barrel shape also assists in creating a hydrodynamic oil film, and improves stability and reduces clearances by allowing for the natural secondary motion of the piston. The proportions of the barrel shape – i.e., the curvature of the bulge – have a large effect on piston/liner surface generation.

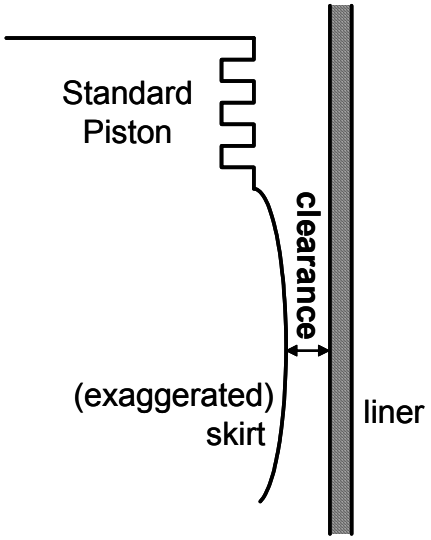

Figure 1-3: Piston with a barrel-shaped skirt

The waviness and roughness of the skirt also affect friction. Figure 1-4 shows a schematic of worn and unworn piston surfaces. For an unworn piston, the affect of the waviness dominates any roughness affects, because the waviness is on a larger scale. In this case, friction is dominated by the contact of the peaks of the waviness with the cylinder liner, causing boundary friction to occur. Contact occurs only at the high points of the machining grooves, with the height of those points determining when and how much contact occurs. As this type of contact continues, however, the peaks are worn down, as shown in the figure. In the worn case, the texture of the flat "plateaus" that has replaced the waviness peaks may become dominant. In this case, the height of flat surface roughness determines the extent of any asperity contact.

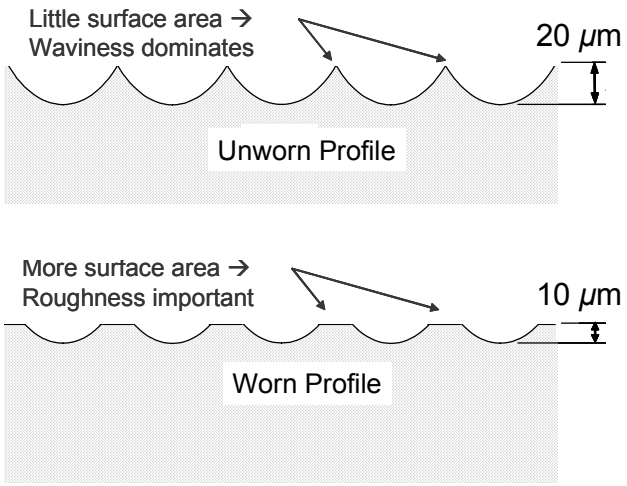

Figure 1-4: A side view of skirt waviness, worn and unworn cases.

1.5.3. Dynamic Phenomena in the Piston-Liner System

The piston is subject to different temperatures, pressures, and reaction forces over the course of the engine stroke. The asymmetric geometry of the crank and connecting rod result in cyclic side-forces between the piston skirt and liner which, together with cylinder gas forces, cause the piston to displace within the cylinder, and also tilt about the pin axis. The major feature of this secondary motion is its tendency to hug one side of the cylinder for most of a stroke, then transfer quickly to the other side, resulting in a "slap" as it contacts the opposite surface. This slap can contribute to engine noise and vibration, as well as friction. The slap and subsequent motion on the major thrust side of the piston, following combustion (and thus under high gas pressure conditions) is responsible for a large portion of the piston/liner friction.

Other dynamic phenomena contribute to piston friction and motion. The bore distortion of the cylinder, due to gas forces and thermal gradients, can have a large effect. Also, other secondary motions of the piston can affect both friction and noise. For example, after the slap, the piston continue to vibrate/oscillate until the oscillations are damped out. The extent of this oscillation depends on the contact velocity as well as the amount of damping (usually from an oil film) present, and can affect the friction, noise, and vibration of the engine.

1.6. Overview of lubricant properties and requirements

Modern engine lubricant must perform many different functions, and fulfill many requirements. To this end, the typical lubricant contains a number of components and additives, designed to control viscosity, reduce boundary friction and wear, control lubricant degradation, and perform numerous other functions. While the lubricant viscosity is the focus of this study, other requirements should be taken into consideration in the design of an engine lubricant.

One of the main lubricant requirements is stability. The oil must maintain a stable state at all temperatures and conditions, so that it does not either react to create corrosive elements or form deposits that can reduce engine performance. The lubricant must also be able to mitigate the effects of any compounds that are formed in the engine or enter via intake air. Detergents and dispersants allow the oil to keep such components in suspension – preventing them from being deposited on surfaces or creating wear - and to inhibit reactions that lead to undesirable products such as acidic compounds [11].

In addition to these functions, the lubricant often also contains compounds that reduce wear and control viscosity. Anti-wear additives can be used to reduce wear due to metal-to-metal contact, while other additives are used to control attack on piston, cylinder and ring surfaces by acidic combustion products. The viscosity must also be controlled so that it maintains an acceptable value at both cold-start and running temperatures. Viscosity Index (VI) improvers can be used to reduce the variation of viscosity with temperature, so that the oil can be thin enough at start-up to lubricate the engine but not too thin at high temperatures to allow excessive boundary contact at running conditions [11]. One side effect of these VI improvers is to make the oil viscosity depend not only upon temperature but upon the shear rate in the oil. Not all lubricants contain VI improvers, but for those that do this viscosity variation must be taken into account.

1.7. Overview of liner surface structure

While they may appear smooth to the naked eye, the surfaces of both the rings and the cylinder walls are rough on the scale of interest – the thickness of the oil film separating the two. The texture of these surfaces can greatly affect both the amount of contact that occurs among asperities and the flow of oil between them. Understanding the effect of surface texturing on the interaction between the surfaces, and between the lubricant and the surfaces, is essential in understanding the lubrication of components currently in use and designing new surfaces to reduce friction.

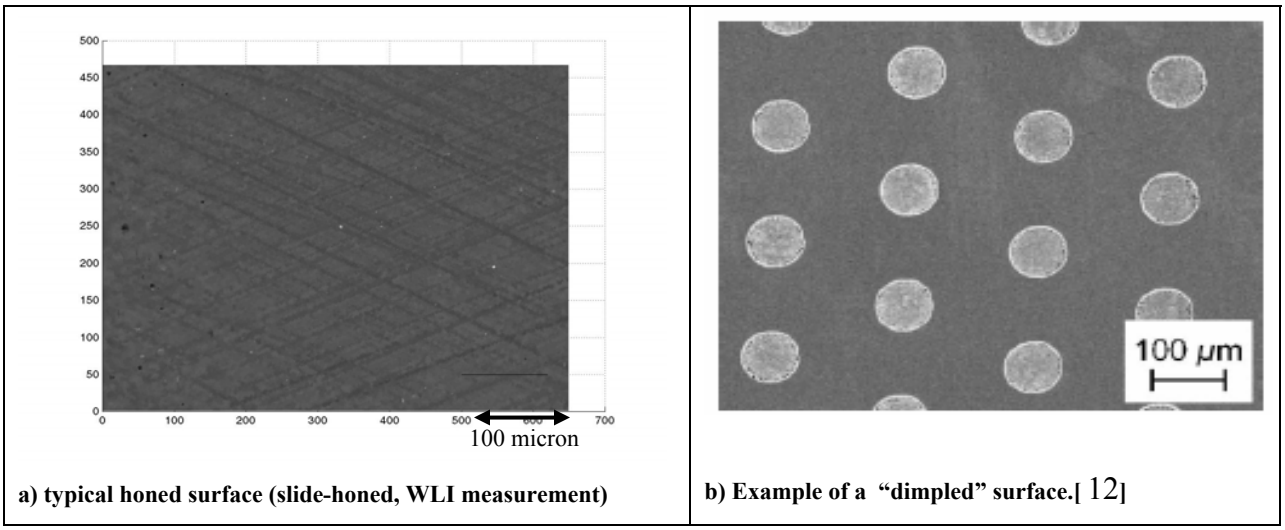

a) typical honed surface (slide-honed, WLI measurement)

b) Example of a "dimpled" surface.[12]

Figure 1-5: Typical examples of honed and laser-textured surfaces

Two examples of surface finishes are shown in Figure 1-5. Figure 1-5a shows an example of a surface commonly found on cylinder liners today – a plateau finish clearly showing the cross-hatch marks that result from the honing process. Figure 1-5b shows a less common texture, the surface has a dimpled pattern created by laser machining. While very uncommon at present, such designed surfaces are the subject of numerous studies and may be a key part of decreasing sliding friction and wear between the rings and liner.

1.7.1. Current production cylinder liner finishes

Today, most cylinder liner surfaces have a honed finish whose properties are stochastically controlled. That is, statistical parameters such as the surface roughness and skewness are determined by the honing process, but the placement of specific features in specific locations is not possible. A typical honed surface, of which an example profile is shown in Figure 1-6 and a surface view in Figure 1-5a, has a negative skewness and a cross-hatch pattern of grooves, both created by the honing procedure.

Figure 1-6: Typical plateau honed profile

A typical honing tool is shown in Figure 1-7. The tool consists of a head with honing sticks or stones that are covered with abrasive particles, and are held outward radially by springs. The head is spun and at the same time moved axially in and out of the cylinder. The honing

sticks are pressed outward into the bore and polish the surface. The process generally proceeds from a coarse grit to a fine one, so that deep grooves and large ridges are made during the initial rough honing passes. Then, the ridges are worn down to a relatively smooth finish by the subsequent fine passes, while the deep valleys remain. Such a process generally results in a plateau finish – a surface with negative skewness - in which the surface is relatively flat with many deep valleys. Such negatively skewed surfaces are thought to reduce friction by effectively breaking in the liner before actual engine use, and thus reducing actual breaking–in time, as well as by reducing asperity contact between ring and liner in a mixed lubrication regime [13,14,15].

In addition to creating a plateau surface, the combination of the rotating and axial feeding movements of the honing machine creates angled grooves on the surface, as shown in Figure 1-8. The relation between the rotation and feeding rates determines the angle of the cross-hatch grooves. The size and angle of these grooves has an influence on friction as well as oil consumption and wear. Several studies have predicted an increase in oil film thickness and decrease in friction for more transverse (relative to the cylinder axis) textures [13-17], although concerns about oil consumption and scuffing wear prevent very shallow-angle cross-hatch grooves from being implemented in production cylinder liners.

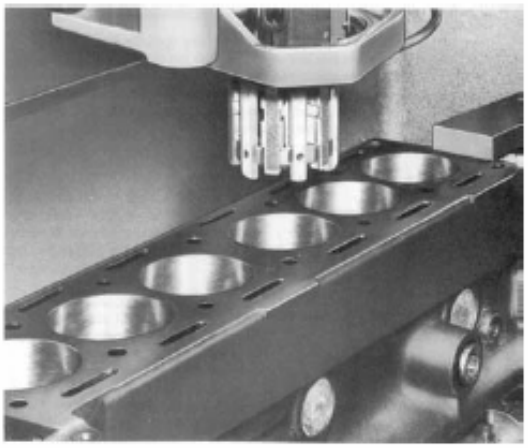

Figure 1-7: Typical cylinder bore honing tool [16]

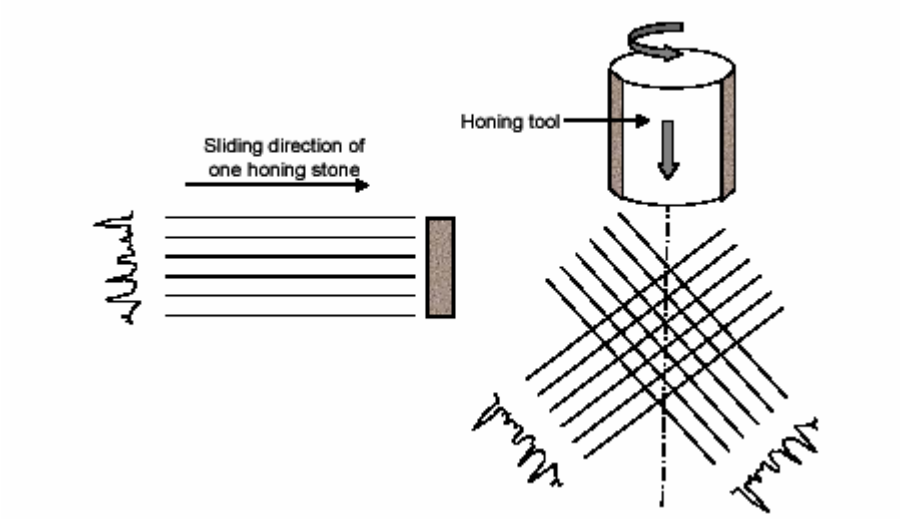

Figure 1-8: Schematic of honing process [15]

1.7.2. Advanced finishes and textures

Deterministically controlled textures, in which individual features, such as the dimples shown in Figure 1-5b, are added to a surface, are already in use in some industries and show promise for friction and wear reduction in engine applications. For example, very small "micro-texturing" has been added to the "landing" sections of magnetic storage media for several years, to prevent stiction when recording heads contact the surface [18]. Although the mechanism for friction reduction here is different from that encountered in the case of the piston ring/liner interface, the success of this technique has encouraged other investigations into the possibility of engineering the surface structure.

Numerous studies, both analytical and experimental, have considered the effect of advanced textured surfaces on friction, wear, and other parameters in sliding applications. Research on face-seals, where loads and speeds are approximately constant during service, has shown great potential for increasing load capacity and lifetime with the addition of micro-texturing. Some experimental prototypes have been successfully field-tested in pumps, where they showed increased load capacity and greatly decreased wear over standard seals [19]. Studies of reciprocating sliding conditions have also indicated that friction may be reduced, although there is a lack of agreement over the mechanism for this effect. Still, both analytical and experimental results have shown potential for friction reduction, and laser-textured cylinder liners that promise low wear and oil consumption have been made commercially available by Gehring GmbH [20] in Germany.

Several methods are available for creating micro-textured surfaces, including chemical etching, machining, abrasive-jet machining, and laser texturing. Each method has advantages and disadvantages, and some may be more appropriate for use in a given application than others. Etching, for example, is versatile in the shapes it can produce, but the process is time-consuming and the profiles of the features are determined by the chemical erosion process and cannot be controlled (i.e., round-profiled dimples cannot be produced). Regular and abrasive-jet machining also have some limitations on profile shape, and may not be appropriate for cylinder

liner texturing if machining heads are too large to access the inner liner surface. Laser texturing technology is currently believed to be a very promising technique based on its flexibility and speed [8]. A possible drawback is that the laser technique may create "burrs" of melted and re-deposited material around the edges of features so that surfaces may require a subsequent polishing step, however this problem may be solved with more optimized techniques in the future. An example of a laser-machining station is shown in Figure 1-9.

Figure 1-9: Typical laser texturing machinery (from Control Micro Systems, Inc.)

.

1.8. Areas of Lubricant and Surface Analyses

Subsequent to the initial mechanical design oriented study, we continued to investigate methods by which ring/liner friction can be reduced in the Waukesha VGF 18GL engine via lubricant and surface design. We focused on lubricant viscosity and surface finish of the cylinder liner. For both studies, existing ring-pack friction and lubrication models were used, with minor modifications as required to complete the study.

In the area of lubricant properties, viscosity and its dependence on temperature and shear rate were considered. The role of lubricant viscosity in controlling the balance between hydrodynamic and boundary friction was studied, as was the effect of variation of viscosity during the engine cycle. Effects of viscosity on both friction and wear were analyzed. Also, some consideration was given to boundary friction coefficient and its role in ring/liner friction.

In the area of surface texturing, a parametric study was performed to evaluate the effects of both grooved and dimpled textures on the cylinder liner. Simplified surfaces were used to calculate flow and stress factors for the cases considered, which were then used in the ring-pack model to predict ring/liner friction. While the model used did not allow a detailed analysis of the effects of these textures on asperity contact and oil flow, this type of parametric study can give an indication of which textures are effective and how changing the different parameters affects friction and wear.

The possibility of optimizing the lubricant and surface together was also investigated. With this combined approach, a greater friction reduction is possible than in the individual cases, and it is also possible to reduce negative side-effects such as increased wear and oil consumption.

2. Model Formulation: Ring-Pack Lubrication and Friction

2.1. Ring-pack modeling

The ring-pack simulation used in this study was developed by Dr. Tian Tian [2] at MIT. In addition to modeling friction and lubrication between the ring and liner, the package contains an advanced ring dynamics module, allowing it to analyze details of ring movement such as flutter and collapse, and calculate parameters such as the ring dynamic twists and gas blow-by flows. In the study of surface finish a modified version of this model, developed by Jeffrey Jocsak [15] also at MIT, was used. This modified package includes sub-models that can account for a greater variety of surface textures than the original program, in both contact and fluid flow analysis. It is used concurrently with a numerical simulation created by Yong Li of MIT, which is used for the calculation of the flow and stress factors which are used in the analysis of rough surface fluid flow. A general diagram of the ring/liner system analyzed in these models is shown in Figure 2-1.

Calculation of ring/liner friction requires simultaneous solution of several relationships: a balance of radial forces on the ring must be satisfied, along with mass and momentum conservation for the lubricant flowing under the ring and a contact relationship for asperity contact. These relationships are interrelated by the oil film thickness and oil wetting locations on the ring. The hydrodynamic pressure, P_{hyd}, is strongly dependent on film thickness and wetting location, while the amount of asperity contact that occurs also depends on the film thickness. As the ratio between these two pressures changes, the radial force balance changes also. A solution is found at an oil film thickness and wetting condition at which the ring load is supported by asperity, oil and gas pressures, and all boundary conditions are satisfied.

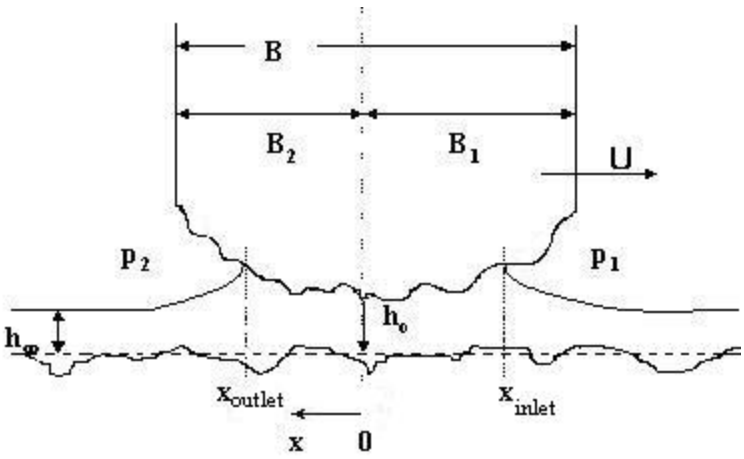

Figure 2-1: Schematic of ring/liner system. Surface roughness and ring curvature are exaggerated.

2.2. Modes of ring/liner lubrication

The ring can experience three modes of lubrication - hydrodynamic, mixed, and boundary - illustrated in Figure 2-2. In pure hydrodynamic lubrication, there is no contact between the ring and liner, and the ring load is entirely support by hydrodynamic pressure in the oil film. In this regime, the ring/liner friction results entirely from shear stress within the oil. In pure boundary lubrication, the entire ring load is support by solid-solid contact between the ring and liner, with no hydrodynamic contribution. In this case, ring/liner friction consists entirely of rubbing friction losses. When the ring load is partially supported by the oil pressure, and partially by asperity contact, mixed lubrication occurs. In this situation, friction losses stem from both oil shear and metal-metal rubbing.

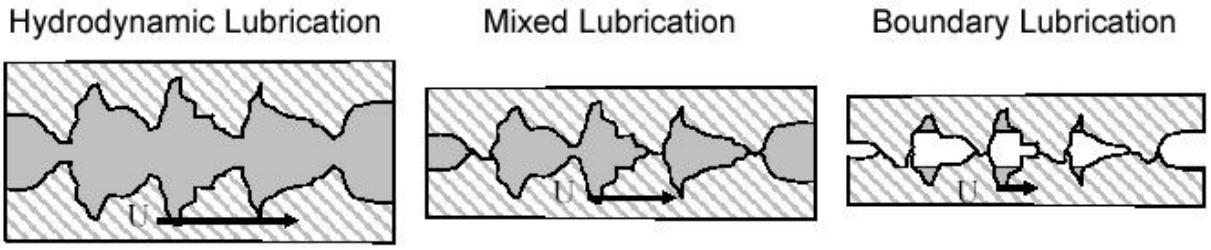

Figure 2-2: Modes of ring/liner lubrication

In the current model, the two surfaces are described stochastically, so it is not possible to ascertain whether any given asperity (local roughness peak) is contacting any other asperity. Instead a statistical limit is used, which determines the oil film thickness at which it is assumed negligible asperity contact occurs. This statistical limit is based on the combined roughness of the two surfaces, σ (where roughness is defined as the standard deviation of the surface height, measured from the mean):

$$\sigma = \sqrt{\sigma_{liner}^2 + \sigma_{ring}^2} \tag{2.1}$$

where σ is the combined surface roughness, σ_{liner} is the liner roughness, and σ_{ring} is the ring roughness. The amount of contact occurring is assumed to be negligible when the nominal separation between ring and liner and is greater than some factor, Ω, times this combined roughness. The model used in this study uses a value of $\Omega = 4$, where at the surface separation of $h = \Omega * \sigma = 4\sigma$, statistically, the probability of contact is less than 2%. Then, it is assumed in the analysis that:

$$\begin{aligned} &\frac{h}{\sigma} \le \Omega = 4 \quad && contact\ \ occurs \\ &\frac{h}{\sigma} > \Omega = 4 \quad && no \quad asperity\, contact \end{aligned} \tag{2.2}$$

where h is the mean oil film thickness.

2.3. Radial force balance

The ring load, including ring tension and gas pressure behind the ring, must be supported by some combination of asperity contact pressure, hydrodynamic pressure in the lubricant film, and gas pressures acting on the ring face. This balance is represented by the equation:

$$\begin{aligned} &\sum F_r = 0 \\ &= \int_{x_1}^{x_2} P_{hyd}\, dx + \int_{-b_1}^{b_2} P_c\, dx + P_1(B_1 + x_1) + P_2(B_2 - x_2) - P_b(B_1 + B_2) - T_r(B_1 + B_2) \end{aligned} \tag{2.3}$$

where P_{hyd} is the hydrodynamic pressure in the oil film, P_c is the asperity contact pressure between the ring and liner, P_1 is the gas pressure on the upper (combustion chamber) side of the ring, P_2 is the gas pressure on the lower (crank case) side of the ring, P_b is the gas pressure behind the ring, B_1 and B_2 are the upper and lower widths of the ring, x_1 and x_2 are the upper and lower wetting locations (x_1 is negative), and T_r is the ring tension, as shown in Figure 2-3. The ring inertia is not included in the radial force balance because it is much smaller than the other terms [2].

.

Figure 2-3: Schematic of

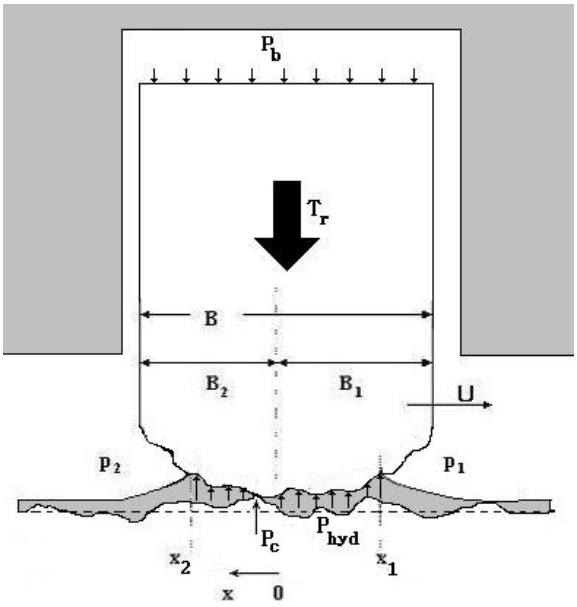

ring/liner system

This relationship must be solved iteratively with asperity contact and hydrodynamic models, in order to determine oil film thickness, wetting locations, and pressure distribution in the lubricant

2.4. Asperity contact model

When solid to solid contact occurs between the ring and liner, an analysis that is based on the Greenwood and Tripp [21] asperity contact model, using a correlation developed by Hu [22], is used. Greenwood and Tripp's model describes the relationship of the elastic pressure of two contacting asperities with the distance between them:

$$P_c = \begin{cases} K' E' A\left(\Omega - \dfrac{h}{\sigma}\right)^z & \dfrac{h}{\sigma} \le \Omega \\ 0 & \dfrac{h}{\sigma} > \Omega \end{cases} \tag{2.4}$$

where P_c is the asperity contact pressure, K' is a constant related to the asperity geometry and distribution, E' is a constant related to the properties of the contact materials, A is a constant that can be used to calibrate predictions with measured data, σ is the combined roughness of the two surfaces, h is the nominal distance between the surfaces, Ω is the ratio of h/σ beyond which contact pressure is assumed to be negligible, and z is a constant. The coefficient K' is given by:

$$K' = \frac{8\sqrt{2}}{15}\pi(N\beta'\sigma)\sqrt{\frac{\sigma}{\beta'}} \tag{2.5}$$

where N is the number of asperities per unit contact area, and β' is the asperity radius of curvature. The coefficient E' is given by:

$$E' = \frac{2}{\left(\frac{1-\nu_1^2}{E_1}\right) + \left(\frac{1-\nu_2^2}{E_2}\right)} \tag{2.6}$$

where E_1 and E_2 are the Young's moduli for the two contacting surfaces, and ν_1 and ν_2 are their corresponding Poisson's ratios.

The relationship given in Eqn. 2.4 must be integrated over the apparent contact area to obtain a total contact force for the ring and liner. This can be done numerically, if deterministic surfaces are provided, or a stochastic model can be used. The analytical method used in this study uses a stochastic model, based on the Pearson system of frequency curves, which can describe surface characteristics based on RMS roughness, skewness, and kurtosis [23] (for definitions of Sk and Ku see subsequent sections). When reasonable assumptions are made for the values of asperity density and radius of curvature, this model can be used for predicting asperity contact pressure between ring and liner.

This asperity contact model assumes that deformation of the asperities is entirely elastic, and that plastic deformation does not occur. Although it is unrealistic to assume that this is the case in an engine, especially during the break-in period, it has been shown by Greenwood & Tripp that the asperity contact pressure calculated for pure elastic deformation is very similar to that calculated with plastic deformation taken into account. Certain assumptions about asperity shapes and distribution are also made in this model, which are described in greater detail in Ref. [21]. Also, it should be noted that surface coatings such as oxide films or chemical layers created by friction modifiers have not been considered.

2.5. Lubricant flow and stress conditions – averaged Reynolds analysis

When hydrodynamic or mixed lubrication occurs, an averaged flow-factor Reynolds analysis is used to model the lubricant pressure and flows, and the interaction between the lubricant and surface asperities. Hydrodynamic support of the ring load depends on a "wedge" effect in which relative motion between sliding surfaces and changing flow area combine to increase pressure in the lubricant. The fluid pressure is then able to support an external load. Because of this effect, a positive pressure increase will occur in the oil in the converging section of the ring/liner interface, and pressure will decrease in the diverging section, as shown in Figure 2-4. The figure also shows cavitation in the oil film, which may or may not occur, depending on engine parameters and running conditions. Cavitation and oil detachment conditions are discussed further below. If the net pressure in the lubricant is positive the ring load can, at least partially, be supported by this hydrodynamically generated oil pressure.

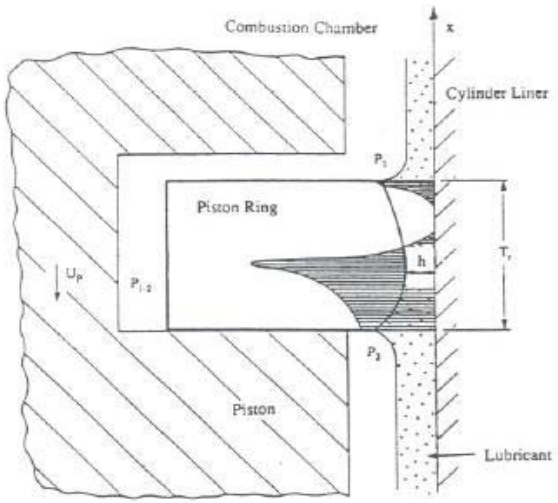

Figure 2-4: Schematic showing pressure distribution in the oil between ring and liner [14]

Analysis of the lubricant pressure and flow between ring and liner is based on Reynolds' equation, which is applicable for thin film flows where viscous phenomena dominate fluid inertia. The Reynolds relationship is derived from conservation of momentum for the fluid (Navier-Stokes relations) and conservation of fluid mass (Continuity), and (for a one-dimensional system) is given by:

$$\frac{\partial}{\partial x}\left(\frac{h^3}{\mu}\frac{\partial p}{\partial x}\right) = -6U\frac{\partial h}{\partial x} + 12\frac{\partial h}{\partial t} \tag{2.7}$$

when both sliding surfaces are smooth, and h is the nominal separation between the surfaces, μ is the fluid viscosity, p is the pressure within the fluid, and U is the relative sliding speed.

In reality, the sliding surfaces are never perfectly smooth. When the oil film thickness is much larger than the roughness of both surfaces, this roughness has very little effect and can be neglected. However, when the oil film thickness and surface roughnesses are of the same order of magnitude, the effects of the surface texturing must be considered.

Both deterministic and stochastic methods are available for describing roughness effects. Deterministic techniques include more detail about actual surface features, and can account more accurately for fluid flows and asperity contact between the ring and liner. However, such techniques are complex and time-consuming to apply, and may not be necessary when a simpler understanding of trends and general effects of different surface parameters is desired. This study uses a stochastic approach, based on the averaged flow factor method of Patir and Cheng [24].

The averaged flow factor technique uses several factors to account for the differences between flow between two smooth surfaces, and flow between rough surfaces. The Reynolds equation for smooth-walled flow is still used, together with three factors which account for the averaged effects of surface roughness:

$$\frac{\partial}{\partial x}\left(\phi_p \frac{h^3}{\mu}\frac{\partial p}{\partial x}\right) = -6U\frac{\partial}{\partial x}(h\cdot\phi_g + R_q\cdot\phi_s) + 12\frac{\partial h}{\partial t} \tag{2.8}$$

where ϕ_p is the pressure flow factor, ϕ_g is the geometric flow factor, ϕ_s is the shear flow factor, and R_q is the combined RMS roughness of the surfaces. Each factor is determined for a given surface, and accounts for the effect of the surface texturing on a given aspect of the fluid flow. The pressure flow factor represents the effect of the roughness on pressure-driven flow, while the shear flow factor represents the effects of surface roughness on shear-driven flow.

The geometric flow factor simply accounts for the fact that, as rough surfaces get closer together, they contact. The film thickness, h, used in the Reynolds equation is the nominal film thickness, taken as the mean distance between rough surfaces. However, the thickness required for shear flow calculation is the *mean* film thickness, which is equal to h in full hydrodynamic lubrication, but diverges from it when asperity contact occurs. When contact occurs, it is assumed that the overlapping asperities are simply sheared off, essentially changing the distribution of surface heights. Then, the location of the surface mean changes. The geometric flow factor takes this into account. When two surfaces are not contacting there is no change in surface mean heights and $\phi_g = 1$, nominal and mean surface separations are the same. When contact occurs, the mean film thickness becomes larger than the nominal, and $\phi_g > 1$.

Several methods for calculating flow factors are available. The technique used for factor calculation in this study is described in more detail in Section 2.7, below.

2.6. Boundary conditions

In addition to the flow factors, several boundary conditions are required to solve the Reynolds relationship given above. Continuity of pressures is required, so that the oil pressure at the top oil attachment point is equal to the gas pressure above the ring (P_1) and the oil pressure at the lower oil attachment point is equal to the gas pressure below the ring (P_2):

$$\begin{aligned} P(x_1) &= P_1 \\ P(x_2) &= P_2 \end{aligned} \tag{2.11}$$

Also, at the inlet, conservation of mass must be satisfied, so that the amount of oil flow under the ring at the inlet must be equal to the supply that was present on the liner prior to the arrival of the ring:

$$Q(x_{inlet}) = Uh_\infty \tag{2.12}$$

where $Q(x_{inlet})$ is the volumetric oil flow rate (per unit width) at the oil attachment point, and h_∞ is the oil film thickness before attachment occurs. This condition is not valid when the ring inlet

is fully-flooded - when there is more oil available than can be accommodated under the ring, and the excess is deposited on the leading ring face, as shown in Figure 2.5. In this case, the oil flow at the ring inlet is assumed to be equal to the amount flowing under the height of the ring surface at inlet:

$$Q(x_{inlet}) = U \cdot h(x_{inlet}) \tag{2.13}$$

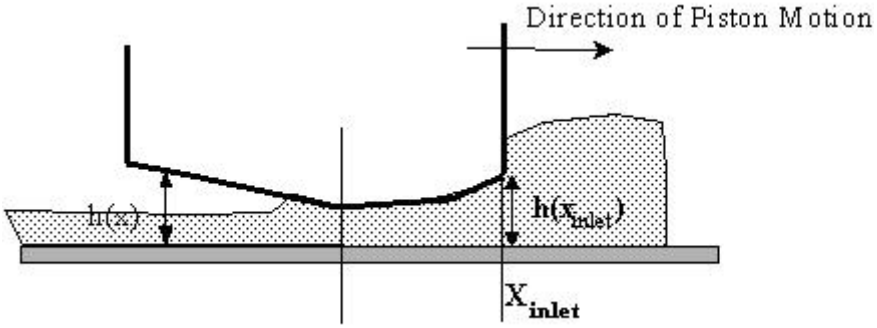

Figure 2-5: Illustration of fully-flooded inlet condition

An outlet condition must also be specified. A commonly used outlet condition is the Reynolds boundary condition:

$$\left.\frac{dp}{dx}\right|_{x=x_{outlet}} = 0 \tag{2.14}$$

which states that the pressure gradient in the oil must disappear at the ring outlet. This boundary condition can apply near the mid-stroke region of the cycle, where high relative speeds maintain hydrodynamic support of the ring, and at low enough gas pressures so that cavitation is not prevented. Near the end-strokes the Reynolds outlet condition is not applicable because, along with mass conservation, it requires oil to accumulate under the ring faster than it is being supplied at the inlet. In this region, then, a film-non separation boundary condition [25] is used, in which it is assumed that all of the oil exiting the ring/liner interface at the outlet stays attached to the ring, where it accumulates:

$$q_{x,outlet} = a \tag{2.15}$$

where $q_{x,outlet}$ is the flow rate of oil at the oil detachment point, and a is the accumulation rate of oil on the ring, defined as:

$$a \equiv h(x_{outlet}) \cdot \frac{dx_{outlet}}{dt} \tag{2.16}$$

2.7. Determination of flow and stress factors

The flow and stress factors that are used in the averaged Reynolds equation, and to determine shear stress are calculated deterministically, using the outputs from a numerical program developed by Yong Li at MIT. This model determines fluid flows and stresses between a smooth surface and the rough surface of interest, represented by a numerical matrix of surface height values. This matrix may be measured from an actual surface, (for example, using white-light interferometry) or generated analytically, as was done in this study. Comparing the deterministically calculated "actual" flows and stresses from this program to those calculated assuming smooth conditions and nominal surface separations provides the flow and stress factors.

Figure 2-6 outlines the program schematically. Conservation of mass and momentum are applied for the fluid, for each element in a grid. In the figure, q_x and q_y are the flows through a single control volume element in the x and y directions, respectively, and Δx and Δy are the distances between mesh points, which must be supplied as input. The cyclic boundary condition requires flows leaving the bottom of the flow region to re-enter at the top, thus conserving mass in the system. In the case of a piston ring, which can experience tangential oil flows, this is a more realistic boundary condition than the non-flow boundary condition applied by Patir and Cheng.

Pressure flow and stress factors are obtained by applying a pressure gradient across the system and calculating the resulting flow rate and shear stress. Shear factors are obtained by applying a relative motion to one surface, and calculating the resulting flows and stresses. All of these calculations must be made at a number of different mean film thicknesses, as the factors are functions of oil film thickness (or, more precisely, of the ratio of oil film thickness to surface roughness, h/σ.)

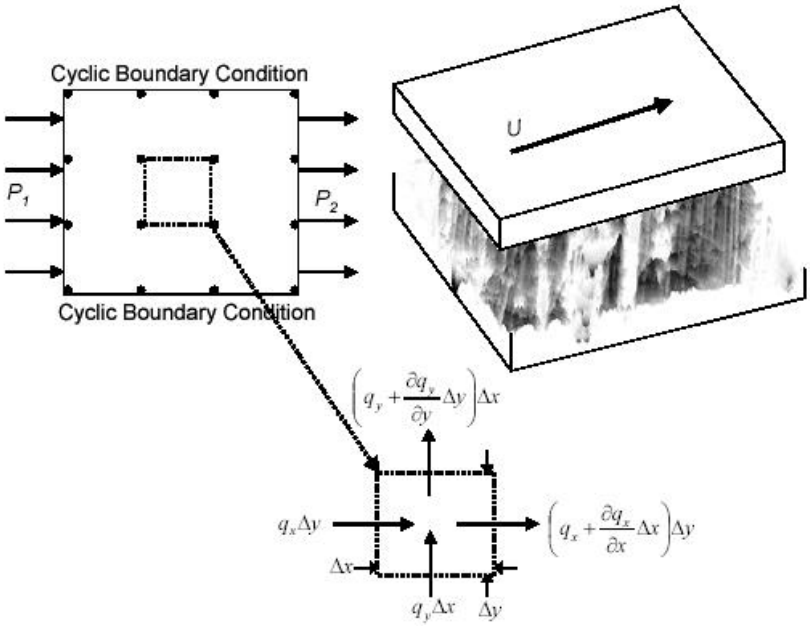

Figure 2-6: Schematic for Li's deterministic fluid flow and stress program

Once the flows and stresses are calculated numerically, the pressure and shear flow and stress factors are calculated by comparing these values to those calculated for smooth surfaces under the same flow conditions, and with the same nominal film thicknesses. The geometric flow and stress factors can be calculated from geometry only, and are defined by:

$$\phi_g = \frac{1}{h}\cdot\frac{1}{m(n-1)}\sum_{i=1}^{n-1}\sum_{j=1}^{m} H_s \tag{2.17}$$

$$\phi_{fg} = \frac{1}{h}\cdot\frac{1}{m(n-1)}\sum_{i=1}^{n-1}\sum_{j=1}^{m} \frac{1}{H_s} \tag{2.18}$$

where ϕ_g is the geometric flow factor, ϕ_{fg} is the geometric stress factor, m and n are the number of nodes in the x and y directions, h is the nominal surface separation, and H_s is the actual surface separation (when contact occurs $H_s = 0$). When there is no contact between the surfaces, both geometric factors are unity, the nominal and mean film thicknesses are equal. When contact occurs, the geometric stress factor, ϕ_{fg}, becomes unbounded and cannot be calculated. In these cases, H_s is set to a minimum height at which a limiting shear stress is assumed to occur. A detailed explanation for this substitution is given in [15].

The other flow and stress factors require input from the Li's numerical simulation for their calculation. With these values, calculation of flow factors proceeds from the definitions of the factors - each is defined as the ratio of actual flow to that which is predicted by a smooth-wall model:

$$\phi_p = \frac{q_p}{\left(\frac{h^3}{12\mu}\frac{\Delta P}{\Delta x}\right)} \tag{2.19}$$

where ϕ_p is the pressure flow factor, q_p is the deterministically calculated flow between the two surfaces due to a pressure gradient, h is the nominal surface separation, μ is the fluid viscosity and $\Delta P/\Delta x$ is the applied pressure gradient;

$$\phi_s = \frac{q_s}{\left(\frac{U \cdot R_q}{2}\right)} \tag{2.20}$$

where ϕ_s is the shear flow factor, q_s is the flow between the two surfaces due to a relative velocity, U is the relative velocity between the surfaces, and R_q is the combined surface roughness (R_q is present in the denominator because it also appears in the averaged Reynolds equation modifying ϕ_s, see. Eqn. 2.8);

$$\phi_{fp} = \frac{\tau_p}{\left(\frac{h}{2}\frac{\Delta P}{\Delta x}\right)} \tag{2.21}$$

where ϕ_{fp} is the pressure stress factor and τ_p is the shear stress in the fluid due to an applied pressure gradient and;

$$\phi_{fs} = \frac{\tau_s}{\left(\frac{\mu U}{h}\right)} \tag{2.22}$$

where ϕ_{fs} is the shear stress factor, and τ_s is the shear stress in the fluid due to a relative motion between the surfaces.

Each of the flow and stress factors are calculated for a number of film thicknesses. Once these values are obtained, a curve-fitted equation is derived for each, which is then used for flow factor calculation in the ring-pack simulation program.

bA number of assumptions are made in the numerical calculation program, and some inherent limitations dictate the manner of program use and the situations to which it can be applied. The size of the rough surface "patch" analyzed must be chosen with care, in order to be both small compared to the actual expected sliding area of ring and liner, and large compared to the surface texturing of interest. This is because the method makes the assumption that the effects of surface texturing can be well-represented by the averaged effect of the combined features, without taking into account the effects of each feature alone. Then, the patch must contain a large enough sample of the pattern of interest to adequately represent all of the features

and evaluate averaged effects. Also, since calculations are made based on sliding between nominally parallel surfaces, the patch must be small compared to the wetted area between ring and liner so that the curvature of the ring does not cause calculation inaccuracies. These requirements necessarily limit the size of surface features and patterns that can be studied using the averaged flow factor method, which must be small compared to the ring/liner wetted area.

Several assumptions are also made in the numerical calculations of fluid flows and stresses. Asperity level cavitation is not taken into account, so that negative pressures do develop in diverging areas. In reality, cavitation is likely to occur when dissolved air leaves solution in the oil, at approximately ambient pressure. While the no-cavitation assumption was also made by Patir and Cheng [24], further investigation of micro-scale cavitation effects is required. Also, realistic deformation of surfaces, upon contact, is not considered. Instead it is assumed that contacting surfaces shear off cleanly, and the removed portions are then no longer part of the calculation. Because the simulation is numeric, and thus based on discrete data points, a method of interpolation is also required. A linear interpolation method is imposed between surface height data points, and a viscous wedge flow solution applied. Further information about this model and its limitations are given in [15].

2.8. Calculating ring/liner friction

The above equations must be solved simultaneously to find the film thickness and wetting locations of the lubricant. Once this has been done (an adjustable step-size iterative algorithm is used), the results can be used to calculate the ring/liner friction (as well as many other parameters). The total ring/liner friction force is the sum of friction due to asperity contact and that due to shear in the lubricant.

The contact friction is assumed to be proportional to the asperity contact pressure, where the proportionality constant used is the boundary friction coefficient, f_b:

$$F_{f,asp} = \int f_b P_{asp} dA \tag{2.23}$$

The hydrodynamic component of friction results from shear stress within the oil, and is derived from Newton's relationship:

$$\tau(x) = \mu \left. \frac{\partial u}{\partial y} \right|_{y=0} \tag{2.24}$$

where μ is the oil viscosity, u is the fluid velocity in the x direction, and the y direction is across the fluid film. Substituting in for u:

$$F_{f,hyd} = \int_{wettedarea} \left(\frac{\mu U}{h} \left(\phi_{fg} + \phi_{fs} \right) - \phi_{fp} \frac{h}{2} \frac{dp}{dx} \right) dA \tag{2.25}$$

The total ring/liner friction force is then given by:

$$F_f = F_{f,asp} + F_{f,hyd} \tag{2.26}$$

This friction force is useful for assessing where, during the engine cycle, friction is generated, and what parameters contribute to friction. For reporting actual friction losses in an engine, however, another measurement is used. The work lost to friction, rather than the friction force, is the important parameter to consider when assessing a low-friction design. This is because this work determines the amount of extra fuel that will be required to overcome friction - the more fuel necessary, the lower the engine efficiency. Friction work is reported as the FMEP, friction mean effective pressure, which is the friction work normalized by engine displacement, and is given by:

$$FMEP = \frac{\int_{cycle} F_f dx}{V_d} \tag{2.27}$$

where V_d is the displaced volume of the cylinder (or of the entire engine, if the friction work evaluated is also for the entire engine).

2.9. Model applicability and limitations

Although it takes into account many of the complexities of the power cylinder system, the ring model used is nevertheless an approximation of reality, and is based on several assumptions that limit its applicability. Some of these are inherent in the averaged Reynolds method itself, while others stem from limitations in the current understanding of related phenomena.

Because it uses an averaged flow factor method, rather than a deterministic fluid analysis, the model used is limited in the surfaces to which it is applicable, as well as in the phenomena it can describe. It is inaccurate at very small film thicknesses (h/σ close to 1 or less) because, when it is continually interrupted by asperity peaks and flow blockages, the fluid flow is more strongly influenced by the actual, deterministic surface features than average effects. Also, textures to be analyzed cannot have features that are too large or "non-smooth." In the former case, the features and pattern under study must be small compared to the ring width, or the assumption that the cumulative effect of the texture features can be well-represented by average factors will be violated. (Details of patch size selection criteria are given in [15].) In the latter case, some textures may violate basic assumptions in development of the Reynolds equation, so that the Reynolds analysis itself may not be applicable for these surfaces.

One of the simplifications made in the development of the Reynolds equation is that, because the oil film is thin, there is no pressure gradient across the film thickness. However, for surface features that are very deep, have non-smooth edges, or otherwise cause too much disruption to a laminar flow, this will not apply. Figure 2-7 illustrates a case in which vortices appear in a deep feature, violating the stated assumption. In other cases sharp edges may cause

turbulence, features may be too close together, or other phenomena may disrupt the assumed flow pattern [26]. When textures of this nature are to be analyzed, a more detailed analytical method should be employed.

Also, in the calculation of the flow and stress factors, it is assumed that the gap between the two surfaces is completely filled with oil. In an actual engine it is likely that the ring/liner clearance will not be entirely filled, especially when surface texturing is present. For example, lubricant may not entirely fill a honing groove, or may be pushed to one side of the groove by pressure from the gases and ring movement, leaving a non-lubricated region. The averaged flow factor analysis does not account for this type of situation.

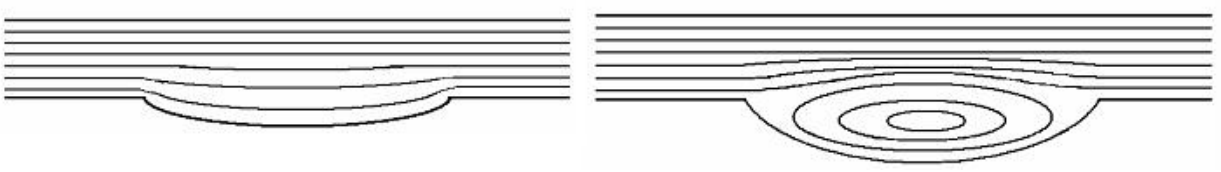

Figure 2-7: The averaged flow factor method is not applicable when surface features are too disruptive

Another limitation of the averaged method lies in its lack of ability to account for non-averaged phenomena. The averaged flow-factor analysis cannot describe many details of the flow and contact between ring and liner that may be of great importance in the actual ring/liner system. For example, flow of lubricant along honing grooves may play a major role in lubricant transport and friction, but this phenomenon cannot be modeled with the averaged method. Again, when phenomena of this nature is of interest, a more detailed, deterministic method is required.

In addition to some inherent limitations in the ring lubrication model itself, a limited understanding of related phenomena has lead to some simplifications. Oil transport is a very complicated phenomenon, and all of the mechanisms that affect it are currently not understood. Thus, the oil transport model used in the ring-pack analysis is necessarily simplified. In all of the analyses discussed, it is assumed that ample lubricant is available to the oil control ring, as well as to the second ring on down-strokes. Transport of oil into the "dry region" of the liner is not well-understood and the results shown should be considered to be preliminary. Also, all results shown are calculated on the pin side of the piston, and effects of piston rotation and secondary motion are not considered. Although it is possible to consider piston secondary motion with the current ring-pack model, the added complication of including this effect may have impeded clear understanding of the parameters under study, and so it was not included.

3. Effects of Engine Operating Conditions on Piston-Ring Friction

3.1. Modern Internal Combustion Engine Operating Conditions

Modern internal combustion engines operate in a variety of speed and load conditions depending on their application. In passenger cars and larger transport trucks, loads and speeds vary considerably due to the variety of driving conditions encountered. Racing engines typically operate at high speeds and high loads. Stationary power generation engines operate in high load, low speed conditions because the high load generates more power and the low speed is needed to interface with the electric generator and the power grid.

Both engine speed and load affect the friction generated between the piston rings and the liner. In addition, oil supply plays a very important role in ring-liner lubrication. In the sections that follow, these effects are analyzed separately and general trends are then developed for the dominant contributors to piston ring friction in the different engine operating conditions.

3.2. Effect of Engine Speed

The effect of engine speed on the friction generated between the piston rings and the liner can be seen from the relations developed in Section 2 and Appendix A. In Eq. (A.5), the second term involving the pressure gradient integrated over the wetted width typically ends up resulting in a much smaller contribution than the first term. Therefore, friction scales roughly as follows:

$$F_f \sim \frac{\mu U}{h} B \tag{3.1}$$

where h is the oil film thickness and B is the ring axial width. The minimum oil film thickness can be related to the piston velocity through the following scaling relationship:

$$h \sim \sqrt{\frac{\mu U B}{p}} \tag{3.2}$$

where p is the pressure in the oil film, which is assumed to be a sole function of x as shown in [2]. Combining Eq. (3.1) and Eq. (3.2), it can be seen that the friction power loss scales with piston speed as follows:

$$P_f \sim \mu^{1/2} U^{3/2} \tag{3.3}$$

The viscosity term is included in this relationship because it depends on the piston speed. The extent of this dependence varies according to the type of oil under consideration. In the case of multigrade oils, which are considered to be shear-thinning fluids, the viscosity is controlled by the shear rate, which depends directly on the piston speed, as explained in Appendix A. As piston speed increases, the viscosity will decrease, and therefore the net effect of these changes on friction power loss is the result of a compromise between them.

For a single grade oil, the viscosity of the oil depends only on its temperature, which is controlled primarily by the temperature distribution along the liner. As piston speed increases, the liner temperature may increase, causing a reduction in lubricant viscosity. Therefore, for the case of single grade oils, friction power losses only increase with higher engine speeds if the reduction in lubricant viscosity does not offset the increase in piston speed.

It should be noted that Eq. (3.3) is only valid for hydrodynamic or mixed lubrication. The dependence of friction power loss on piston velocity would be linear for pure boundary lubrication conditions.

It should also be noted that for a given set of engine geometric parameters (crank radius, connecting rod length, etc.), the piston speed is directly related to the rotational speed of the crankshaft [27]. Therefore, the piston speed can also be replaced by the rotational speed of the engine crankshaft in Eq. (3.3). This modified form of Eq. (3.3) will be used later in this Section.

3.3. Effect of Engine Load

The effect of engine load on friction is less straightforward. In order to maintain constant engine speed when the load on the engine increases, the amount of air and fuel brought into the cylinder to be compressed and burned during combustion must be increased. As a result, higher peak pressures are reached in the cylinder.

The friction generated by the piston rings is significantly affected by the pressures attained in the cylinder throughout the engine cycle. The cylinder pressure controls the land pressures, which affect the ring dynamics and therefore the lubrication conditions encountered by the rings throughout the engine cycle. Although in general, the contribution of friction as a percentage of the engine's indicated power output reduces as load increases, major changes in load may result in a change in the type of piston ring-liner friction that dominates in different parts of the cycle. This is best illustrated through the use of an example, which is described in the following section.

3.4. Illustration of Effect of Speed and Load on Piston Ring Friction

To illustrate the effect of speed and load on friction, the friction model introduced in Section 2 was used to analyze the piston ring friction generated throughout the cycle in a Waukesha natural gas power generation engine for different operating conditions. More detailed specifications for the engine are provided in a later section. Since it is used in power generation applications, it is designed for low speed, high load operation (1800 rpm and 200 psi BMEP). The results in this section were all obtained assuming the maximum oil supply condition (OS1).

Figure 3-1 shows the friction power losses of each of the piston rings throughout the engine cycle at the standard low speed, high load operating condition. It can be seen from the figure that the highest contributors to friction in the engine cycle are the top ring around top dead center (TDC) of compression/expansion and the oil control ring throughout the engine cycle.

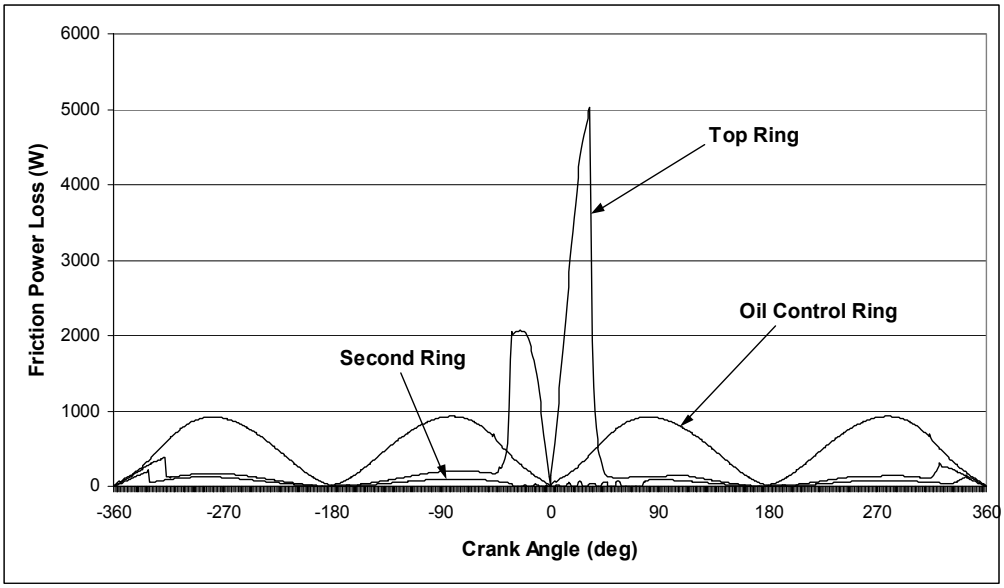

Figure 3-1: Friction Power Loss Contributions in the Piston Ring Pack

This is confirmed in Figure 3-2, which shows the FMEP contributions of each of the piston rings. The determination of FMEP from friction power losses is derived in Appendix B. This figure also shows the FMEP contributions from each of the rings from boundary lubrication. It is clear that most of the top ring friction comes from boundary lubrication in the part of the cycle around TDC of the compression/expansion strokes.

To demonstrate the effect of varying engine load, a different set of cylinder pressure data was used as an input into the friction model. This pressure data was taken from another engine, but nevertheless it can still be used to illustrate the effect of decreasing engine load on friction. The peak pressure is approximately 20 bars for this case compared to a value of 80 bars at the standard operating condition. Figure 3-3 shows the friction power losses of each of the piston rings throughout the engine cycle, and Figure 3-4 shows the FMEP contributions of each of the rings. By comparing these figures with the earlier results for the higher load conditions, the effect of reducing engine load on friction can immediately be seen. In this case, the contribution of the top ring friction generated near TDC of compression/expansion is reduced and the portion of top ring friction coming from boundary lubrication conditions is lower as well, indicating a higher overall contribution from top ring friction generated at midstroke. The main contributor to friction in the low load case is clearly the oil control ring.

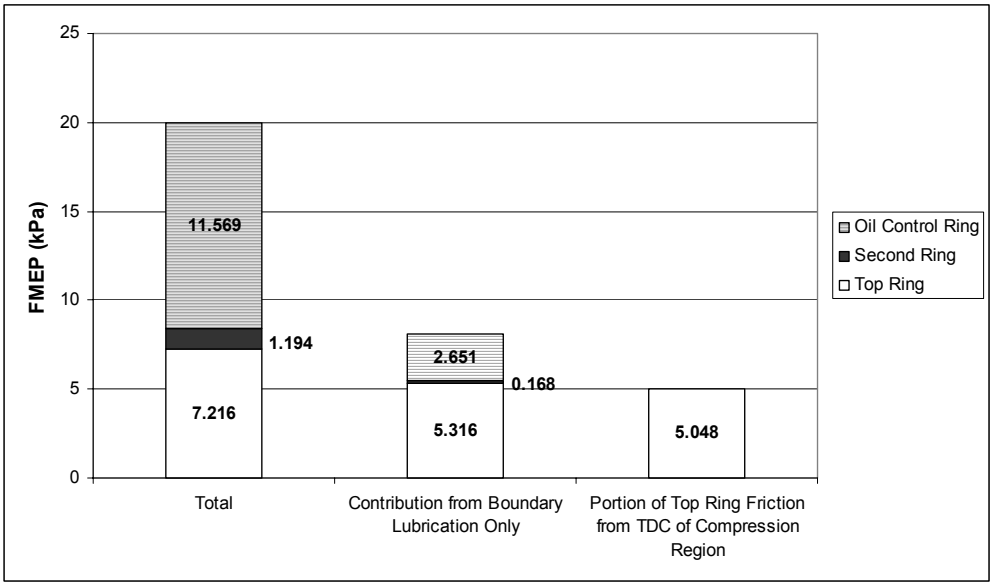

Figure 3-2: FMEP Contributions in the Piston Ring Pack

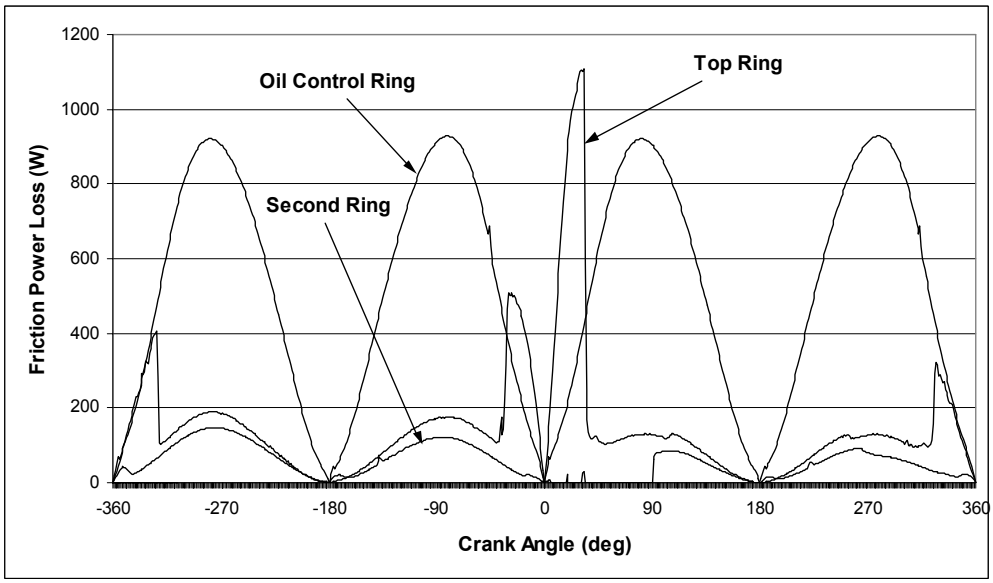

Figure 3-3: Friction Power Loss Contributions of the Ring Pack at Lower Load Condition

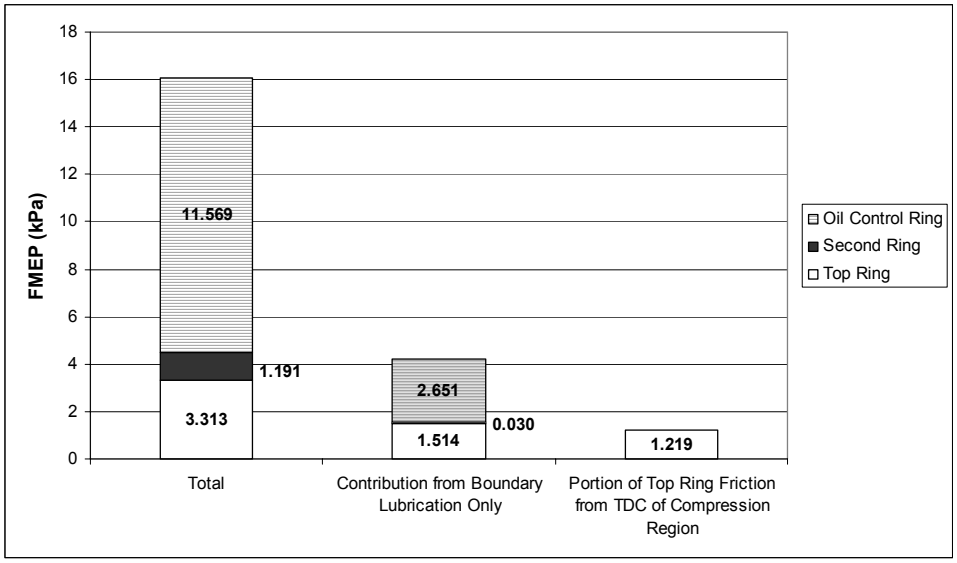

Figure 3-4: FMEP Contributions of the Ring Pack at Lower Load Condition

To illustrate the effect of engine speed, results were obtained for an engine speed of 3000 rpm for the same cylinder pressure data used to generate the low load, low speed case. It should be noted that the increased engine speed may have an effect on the liner temperature distribution and therefore on the lubricant viscosity. Justification for neglecting this effect can be provided using the Waukesha engine data for this specific case. According to Eq. (3.3), for an increase in engine speed from 1800 to 3000 rpm to be offset by a change in oil viscosity, the viscosity would need to be reduced by a factor of approximately 4.5. According to the Vogel Equation, which is used by the model to determine the viscosity of the oil at a specific temperature along the liner, the change in temperature that would be required to achieve a reduction in viscosity by a factor of 4.5 would be between 50 and 100°C, depending on the point in the engine cycle under consideration [2]. Such a change in liner temperature could not feasibly result from this change in engine speed. Therefore, the effect of the change in viscosity can be neglected in this case. This analysis also shows that in general, for the purpose of comparing the main contributors to friction between a low speed and a high speed case, the effect of the change in viscosity can safely be neglected.

With this in mind, the friction power losses of the piston ring pack and the FMEP contributions are plotted again in Figure 3-5 and Figure 3-6, respectively, for the high speed case.

In this case, the contribution of the top ring friction from boundary lubrication around TDC of compression/expansion is reduced even more compared to the low load, low speed case, although this difference would be less significant if the higher cylinder pressure data corresponding to the higher speed were used. Still, for this case, the portion of the total top ring friction from hydrodynamic lubrication conditions during the midstroke region of the engine

cycle is larger. This result is expected because of the stronger dependence of friction power losses on engine speed in hydrodynamic lubrication conditions compared to boundary lubrication conditions. It can also be seen from these results that friction from the oil control ring is the most significant contributor to piston ring pack friction in the low load case.

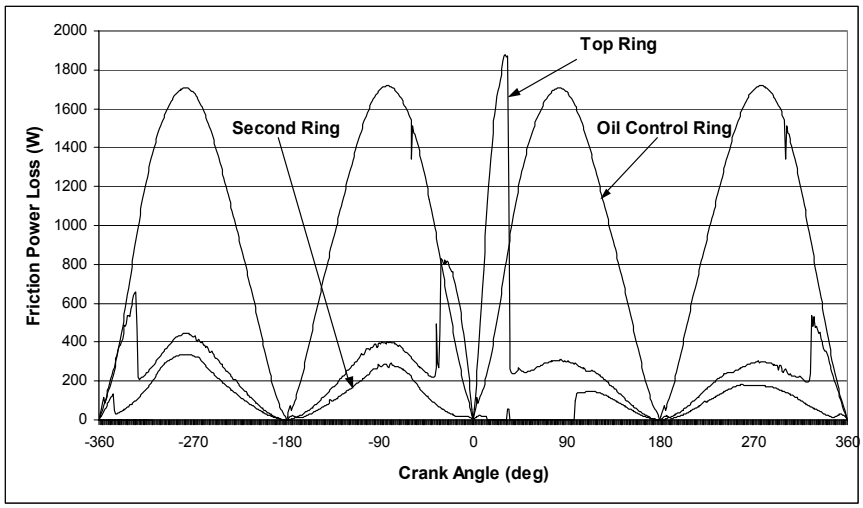

Figure 3-5: Friction Power Losses in the Piston Ring Pack at Low Load, High Speed

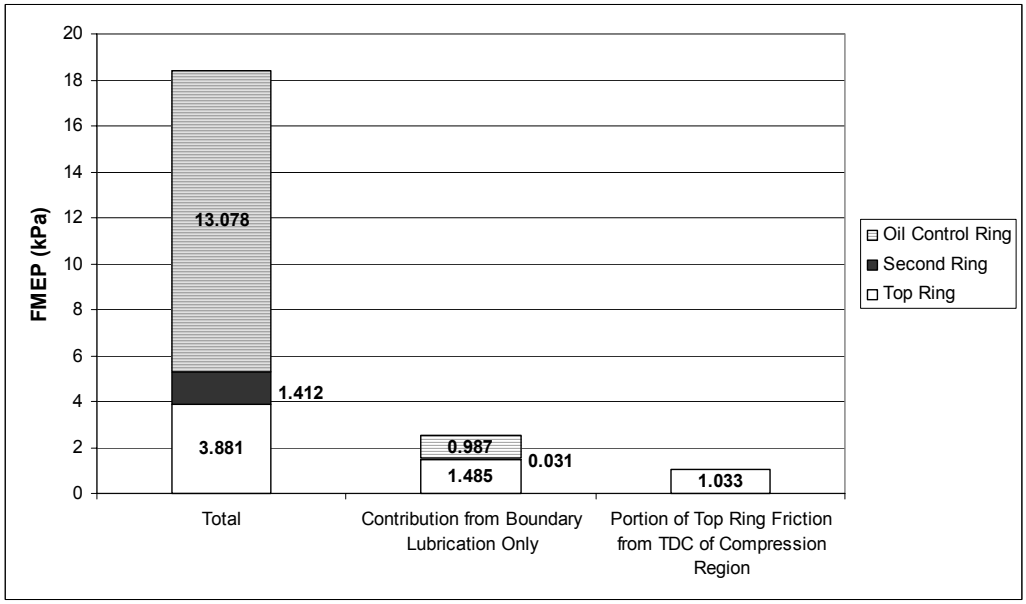

Figure 3-6: FMEP Contributions in the Ring Pack at Low Load, High Speed

The scaling relationship between friction power loss and speed can also be seen from these results. Comparing Figure 3-5 and Figure 3-6, around TDC of compression/expansion, the ratio of top ring friction power loss for the high speed case to the low speed case is about 1900/1100=1.7, which is roughly the same as the ratio of the engine speed, 3000/1800=1.7. This was expected for pure boundary lubrication conditions. In the midstroke region, the ratio of peak top ring friction power losses during the intake stroke is roughly 443/200=2.2, which is approximately equal to the engine speed ratio as defined in Eq. (3.3), namely (3000/1800)3/2=2.2.

3.5. Effect of Oil Supply on Piston Ring Friction

The amount of oil supplied to the different piston rings throughout the engine cycle has a significant effect on the friction and lubrication conditions between the rings and the liner. In Section 2, the approach used to model oil supply in this study was described. This involved evaluating each of the reduced friction designs at both a maximum (OS1) and minimum (OS2) oil supply condition, since the exact oil supply rate is unknown. In the previous section, all of the results were obtained assuming the maximum oil supply condition (OS1). It turns out that for all of the speed and load conditions that were investigated in the previous section, the results are quite similar for the OS2 case. The main difference is that the top ring contributes more significantly to friction in all speed and load conditions because of the reduced oil supply. Previous studies conducted using the friction model have shown that the top ring typically encounters boundary lubrication conditions throughout a considerable portion of the engine cycle for the minimum oil supply condition [28].

It was also briefly noted in Section 2 that the amount of oil on the liner in the region above TDC of the oil control ring was set to zero in the first cycle of the calculation. This is because the oil control ring can never travel above its own TDC position, and there is thus no direct oil supply to the upper rings between TDC of the oil control ring and TDC of the top ring. As a result, the only source of oil to this part of the liner is what is brought into this region by the top ring or the second ring in subsequent cycles. There is therefore much less oil supply to this section of the liner, and it is thus hereafter as the 'dry region.' The dry region is illustrated in Figure 3-7 below.

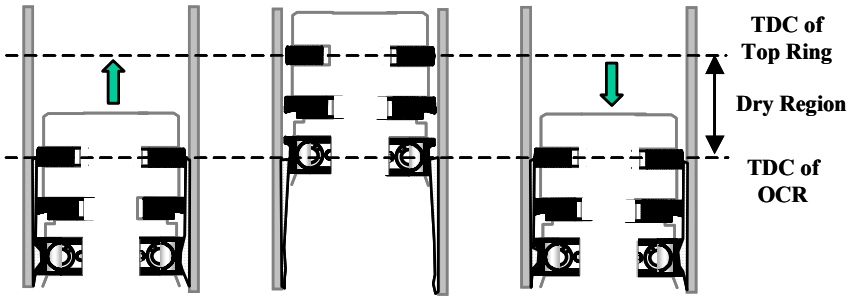

Figure 3-7: Illustration of the Dry Region

It may be possible to bring oil into this region in certain circumstances. The effect of the presence of oil in the dry region during the first engine cycle should be investigated in order to understand the implications of the assumption of zero initial oil film thickness along the liner in this region, since it was used throughout this study. In the remainder of this section, the impact of the initial oil film thickness on the evolution of the lubrication conditions in the dry region will be discussed, and the effect of the oil film thickness in this region on friction will be identified.

Figure 3-8 shows the evolution of the lubrication conditions in the dry region for the case where no oil is initially assumed to be present. Figure 3-8 a), b), and c) show the oil film thickness on the liner before (light black line) and after (dark black line) passage of the top ring during the first, second, and third cycles, respectively. As can be seen from these plots, there is no oil in the dry region, which extends from roughly 40 degrees before to 40 degrees after top dead center (TDC is located at 0 degrees in these plots). However, there is a slight difference between the exact amounts of oil brought into this region by the top ring in the compression stroke and brought out during the expansion stroke. This can be seen by comparing Figure 3-8 a) and Figure 3-8 b). In Figure 3-8 a), the liner oil film thickness before passage of the top ring is slightly smaller than the film thickness left behind by the top ring as the top ring enters the dry region during the compression stroke. Then, on the expansion stroke, the liner oil film thickness is unchanged after the passage of the top ring, and therefore, the additional oil that was brought into the region during the compression stroke remains on the liner for the next cycle. In Figure 3-8 b), during the second cycle, the location of the nonzero oil film thickness is advanced from 33 to 31 degrees before TDC. Similarly, the nonzero oil film thickness location is advanced from 31 to 30 degrees before TDC between the second and the third cycle. After 4 cycles, there is no further advancement of the nonzero oil film thickness, and the dry region is therefore fully evolved. It can be concluded from this analysis that if zero oil film thickness is initially assumed to be present in the dry region, it is unlikely that this region will become wetted during any subsequent engine cycle.

For comparison, model predictions were also obtained assuming that the oil film thickness in the dry region was initially 1 micron. Figure 3-9 a), b), and c) show the liner oil film thickness before (light black line) and after (dark black line) passage of the top ring for the third, fourth and fifth cycles, respectively. Figure 3-9 a) shows that in the third cycle, oil is available in the dry region until about 5 degrees before TDC, at which point oil starts to accumulate under the top ring and no oil is left behind on the liner. Just before this occurs, between 10 and 5 degrees before TDC, a larger oil film thickness is left on the liner after passage of the top ring than before, and the top ring is clearly releasing some of the oil that was accumulated in the earlier part of the stroke. Then, after passing TDC, on the expansion stroke, the liner oil film thickness before and after passage of the top ring is the same, which indicates that the top ring does not carry out the oil that was brought into this region. As a result, in the fourth cycle, as shown in Figure 3-9 b), a much larger oil film thickness is available to the top ring before it reaches TDC compared to the third cycle. The top ring releases some of its accumulated oil just before TDC, but this time, it carries out all of the oil from in this region to the other parts of the cycle, as indicated by the zero oil film thickness after passage of the top ring during the

expansion stroke. In the fifth cycle, as shown in Figure 3-9 c), the top ring is able to bring some oil into the dry region, much like the case in the third cycle. In fact, the fifth and third cycles are almost identical. This is also true for all of the subsequent even cycles. It can thus be concluded from this analysis that if nonzero oil film thickness is initially assumed to be present in the dry region, a balance is eventually reached in which the amount of oil brought into the dry region in odd cycles is balanced by the amount of oil brought out during even cycles.

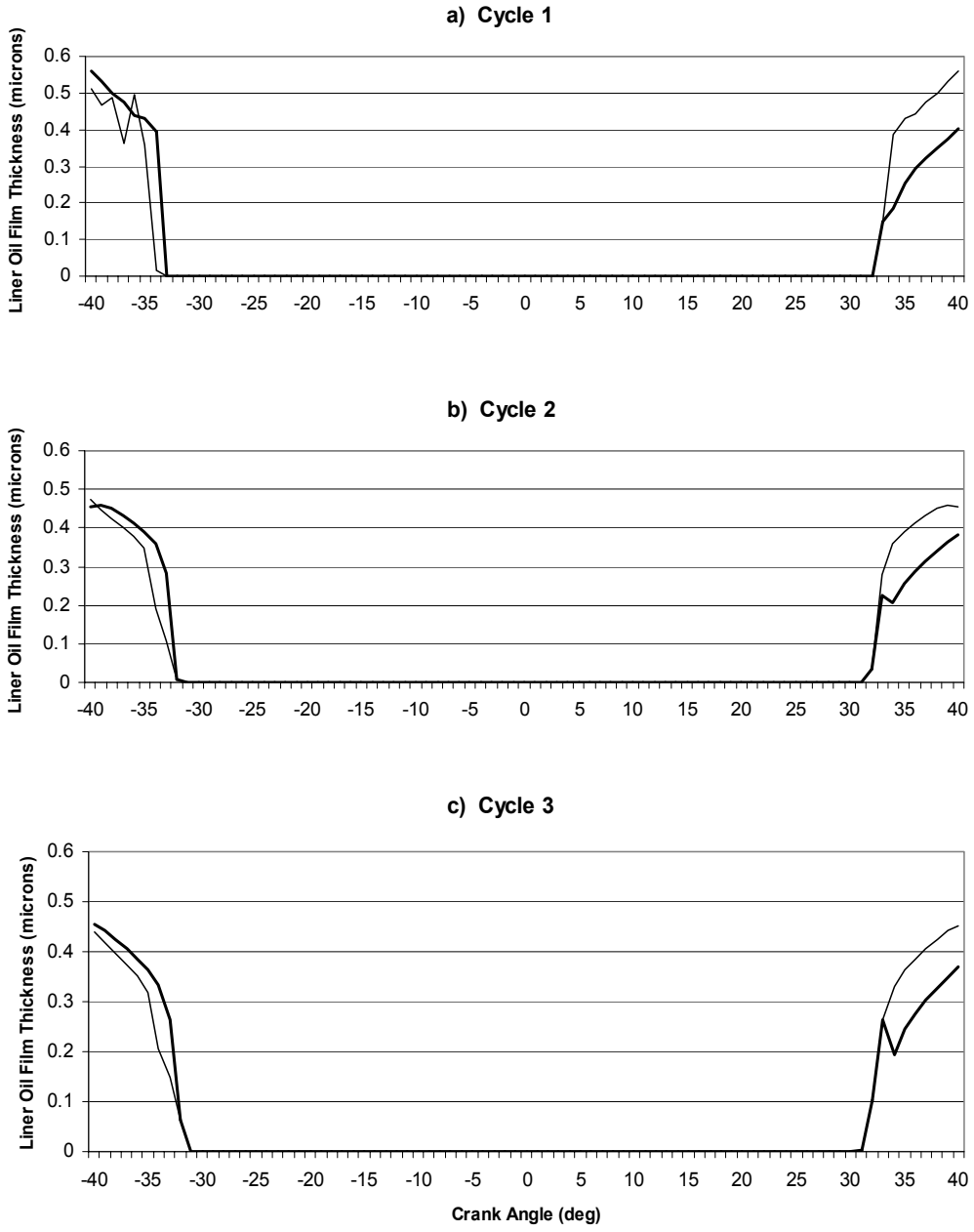

Figure 3-8: Evolution of the Dry Region

The effect of the oil film thickness in the dry region on friction is the most relevant issue in this study. For the cases in which zero initial oil film thickness was assumed in the dry region, the model predictions indicated that the top ring was in pure boundary lubrication near TDC of the compression/expansion strokes, and that this contributed to high friction power losses. If oil could be brought into the dry region, then the top ring would no longer be in pure boundary lubrication, and the friction generated due to boundary contact would be reduced. Figure 3-10 and Figure 3-11 below show the friction power loss and FMEP contributions, respectively, for the case where initial oil film thickness in the dry region is assumed to be 1 micron. As can be seen from the figures, the main contributors to friction are still the top ring and the oil control ring, but the relative contribution of the oil control ring is larger. The lower FMEP contribution from the top ring around TDC of compression/expansion is a result of the larger portion of the overall radial load acting on the back of the ring being supported by hydrodynamic pressure. Since hydrodynamic friction is typically much smaller than boundary friction, if a greater portion of the load is sustained by hydrodynamic lubrication, the overall friction losses are reduced.

More detailed studies with the friction model in the past have indicated that it is difficult to bring oil into the dry region on the pin side of the piston [28]. It was also shown in these studies that if piston tilt is sufficiently large, the top ring can bring oil into the dry region on the minor thrust side of the piston, due to the large oil film thickness that is untouched by the rings on the intake stroke which becomes available just before the top ring enters the dry region on the compression stroke. Significant bore distortion, leading to poor conformability of the oil control ring and the second ring, was also identified as a possible method by which oil could become available to be brought into the dry region [28].

It is therefore unlikely that any significant amount of oil exists in the dry region on the pin side of the piston. Therefore, for the remainder of this study, model predictions were obtained assuming that the oil film thickness in the dry region is initially zero. The implications of this assumption will be mentioned where appropriate.

3.6. Summary of the Effects of Engine Operating Conditions on Ring Friction

Table 3-1 below identifies the main contributors to friction in different engine operating conditions.

It should be noted that this table is only valid for engines using single grade oil. As was pointed out in Section 3.2, for multigrade oil, the engine speed has a strong dependence on the viscosity of the lubricant, and therefore it is difficult to draw conclusions about the main contributors to friction in this case.

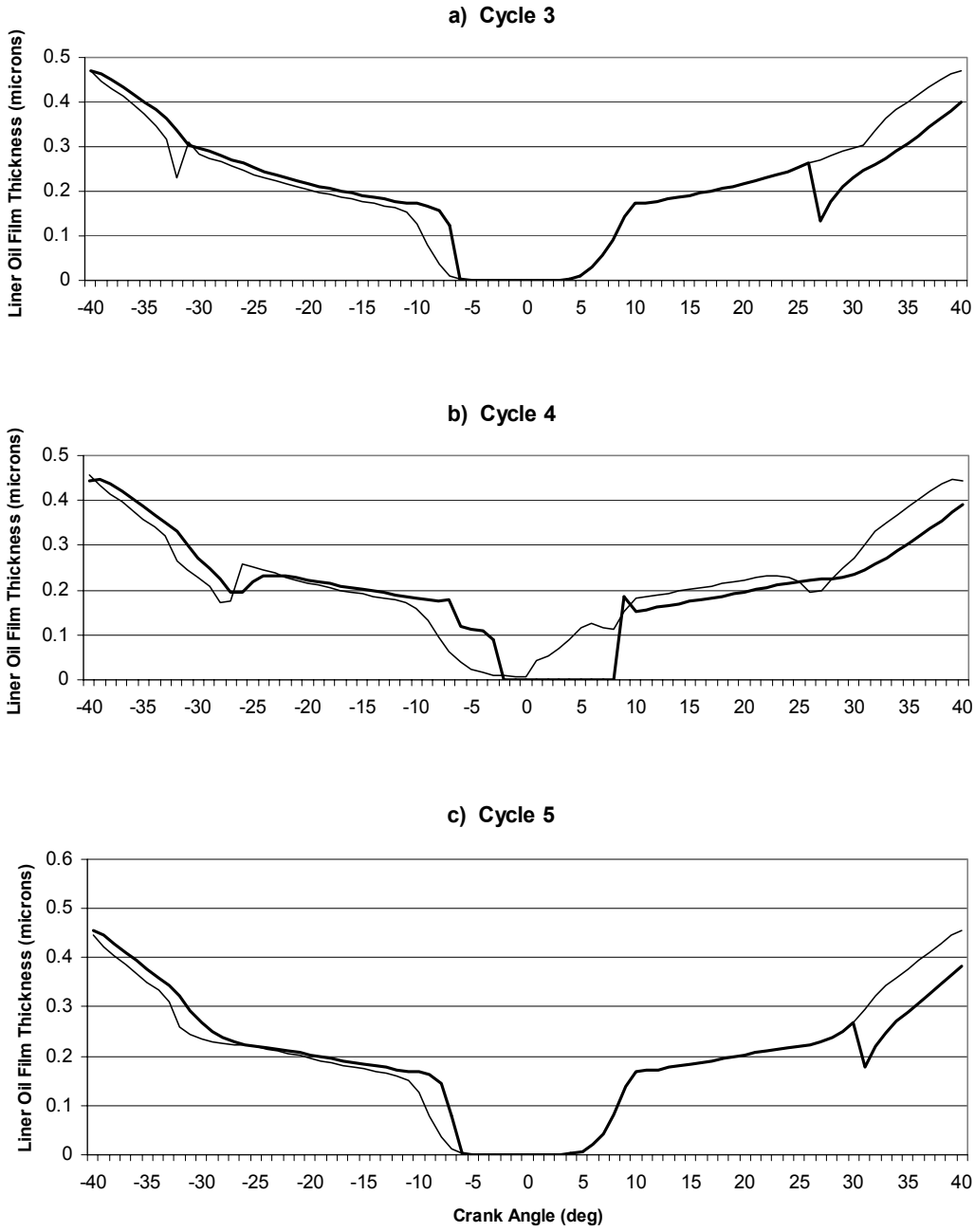

Figure 3-9: Evolution of the Dry Region with Nonzero Initial Oil Film Thickness

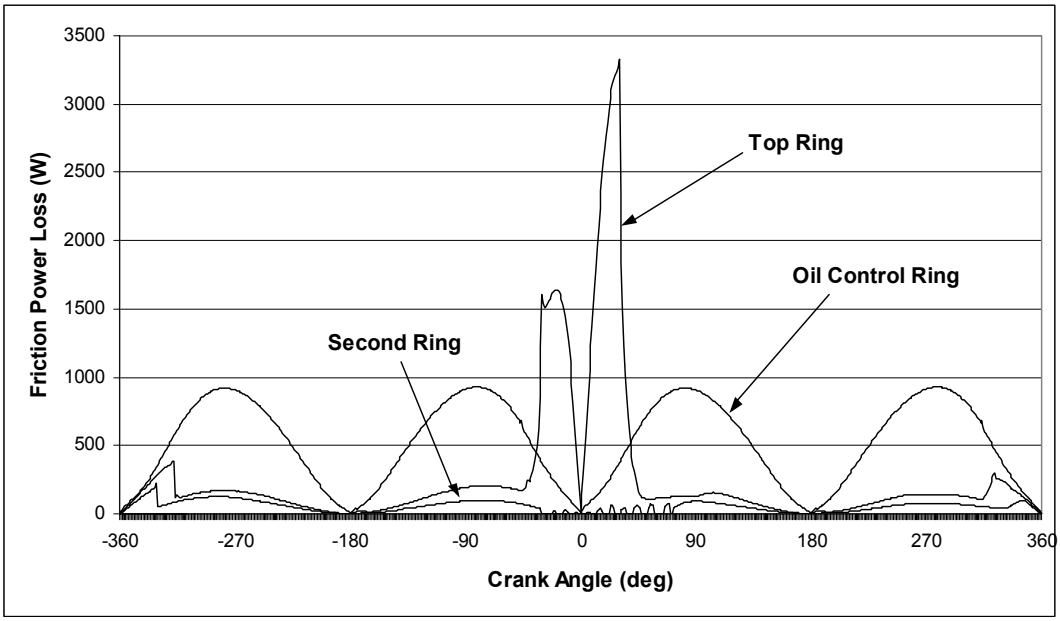

Figure 3-10: Friction Power Losses in Dry Region with Nonzero Initial Oil Film Thickness

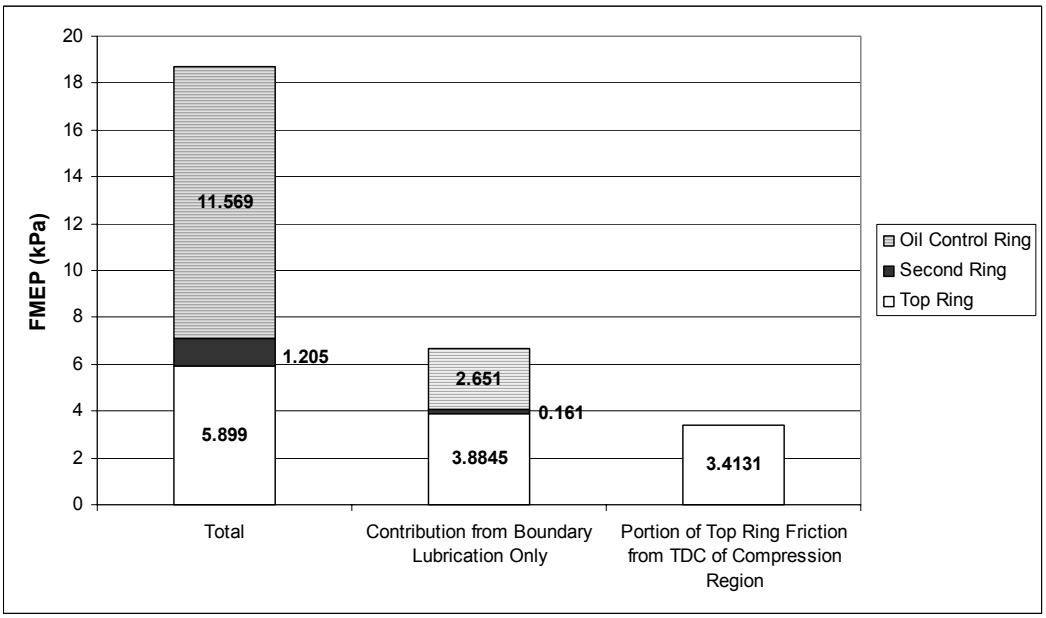

Figure 3-11: FMEP Contributions in Dry Region with Nonzero Initial Oil Film Thickness

Table 3-1: Summary of Main Contributors to Friction for Different Engine Operating Conditions

		Increasing contribution from top ring boundary friction around TDC of compression →	
		Low load	High load
Boundary friction power loss increasing as U ↓ Hydrodynamic friction power loss increasing as $\mu^{1/2}U^{3/2}$	Low speed	-Oil control ring throughout engine cycle	-Oil control ring throughout engine cycle -Top ring around TDC of compression/expansion
	High speed	-Oil control ring throughout engine cycle	-Oil control ring throughout engine cycle -Top ring around TDC of compression/expansion

The next section discusses the development of friction reduction strategies for high load, low speed engines using single grade oil because in this case, high pressures are generated and severe lubrication conditions are present due to the effect of engine speed on oil film thickness. It was therefore the most interesting case to consider in order to study friction and oil transport. In addition, since both the top ring near TDC of compression and the oil control ring throughout the engine cycle contribute most significantly to friction power losses at this speed and load, the same strategies developed to reduce friction in this case could be applied to reduce oil control ring friction in the lower load condition.

For high load, low speed operating conditions, the largest contributors to friction were identified as the top ring around TDC of compression and the oil control ring throughout the engine cycle. In the sections that follow, physical explanations for each of these high contributions are provided.

3.7. Physical Insight on Friction in High Load, Low Speed Engines

3.7.1. Top Ring Contribution around TDC of Compression

The high friction generated by the top ring in the region around TDC of compression is a result of the combination of poor oil supply to the top ring in the dry region, and high pressure generated in the cylinder by compression and combustion. In high load operating conditions, high peak pressures are generated in the cylinder by compression and combustion. As the pressure in the cylinder rises during the compression stroke, the top ring gradually conforms to the lower groove flank, as shown in Figure 3-12 below. No oil is depicted between the top ring and the liner in this figure in order to reflect the poor oil supply to this region, which was discussed in Section 3.5.

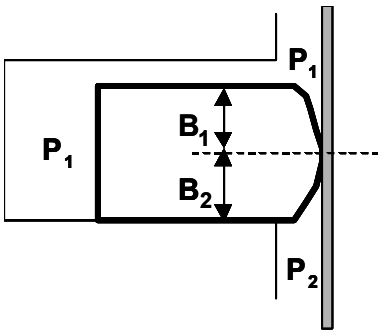

Figure 3-12: Illustration of the Top Ring near TDC of Compression

If no oil is assumed to exist between the ring and the liner in this region around TDC of compression/expansion, and the top ring is assumed to conform well to the lower groove flank, the friction force acting on the top ring is from pure boundary lubrication conditions and can thus be estimated as the product of the radial load acting on the back of the ring and the coefficient of friction:

$$F_f = a_{asp}\left[(p_1 - p_2)B_2 + W\right] \qquad (3.4)$$

where aasp is the coefficient of friction between the ring and the liner, and W is the ring load due to tension.

The power loss due to friction is the product of the friction force in Eq. (3.4) and the piston speed at that instant. Although the piston speed is small near TDC, the friction force is very high and therefore the product of friction and piston speed is large, as was shown in Figure 3-1 for the Waukesha natural gas engine. Significant top ring friction power losses occur in this region of

the engine cycle as a result. This effect would be even more significant in larger diesel engines, where the peak cylinder pressure can reach 200 bars.

3.7.2. Oil Control Ring Contribution throughout Engine Cycle

The high friction generated by the oil control ring throughout the engine cycle is a result of its high tension. Here, the tension is generated by the ring's own elasticity, and is thus equivalent to the amount of force required to close the ring gap in order to fit the ring inside the cylinder bore. As explained in Section 1, the principal function of the oil control ring is to regulate the amount of oil that reaches the upper rings. As a result, the high tension is necessary in order to promote conformability of the oil control ring to the bore. Good conformability is difficult to achieve in practice because of the non-uniform distortion of the cylinder bore due to mechanical deformation and thermal gradients. As a result, the best way in which to ensure adequate conformability of the oil control ring to the bore is by designing the oil control ring with a high tension.

The high tension force acting on the small lands of the oil control ring results in a high unit pressure exerted on the oil film under the lands. This idea is illustrated in below in Figure 3-13.

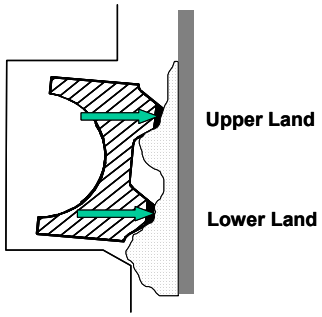

Figure 3-13: Illustration of Effect of Oil Control Ring Tension on Oil Film Thickness

As a result, the oil film thickness that passes under the oil control ring is reduced and adequate oil control is achieved in this way. This can be seen by consideration of the radial force balance in Eq. (2.3). Assuming that the land pressures around the oil control ring are equal and close to atmospheric pressure, they can be neglected in this analysis. Therefore, the force due to ring tension is balanced by the pressure generated in the oil film:

$$W = \int_0^B p dx \qquad (3.5)$$

Here, for simplicity, the oil control ring is assumed to be fully-flooded with oil, and therefore the pressure developed in the oil film is related to the load due to tension through the following scaling relationship:

$$p \sim \frac{W}{B} \tag{3.6}$$

Now, scaling the Reynolds' equation yields the relationship between the pressure developed in the oil film and the film height:

$$h \sim \sqrt{\frac{\mu UB}{p}} \tag{3.7}$$

Eq. (3.6) shows that a high ring load due to tension results in higher pressure developing in the oil film, which reduces the film thickness according to Eq. (3.7). The reduced film thickness leads to higher friction between the ring and the liner according to Eq. (3.1).

If no oil were to exist between the oil control ring and the liner, the high tension force would result in more severe asperity contact pressure which would result in higher friction.

Therefore, regardless of the amount of lubrication under the oil control ring, the high tension generates high friction between this ring and the liner. In the Section that follows, several design strategies will be developed to reduce the friction generated by both the oil control ring and the top ring along the liner.

4. Effects of Piston-Ring Design in Friction Reduction Strategies

The following Section contains a description of recommended strategies to reduce the friction generated by the main contributors identified in Section 3. The relative friction reduction potential of each design strategy is investigated using the modeling tools described in Section 2. Adverse effects that may result from implementation of the designs are discussed, and additional designs to minimize these adverse effects are developed and recommended.

4.1. Top Ring

An equation describing the friction generated by the top ring along the liner in the region near TDC of compression was given in the previous Section (Eq. (3.4)). Due to the high pressures generated near TDC of compression, the pressure term typically exceeds the ring load due to tension by at least an order of magnitude. Therefore, designs to reduce friction should be focused on reducing the contribution from the pressure difference acting on the lower part of the top ring. Since the pressure difference is controlled by the compression and combustion process, which will not be changed in this study, the most effective way to reduce top ring friction in this region is by reducing the area exposed to the high pressure difference (B2 in Figure 3-12).

At this point, it should be noted that this design strategy was developed assuming that there is no oil in the dry region. Pure boundary lubrication conditions were indeed predicted to be

present in the dry region by the model, as was discussed in Section 3.5. However, it was also pointed out in this section that in certain circumstances, oil can be brought into the dry region and mixed lubrication may be achieved. If this were the case, the suggested design strategy of reducing B2 would still reduce friction, but it would be slightly less effective because in mixed lubrication conditions, the portion of the net radial load supported by the oil film is much greater than the portion supported by asperity contact. The reduction in B2 would still reduce boundary friction by reducing the net radial load, but since the part of the load supported by hydrodynamic pressure is generally larger than that supported by asperity contact, the strategy would be less effective at reducing friction overall if oil were present in the dry region.

There are several practical ways in which the reduction of B2 can be accomplished, and they are described in the sections that follow.

4.1.1. Skewed Barrel Profile

The top ring can be manufactured such that the physical length of the region below the minimum point is reduced. This is generally referred to as a skewed barrel profile design. Such a design clearly reduces the area over which the high pressure difference acts, which reduces the friction generated between the top ring and the liner in this region. This design was investigated in some of the previous studies described in Section 1, and a reduction in friction was observed by its implementation [29,30]. The design is illustrated below in Figure 4-1, where it is compared to a symmetric barrel profile.

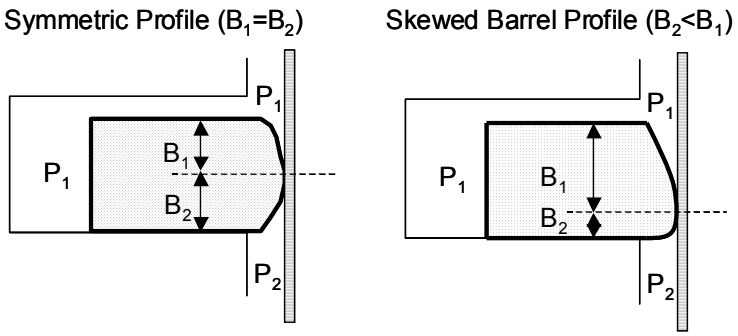

Figure 4-1: Illustration of Skewed Barrel Profile Design

4.1.2. Top Ring Groove Upward Tilt

The high pressures generated in the cylinder due to compression and combustion force the top ring to conform well to the lower groove flank around TDC of compression. As a result, if an upward groove tilt angle were introduced in the top ring groove, the point on the ring that is closest to the liner (the minimum point) would move down along the profile if the top ring were to conform to the upward tilted groove around TDC of compression. This idea is illustrated below in Figure 4-2. As would be the case for the skewed barrel profile design, this design

would result in a reduction of area over which the high radial pressure difference acts, and would therefore reduce friction.

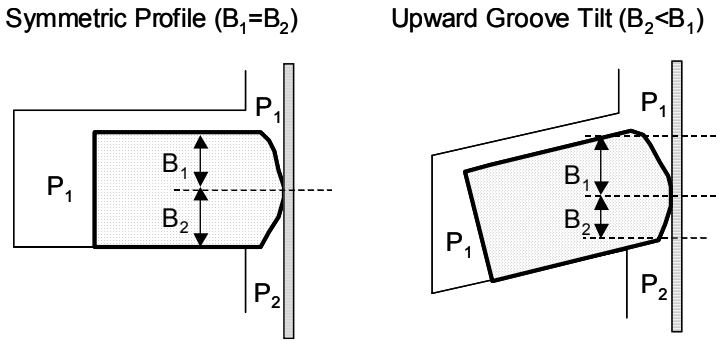

Figure 4-2: Illustration of Top Ring Upward Groove Tilt Design

4.1.3. Reduced Top Ring Axial Height

One other method by which to reduce the area over which the high radial pressure difference acts around TDC of compression would be to reduce the overall axial height of the top ring. This would reduce both B1 and B2, and since the high pressure difference acts over B2, friction could be reduced using this design. This idea is illustrated below in Figure 4-3.

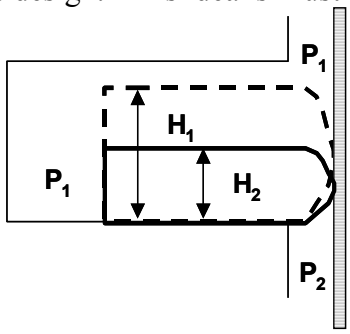

Figure 4-3: Illustration of Reduced Axial Height Design

4.2. Oil Control Ring

4.2.1. Reduced Tension Oil Control Ring

Since the friction generated by the oil control ring is a result of its high tension, the best way in which to reduce oil control ring friction would be to reduce the ring tension. This would almost certainly be accompanied by an increase in oil consumption due to poorer conformability. This will be discussed in more detail in the following section, and designs will be recommended to compensate for this adverse effect.

4.3. Adverse Effects of Reduced Friction Designs

4.3.1. Reduced Ring Life

Reduced ring life was reported in previous studies that were conducted on reduced axial height rings. In particular, Hill and Newman identified reduced axial height as causing reductions in axial stiffness [10]. Based on their experimental results, they concluded that compression rings should be at least 1.5 mm in axial height. Failures were observed and the tests had to be terminated after 50 hours when rings whose axial heights were below this value were used in their study.

4.3.2. Increased Top Ring Groove Wear

One of the adverse effects of the upward top ring groove tilt design is that it can result in increased top ring groove wear. When the cylinder pressure rises sufficiently to push the top ring downward to conform to the groove, concentrated contact is first made at the outer diameter (OD) corner of the lower groove flank because of the upward tilt angle. This effect is illustrated in Figure 4-4 below, in which the contact pressure distribution between the ring and the lower groove flank is compared between the baseline design with no upward groove tilt and the upward groove tilt design. The graph shows the contact pressure distribution between 100 degrees before TDC and 100 degrees after TDC since this is the region of interest in the engine cycle. As can be seen in the graph, fairly uniform contact pressure distribution is achieved from ID to OD in the baseline design, although there is a slight increase in the contact pressure at the OD corner for this design. This is because the high pressure above the top ring in the area between the groove edge and the liner can cause the ring to rotate around the OD corner by a small amount close to TDC of compression. The upward groove tilt design therefore results in a large concentrated contact pressure at the OD corner of the groove.

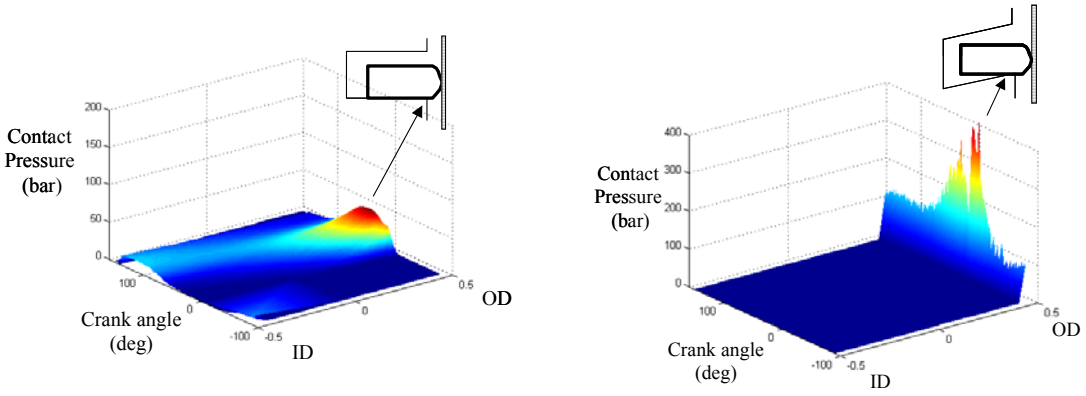

Figure 4-4: Effect of Upward Top Ring Groove Tilt

Because of the highly concentrated contact pressure at the OD corner of the upward tilted top ring groove, this corner will be subjected to significant wear and will likely flatten out over

time. As a result, the upward groove tilt angle will gradually decrease until the design is effectively undone and the groove is no longer tilted. Clearly, a design to compensate for this effect is needed if this upward groove tilt design is to be useful for practical purposes. Such a design will be recommended in Section 4.4.1.

4.3.3. Increased Oil Consumption

In Section 4.2.1, it was noted that reducing oil control ring tension will compromise the ring's conformability to the liner, which will likely result in increased engine oil consumption. In reality, this depends on whether or not the oil that passes the oil control ring-liner interface is able to reach the combustion chamber. It also depends on the extent of the bore distortion in the engine, which is not known exactly. Nevertheless, it is likely that if a significant amount of excess oil passes the oil control ring-liner interface, at least part of this oil will reach the crown land and will be consumed. Therefore, the reduced tension oil control ring design should be implemented with another design to compensate for the likely increase in oil consumption. Two designs that could potentially achieve this purpose will be described in Sections 4.4.2 and 4.4.3

4.4. Designs to Compensate for Adverse Effects

4.4.1. Effect of Top Ring Static Twist on Top Ring Groove Wear

As discussed in Section 4.3.2, the upward top ring groove tilt design results in a large concentrated contact pressure at the OD corner of the groove, which can quickly wear the OD corner and render the design ineffective. One way in which to compensate for this effect is by introducing a positive static twist in the top ring. This can be accomplished by adding a small groove in the in the upper ID corner of the top ring.

If there is no groove in the upper ID corner of the ring, the cross-section is approximately symmetric. As a result, when the ring is installed in the cylinder bore and the radial load due to tension is applied, pure bending occurs about the axis that is normal to the plane of the ring as the ring gap is closed. If a small section of material is removed from the upper ID corner of the ring, the cross-section becomes asymmetric, and the location of the centroid and the angle of the principal axes of the cross-section will change. As a result, when the ring is installed in the cylinder bore and the uniform radial load due to tension force is applied, the cross-section will be subjected to a twisting moment as well as a bending moment.

If a certain amount of material is removed from the upper ID corner of the ring such that the positive twist introduced by this change is larger than the upward groove tilt angle, the ring will settle down on the lower groove flank much more gradually as the cylinder pressure rises during the compression stroke. As a result, a more uniform contact pressure distribution between the ring and the lower groove flank will be achieved with such a design, as illustrated in Figure 4-5 below. This will prevent the upward groove tilt design from becoming worn. The contact pressure distribution in the case of the upward groove tilt combined with the positive top ring

static twist yields roughly the same uniformity in the contact pressure distribution as the baseline design with no upward groove tilt. It is therefore reasonable to expect that this design would wear no less than the baseline design. The combination of the upward groove tilt with the positive top ring static twist thus reduces friction without introducing any adverse effects.

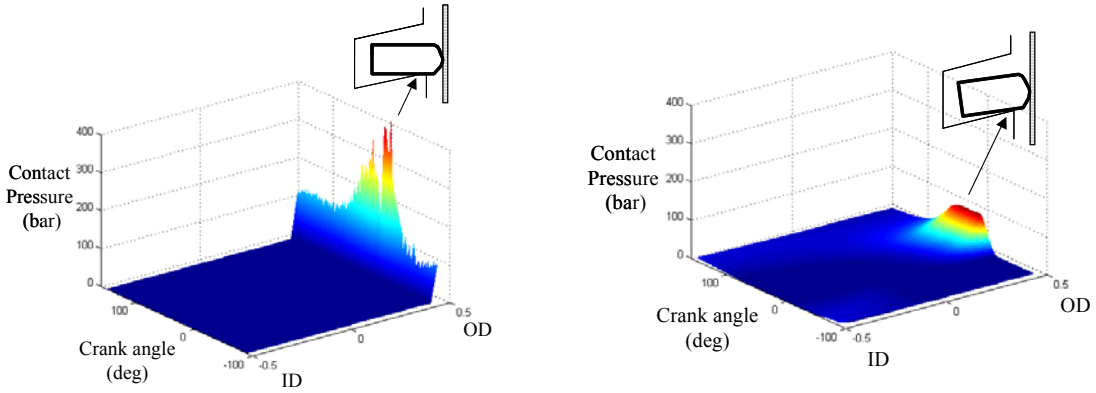

Figure 4-5: Effect of Top Ring Static Twist

4.4.2. Effect of Second Ring Design on Oil Consumption

The second ring is typically designed with either a positive static twist or a negative static twist. With a positive static twist, the ring is more stable and therefore no ring flutter occurs near TDC of compression. A complete description of the flutter phenomenon as well as a more thorough discussion of the link between static twist and ring stability can be found in [31]. It is commonly believed that second ring flutter near TDC of compression results in oil transport to the crown land and eventually to oil consumption. As a result, the second ring is often designed with a positive static twist so that no flutter occurs around TDC of compression.

One of the consequences that can occur as a result of the use of such a design is that the second ring can remain fixed on the lower groove flank for most of the cycle. This is because a second ring with positive static twist can seal the path where gas would normally flow to the lower lands, as shown below in Figure 4-6. As a result, there is a significant pressure rise in the second land and this pressure cannot be relieved to the lower lands through the blocked path. Because of the inability of the gas to flow from the second land to the lower lands, pressure in the second land builds, and can exceed the cylinder pressure near the end of the expansion stroke. At the beginning of the exhaust stroke, this pressure difference tends to force the top ring to lift, whereas the downward pointing inertia force pushes the top ring down, resulting in a phenomenon called top ring reverse flutter. Previous studies have shown that top ring reverse flutter may be an important source of oil consumption [31,32,33].

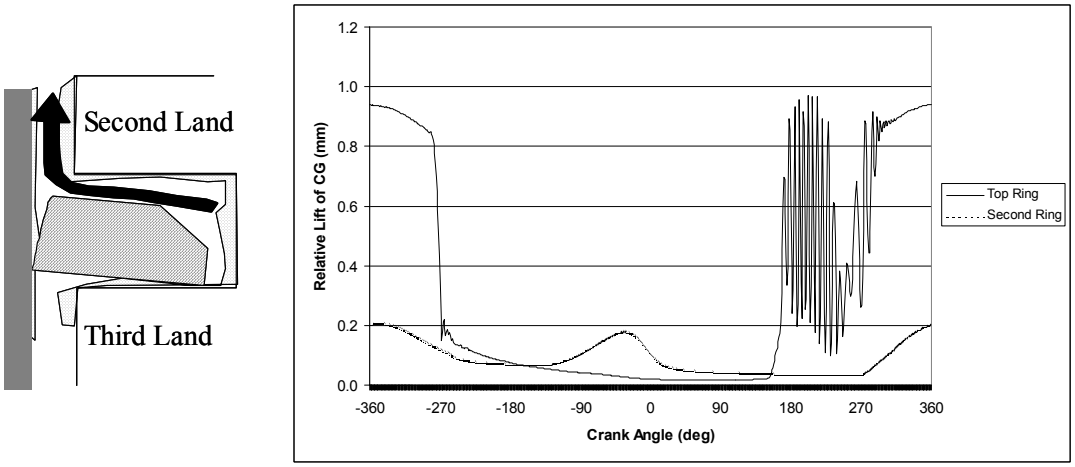

Figure 4-6: Top Ring Reverse Flutter

There is another potential adverse consequence that can result from the use of a second ring with positive static twist. With a larger second ring static twist, a more significant portion of the taper face becomes exposed to the higher second land gas pressure. Due to the sealing created between the second ring and the top OD corner of the second ring groove, the high gas pressure can push the ring inward to allow the gas flow to pass through the ring-liner interface. This is a phenomenon called second ring collapse, and it is illustrated in Figure 4-7 below. Operating conditions and designs to avoid second ring collapse are discussed in [31]. Second ring collapse is undesirable for oil consumption because it allows a significant amount of gas to flow past the ring-liner interface and to reach the third land, where pressure builds up and gas flow can subsequently carry oil into the second ring groove and upwards towards the combustion chamber.

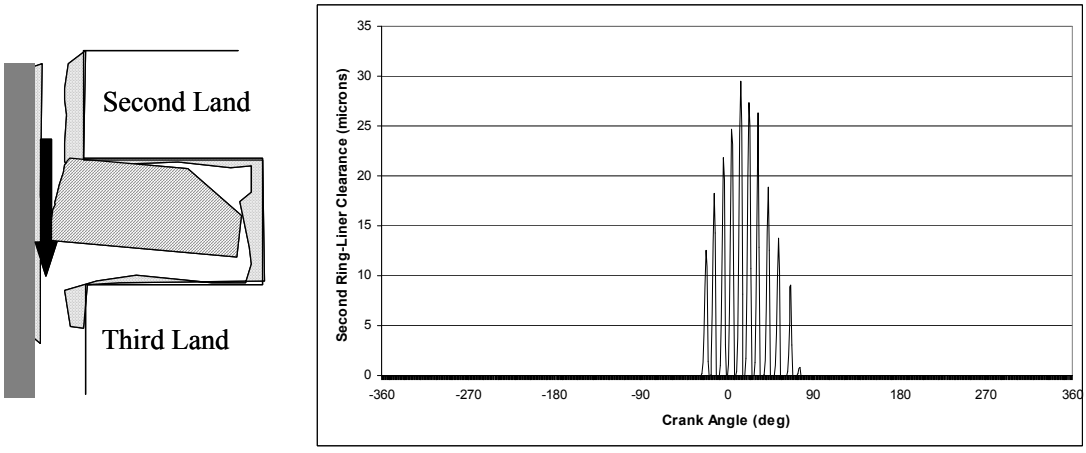

Figure 4-7: Second Ring Collapse

A second ring with a negative static twist allows the gas flow to penetrate to the lower lands from the second land, and therefore eliminates top ring reverse flutter, and the potential second ring collapse. This result is illustrated in Figure 4-8.

The elimination of top ring reverse flutter through the use of the negative static twist second ring design has the potential to reduce oil consumption in the engine. It is therefore recommended that this design be used with the reduced tension oil control ring so that the reduction in tension does not significantly increase oil consumption overall.

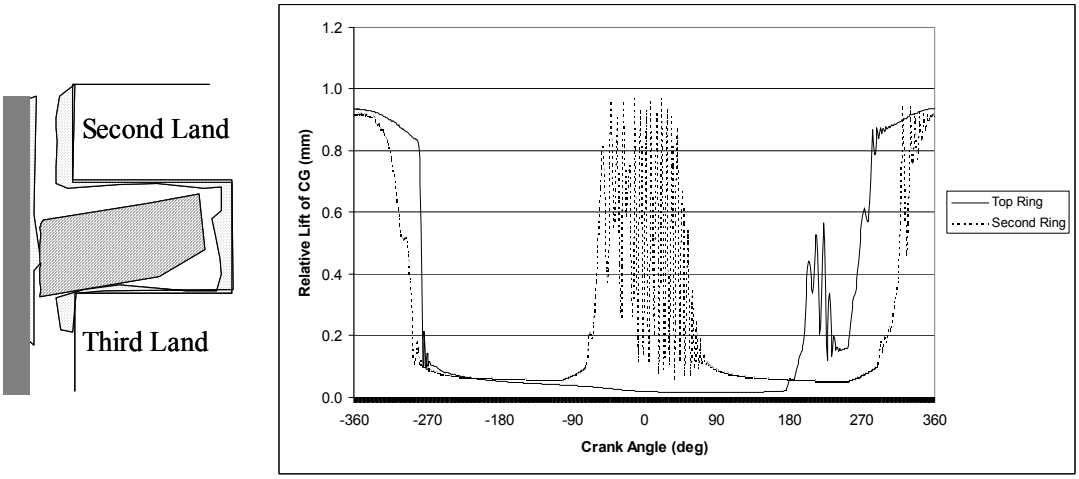

Figure 4-8: Second Ring with Negative Static Twist

4.4.3. Effect of Oil Control Ring Conformability on Oil Consumption

Another design strategy that could be used in combination with the reduced tension oil control ring to compensate for the increased oil consumption is the reduction of the radial thickness of the cross-section of the oil control ring. If the cross-sectional area is reduced, the moment of inertia is also reduced. This is because the moment of inertia is determined by the sum of the squares of the radial distances between the centroid of the cross-section and the origin at each element of area of the ring. Therefore, if the overall area is reduced, there are fewer contributions to the overall area, and the moment of inertia is thus reduced. If this is the case, bending is promoted about the axis perpendicular to the plane of the ring, leading to improved conformability.

However, designing the oil control ring with a smaller area results in a reduction in the structural strength of the ring, which may compromise ring life. A stiffer material could be used to compensate for this effect, but this would result in a decrease in conformability overall, since the stiffness of the material has a more significant effect on conformability than the cross-sectional area of the ring. Therefore, the improvement in conformability that can be achieved by a reduction in the cross-sectional area of the ring is limited by structural considerations, and may not be the most effective design strategy.

4.5. Additional Design Limitations

4.5.1. Manufacturing Limitations

Typical axial heights of piston rings range from 1 mm to 4 mm. As a result, machining the rings to precisely match the design specifications is difficult, and tolerances are often on the order of the design values themselves. Care thus needs to be taken when developing designs to ensure that allowances are made for such tolerances.

Certain designs are limited by these tolerances. In particular, the top ring profile can only be machined within certain tolerances, and as a result, there are limitations on the design values that can be specified.

In this study, the effect of producing designs at the limits of the various tolerances was evaluated using the modeling tools. In other words, the friction reduction potential of each of the designs was assessed for each case with an upper and a lower limit representing the extreme cases for machining the rings at the edge of the tolerance ranges. This facilitated the optimization of the final designs to ensure that a reduction in friction was predicted by the modeling tools.

4.5.2. Transition to Boundary Lubrication at Midstroke

In several of the designs presented in the previous sections, the physical length between the top ring's minimum point and its lower edge in the untwisted state (B2 in Figure 3-12) was reduced. If this length is reduced significantly, it can result in the onset of boundary lubrication conditions throughout the entire engine cycle.

For most of the engine cycle, the top ring is typically designed to be in hydrodynamic lubrication, except near dead centers when piston speed is reduced significantly and hydrodynamic lubrication cannot be sustained. If B2 is reduced beyond a certain extent, the top ring will become fully-flooded at the leading edge on downstrokes. This is because the oil supply is fixed, but the amount of space available under the ring is decreasing as B2 is reduced. Once the top ring becomes fully-flooded on downstrokes, because of the fixed oil supply, less oil can fit under the ring as B2 is reduced further. Therefore, further reduction in B2 results in a reduction in oil film thickness, ho, and eventually, the condition defined in Eq. (2.2) is met and boundary lubrication conditions are present even in the midstroke regions of the engine cycle. As was pointed out throughout this study, boundary friction losses are much higher than friction losses from hydrodynamic lubrication, and therefore the onset of this condition throughout the cycle causes a significant increase in the friction generated by the top ring along the liner. This condition thus sets an upper limit on the potential reduction of B2 through a reduction in axial height or through the use of a skewed barrel profile.

In general, as long as boundary lubrication conditions are not present in the midstroke regions of the engine cycle, the top ring friction generated in the midstroke region is a negligible part of the total friction generated by the top ring for high load, low speed operating conditions. However, as pointed out in Section 3, for low load, high speed conditions, midstroke friction

generated by the top ring becomes significant. Although the present study focuses on high load, low speed engines, an approach to identify strategies for the reduction of top ring midstroke friction was also suggested. This was included because once the contribution of the top ring friction generated around TDC of compression/expansion is reduced through various design changes, the top ring friction at midstroke is the next area which can be targeted for further friction reduction.

4.6. Application of Reduced Friction Design Strategies to a Natural Gas Power Generation Engine

In the following Section, the reduced friction strategies developed in Section 4 are applied to re-design the piston rings of a natural gas power generation engine with the goal of reducing friction to improve the engine's efficiency. Model predictions are first obtained to compare the effectiveness of each of the low-friction design strategies in the Waukesha engine. Based on the results of this comparison, several low-friction designs were selected for experimental investigation. The logic behind this selection process is briefly described. The experimental procedure used to evaluate the designs is then described in detail in a later section, and the results are presented and compared with the corresponding model results for those specific changes.

4.6.1. Description of Engine and Relevant Specifications

The engine selected for this study was a Waukesha spark-ignited natural gas power generation engine. Relevant specifications for this engine are shown in below in **Table 4-1**. The operating condition selected for this study was based on a typical operating condition that is ideal for interfacing with power generation equipment. It should be noted that all of the model predictions that will be presented in the sections that follow are based on normalized design values so that the current design values remain confidential.

Table 4-1: Waukesha Engine Specifications

Engine Configuration	6 Cylinders, Inline
Displacement	18 liters
Bore, Stroke	152 mm, 165 mm
Speed	1800 rpm
Load Condition	1360 kPa BMEP

4.6.2. Reduced Friction Designs and Model Predictions

In the section that follows, model predictions are presented to illustrate the effect of implementing the different design strategies investigated in this study on friction in the Waukesha engine. The results are presented in terms of FMEP, which is the integrated effect of the friction power losses over the engine cycle, normalized by the engine's displaced volume. Details on the determination of FMEP from friction power losses throughout the engine cycle are given in Appendix B. In this study, model predictions were obtained for both oil supply conditions, OS1 and OS2, to bracket the actual FMEP between the upper and lower limits.

4.6.2.1. Reduced Tension Oil Control Ring

Model predictions for the effect of reducing oil control ring tension on friction in the Waukesha engine are presented in the figures below. Figure 4-9 and Figure 4-10 show the effect of reducing oil control ring tension on oil control ring FMEP and total ring pack FMEP, respectively.

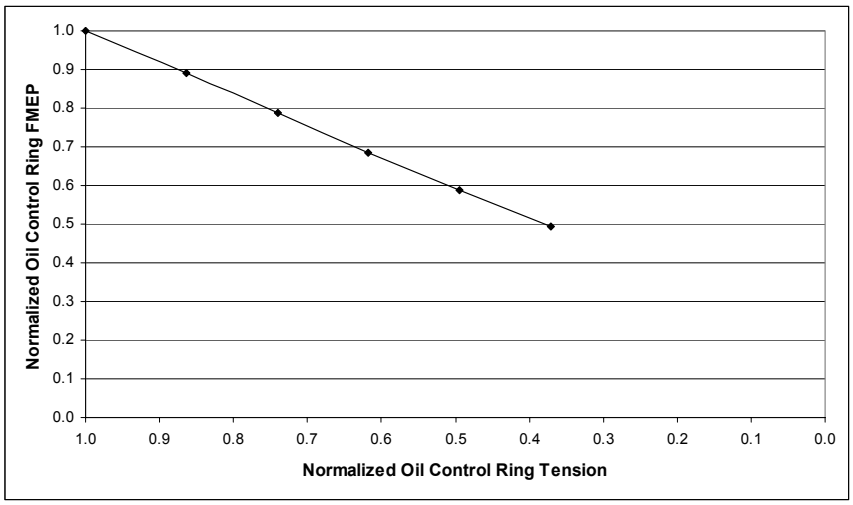

Figure 4-9: Effect of Oil Control Ring Tension on Oil Control Ring FMEP

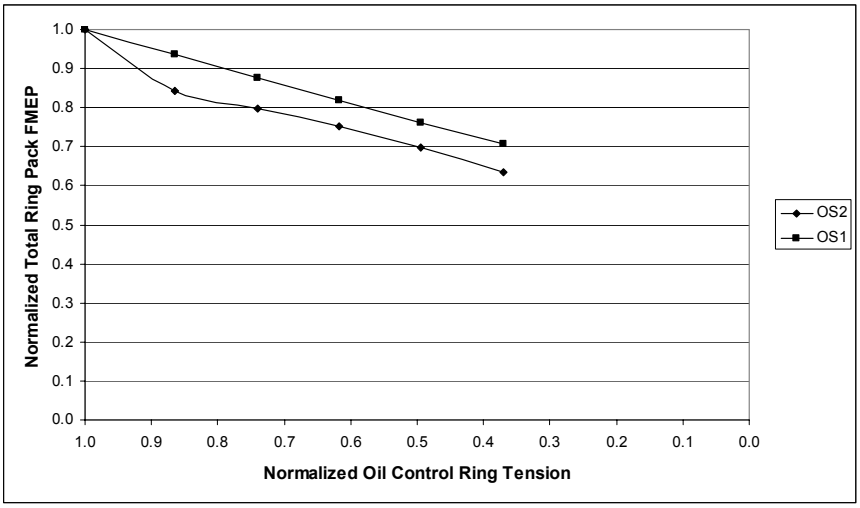

Figure 4-10: Effect of Oil Control Ring Tension on Total Ring Pack FMEP

It should be noted that in Figure 4-10, there is no distinction between OS1 and OS2 as the oil supply conditions do not affect the oil control ring, which is assumed to be fully-flooded on both upstrokes and downstrokes in the model as discussed in Section 2. It can be seen in the above figures that if oil control ring tension were reduced by half of its total value, oil control ring FMEP would be reduced by 40% and total ring pack FMEP would be reduced by 30-35%.

The sharp decrease in total ring pack FMEP in the case of OS2 for a reduction in oil control ring tension from a normalized value of 1.000 to 0.864 can be attributed to the top ring gaining hydrodynamic lubrication on the expansion stroke for the cases where the tension is below the normalized value of 0.864. If the tension is larger than this value, the oil control ring leaves an insufficient amount of oil on the liner and the top ring is in pure boundary lubrication conditions throughout the engine cycle.

4.6.2.2. Skewed Barrel Top Ring

Model predictions for the effect of a skewed barrel top ring profile on top ring friction in the Waukesha engine are presented in the figures below. In Section 4.1.1, the effect of decreasing B2 on friction was discussed. Figure 4-11 and Figure 4-12 show the effect of the reduction of B2 on top ring FMEP and total ring pack FMEP, respectively.

As can be seen from the figures, the introduction of a skewed barrel profile can reduce top ring FMEP by up to 45% irrespective of the oil supply condition, and total ring pack FMEP by 15-25%. The reduction in total ring pack FMEP is larger for the case of OS2 because the top ring contributes much more significantly to the total ring pack FMEP due to the poorer oil supply assumed in this case.

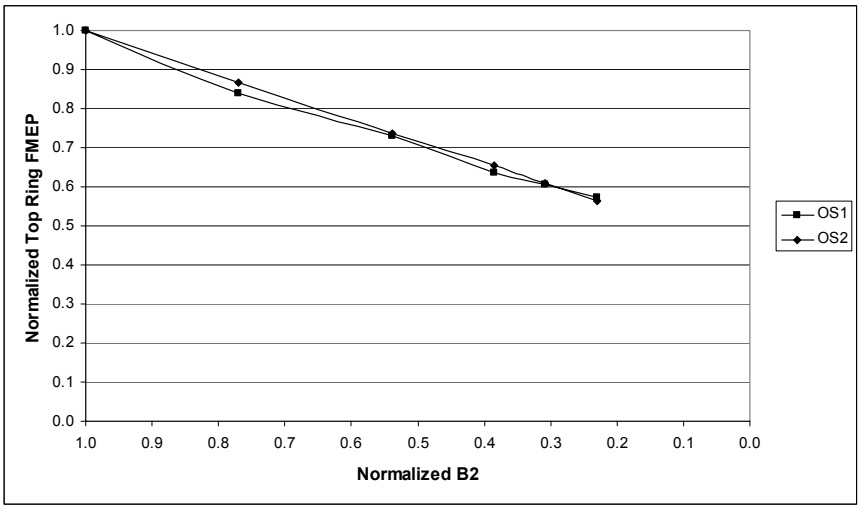

Figure 4-11: Effect of Skewed Barrel Profile on Top Ring FMEP

4.6.2.3. Reduced Axial Height Top Ring

Model predictions for the effect of reducing the axial height of the top ring on friction in the Waukesha engine are presented in the figures below. Figure 4-13 and Figure 4-14 show the effect of the reduction of axial height on top ring FMEP and total ring pack FMEP, respectively.

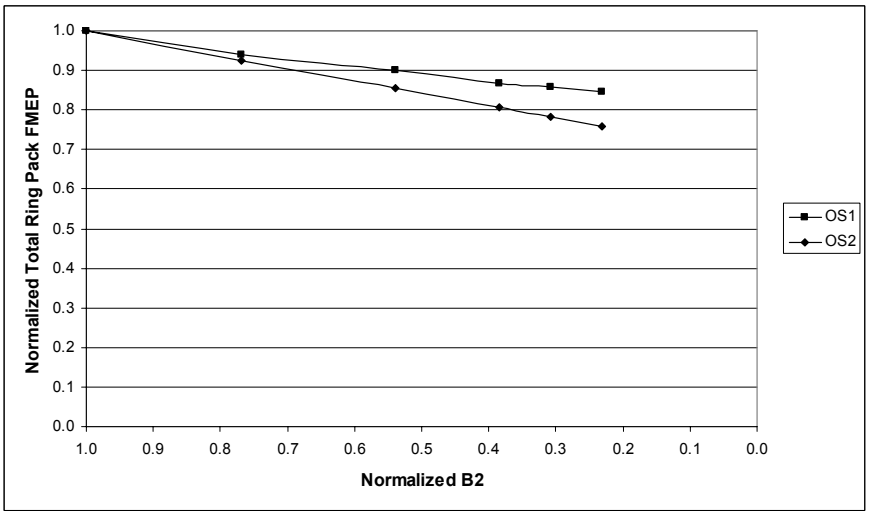

Figure 4-12: Effect of Skewed Barrel Profile on Total Ring Pack FMEP

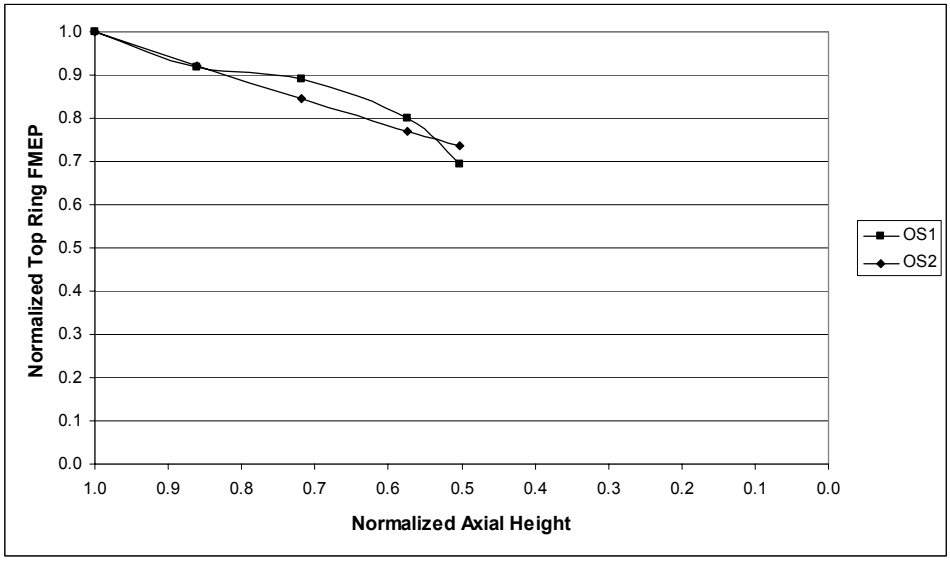

Figure 4-13: Effect of Top Ring Axial Height on Top Ring FMEP

As can be seen in the figures, a reduction in the axial height of the top ring can result in a reduction in top ring FMEP of up to 25%, regardless of the oil supply condition. For the case of the total ring pack, FMEP can be reduced by 10-15% by a reduction in top ring axial height. Again, as in the case of the skewed barrel profile, the reduction of total ring pack FMEP is higher for the case of OS2 because of the larger contribution of the top ring to total ring pack friction in that case.

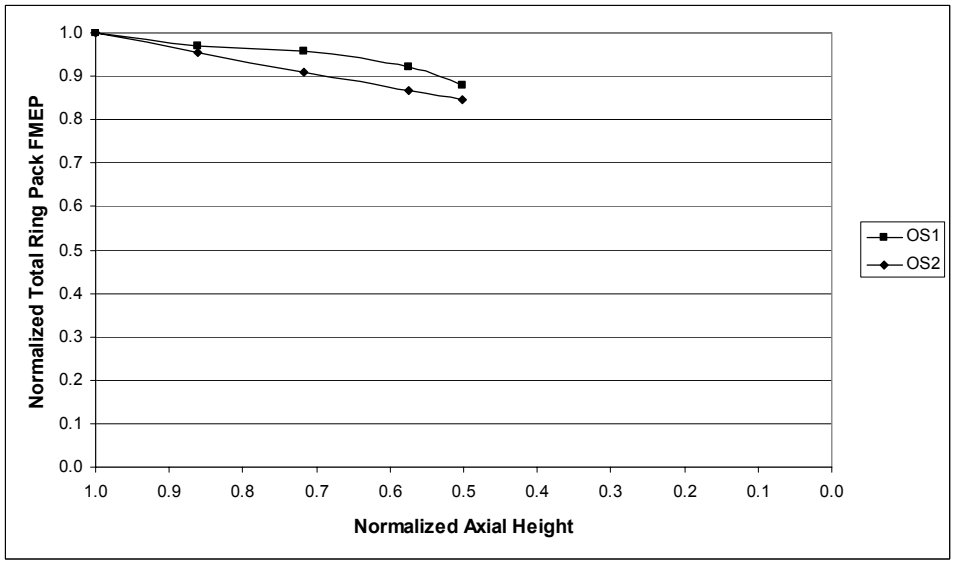

Figure 4-14: Effect of Top Ring Axial Height on Total Ring Pack FMEP

It should be noted that since the focus of this study is on the reduction of top ring boundary friction around TDC of compression, the objective is to reduce B2 and therefore either the skewed barrel profile or the axial height reduction should yield similar results. However, the

reduced axial height rings have been shown to have lower structural strength, leading to earlier failure, as discussed in Section 4.3.1. Therefore, the skewed barrel profile design is more advantageous from the standpoint of ring life and reduced friction.

4.6.2.4. Upward Top Ring Groove Tilt

Model predictions for the effect of increasing the top ring groove tilt on friction in the Waukesha engine are presented in the figures below. Figure 4-15 and Figure 4-16 show the effect a top ring groove with an upward tilt on top ring FMEP and total ring pack FMEP, respectively.

As can be seen in the figures, the upward top ring groove tilt can result in a reduction in top ring FMEP of up to 25%, regardless of the oil supply condition. For the case of the total ring pack, FMEP can be reduced by 10%.

There are several trends that can be observed from these figures that require more detailed explanation. Firstly, for the case of both OS1 and OS2, for an increase in groove tilt beyond a normalized value of 0.571, the FMEP remains fairly constant. This can be explained by considering the dynamics of the top ring as it travels in the dry region. The development of this upward groove tilt strategy assumed that the top ring would conform fairly well to the lower groove flank and that as a result, the position of the minimum point on the top ring would be lower on the profile when the groove tilt was increased. However, the top ring does not actually conform very well to the lower groove flank during this part of the engine cycle. This is confirmed by the model predictions, and is illustrated by a plot of the top ring twist as shown below in Figure 4-17 for the case of three upward groove tilts with normalized values of 0.429, 0.857 and 1. It should be noted that the small fluctuations in the ring twist Figure 4-17 are a result of the instability of the ring in this configuration due to the concentrated outer diameter contact on the lower groove flank. As can be seen from this figure, the top ring twist increases between groove tilts of 0.429 and 0.857, but between 0.857 and 1, there is no significant increase. As a result, the minimum point position does not change and there is no reason to expect a reduction in FMEP.

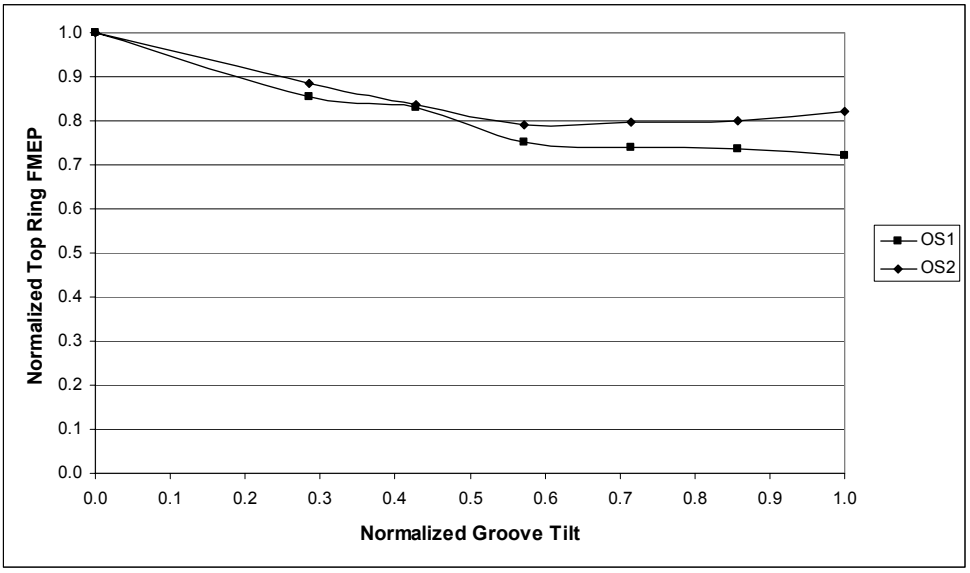

Figure 4-15: Effect of Top Ring Groove Upward Tilt on Top Ring FMEP

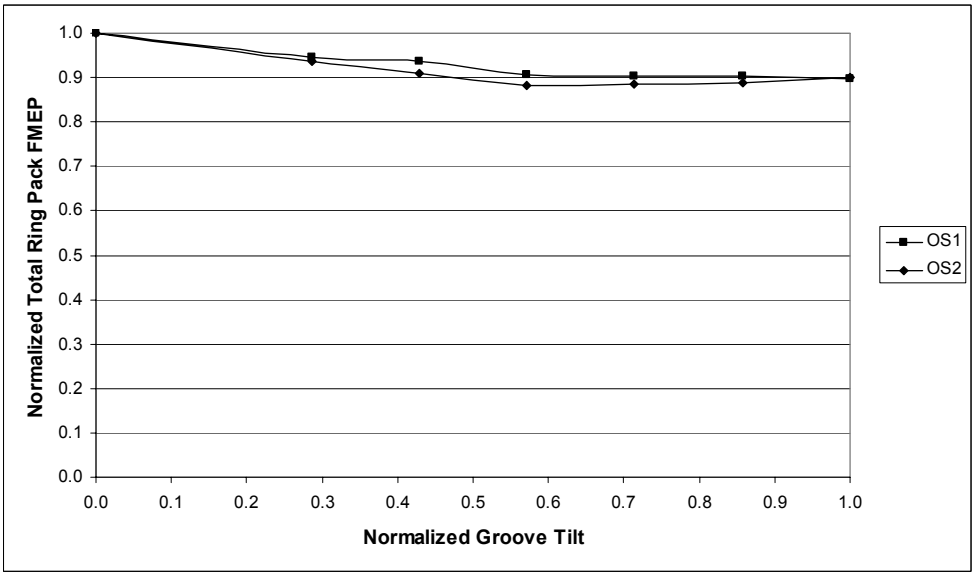

Figure 4-16: Effect of Upward Top Ring Groove Tilt on Top Ring FMEP

Before providing insight into this apparent limit in top ring twist that is reached after a certain groove tilt is exceeded, the governing forces and moments acting on the top ring to create the positive twist around TDC of compression must first be described. The positive top ring twist around TDC of compression is a result of the counterclockwise net moment acting on the top ring during this period. In Figure 4-18, the integrated moments acting on the top ring around TDC of compression are plotted, along with the resulting top ring dynamic twist. The convention adopted in this figure is that a positive moment results in a positive or

counterclockwise twist. It can be seen from Figure 4-18 that there is a clockwise moment exerted by the high gas pressure acting on the part of the top ring surface that is exposed to the clearance between the groove and the liner. Moments due to gas pressures acting on the rest of the top and bottom ring surfaces are balanced, because of the ability of the high-pressure gas to penetrate to the region below the ring due to the ring-groove configuration, as can be seen in the illustration of the top ring-groove configuration in Figure 4-19. The net moment due to the high gas pressure acting on the ring in the clearance between the groove and the liner is roughly balanced by the counterclockwise moment from asperity contact between the bottom face of the ring and the lower groove flank. The unbalanced positive moment acting on the top ring that results in the positive twist around TDC of compression comes from the force due ring-liner interaction.

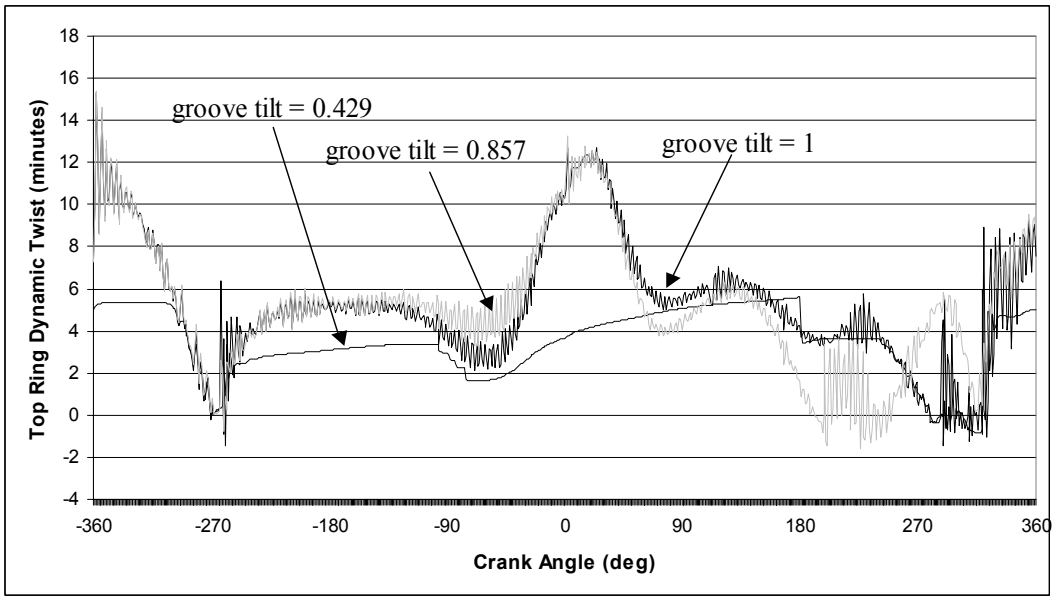

Figure 4-17: Effect of Groove Tilt on Top Ring Dynamic Twist

To better explain the source of this moment, a simple diagram illustrating the forces and acting on the top ring around TDC of compression is shown in Figure 4-19. For illustrative purposes, without loss of generality, the second land pressure is assumed to be zero. The net force exerted by the ring on the liner due to the radial pressure difference is balanced by a reaction force of equal magnitude from the liner on the ring, which is concentrated around the minimum point. For simplicity, this force is assumed to act through the minimum point. There is thus a net positive moment acting on the ring because the line of action of the resultant of the pressure force acting on the inside surface of the ring is below the line of action of the resultant force acting at the minimum point.

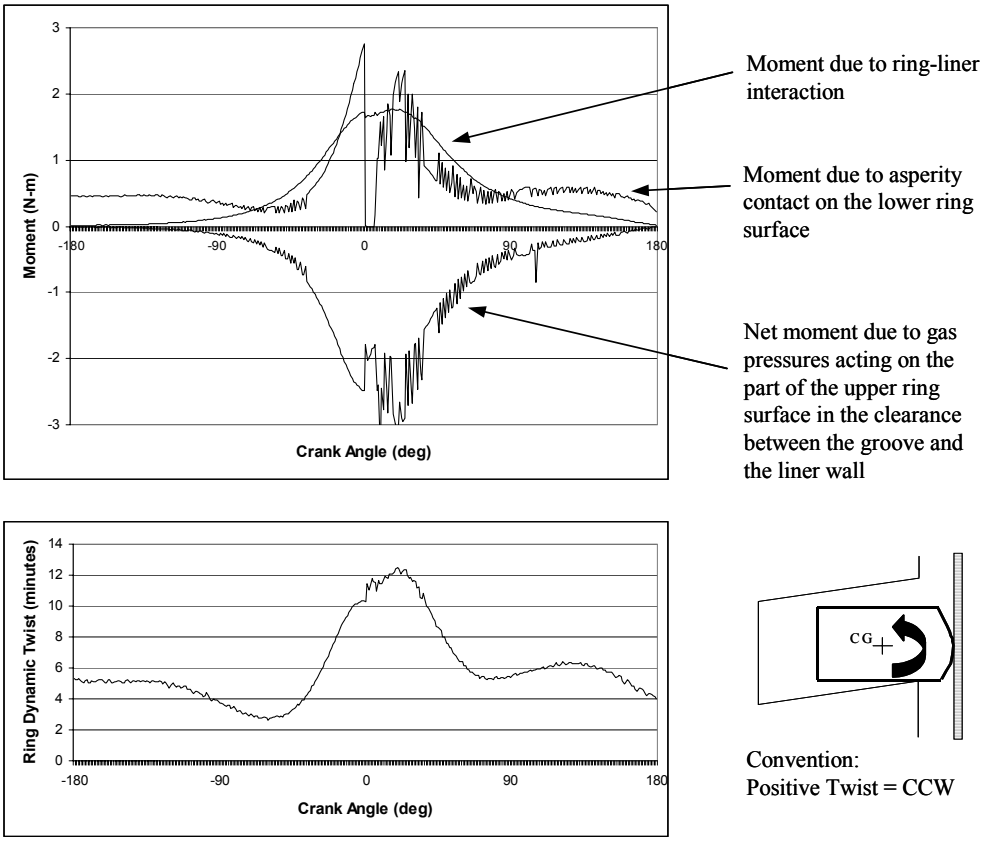

Figure 4-18: Top Ring Moments and Twist

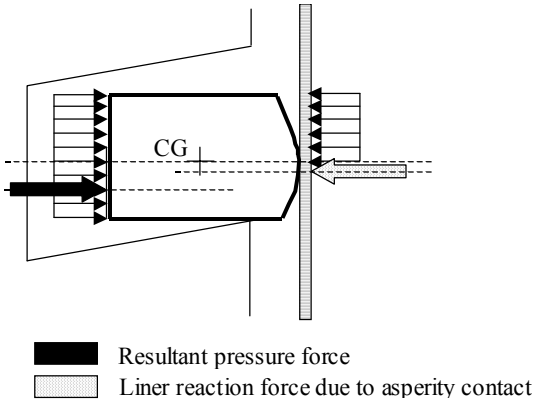

Figure 4-19: Illustration of Moments due to Ring-Liner Interaction

Now that the governing forces that lead to the top ring twist around TDC of compression have been described, insight can be given to explain the effect of increasing groove tilt on top ring twist. The difference in the top ring dynamic twist observed when top ring upward groove tilt is increased is actually a result of the change in the moment acting on the lower face of the top ring due to oil and gas pressure. When the upward groove tilt is small, there is less space between the lower ring surface and the groove and therefore more of the force acting on the lower ring surface comes from oil squeezing from the oil layer between the lower ring flank and

the lower groove flank. As groove tilt is increased, more space exists between the ID of the lower surface of the top ring and the lower groove flank, and therefore there is less contact with oil. As a result, less negative moment is generated by oil squeezing and therefore the ring tends to twist more positively. This is shown below in Figure 4-20, which shows the integrated moment due to oil squeezing acting on the lower flank of the top ring for normalized groove tilts of 0.571 and 0.714, respectively. As can be seen in this figure, for a normalized groove tilt of 0.571, the integrated moment due to oil squeezing acts to create a positive twist at first, but then as the ring twists, the direction of this moment reverses due to the increasing contact area with the oil towards the ID of the top ring and the net oil squeezing moment becomes negative. For the case of a normalized groove tilt of 0.714, the oil squeezing moment is always positive because the larger groove tilt creates more space between the top ring and the lower groove flank towards the ID corner of the ring and therefore there is no contact with the oil to create a negative moment.

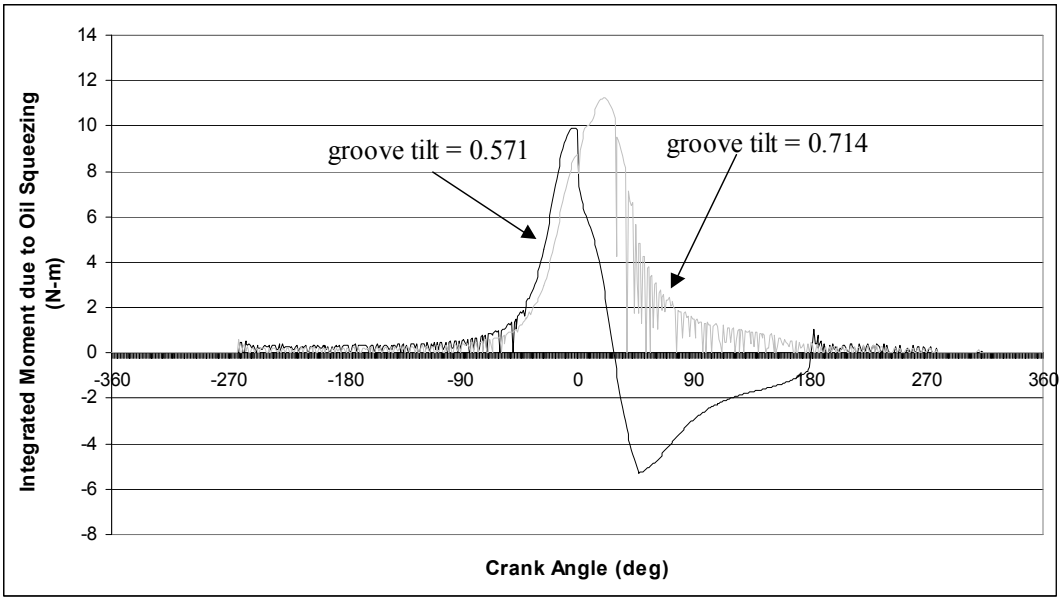

Figure 4-20: Effect of Groove Tilt on Oil Squeezing

Beyond a certain increase in groove tilt, there is no noticeable difference in the ring twist because no contact is made with the oil film between the lower ring surface and the groove and therefore further increase in groove tilt angle has no effect on top ring dynamics.

In summary, the net positive top ring twist that occurs around TDC of compression comes from the unbalanced moment due to ring-liner interaction. As groove tilt is increased, the contribution of the negative moment from oil squeezing between the lower ring surface and the lower groove flank decreases because less contact is made with the oil film. This occurs until a certain groove tilt is exceeded, at which point no further contact is made with the oil film. Therefore, there is no further increase in top ring positive twist beyond that groove tilt.

5. Effects of Lubricant Viscosity in Ring-Pack Friction Reduction Strategies

This study focuses on the effects of lubricant viscosity, and its variation during the engine cycle, on ring/liner friction. A brief study of boundary friction coefficient is also included, as it can have a large effect on friction, and can be controlled to some extent by lubricant additives. The objective is to determine an optimized viscosity, including variations during the engine cycle, for the given engine design and operating conditions.

Both idealized and more realistic cases are considered. First, ideal cases where the lubricant viscosity at each crank angle can be independently controlled are studied, to illustrate potential benefits in a well-controlled scenario. Then, a parametric study of more practical cases is presented, based on realistic lubricant dependencies on temperature and shear rate. Also, different ring tension and roughness parameters are studied to find any interaction between these factors and lubricant effects.

While friction reduction is the focus of the current effort, other factors such as wear must also be addressed. A simple study of the effects of lubricant viscosity on wear is presented, with a slight benefit observed when viscosity variation during the engine cycle can be controlled.

It should be noted that, for most of the analyses below, the focus is on the oil control ring only, and not the entire ring pack. Figure 3-2 shows that the OCR is the largest contributor to ring-pack friction in the Waukesha engine. The top ring also contributes significantly to the total friction, but, as shown in Figure 3-11, most of this contribution comes from boundary friction in the dry region. The high friction in the dry region is due, in part, to very poor lubrication, so that controlling the lubricant viscosity should have little to no effect on friction generated here. Model results indicated that viscosity may have some influence on dry region width, and thus friction, but these results are preliminary, and are discussed briefly in section 5.4.

5.1. Effects of Lubricant Viscosity on Hydrodynamic and Boundary Losses

Two lubrication regimes contribute to friction losses for each ring: hydrodynamic losses result from shear stress within the lubricating oil, and boundary losses from rubbing between the two contacting solid surfaces. The relative contribution of each mode to total friction for a given ring depends on how well the ring-liner load can be supported by the oil film. At high enough speed and viscosity, the oil film can fully support the ring load, resulting in pure hydrodynamic lubrication. For lower speeds and/or low viscosities, a thinner film is generated and may be thin enough to allow some asperity contact to occur, resulting in mixed lubrication. At very low speeds or viscosities (or very low oil availability, as in the case of TDC combustion for the top ring) the oil film can break down, and the ring load is entirely supported by asperity contact.

The lubrication regimes of the ring during the engine cycle can be related to the ring speed, U, and lubricant viscosity, ν, for a given load. Figure 5-1a shows how the ring/liner friction coefficient varies with a bearing number $N=10*U*\nu$ for baseline engine parameters (the factor 10 was chosen so that the bearing number ranges approximately between 0 and 1). In Figure

5-1a, the oil film thickness and friction coefficient for the OCR are plotted. As the bearing number approaches 0, film thickness decreases and hydrodynamic support is lost. Asperity contact supports the load, and the coefficient of friction increases to the boundary friction coefficient, $f_b = 0.1$ in this case. For high bearing number, friction increases as shear stress – proportional to U and ν - increases. In the mid-range, friction coefficient drops as the balance between boundary and hydrodynamic lubrication changes.

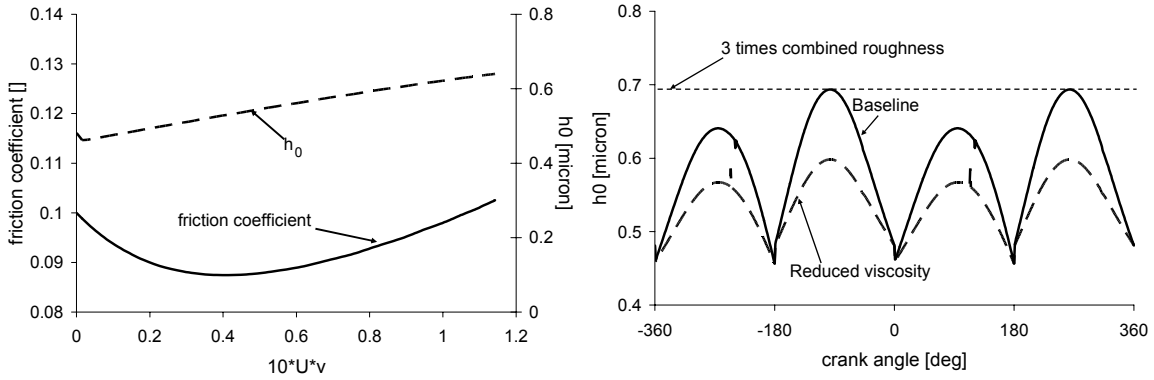

a)friction coefficient and h0 dependence on bearing # **b)minimum film thickness, for an engine cycle**

Figure 5-1: Effects of speed and viscosity on ring-liner separation (minimum film thickness) and friction, lower land OCR

Figure 5-1b shows the film thickness between the lower land of the OCR and the liner for an engine cycle, in the Waukesha engine studied (-360^o is the beginning of the intake stroke), for two lubricant viscosity cases. Results for the upper land are the same – only one is shown for illustrative purposes. Viscosity variation during the engine cycle for the baseline and reduced-viscosity cases are shown in Figure 5-3. Film thickness is small near dead-centers, because U=0 and hydrodynamic support is lost (film thickness does not go to 0 because of the ring and liner roughness – there is still some oil trapped in the valleys when peaks are contacting.) Near mid-strokes piston speed is high, and film thickness is also large. The line "3 times combined roughness" indicates the film thickness that is three times the combined roughness of the ring and liner, at which there is a 5% chance of metal to metal contact. Comparing to Figure 5-1a, the film thicknesses shown in Figure 5-1b indicate that hydrodynamic lubrication dominates near mid-strokes (although there is a very small amount of asperity contact), while boundary contact supports most of the ring load near dead centers. In the reduced viscosity example, film thicknesses are lower, because the less viscous oil is less able to support the ring load.

This distribution of friction regimes is also shown in an analysis of ring/liner friction force. Figure 5-2a shows friction force, per crank angle, for a single (intake) stroke in the Waukesha engine, for the lower land only. In general, results for only the lower land are shown, except when noted, for simplicity in showing trends. The upper land shows the same trends in all cases. In the ring-pack simulation program used, asperity contact is assumed to occur only for film thicknesses less than four times the combined roughness of the surfaces. For larger film thicknesses, the chance of boundary contact (less than 2%) is assumed to be small enough to be negligible. In all other cases, the boundary contact pressure is calculated according to the model given by Greenwood and Tripp [21].

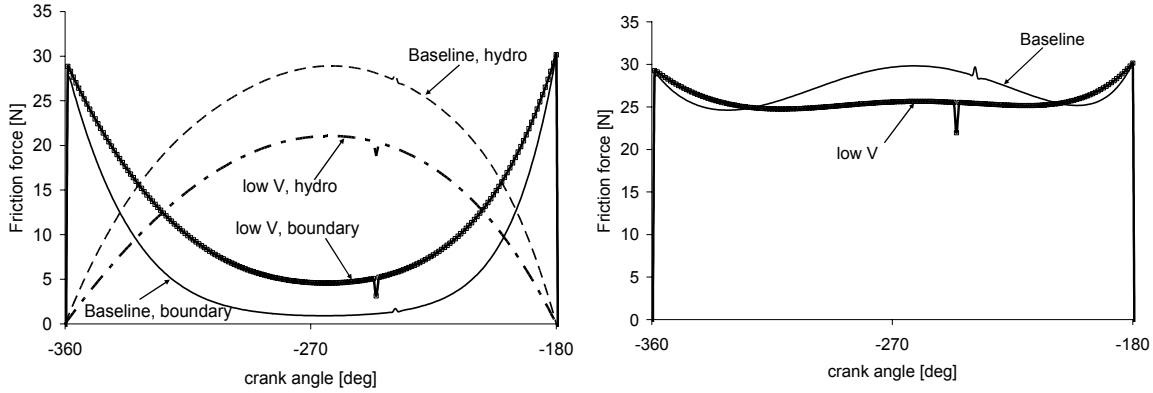

a)Ring/liner friction force, hydrodynamic and boundary **b)Ring/liner friction, total**

Figure 5-2: Effect of viscosity on hydrodynamic and boundary friction, intake stroke, lower land OCR

In the figure, boundary friction is high near dead-centers, where oil film thickness is small, while hydrodynamic friction is high near mid-stroke where piston speed and film thickness are large. For the lower viscosity lubricant, the hydrodynamic friction is reduced, while boundary friction is increased, corresponding to the reduction in oil film thickness shown in Figure 5-1b. Figure 5-3 shows the viscosities of the two cases compared. The variation in viscosity with crank angle is due to the dependence of viscosity on temperature, which is high near TDC and decreases to a minimum value at BDC. Viscosity values for two strokes are shown, to indicate the full range of viscosity variation during an engine cycle.

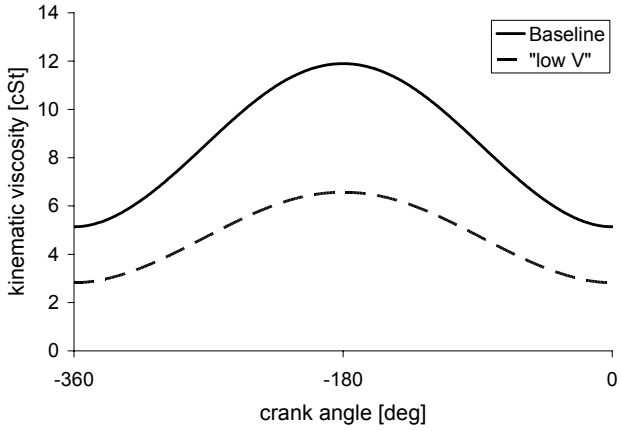

Figure 5-3: Viscosity change during the engine cycle, Baseline and low-viscosity cases. Intake and compression strokes shown

The power lost to ring/liner friction is proportional to the ring/liner friction force and the piston speed at which that force is generated. Although the friction force near dead-centers is of a similar magnitude to the friction force near mid-stroke, mid-stroke power losses are much higher because of the dependence on piston speed. Changes in mid-stroke friction force, then, have a greater effect on total cycle friction than changes in end-stroke friction force. Figure 5-4, which shows the friction work loss per crank angle associated with the friction forces shown in Figure 5-2, illustrates this.

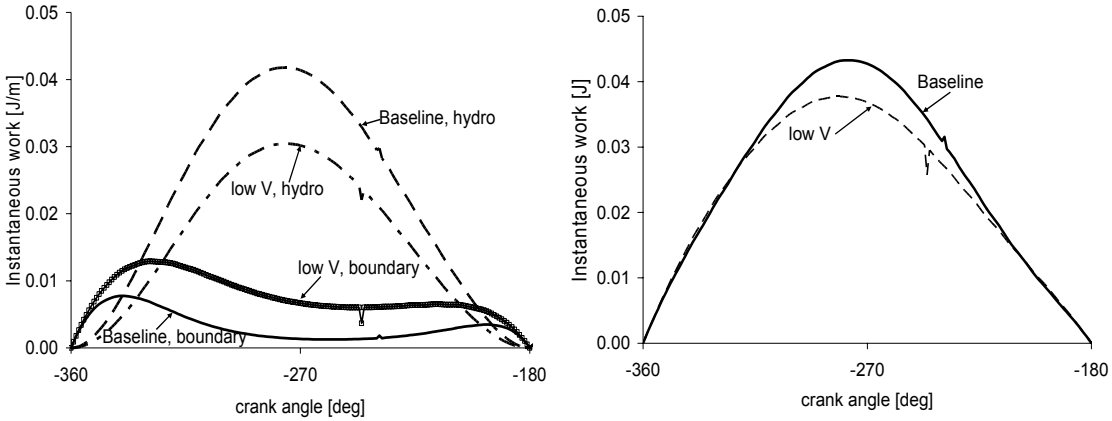

a)Ring/liner friction power loss, hydro and boundary b)Total ring/liner friction power loss, for 2 viscosity cases

Figure 5-4: Effect of viscosity on boundary and hydrodynamic friction work, per crank angle, intake stroke, lower land of OCR

Figure 5-4a shows the boundary and hydrodynamic work losses. For the baseline case, most of the frictional energy losses are due to hydrodynamic lubrication near mid-stroke. For the lower viscosity case, there is an increase in boundary losses at mid-stroke because of the increase in asperity contact there, with a corresponding decrease in hydrodynamic losses. The balance between these two changes determines the extent of the change in overall friction, which is shown in Figure 5-4b. In this figure, it is clear that the mid-stroke effects of changing viscosity almost entirely determine the change in overall friction, for this example, with only minimal contribution from the dead-center region.

The hydrodynamic/boundary friction trade-off occurs not only during the engine cycle, but for the ring pack as a whole. Figure 5-5 illustrates the trade-off between hydrodynamic and boundary lubrication for total cycle friction for the entire Waukesha engine ring-pack. The figure shows the same trends presented above – friction tends to decrease with viscosity as long as the oil is viscous enough to support hydrodynamic lubrication. When viscosity gets too low, friction begins to increase, as boundary friction becomes large. An ideal viscosity is found at the balance of these trends, where a minimum friction loss is found. The goal of this study is to define this ideal viscosity, taking into account viscosity variation during the engine cycle, for the Waukesha engine.

5.2. Viscosity Variation During the Engine Cycle – Idealized Cases

Ring/liner friction is closely related to lubricant viscosity - if viscosity variation during the engine cycle can be controlled, friction reduction may be possible. Several idealized cases were investigated analytically to assess this possibility. The main conclusion of these analyses is that viscosity in the mid-stroke region, where ring speed is high, is the most important parameter to control. Controlling viscosity near dead-centers was the focus of the investigation, and was shown to provide only a small possible friction reduction benefit. A greater advantage of controlling dead-center viscosity may lie in wear reduction, which is discussed in section 5.6.

Two categories of idealized cases were considered: (a) in which viscosity is held constant throughout the cycle, and (b) in which viscosity is increased or held high near dead-centers, to reduce dead-center asperity contact. Initially, the mid-stroke viscosity in each of these cases is kept the same as the baseline case, so that the effect of the viscosity variation can be assessed independently of overall mean viscosity effects. The mid-stroke viscosity was chosen as a reasonable "mean" viscosity both because it is close to the actual mean for the baseline case, and because the mid-stroke region is the source of most of the ring frictional losses. The effect of reducing overall viscosity in both cases (a) and (b) was also evaluated. Viscosity variation during an engine cycle for the example cases discussed, as well as the baseline case, is shown in Figure 5-6.

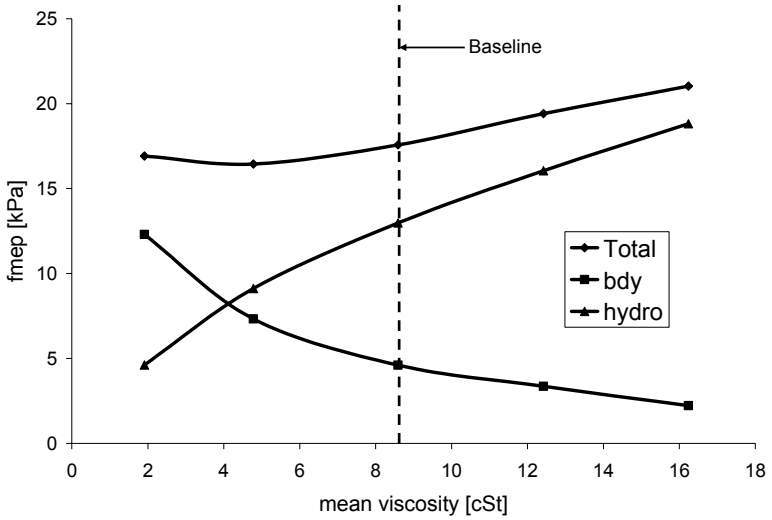

Figure 5-5: Trade-off between hydrodynamic and boundary friction for the baseline ring-pack. Oil is a straight-weight oil (no shear thinning). Fmep is the friction mean effective pressure, a measure of total friction power loss over the engine cycle.

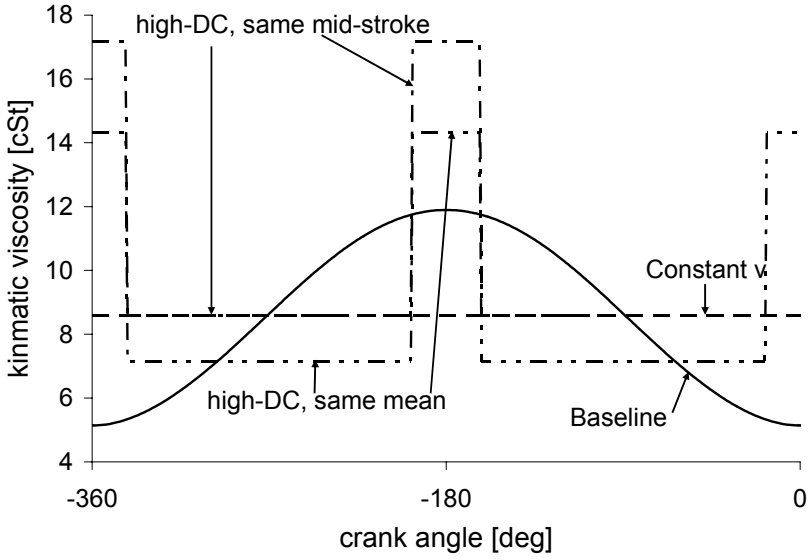

Figure 5-6: Viscosity variation during an engine cycle for three representative cases

5.2.1. Case (a) – Viscosity held constant throughout the stroke

Only a small change in friction was observed between the baseline and constant viscosity caseb. This is because, for the baseline case, the mean viscosity occurs near mid-stroke, so that any viscosity effects that occur before mid-stroke tend to cancel out those that occur after. Figure 5-7 shows this effect, where the friction forces and frictional power losses for these two cases are plotted. In the beginning of the stroke, the viscosity of the baseline lubricant is lower than that in the constant viscosity case, so that baseline hydrodynamic friction is lower, and boundary friction is higher, than for the constant viscosity case. The opposite occurs in the second part of the stroke, so that the overall result is the shift observed, and the overall change in friction is relatively small.

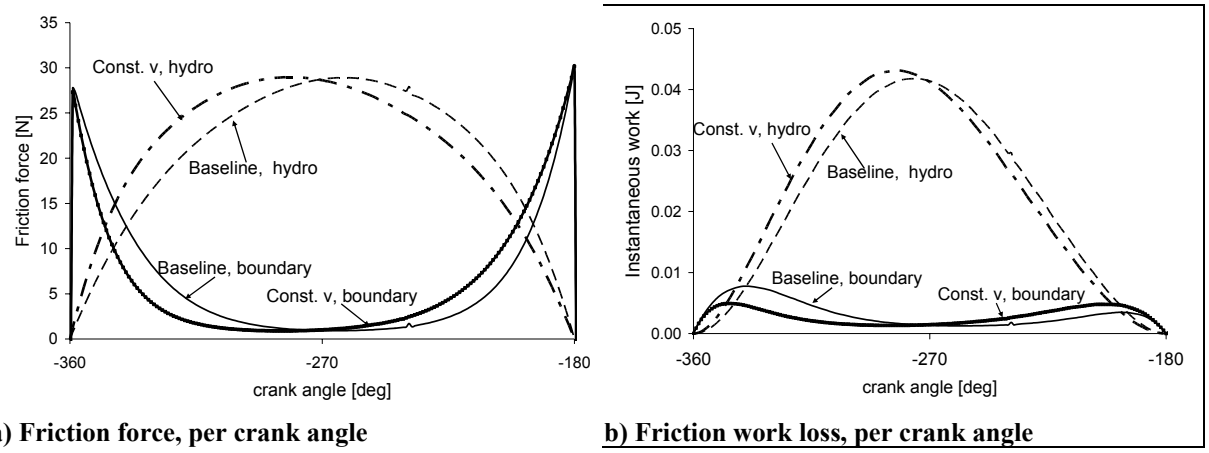

a) Friction force, per crank angle **b) Friction work loss, per crank angle**

Figure 5-7: Constant viscosity case compared to baseline viscosity case, lower land OCR

This is further illustrated in Figure 5-8, which shows the same friction work as a function of piston speed during the intake stroke (other strokes show the same trends), where the arrows indicate the direction of increasing crank angle. This figure shows clearly the effects of the changing viscosity – plotting the friction force vs. piston speed for a stroke removes the effect of the speed, so that viscosity effects are seen more clearly. Figure 5-8a shows that friction for the baseline case is lower than average in the first part of the stroke (where viscosity is lower) and higher in the second. Over the entire stroke, the friction in these two periods averages to a value that is close to that for the constant viscosity case. For the constant viscosity case, there is almost no difference between friction in the first and second parts of the stroke.

Figure 5-8b shows the effect of changing viscosity when the viscosity is held constant during the stroke (the study of mean viscosity effects is further discussed below). The lower viscosity case clearly has lower frictional losses, with the majority of the friction reduction occurring near mid-stroke, due to decreased hydrodynamic friction. This figure shows that the effects of viscosity are largest near mid-stroke, and are small near dead-centers, for this viscosity range. This phenomenon contributes to the relatively small friction benefit predicted for the second idealized case considered, which is summarized below.

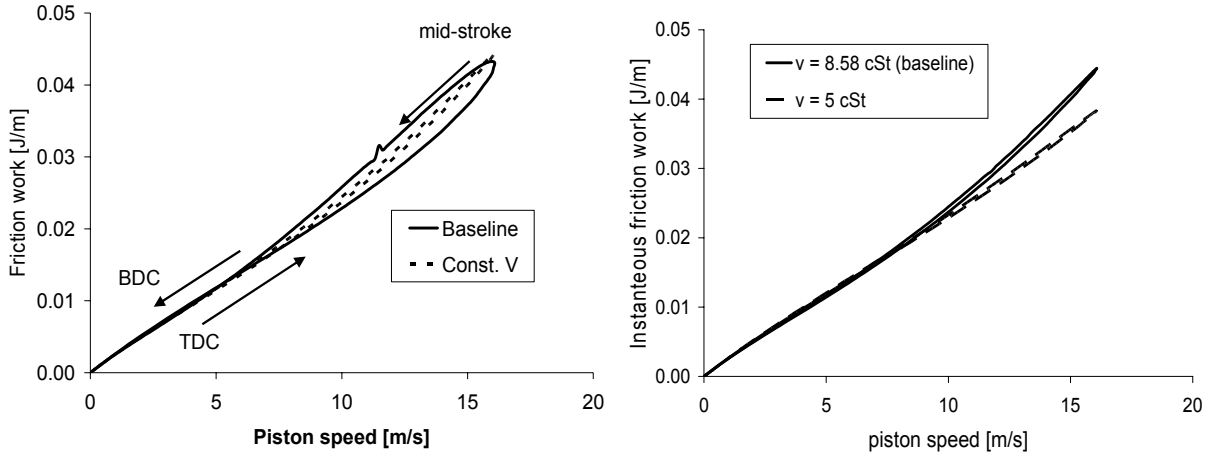

a) Instantaneous friction work, as a function of piston speed

b) Effect of mean friction reduction, constant viscosity case

Figure 5-8: Effect of viscosity temperature dependence, comparing baseline and constant viscosity cases, intake stroke, lower land, OCR

5.2.2. Case (b) – Viscosity held high at dead-centers – "High-DC" cases

Several different viscosity profiles were investigated in which viscosity near dead-centers was held high and viscosity near mid-stroke was held constant or reduced. In one group, a mean viscosity that was the same as the baseline case was maintained, and the width of the high-viscosity peak was varied (number of crank angles for which viscosity was held high). In a second group, the mid-stroke and dead-center viscosities were held constant, with the mid-stroke viscosity matching the baseline case, while the width of the high-viscosity peak was varied. In both groups the end-stroke viscosity was maintained at twice the mid-stroke viscosity. These viscosity variation cases are referred to as "high-DC", for the high viscosity found near dead-centers, and some examples are shown in Figure 5-9. Example results from both groups are presented below.

When the mid-stroke viscosity is kept the same as the baseline case, there is only a small difference in friction between the baseline and high-DC cases – and almost no difference in frictional losses between the high-DC and constant viscosity cases. Two examples are shown, one in which the transition from high to low viscosity occurs near the crank angle at which boundary and hydrodynamic friction are equal (about 18^{o} ATDC), and one in which the transition occurs earlier (closer to dead-center) than this, at 12^{o} ATDC (see Figure 5-11a). Figure 5-10 shows both high-DC cases compared to the constant viscosity case, which shows the effects of the viscosity variation more clearly than comparison with the baseline. Both high-DC viscosity strategies cause boundary friction to decrease near dead-centers, with a corresponding increase in hydrodynamic friction due to the increased viscosity compared to the constant-viscosity case.

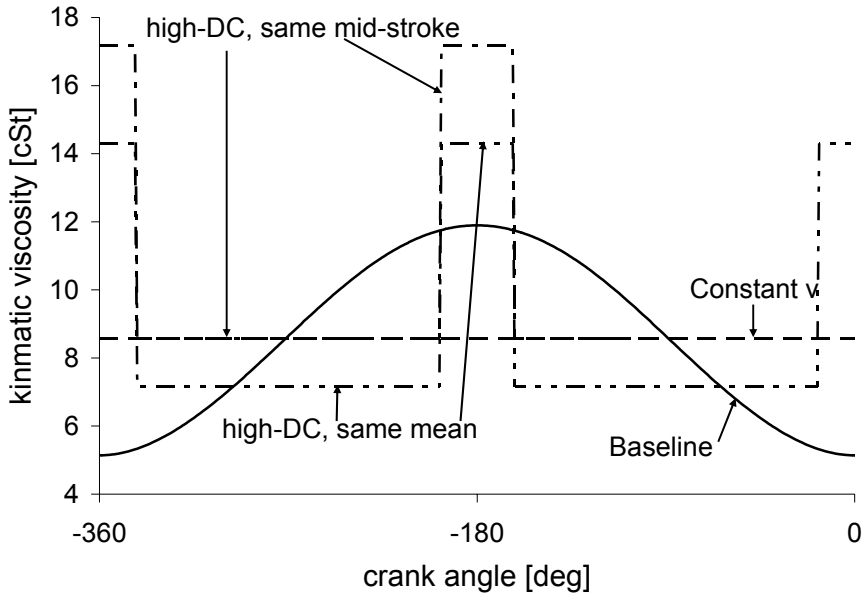

Figure 5-9: Example high-DC cases, viscosity variation during the engine cycle

Figure 5-11b shows the net result of these changes. For the 18^{o} case, there is a net reduction in friction close to dead-centers, but a net increase as the piston speed increases and hydrodynamic friction becomes important, at around 12 ^{o} ATDC, (at the beginning of the stroke only). The result is zero net change in fmep compared to the constant-viscosity case – the reduction in boundary friction and increase in hydrodynamic cancel each other. For the12 ^{o} case, there is the same net decrease in friction near the end-strokes, and the transition is timed well so that there is only a small subsequent increase in hydrodynamic friction. The result is a net decrease in fmep, compared to the constant viscosity case. However, because the net reduction in friction is so small (note that the scale on the friction axis in Figure 5-11b is magnified) and the contribution to friction power loss near dead-centers is small, this reduction is negligible. Results for both cases are summarized in Table 5-1.

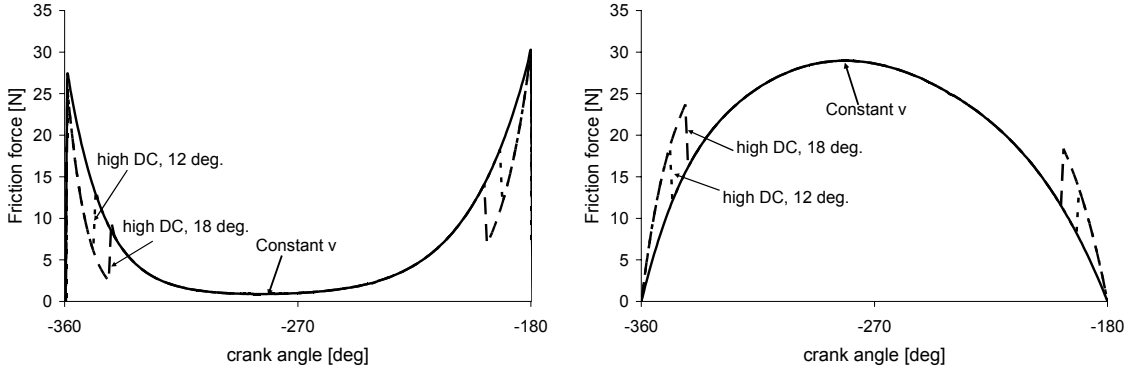

a) Boundary friction, constant viscosity and two high-DC cases, intake stroke

b) Hydrodynamic friction, constant viscosity and two high-DC cases, intake stroke

Figure 5-10: Effect of high-DC viscosity variation on hydrodynamic and boundary friction

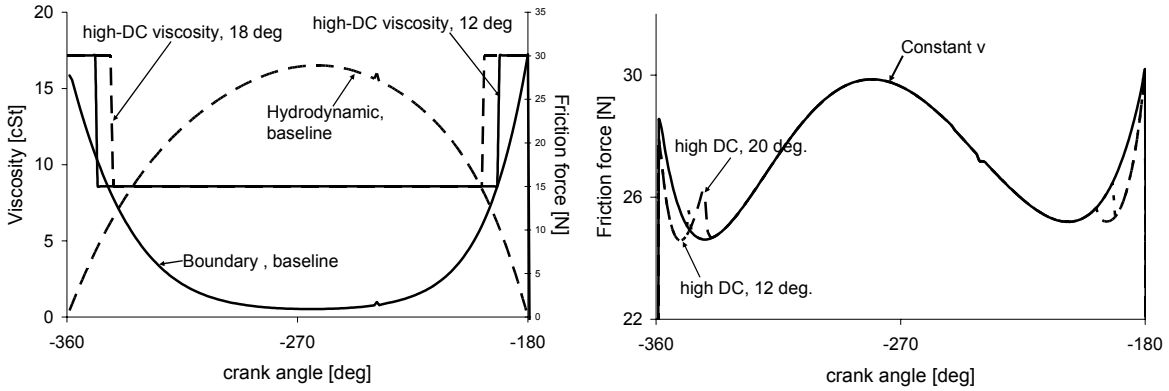

a)The transition crank angles for high-DC cases were based on the hydrodynamic/boundary transition

b) Total friction force for constant viscosity and two high-DC cases, intake stroke

Figure 5-11: Effect of high-DC viscosity on total ring/liner friction

A case in which mean, rather than dead center, viscosity was held the same as the baseline case was also considered. In the example shown in Figure 5-12, the high/low viscosity transition occurred at 18^{o} ATDC. An overall reduction in friction of ~4% from the baseline was observed for this case, but the reduction was due entirely to a decrease in mid-stroke hydrodynamic friction, and did not stem from effects in the dead-center region. The same friction reduction could have been obtained with a constant-viscosity strategy, with the constant viscosity the same as occurs the mid-stroke region of this high-DC case.

Figure 5-12 shows a comparison of the hydrodynamic, boundary, and overall friction forces for this high-DC and constant-viscosity cases. The high-DC case shows lower hydrodynamic friction near mid-stroke, as well as lower boundary friction near dead-centers, compared to the constant viscosity case, as expected based on the viscosity distribution. The high-DC case also shows higher boundary friction near mid-stroke and higher hydrodynamic friction near dead-centers, however, because there is a trade-off between the two lubrication regimes when viscosity changes. The boundary friction reduction near dead-centers is entirely offset by the increase in asperity contact near mid-stroke (see Table 5-1), while the reduction in mid-stroke hydrodynamic friction produces a net decrease in hydrodynamic losses. The net result, as shown in Figure 5-12b, is an overall friction reduction of about 4%.

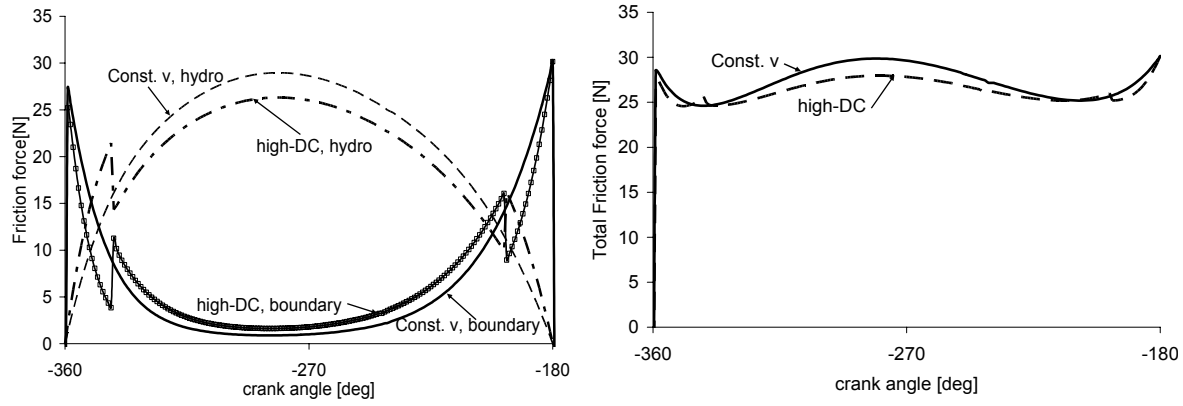

a) Hydrodynamic and boundary friction forces

b) Total friction force

Figure 5-12: Comparison of friction force in high-DC and constant viscosity cases, lower land, OCR

These examples show that, for the cases studied, controlling viscosity near dead-centers has almost no effect on total cycle friction. One reason for this is that any reduction in boundary friction near dead-centers is always at least partially offset by a corresponding increase in hydrodynamic friction. If the high/low transition is not well-placed, the increase in hydrodynamic friction may become large and result in a net increase in friction, rather than the desired decrease. If another method of reducing boundary friction – for example, with surface modifiers – can be used, and this increase in hydrodynamic friction can be avoided, a larger friction reduction benefit is possible, both at dead-centers and throughout the stroke.

Another factor leading to lack of benefit in controlling end-stroke viscosity is that the contribution to overall friction from dead-centers is only a small fraction of the total cycle losses. Although friction forces may be high, the slow piston speeds in this region keep friction power losses low. Dead-center boundary friction (where the "dead-center region" is taken as +/-18 crank-angle degrees around each ring-reversal) accounts for only a few percent of the total ring friction, as shown in Figure 5-13. Then, any friction reduction associated with reducing boundary friction here cannot exceed this relatively small amount.

Table 5-1: Effects of different viscosity variation cases on friction, constant mid-stroke viscosity

	Fmep, [kPa]	Fmep, bdy [kPa]	Fmep, hydro [kPa]	Fmep change, from baseline
Baseline	11.14	1.19	9.95	--
Constant viscosity	11.25	1.02	10.23	+1%
High–DC, same mid-stroke, 18 deg	11.25	0.88	10.34	+1%
High-DC, same mid-stroke, 12 deg	11.25	0.97	10.28	+1%
High-DC, same mean, 18 deg	10.72	1.32	9.4	-4%

5.2.3. Changing Mean Viscosity

Friction depends on both viscosity variation during the cycle and the overall mean cycle viscosity. The three viscosity variation cases (baseline, constant viscosity, and high-DC) considered above were evaluated for different mean viscosities. For the high-DC case, the dead-center viscosity was held constant, and the mid-stroke viscosity reduced. As was indicated in Figure 5-5, overall ring friction changes with viscosity, and a minimum fmep is found at a balance between hydrodynamic and boundary friction during the ring cycle. This study showed that the minimum friction loss obtainable is approximately the same for each viscosity condition.

Figure 5-14 shows the change in total cycle friction losses for the OCR for the baseline viscosity profile, with the corresponding boundary and hydrodynamic components. As the figure shows, there is the potential for an ~10% reduction in ring friction from the current baseline. This reduction results from a decrease in hydrodynamic friction in the mid-stroke region.

In Figure 5-15, the results for the three cases are compared, and plotted against mid-stroke viscosity. There is almost no difference between the three viscosity strategies for the range of viscosities studied, with the high-DC case showing a small (less than 1%) reduction in minimum friction. As in the case described in section 5.2.2, the high-DC case does provide a consistently lower boundary friction loss than the baseline case, but this is offset by a matching increase in hydrodynamic friction (see Figure 5-16). Again, it is shown that the major effect of viscosity on friction is in the mid-stroke region, and controlling dead-center viscosity has a relatively small effect.

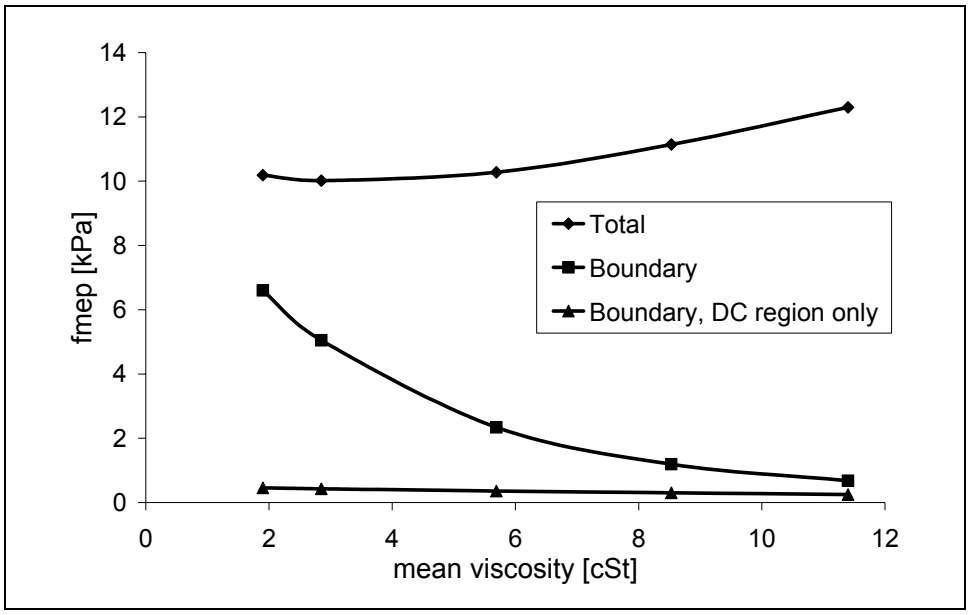

Figure 5-13: Friction forces and friction power loss, baseline viscosity

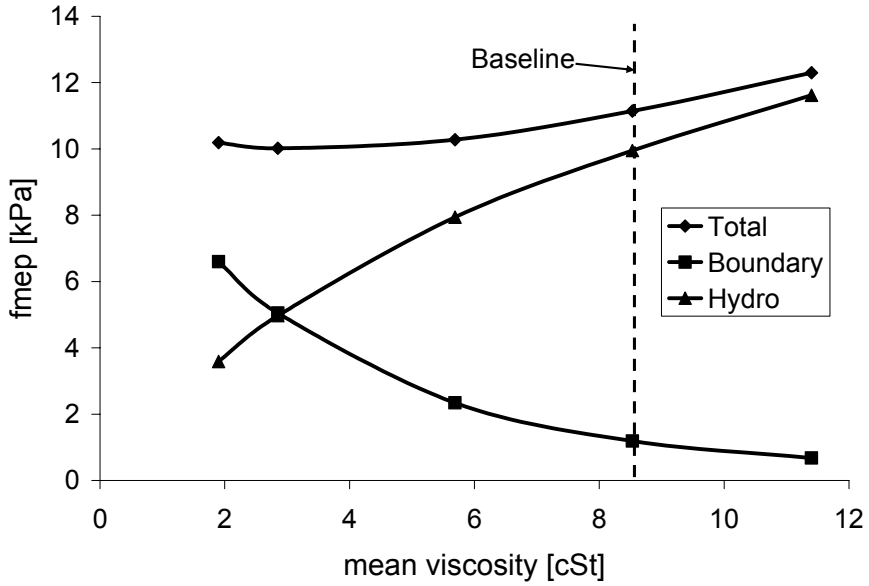

Figure 5-14: Hydrodynamic vs. boundary friction trade-off for the OCR, baseline viscosity variation

It should be noted that, although there is only a small friction benefit in controlling dead-center viscosity, there may be a wear benefit. High boundary friction is an indicator of wear. Although reducing the high friction near dead-centers may not substantially reduce frictional losses, reduction of asperity contact in this region should cause a wear reduction. A simple analysis of this possibility was performed, and is discussed briefly in section 5.6.

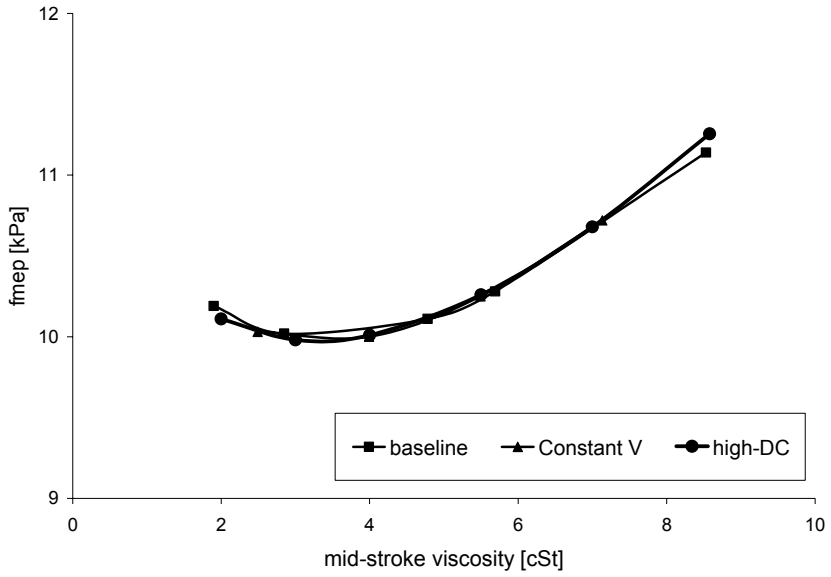

Figure 5-15: Reduction in total cycle friction with mean viscosity, three viscosity variation cases, OCR.

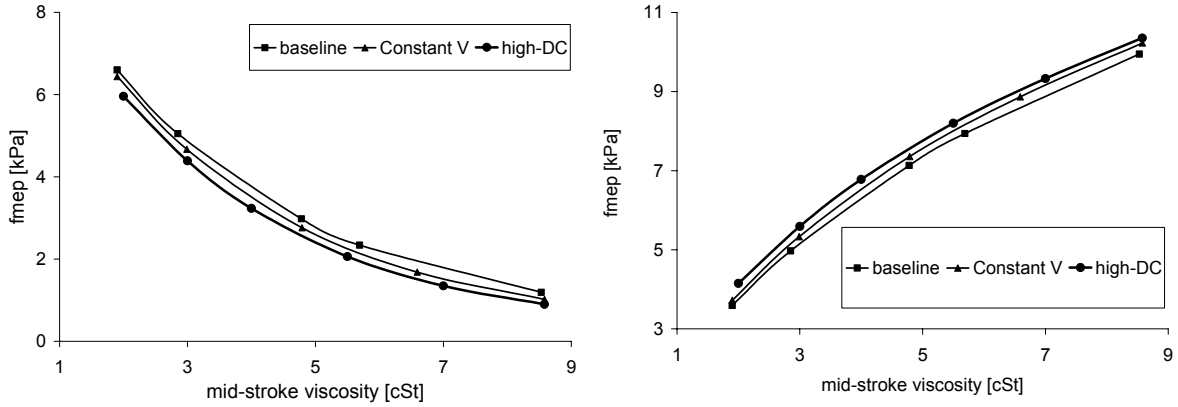

a)Fmep from boundary friction **b)Fmep from hydrodynamic friction**

Figure 5-16: Hydrodynamic and boundary contribution to total fmep, three viscosity cases

5.3. Viscosity Variation During the Engine Cycle – Real Engine Conditions

Although it is useful to study idealized conditions to evaluate viscosity control strategies and best-case scenarios, in the engine the realistic temperature and shear-rate dependence of the

lubricant viscosity must be taken into account. The effects of both temperature and shear rate parameters were studied, and results are summarized below. In the case of temperature dependence, the effects of the "steepness" of the variation – the strength of the viscosity temperature dependence – were considered. In the case of shear rate dependence, the high/low shear transition region was studied, and parameter values assigned to mimic an idealized case discussed above – high viscosity near dead centers and low near mid-stroke.

5.3.1. Lubricant viscosity parameters

The dependence of lubricant viscosity on temperature and shear rate were modeled by commonly used relationships: the Vogel equation for temperature dependence, and the Cross equation for shear rate dependence. These equations and the parameters used in them are described below.

5.3.1.1. Temperature Dependence

Because the oil film is very thin, the temperature across the film (in the radial direction) is assumed to be constant. Then, for each axial lubricant element, the viscosity is assumed to be constant across the film thickness and dependent on the oil temperature, as described by the Vogel equation:

$$\nu = z \cdot e^{\left(\frac{T_1}{T_2+T}\right)} \tag{5.1}$$

where ν is the kinematic viscosity of the lubricant, z is an oil "thickness" parameter, T_1 is an overall temperature-viscosity dependence parameter, T_2 is a lower bound parameter that is related to the glass transition temperature of the lubricant, and T is the lubricant temperature. Increasing T_1 increases the change in viscosity for a given temperature change, while increasing T_2 has the opposite effect. For a small T_1 or large T_2, the viscosity can become virtually independent of temperature.

To evaluate the effect of the strength of the viscosity-temperature relationship, lubricants with several values of T_1 were compared (while z was changed accordingly to keep mid-stroke viscosity constant). Figure 5-17 shows viscosity as a function of temperature for a few of the T_1 values studied. The liner temperatures at TDC for the top ring and BDC for the OCR are shown. A square-root distribution is assumed for the liner, bounded between these two temperatures.

5.3.1.1. Shear-Rate Dependence

The large temperature variations in the internal combustion engine cause large variations in viscosity, as shown in Figure 5-17. Viscosity index improvers (VII's), are added to many engine lubricants to decrease this dependence of viscosity on temperature. A side effect of such additives is to cause shear thinning in the lubricant – the viscosity becomes dependent on the oil shear rate, where high shear rates cause the oil viscosity to be reduced.

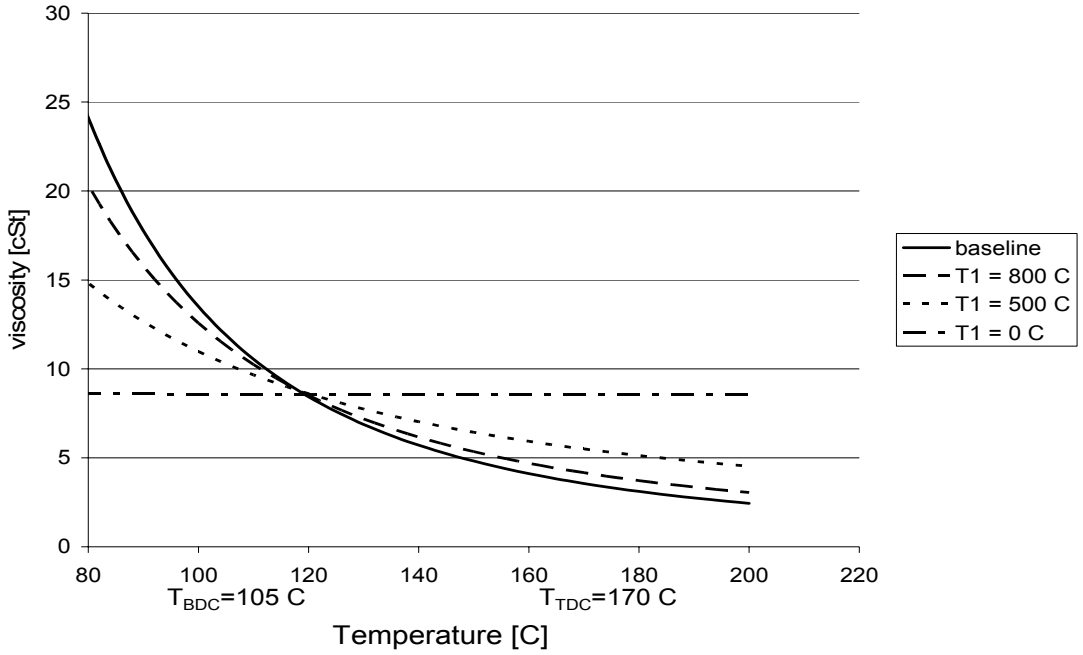

Figure 5-17: Examples of viscosity variation with temperature.

The Cross relationship was used to model the dependence of viscosity on shear rate:

$$\nu = \nu_0 \frac{1 + \frac{\nu_\infty}{\nu_0}\left(\frac{\gamma}{\beta}\right)^m}{1 + \left(\frac{\gamma}{\beta}\right)^m} \tag{5.2}$$

where ν_0 is the low shear viscosity (obtained from the Vogel equation, above), ν_∞/ν_0 is the ratio of high shear viscosity to low shear viscosity, γ is the lubricant shear rate, m is a parameter governing the width of the low shear-high shear transition region, and

$$\beta = 10^{c_1 + c_2 T} \tag{5.3}$$

is the critical shear rate, which controls the shear rate at which the low shear/high shear transition occurs (c_1 and c_2 are parameters controlling β). Figure 5-18 shows several typical viscosity-shear rate relationships that were used for the current study, with parameters given in

Table 5-2 (in section 5.3.3).

For very low and very high shear, viscosity is approximately constant. A transition region, whose width is determined by the parameter m and whose location is determined by β, the critical shear rate, separates the high and low shear regions. In the case of piston rings, the lubricant between ring and liner generally experiences a higher shear rate than the critical shear rate for almost the entire cycle, with the exception of a few crank angles near dead centers. Then, the lubricant is essentially dependent only on temperature. The value of the critical shear rate was adjusted in this study, to assess the effects of having the transition occur during the ring stroke.

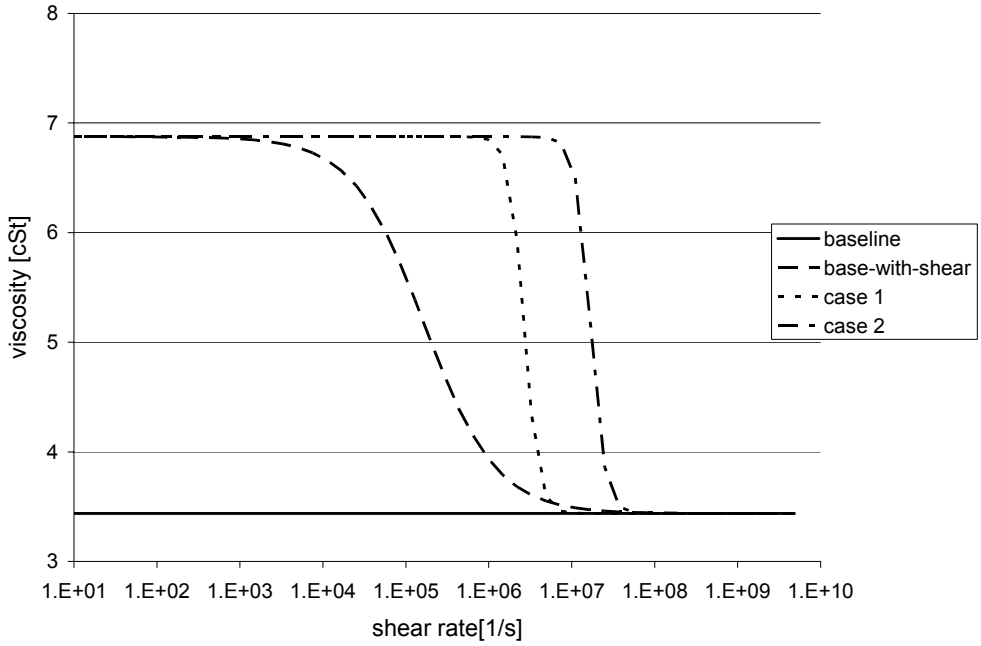

Figure 5-18: Viscosity variation with shear rate, for cases studied

5.3.2. Temperature Dependence - OCR

The parameter T_1 was varied in order to vary the degree to which viscosity changes with changing temperature, while z was also changed proportionally, in order to maintain a constant average viscosity for the cycle. For all of the cases studied, the mean viscosity occurred near mid-stroke, so maintaining a constant mid-stroke viscosity was equivalent to maintaining a constant mean, with the amount of viscosity variation between TDC and BDC varying between cases. A range from a high temperature dependence to no dependence ($T_1 \sim 0$) was considered. Figure 5-19 shows the lubricant temperature change for an engine cycle, and the corresponding cycle lubricant viscosities for each case.

For each case considered, the viscosity variation is close to symmetric about mid-stroke – that is, it is low on one side (either the beginning or end of the stroke), passes through mid-stroke at close to the mean viscosity, then is high on the other, as shown in Figure 5-19b. This is the same phenomenon that was described in the ideal, constant-viscosity case studied in section 5.2.1. As in that case, the resulting change in friction is small, because the friction changes due to changing viscosity during each half of the stroke largely cancel each other out.

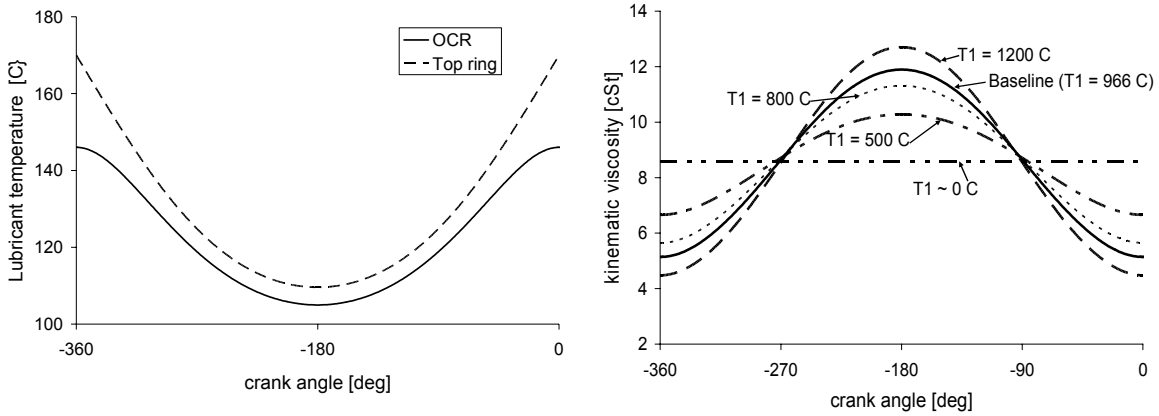

a) Temperature variation of oil film in the engine

b) Variation of viscosity for an engine cycle, 2 strokes

Figure 5-19: Variation of viscosity during an engine cycle for test cases considered

Simulations were run considering the different temperature-dependence cases at different mid-stroke viscosity values. An example of a group of profiles with different mean viscosities, with temperature dependency $T_1 = 800^o$ C, is shown in Figure 5-20. Figure 5-20 shows the results of the study – almost no difference in fmep values is seen between the cases. Cases with low T_1 (relatively "flat" profile) showed slightly higher friction at high viscosities, due to a slight increase in hydrodynamic friction, but for the most part all of the cases gave the same friction for the viscosity range studied. This is again due to the effect illustrated in Figure 5-8, section 5.2.1, which indicates that friction generation over a cycle remains approximately constant, for the types of viscosity variations studied here, as long as the variation is symmetric about mid-stroke.

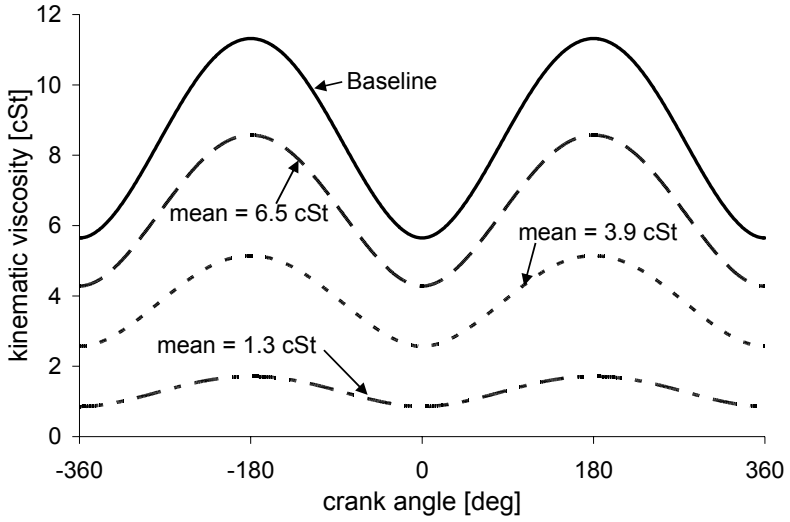

Figure 5-20: Viscosity variation during the engine cycle for changing mean viscosity, T_1 = 800C

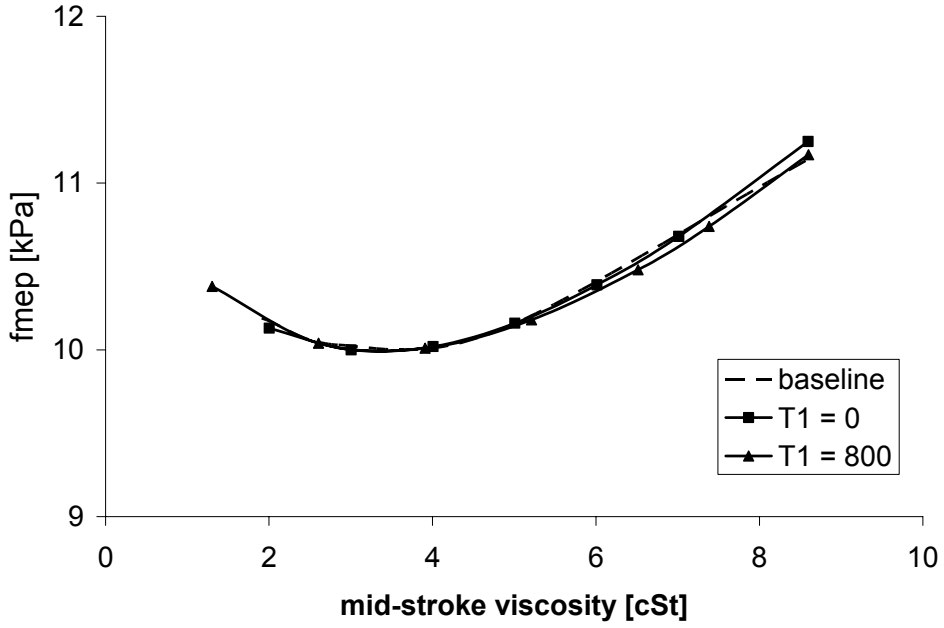

Figure 5-21: Dependence of fmep on mean/mid-stroke viscosity, different temperature dependence cases

5.3.3. Shear Rate Dependence – OCR

In addition to being dependent on temperature, the viscosities of many lubricants are also dependent on the shear rates experienced by the oil. In this study, the critical shear rate and transition region were controlled to study the effects of viscosity transitions taking place during the stroke. This is a method by which to approximate the idealized cases described above, where viscosity can be held high near dead-centers and low near mid-strokes (although the temperature dependence is still present). As is shown below, the results of this study are similar to those of

the idealized case – friction benefits are relatively small – but the reduction in minimum friction that is achieved is slightly larger than in the idealized case, of ~1% below the baseline value.

Many sets of Cross equation parameters were studied, and several examples are presented. The parameters for these examples are given in

Table 5-2, and variation in viscosity during an engine cycle corresponding to the cases presented is shown in Figure 5-22b. As is shown in the figure, the effect of controlling the Cross equation parameters in this manner is to keep viscosity high near dead-centers and lower near mid-stroke, where the temperature dependency of the viscosity (which was kept at the baseline value) also contributes to the variation. The two cases 1 and 2 demonstrate the effects of changing the width of the high-viscosity region.

As in the idealized case, keeping viscosity high near dead centers causes a decrease in boundary friction there, with a corresponding increase in hydrodynamic friction, as is shown in Figure 5-23. When the mid-stroke viscosity is matched with the baseline case, the case 1 viscosity distribution shows a slight reduction in friction, while case 2 shows a slight increase. This is related to the hydrodynamic/boundary friction balance in the engine cycle. In baseline conditions, the high/low viscosity transition for case 2 occurs relatively late in the stroke, in a region where hydrodynamic lubrication accounts for a large fraction of the total ring/liner friction. Then, the effect of the high viscosity is to increase the already high hydrodynamic friction. For case 1, the high viscosity period remains within a zone where boundary friction is dominant, so that the reduction in boundary friction is slightly higher than the increase in hydrodynamic friction.

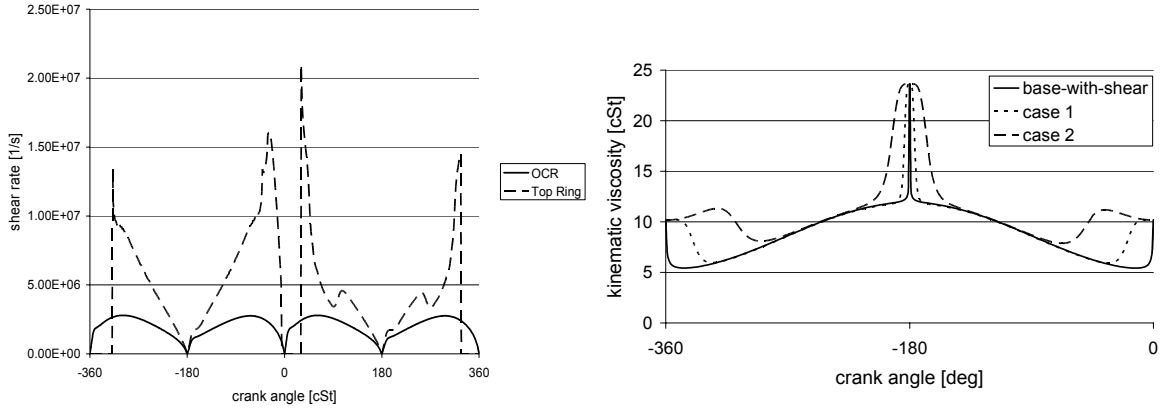

a) shear rate variation during an engine cycle **b) viscosity change during 2 strokes, studied cases**

Figure 5-22: Shear rate variation and viscosity (shear-rate dependent) variation during an engine cycle

As overall viscosity changes, the hydrodynamic/boundary friction balance in the engine cycle changes. In particular, as viscosity is decreased, hydrodynamic lubrication becomes less effective and boundary friction increases. The zone around dead-centers where boundary friction is dominant extends farther toward mid-stroke, and contributes more to total friction losses because it extends into a zone where piston speed is increased. Then, a larger high-viscosity zone, such as occurs in case 2, provides more benefit. This is shown in Figure 5-25,

which shows the effect of changing mid-stroke viscosity on ring friction, for the cases considered. It also explains why no friction benefit is observed in the idealized case at low viscosity – the width of the high-viscosity region in the idealized case is not large enough to provide much friction reduction, because it remains within the low-speed, dead-center region.

Table 5-2: Cross equation parameters for three cases studied

Case	m	$\nu_{high\text{-}shear}/\nu_{low\text{-}shear}$	c_1	c_2	ν_∞/ν_0
baseline with shear*	1	.5	2.3	.0225	0.5
case 1	5	.5	3.8	.0225	0.5
case 2	5	.5	4.3	.0225	0.5

*** 1 This case uses all baseline Cross equation parameters except ν_∞/ν_0=0.5, which adds shear dependence to the baseline case, which is a straight-weight oil.**

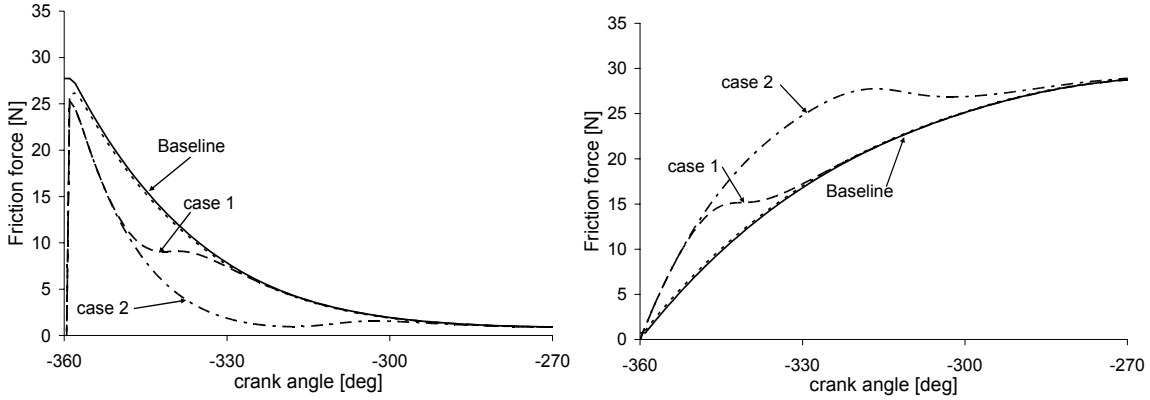

a)Boundary friction near TDC, intake, cases 1 and 2 **b)Hydrodynamic friction near TDC, intake, cases 1 and 2**

Figure 5-23: Hydrodynamic and boundary friction effects in cases 1 and 2

It should be noted that, in Figure 5-25, the ratio of high-shear to low-shear viscosities is not kept constant as mean viscosity changes. This is because, as mean viscosity is reduced, the magnitude of the low-shear viscosity (the high viscosity at dead-centers) decreases, as shown in Figure 5-24a. To counter this decrease and keep dead-center viscosity approximately constant, the high:low viscosity ratio was changed with mean viscosity - example of this are shown in Figure 5-24b.

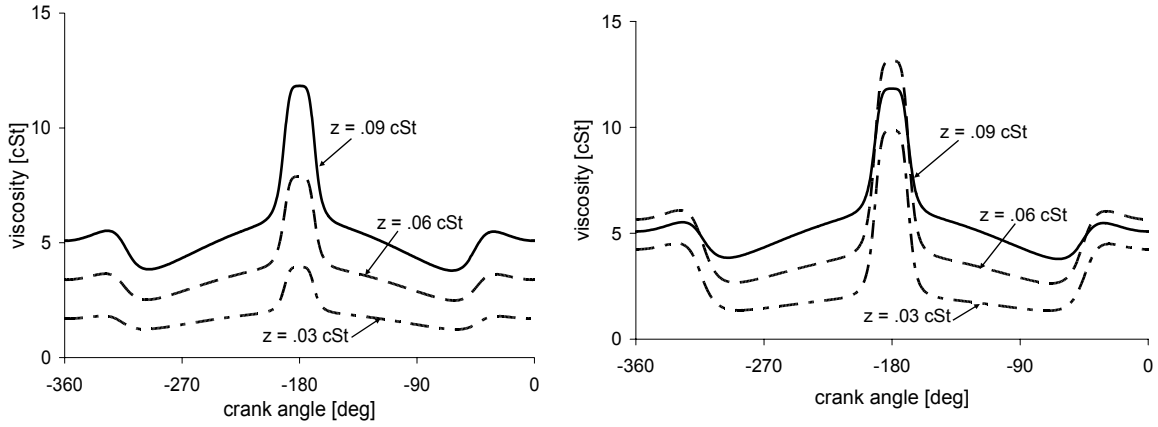

a) High/low shear viscosity ratio kept constant

b)High/low shear viscosity ratio set to maximize friction reduction for a given z value.

Figure 5-24: Viscosity variation during the engine cycle, case 2

Figure 5-25 shows the effects of changing mean viscosity for the cases considered, with the high/low shear viscosity ratio optimized for low friction, at a given mid-stroke viscosity. The figure shows that there is a small friction benefit of ~1% using case 2 parameters. Simply reducing mean viscosity can reduce cycle friction by about 10%, if viscosity variation is controlled in the manner described here, a reduction of ~11% may be possible, from the current baseline oil.

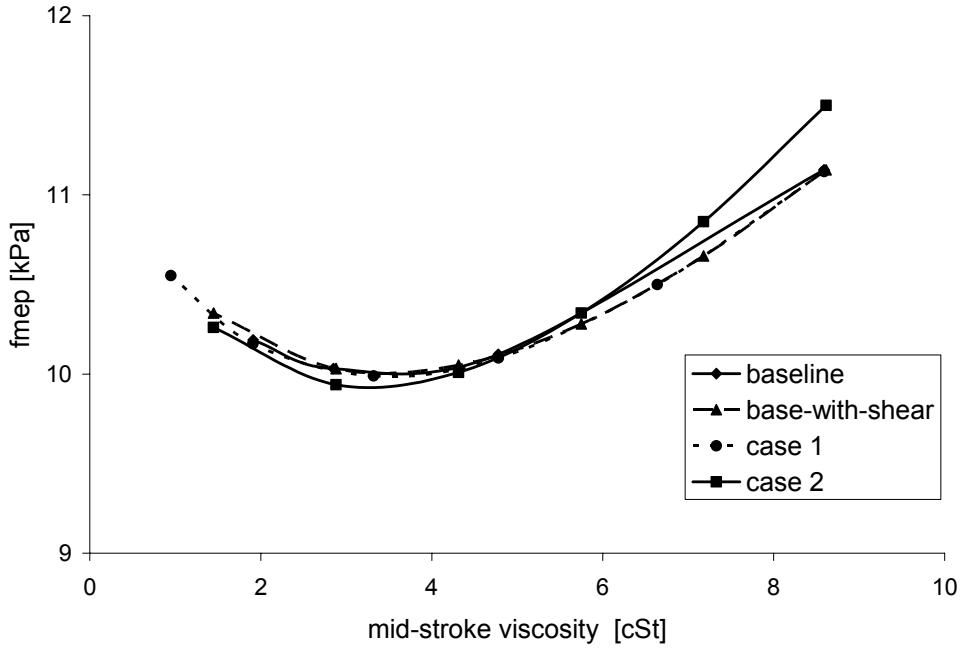

Figure 5-25: Dependence of OCR friction losses on mid-stroke viscosity, for different shear-rate dependence cases

Because their benefits are dependent on reducing dead-center boundary friction, which is only a small contributor to overall friction, the friction reductions offered by controlling viscosity

temperature and shear dependence are small. Still, some benefit may be gained, and, as discussed in section 5.6, there may also be a benefit in wear reduction in keeping dead-center viscosity high.

5.4. Top Ring - Dry Region

The top ring experiences pure hydrodynamic lubrication during most of the stroke, but is subject to a large "spike" of boundary friction near TDC combustion, as shown in Figure 5-26. This spike is caused by a combination of factors: very high post-combustion gas pressures and temperatures, slow piston speed and poor lubrication. Lubricant availability is very poor near TDC because the oil control ring does not reach this area, so the region is lubricated only by oil that is scraped up by the compression and scraper rings. Because of the very harsh conditions, this "dry region" is the site not only of high friction generation but also of high ring/liner wear and possible scuffing failure. It contributes the majority of top ring friction, and approximately 30% of total ring pack friction (see Figure 3-2).

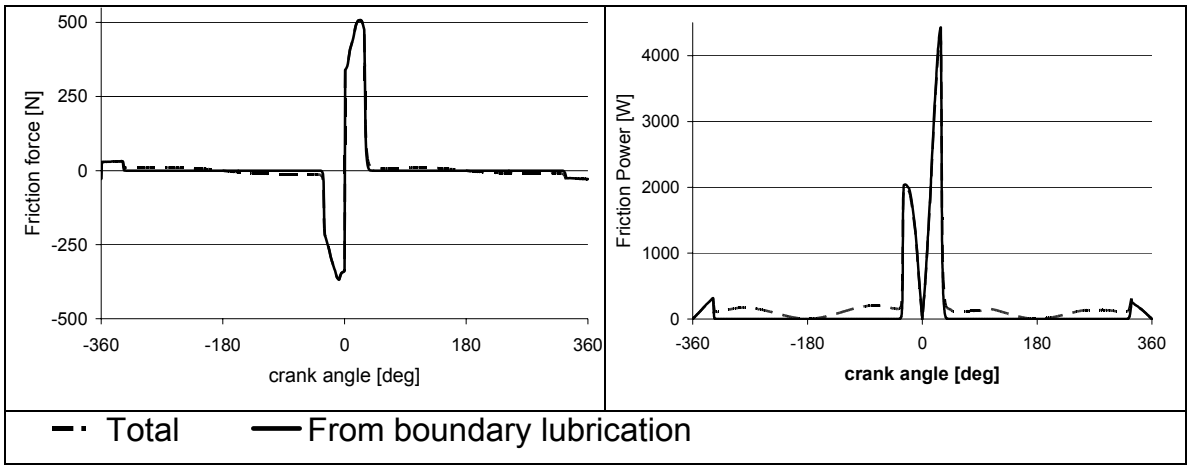

Figure 5-26: Top ring friction force (left) and friction power loss (right) for an engine cycle

Lubricant viscosity does not have a direct affect on top ring/liner friction, because full boundary lubrication occurs there, and the frictional losses are affected only by the boundary friction coefficient. However, the lubricant viscosity may affect this region indirectly, by influencing the size of the poorly lubricated zone. As is shown in Figure 5-27a, simulations show that oil availability in the dry region is greater for thinner lubricants. The result is less asperity contact and a smaller "spike" of high ring/liner force, as shown in Figure 5-27b.

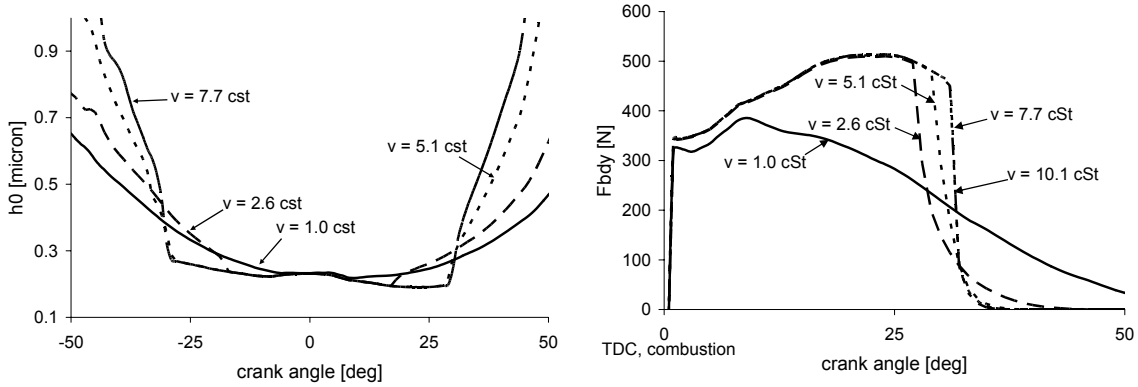

a)Minimum film thickness, h0, near TDC combustion **b)Boundary friction near TDC combustion (0 deg)**

Figure 5-27: Dry region width increases with lubricant viscosity, for the top ring

Figure 5-27a shows the change in dry-region width with oil viscosity, for an idealized case where viscosity is constant throughout the cycle. As the figure shows, the dry region (the relatively flat region, between the sharp drop and subsequent sharp rise in film thickness) increases in width as viscosity increases, approaching a maximum. For very low viscosity (ν = 1 cSt) there is almost no dry width. For viscosities greater than ν~5 cSt, there is very little change in dry region width – a maximum dry width and maximum boundary friction have been reached. Between these values, the size of the un-wetted region increases with lubricant viscosity. This corresponds to the boundary friction force shown in Figure 5-27b. For the lowest viscosity case, the "spike" barely appears and is replaced by a region of gradually decreasing boundary friction. As viscosity increases, the width of the boundary friction "spike" increases with the viscosity until it reaches a maximum.

These results indicate that thinner oils are upscraped into the dry zone more easily than thicker oils, although the details of the mechanism are not well-understood. It is not clear that this is a real effect – simulations may show this effect because of underlying assumptions or simplifications that have not been considered. Also, other studies have shown the opposite trend– an increase in dry-region wetting with higher viscosity. More research is required to determine the extent of viscosity effects on dry region width. Some possible lubricant effects are illustrated in Figure 5-28.

Figure 5-28 illustrates some effects of lubricant viscosity on oil upscraping by the top ring. The extent of the upscraping depends on lubricant availability on the liner before the dry region and the ring/liner clearance, as well as other factors such as the ring load. For thinner lubricants, the distance between ring and liner is smaller, because low viscosity oils create thinner hydrodynamic films in response to ring load (this is illustrated in Figure 5-28b, where h_0 can be used as an indicator of ring/liner clearance). This encourages upscraping. However, there is also less available lubricant for thinner oils, for the same reason – the smaller clearance causes more oil to be scraped down the liner on down-strokes. The balance between these two factors plays a part in determining how much oil is scraped up the liner. Many factors also contribute to oil transport, including oil travel along the piston lands and pumping by the rings.

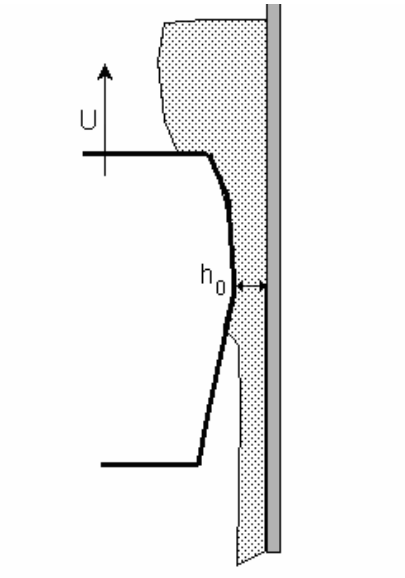

a) upscraping by top ring

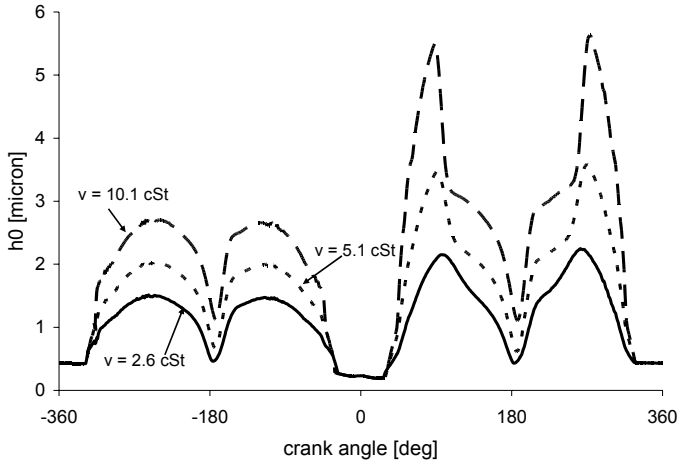

b) ring-liner separation increases with lubricant viscosity (units are cSt)

Figure 5-28: Lubricant upscraping mechanism

The total cycle friction losses for the top ring depend on both transport of oil into the dry region and the ability of the oil to support hydrodynamic lubrication in the rest of the stroke. In Figure 5-29, a minimum fmep, corresponding to a minimum boundary friction, is found at a low viscosity. This viscosity balances between allowing more oil to be transported into the dry region, reducing friction there, but making asperity contact more likely during the rest of the stroke. This is illustrated in Figure 5-27b – for the lowest viscosity of 1cSt, the height of the dry region "spike" is decreased, but its width is increased. The very low viscosity oil was transported into the dry region, but then was too thin to support hydrodynamic lubrication for the entire stroke outside of the dry region. At higher viscosities, boundary friction remains approximately constant with viscosity, consistent with Figure 5-27 (dry region width stays constant), while hydrodynamic friction increases with viscosity, leading to an overall increase in friction.

Comparing Figure 5-29 to Figure 5-14, for the oil control ring, the minimum frictional losses for the two rings occur at approximately the same viscosity. Then, an additional benefit in reduction of top ring friction may occur if viscosity is reduced to this value. A reduction in top ring friction of ~ 30% is possible, which corresponds to a ring-pack friction reduction of ~ 9%. However, increasing oil upscraping may increase oil consumption, which must also be considered in the total engine design. Also, it is not clear whether this is a real benefit, or only appears due to model assumptions or simplifications. More research is required to assess this possibility.

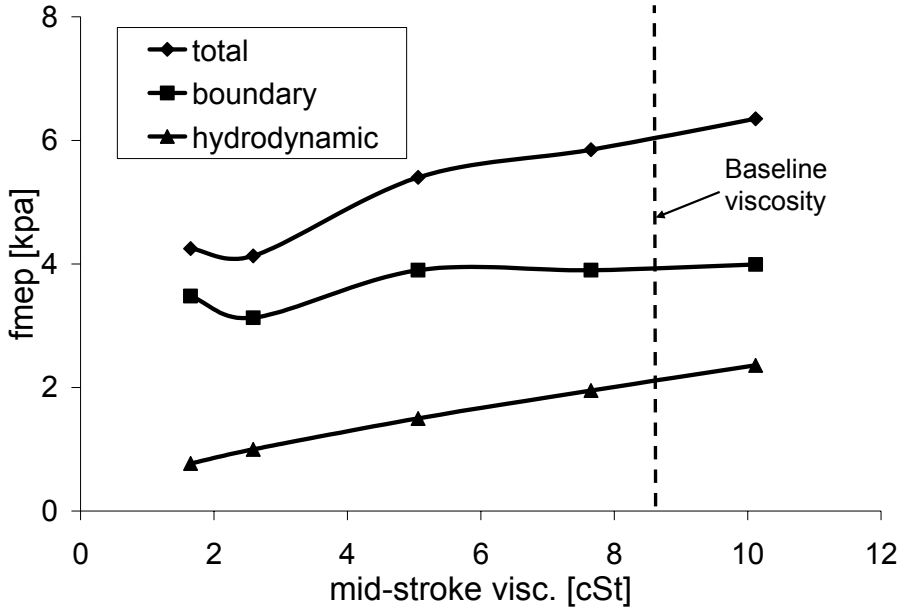

Figure 5-29: Dependence of top ring friction on lubricant viscosity, baseline viscosity case

5.5. Other lubricant properties: Boundary friction coefficient

If ring/liner boundary friction coefficient can be decreased - for example, with surface-modifying lubricant additives - a large friction benefit is possible. Decreasing boundary friction coefficient, f_b, reduces ring/liner friction both directly, by reducing friction due to asperity contact, and indirectly, by allowing lubricant viscosity to be reduced and thus reducing hydrodynamic friction as well. The latter effect occurs because changing f_b alters the balance between hydrodynamic and boundary friction for the ring and liner - a low friction coefficient allows viscosity to be reduced without incurring a large friction penalty because of the increased asperity contact. The lower f_b becomes, the lower the viscosity can become before the corresponding increase in asperity contact - and thus boundary friction - out-balances the reduction in hydrodynamic friction that resulted from the viscosity reduction. This is illustrated in Figure 5-30, which shows the dependence of total ring-pack fmep on boundary friction coefficient for different lubricant viscosities (baseline viscosity-temperature dependence).

As is shown in the figure, at a given viscosity, reducing f_b causes a reduction in total friction - this results from the direct reduction of boundary friction with decreasing friction coefficient that is shown in Figure 5-30b. Also, the viscosity at which the minimum frictional loss occurs decreases with f_b, as does the minimum friction - this is a result of the effect of f_b on the hydrodynamic/boundary friction balance. Reducing boundary friction coefficient has a dual effect on ring/liner friction - it both reduces boundary friction and allows a lower viscosity lubricant to be used, thus reducing hydrodynamic friction – and thus can have a substantial, beneficial effect on overall ring-pack friction.

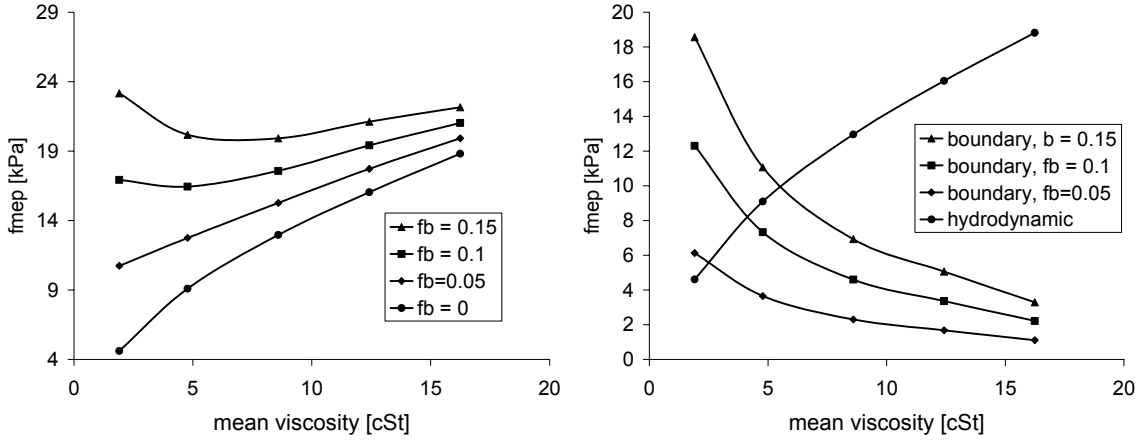

a)Total ring pack friction losses **b) Boundary and hydrodynamic ring-pack losses**

Figure 5-30: Effect of boundary friction coefficient on total ring-pack friction

5.6. Other Considerations: Wear

In addition to frictional losses, wear of the rings and liner must also be taken into account when designing an optimized lubricant. Ring/liner wear leads to leakage of combustion gases out of the engine cylinder ("blow-by") and a corresponding reduction in efficiency and increase in engine emissions. Limiting this degradation of engine performance, and avoiding the need to service and replace parts, requires that ring/liner wear be controlled.

The actual wear of the ring and liner is a complicated and not well-understood phenomenon, and actual wear predictions have not been made in this study. Instead, a factor is calculated, which takes into account two main contributors to wear: asperity contact pressure and sliding distance. The wear factor presented is a mean factor for an engine stroke, and is calculated as the integral of the contact pressure multiplied by the piston speed, integrated over the stroke distance.

The wear factor increases as mean lubricant viscosity is reduced, as is shown in Figure 5-31a, because the amount of asperity contact occurring increases. Figure 5-31b shows that the wear increases strongly even as frictional losses remain low – the minimum fmep is found at a viscosity corresponding to a high wear rate. Then, choosing an ideal lubricant viscosity represents a balance between friction and wear considerations – the desire for low friction must be balanced against a need for low wear.

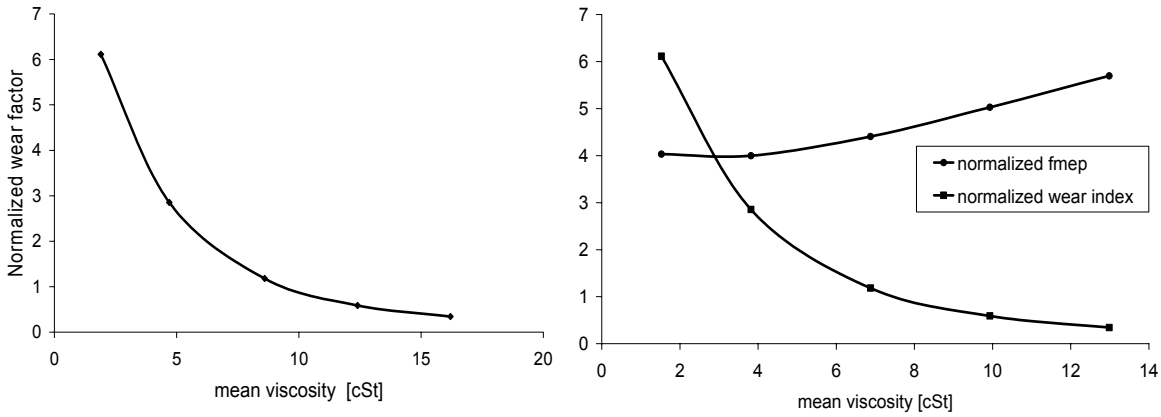

a) Wear increases as viscosity decreases

b) Minimum friction occurs at a large wear factor

Figure 5-31: Effect of lubricant viscosity on friction and wear parameter

It is possible to decrease wear slightly by controlling the viscosity change during the engine cycle, as is shown in Figure 5-32, where the baseline case is compared to a constant-viscosity case and the controlled shear-dependence "case 2", described in section 5.3.3. Maintaining high viscosity near dead-centers can reduce asperity contact in the end-stroke regions, decreasing wear. Figure 5-32a shows that, for a given ring friction loss, the viscosity-shear rate relationship "case 2" shows the lowest wear rate (or, similarly, for a given wear rate case 2 gives the lowest friction). This is because this case maintains the highest dead-center viscosity, and so allows the least asperity contact to occur during the stroke, as shown in Figure 5-32b. In Figure 5-32b, instantaneous wear parameter is shown for the three viscosity cases at the same fmep, which is the baseline fmep = 11.14 kPa.

5.7.Ring Properties: Ring Tension and Surface Roughness

The ring lubrication studies presented above all used the same ring and liner parameters, including ring tension, surface roughness, etc., which are the parameters of the current, baseline set-up of the Waukesha engine and are given in Table 5-3. For a different set of engine parameters viscosity effects may be different - the interaction between the lubricant, engine properties and engine running conditions may change as parameters are varied. To illustrate some of these cross-coupling effects a study of the interaction of two important ring parameters - tension and surface roughness - with lubricant changes is presented. In these studies, the realistic temperature and shear-rate dependencies of the lubricant viscosity are used, as described in section 5.3. Table 5-3 summarizes the range of ring factors considered, including lubricant properties.

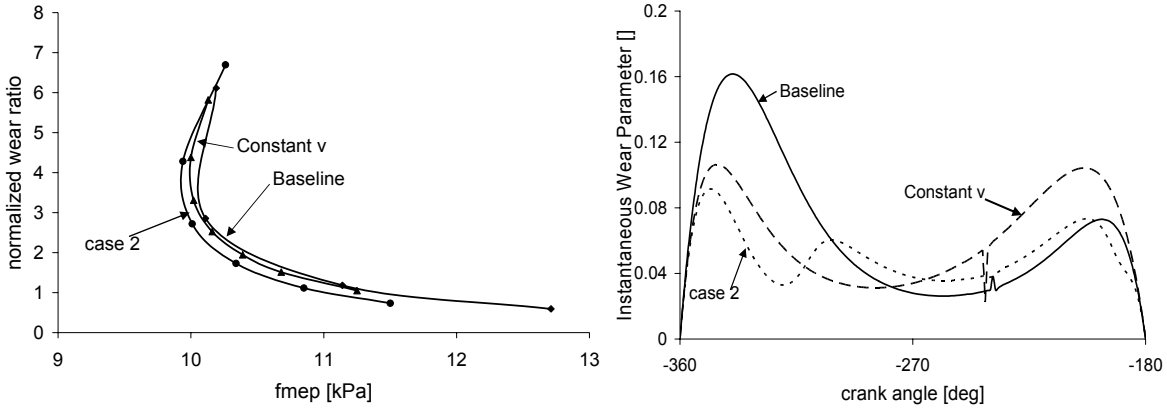

a) Overall cycle wear parameter vs. overall cycle friction losses **b) Instantaneous wear parameter, intake stroke**

Figure 5-32: Changing temperature and shear properties of the lubricant can reduce wear at a given fmep

Table 5-3: Ranges of ring parameters considered

Parameter	Range	Baseline value	Unit
Ring tension	81-40	81	N
Ring surface roughness, R_q	0.05 – 0.2	0.1	micron
Boundary friction coefficient, ring/liner	0.05 – 0.15	0.1	-
T_1, Vogel equation (controls T dependence)	0 - 1200	965.76	^oC
c_1, Cross equation (controls critical shear rate)	2.3 – 4.3	2.3	-
μ/μ_0, Cross equation (controls high/low viscosity ratio)	1-.1	1	-

5.7.1. Ring Tension

The ring tension is one factor that controls the balance between hydrodynamic and boundary lubrication between the ring and liner. For a given viscosity (and sliding speed), as ring tension is reduced asperity contact decreases. Regions of the ring stroke that experience mixed lubrication at high ring tension may experience pure hydrodynamic lubrication at lower tension (see Figure 5-33a). Also, the ring tension can affect the lubricant viscosity, if it is dependent on shear-rate, as shown in Figure 5-33b. A lubricant that is optimized to balance hydrodynamic and boundary contributions to ring friction must take these effects into account.

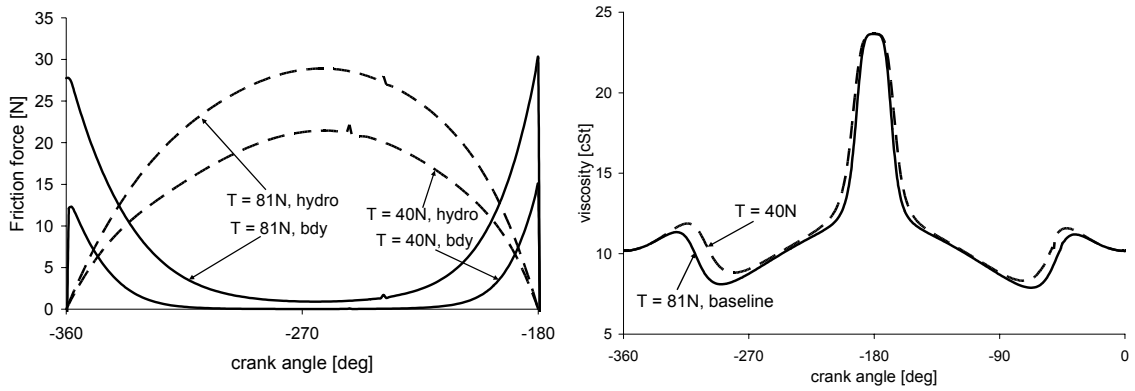

a) Lower ring tension leads to reduced asperity contact and a larger hydrodynamic region

b) Shear rate in the oil depends on ring tension, so lubricant viscosity does as well

Figure 5-33: The lubrication regime of the ring depends on ring tension

The interaction between ring tension and lubricant viscosity is illustrated using the example of the "case 2" viscosity distribution, which is described in section 5.3.2. For this case, the shear-dependence of the viscosity is controlled to produce high viscosity near dead-centers and low viscosity near mid-stroke. The high/low viscosity transition point is matched to the transition between the high boundary friction near dead-centers and high hydrodynamic friction near mid-stroke, for the baseline ring tension of T=81N. When the ring tension is reduced, the case 2 transition point is no longer well-matched to the lubrication regime of the ring.

Figure 5-33a shows that for a ring tension of 40N only a small amount of asperity contact occurs, very close to dead-centers. For the case 2 viscosity distribution, viscosity is still held high outside of this region, because it was intended to apply to a higher tension ring that experienced more asperity contact. In addition to this, as is shown in Figure 5-33b, the high/low viscosity transition occurs even later for the reduced tension ring, because shear rates in the oil are lower. The result of these effects is an increase in friction, compared to the baseline case, because of increased hydrodynamic friction. This is shown in Figure 5-34. For high mid-stroke viscosities (viscosities that are high enough to maintain hydrodynamic lubrication at mid-stroke), the case 2 viscosity distribution gives higher friction than the baseline. As ring tension is decreased, the increase in friction due to the case 2 distribution increases.

Figure 5-34 also indicates that as ring tension is reduced the benefits of using the case 2 strategy at low viscosities are reduced. For T = 40N, the baseline and case2 fmep value are almost the same, for mid-stroke viscosity less than 4cSt. This is because the friction benefit of the case 2 viscosity distribution lies in reducing dead-center boundary friction, and, as ring tension is reduced, boundary friction also decreases. For low ring tensions there is very little benefit to reducing dead-center boundary friction, because the high-boundary region is small and occurs only where piston speeds are low.

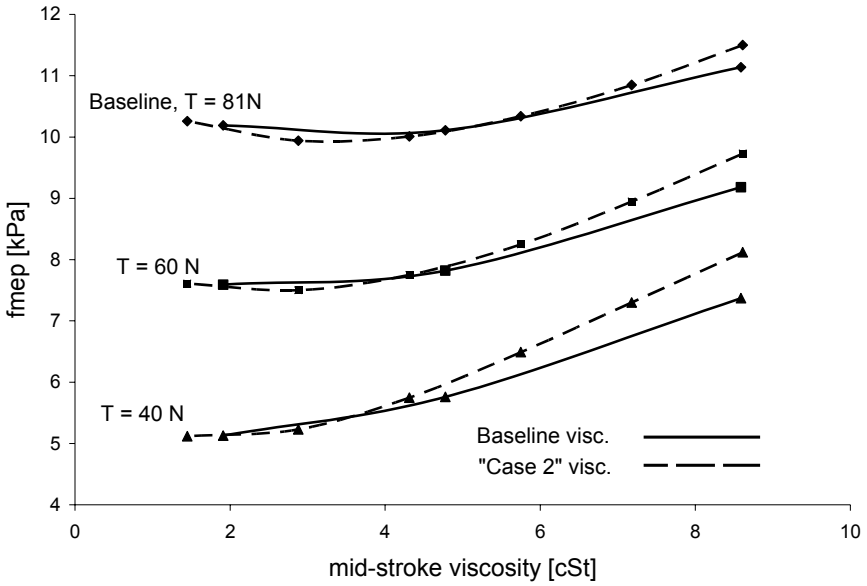

Figure 5-34: Interaction of ring tension and viscosity effects, comparing baseline and "case 2" viscosity distributions

5.7.2. Surface Roughness

Ring friction has a more complicated dependence on surface roughness than on ring tension. Friction may increase or decrease with surface roughness, because roughness (described here by the standard deviation of the surface mean height) affects both asperity contact and hydrodynamic lubrication. For a rougher surface asperities are larger, and so asperity contact occurs at a larger film thickness. Then boundary friction tends to increase with roughness, as shown in Figure 5-35a. However, hydrodynamic friction tends to decrease with roughness, as shown in Figure 5-35b, because of the effect of the surface texture on oil flow and hydrodynamic pressure generation. In general friction tends to increase with ring roughness, but in the region near the baseline roughness of the Waukesha engine, R = 0.1μ, the opposing hydrodynamic and boundary effects make the influence of the roughness less clear. In Figure 5-36 and Figure 5-37, it should be noted that ring friction is lowest for the mid-range roughness R = 0.1μ, and both the less rough and the more rough cases exhibit higher friction.

The constant viscosity and "case 2" viscosity cases are compared to the baseline case, for different roughnesses, in Figure 5-36 and Figure 5-37. Both figures show that for the roughest case, R=0.2μ, viscosity effects are the weakest. This may be because the large asperities prevent a substantial reduction in boundary friction from occurring, negating any benefits from the constant viscosity and "case 2" cases. For the two lower roughness cases, the results are similar. A small reduction in minimum friction is observed for both the constant viscosity and case 2 distributions, while friction is slightly larger at higher viscosities. It appears that a large roughness can negate the benefits of controlling viscosity variation during the cycle (for the cases considered), but for baseline and lower roughness, there is little lubricant/roughness interaction.

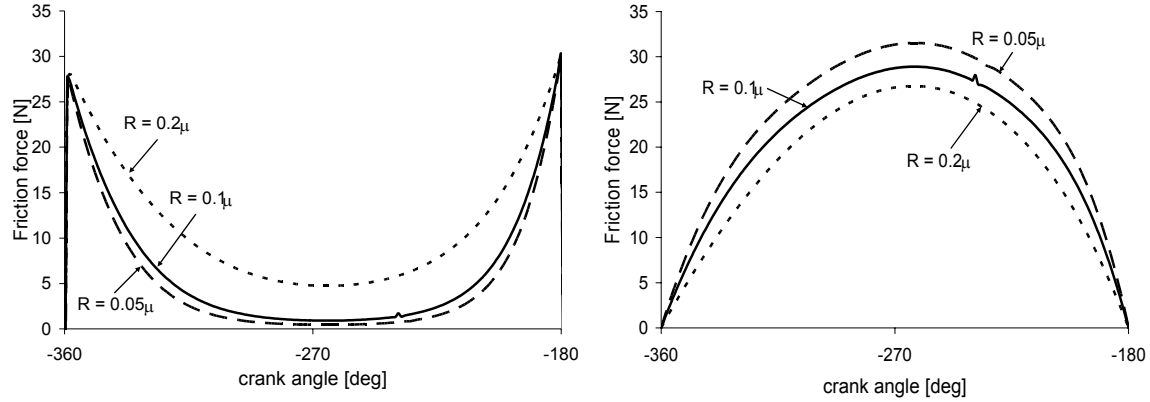

a) Boundary friction **b)Hydrodynamic friction**

Figure 5-35: Effect of ring surface roughness on friction, intake stroke

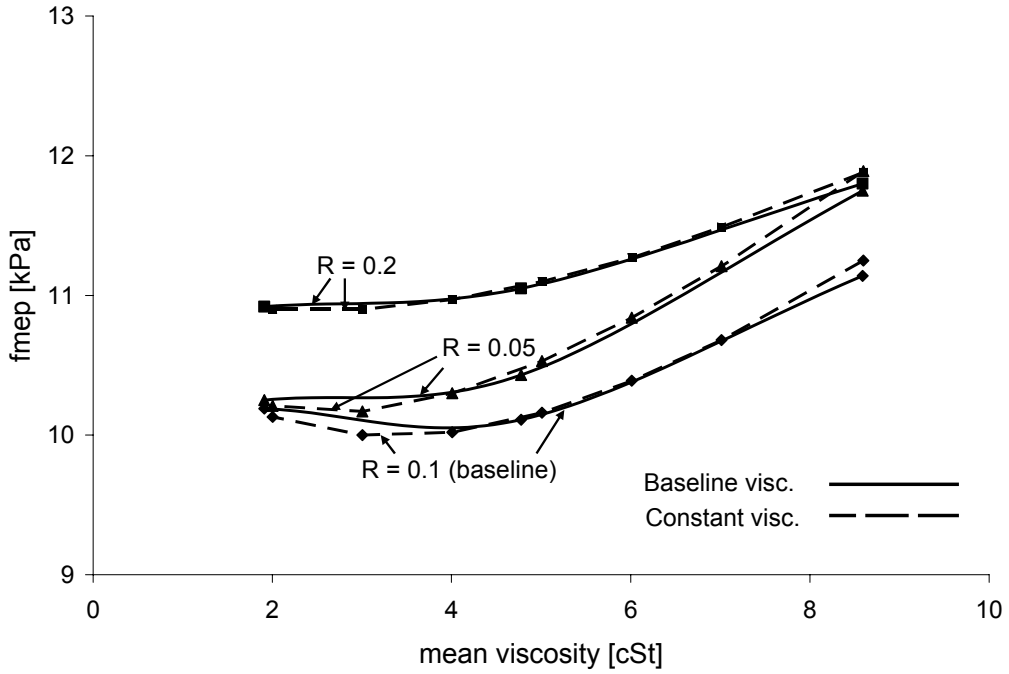

Figure 5-36: Interaction of ring roughness and viscosity effects, baseline and constant viscosity

5.8. Conclusions and Friction Reduction Strategies

The piston rings experience hydrodynamic, boundary, and mixed lubrication modes during engine operation, where the amount of friction loss due to each mode depends on engine design and running parameters. For given parameters, the lubricant viscosity plays a main role in determining the lubrication mode, as well as the frictional losses during the engine cycle. In this study, the role of lubricant viscosity in controlling ring/liner lubrication mode, and thus ring/liner

friction, was considered. The viscosity can be used to optimize the lubrication regime, leading to reductions in friction and wear.

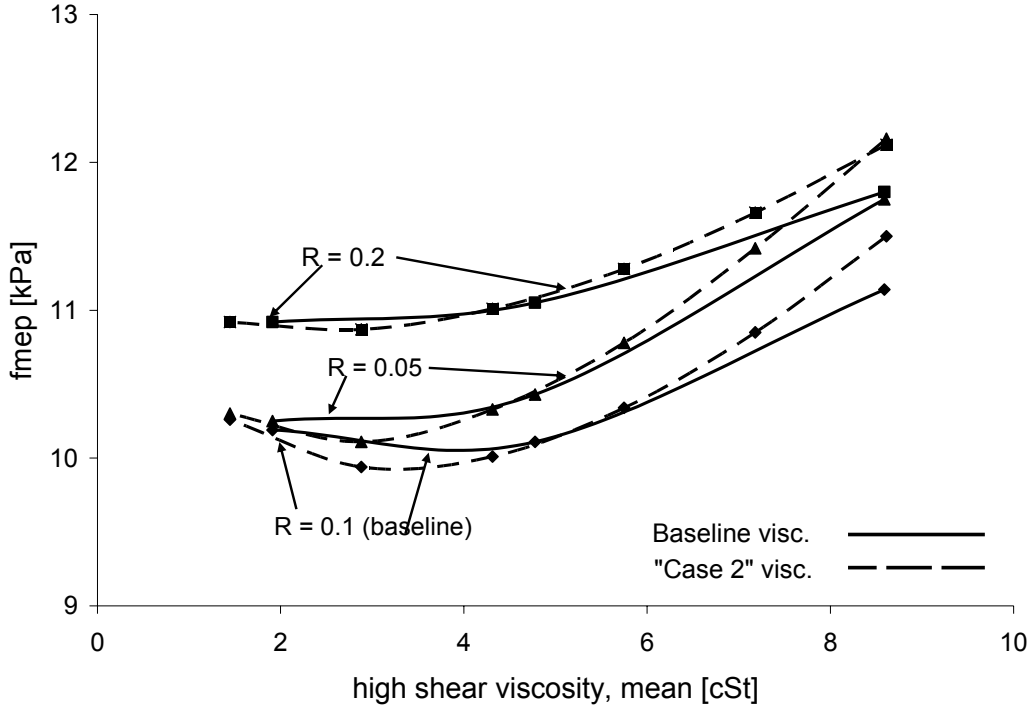

Figure 5-37: Interaction of ring roughness and viscosity effects, baseline and "case 2"

Oil viscosity affects friction directly in the hydrodynamic regime, where hydrodynamic friction increases with viscosity. It also influences boundary friction indirectly by controlling oil film thickness, and thus the amount of asperity contact that occurs. Reducing viscosity can reduce hydrodynamic friction but also causes a decrease in oil film thickness that makes asperity contact more likely. A thicker oil may reduce boundary friction but increase hydrodynamic losses. At the optimum viscosity (the viscosity at which minimum friction losses are incurred) there is a balance between hydrodynamic and boundary friction losses.

As piston speed, ring loading, and other parameters change during the engine cycle, the optimum oil viscosity also changes. Near mid-stroke, high speeds support hydrodynamic lubrication, making a low viscosity lubricant desirable to reduce hydrodynamic losses. Near dead-centers, low speeds cause hydrodynamic support to decrease. Then, a high viscosity oil is desirable, to maintain thicker oil films and reduce asperity contact. If viscosity variation during the cycle can be controlled so that the viscosity is optimum at all times, ring-pack friction reduction is possible. Several idealized and realistic cases were studied to quantify the friction benefit obtainable by controlling viscosity variation during an engine cycle.

Idealized cases with low mid-stroke viscosity and high dead-center viscosity were considered, as were several realistic cases with typical temperature and shear-rate dependencies. It was found that friction reduction is possible when viscosity variation during the cycle is controlled, but it is small compared to the reduction that can be obtained simply by reducing mid-stroke viscosity. Two mechanisms lead to the small size of the friction benefit: the contribution to total cycle ring friction from the dead-center area is small, because of low piston

speeds there; and any reduction in asperity contact is accompanied by an increase in hydrodynamic friction, which cancels out some of the benefit. Oil viscosity near mid-stroke, where most of the ring/liner friction is generated, is the dominant viscosity that controls the overall friction losses for the ring.

A friction reduction of ~10% is predicted for the OCR, from the baseline case, when viscosity is in the mid-stroke region reduced. An additional reduction of 1-2% is possible when dead-center viscosity is held high to reduce boundary friction. For the Waukesha engine, the oil control ring accounts for ~65% of the total ring-pack losses. Then, an OCR friction reduction of 11% leads to a total ring-pack friction reduction of ~7%.

The top ring contributes most of the remainder of the ring-pack friction, but experiences most of its losses (~70%) as boundary friction in the poorly-lubricated TDC region of the stroke. Then, viscosity does not have a large direct affect on top ring friction. However, simulations show an indirect effect, where oil transport into the dry region may increase as viscosity decreases. This leads to a decrease in friction of up to 30%, leading to a ring-pack friction reduction of ~9%. However, the mechanism for this reduction is not clear, and further research is required.

Ring/liner wear was also briefly considered, in a simple analysis of a wear coefficient related to boundary contact force and ring/liner sliding distance. Wear was found to increase strongly with decreasing viscosity, even as friction remains low. In the interest of keeping wear low, then, it may be necessary to accept a higher-than-minimum level of ring friction. Controlling viscosity variation was shown to have some potential benefit in reducing wear, because of the reduction in asperity contact forces near dead-centers, with a wear coefficient reduction of ~42% for the minimum-friction case.

For the Waukesha engine, an OCR friction reduction of ~11% was shown to be possible, translating to a total ring-pack reduction of ~7%. A further reduction in friction from the top ring may be possible, resulting in a total ring-pack friction reduction of ~18%, but the top ring benefit is not well-understood This benefit must be balanced with consideration of wear increases that may occur. If surface modification additives can reduce the boundary friction coefficient for ring-liner contact, even greater friction reductions are possible.

Lubricant properties providing minimum friction for the Waukesha ring-pack are summarized in Table 5-4. The parameters proposed are those for case 2, at the minimum-friction viscosity.

Table 5-4: Cross and Vogel equation parameters for friction reduction

Parameter	Current Value (Unworn)	Proposed	Friction Reduction
z (viscosity "thickness")	.09	.06	7%
c_1 (controls critical shear rate)	2.3	4.3	
m (width of transition region)	1 (more gradual transition)	5 (sharper transition)	

6. Analysis of Effects of Surface Characteristics on Ring-pack Friction

Modification of the surface textures of the ring or cylinder liner may reduce ring/liner friction. Such modification may also increase friction, however, or cause other adverse effects, so care must be taken to match the texturing to the system and conditions under study. Several mechanisms are proposed for the effect of surface finish on friction, including the removal of wear particles from the sliding interface by negative textures, use of negative textures as "lubricant reservoirs" to supply otherwise poorly-lubricated areas, and increase in hydrodynamic support due to "micro-hydrodynamic" action of surface features. In addition, several types of surface modification are considered. These can be separated into the two broad categories of stochastic modifications, including the control of statistical surface parameters such as the roughness and skewness, and deterministic modifications, which consist of placing specific features, such as dimples, at specific locations on the surface.

This study focuses on adding deterministic textures to the cylinder liner, and the effects of such texturing on the hydrodynamic support of the ring load. An averaged Reynolds analysis, using deterministically calculated flow factors, was used to perform a parametric study on both grooved and dimpled textures. The main friction-reducing effect of such textures is to increase flow resistance, thereby increasing oil film thickness. When film thickness is increased, asperity contact is reduced and hydrodynamic friction also decreases, because of the corresponding decrease in oil shear rate. While limitations of the model must be taken into account, results of this study indicate that both grooved and dimpled surface features can cause a reduction in ring/liner friction, where the optimum texture is determined by engine parameters and running conditions.

6.1. Background and review of current surface texture research

Surface texturing has been recognized as a method for enhancing the tribological properties of surfaces for many years. Adding a controlled texture to faces in relative motion can have many positive effects, such as reduction of friction and wear and increase in load capacity. Early studies recognized the potential of microasperities to provide hydrodynamic lift during film lubrication [34-36], while later research indicated that small-scale texturing could also trap wear particles [37] in boundary and dry lubrication. A further use of microtextured surfaces may be found in the use of partial texturing – a textured region can take the place of macro-geometry such as steps or inclined planes meant to provide hydrodynamic lift [38]. All of these effects may decrease friction and wear between two sliding surfaces, but some experimental results also show a negative effect from surface texturing. In some cases texturing is not optimized for a given case, in others there is no optimal case – any kind of texturing may be worse than a smooth surface. Research and analysis presented to date demonstrates both the potential to improve tribological properties via surface texturing, and the need to understand materials, lubricants, and running conditions before a surface texture is applied.

Micro-topography consists of micron-scale surface features, either negative (cut into the "flat" surface) or positive (protruding). Early textures were limited to grooves and troughs, while new techniques have allowed complex patterns of different shapes, including circular, triangular, and other geometric shapes, to be used. Asperity shape, geometry, depth, area ratio (the ratio of asperity to flat area) and orientation can all impact the effectiveness of a given texture.

Several methods are now available for creating this surface micro-topography. Mechanical techniques such as vibrorolling and abrasive machining can be used to create grooves, while other methods including reactive ion etching (RIE), other forms of etching, and lithography can produce a variety of shapes in both metals and ceramics. In recent years laser surface texturing (LST) has emerged as a versatile and high-speed texturing method that can provide well controlled surface characteristics for a variety of materials. This method has been used in the magnetic storage industry for several years, and is currently the focus of several studies [19].

Recent and past studies have explored the effects of these various methods and of different microasperity parameters on friction, wear, and other issues. A limited number of analytical models have been proposed, mostly considering hydrodynamic effects of microtexturing, while the majority of studies have been experimental. The outcome of research to date indicates that optimal surface texturing parameters depend on the running conditions studied and on the dominant mode of lubrication considered. Surface texturing can provide a benefit in several ways: decreasing friction during well-lubricated sliding by providing hydrodynamic lift, acting as reservoirs for lubricant, and removing wear particles from the sliding interface. Each of these modes is discussed in further detail below.

6.1.1. Boundary and non-lubricated sliding

When lubrication is poor (or non-existent) or hydrodynamic lubrication is made difficult for other reasons, the main effect of micro-texturing is likely to be its ability to remove wear particles from the sliding interface. In general, it is expected that this particle-removal action will reduce friction and wear, as in many engineering situations most friction is due to plowing. Suh, et. al [37,39] performed much of the pioneering research in this field, demonstrating that the addition of grooves to a surface caused wear particles to be removed from the interface, and measuring reduced sliding friction for many cases.

Other research, however, has shown that friction can increase when grooves and other textures are added to sliding surfaces. In cases where plowing is not the main friction mechanism, removing particles from between sliding surfaces can cause an increase in friction due to adhesion, because the surfaces can come into closer contact when wear particles are not present to keep them apart. In other cases, a beneficial chemical reaction may generally occur between sliding surfaces and wear particles, and when the particles are removed the reaction no longer occurs. Petersson and Jacobson [40] conducted an experimental study in which adding dimples greatly increased the sliding friction of silicon coated with diamond-like carbon (DLC), because a beneficial tribo-film did not form in the textured case. In other tests, adding texturing can increase friction but the mechanism is not clear. While many studies have shown that

texturing removes wear particles from a sliding interface, a good understanding of the chemical interaction of the two sliding materials is required to predict what effects on friction will be.

In poorly lubricated cases, surface dimples may also decrease friction by acting as "lubricant reservoirs" that help to maintain an adequate lubricant supply. Blatter, et. al [41] demonstrated that the presence of small grooves (on a sapphire disk, sliding against steel) could cause a delay in the loss of lubrication in a case where a small amount of oil was introduced at the beginning of a sliding test, which was then allowed to run until failure (a sudden increase in friction coefficient). For some grooved cases, the number of cycles for which lubricated sliding was maintained was an order of magnitude greater than that for smooth surfaces. Lubricant reservoirs may be particularly useful where lubricant availability is intermittent. In these cases, dimples may act as "lubricant capacitors," storing oil when it is readily available and re-supplying it to the sliding interface when it is scarce.

6.1.2. Hydrodynamic effects

Like large scale converging surfaces, micro-scale asperities can create an asymmetric oil pressure distribution that results in hydrodynamic lift. In cases of mixed lubrication, this added lift can alter the balance between hydrodynamic and boundary lubrication, reducing the amount of asperity contact that takes place, and thus reducing both friction and wear. Also, even when contact does not occur, an increase in oil film thickness reduces shear within the oil, reducing hydrodynamic friction. Several studies, both analytical and experimental, have considered the effects of surface patterns in hydrodynamically lubricated cases.

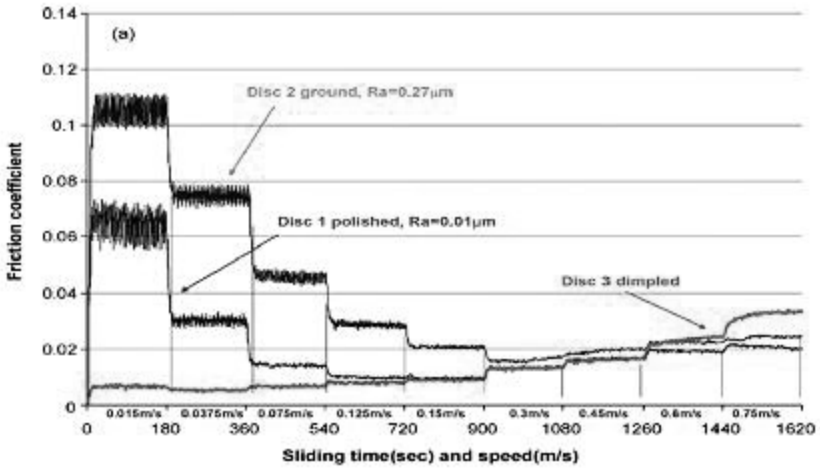

Figure 6-1: Adding dimples delayed the onset of asperity contact in this test, from Kovalchenko, et. al [42]

Because they can assist in creating hydrodynamic pressure in the fluid film, textured surfaces have an effect on the lubrication regime of sliding surfaces. Kovalchenko et.al. looked closely at the lubrication regime effect in a series of experiments using a pin-on-disk test rig with unidirectional sliding, with a textured disk [42]. This study produced Stribeck-like curves for

various lubricants and load conditions, and different dimpled area densities (the depth:diameter ratio for the dimples was maintained at an "ideal" value in all cases). In general, dimpling expanded the range of parameters under which hydrodynamic lubrication took place, extending the non-contact regime to low speeds and viscosities. An example of Kovalchenko's results is shown in Figure 6-1.

Sadeghi, et al. has also demonstrated that texturing can reduce asperity contact, analytically showing that adding dimples in the end-stroke region of a reciprocating slider can reduce overall friction by reducing contact in this area [43]. A deterministic model of mixed lubrication was used in this study, which showed that friction reduction for a reciprocating cycle is possible when round dimples are added to one surface. (The metric for "friction" used here was the cycle average friction coefficient. This over-represents the importance of end-stroke friction compared to friction power loss, which represents the actual energy required to overcome friction.) An example of Sadeghi's predictions are shown in Figure 6-2, which shows an almost complete removal of asperity contact in the textured region.

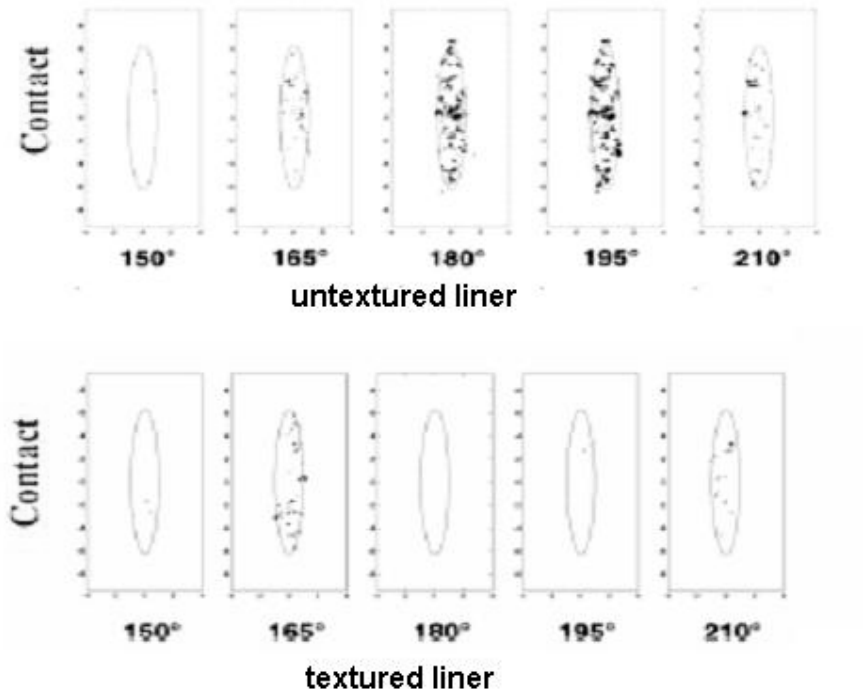

Figure 6-2: Modeling shows a reduction in asperity contact when liner texturing is added [43]

Studies have also shown that friction can be reduced when surface dimples are added even when no contact occurs. Etsion, et. al. have completed several analytical and experimental studies considering the effects of round dimples on sliding friction and load support. Early studies, based on a CFD model in which contact was not considered, predicted increased load support in face seals with the addition of dimples, where the ratio of depth:diameter was the main factor in optimizing the texturing. A depth:diameter ratio of approximately 0.1 was

predicted to be optimal for almost all cases [44]. (As in the case of Sadeghi, the measurement of friction used in Etsion's study is mean cycle friction coefficient.) In-place testing in working pumps showed increased life and reduced wear as predicted [19]. Subsequent analysis of "piston-ring like" cases showed that optimized dimpling could also decrease friction in reciprocating sliding, again, due purely to hydrodynamic friction reduction as asperity contact was not considered. Reciprocating-slider testing showed reduced friction, as well as a dependence on oil supply, suggesting that the dimples were effective only in a well-lubricated regime, and may actually be harmful in poorly-lubricated situations [45,46].

Many other studies, both analytical and experimental, have studied the effects of surface texturing. Stephens and Siripuram [47] as well as Hsu [48] considered the effects of different dimple shapes. Stephens and Siripuram considered circular, square, diamond, hexagonal and triangular cross-sections, and concluded that friction reduction was generally independent of shape. Hsu, however, concluded that dimple shape could have some effect, and that, in particular, shapes with an orientation more perpendicular to the sliding direction could delay the onset of asperity contact. (Results also indicated, however, that round dimples had almost no effect, in disagreement with several others). Other researchers have also predicted that texture orientation has an effect on friction and oil film thickness. Michail and Barber [49] predicted increased oil film thickness for textures more perpendicular to the sliding direction, while Jocsak [15] also predicted increased film thickness and reduced friction for lower honing groove cross-hatch angles (grooves more perpendicular to the sliding direction).

Many experimental and analytical studies have predicted friction reduction with the addition of appropriate texturing to sliding surfaces. As can be seen from this brief literature review, however, there is no general agreement on what types of textures should be added, what texture parameters are the controlling factors in friction reduction, and even what the effects of various texture parameters are. Much work still remains in this field before a good understanding of the effects of surface texturing is achieved.

6.2. Describing surface textures and finishes

Several different systems have been created for stochastically describing surface textures, while in deterministic studies patterns must generally be represented by actual measured or simulated data sets. Both stochastic parameters and deterministic descriptions are used in this analysis of surface texture effects, with deterministic surfaces used to calculate flow and stress factors and stochastic parameters used to define asperity contact mechanics. The deterministic surfaces are generated using a method described in Section 6.4.1, while the system of stochastic parameters used is described below.

Several methods and standards exist for measuring and characterizing surface finish. Techniques such as white-light interferometry (WLI) can give three-dimensional measurements of surface textures, while profilometers and similar instruments provide two-dimensional measurements of surface height along a linear path. Both types of measurement can be used directly when a deterministic description of a given surface is desired. However, in many cases

the use of a deterministic measurement in an analysis or as a description of a given surface is too complicated or time-consuming, and stochastic parameters are used. These parameters statistically describe the variation in height of a surface, and can provide a general understanding of surface characteristics.

There are several different standards which are used to define stochastic parameters for surface measurement, most of which describe only variations in the surface height, and not spatial variations along the length and width. In this study, three parameters are used to describe surface height distribution: the roughness, skewness, and kurtosis. These three parameters are all derived from a statistical analysis of the distribution of surface heights, where the roughness, σ, is defined as the standard deviation of the surface heights, the skewness, Sk, is the third standardized moment about the mean, and the kurtosis, Ku, is the fourth:

$$\sigma = \sqrt{\frac{1}{N}\sum_{i=1}^{N}(x_i - \bar{x})^2} \tag{6.1}$$

$$Sk = \frac{\frac{1}{N}\sum_{i=1}^{N}(x_i - \bar{x})^3}{\sigma^3} \tag{6.2}$$

$$Ku = \frac{\frac{1}{N}\sum_{i=1}^{N}(x_i - \bar{x})^4}{\sigma^4} \tag{6.3}$$

where N is the number of data points included in the distribution, x_i is the surface height at a given point, and $\bar{x}$ is the mean surface height. These parameters can also be defined using the probability distribution function of the surface height distribution, if this function is known.

The surface roughness, σ, is simply the standard deviation of surface heights, and is an approximate representation of the height of the surface asperities above the mean. Skewness can be thought of as the asymmetry of the distribution. A negatively skewed surface has a plateau surface and many low valleys, while a positively skewed one has wide, flat valleys along with high peaks, as illustrated in Figure 6-3a. Kurtosis is often described as the "peakedness" of the distribution, and represents the number of surface height measurements that are very far from the mean. A surface with high kurtosis has a very wide distribution ("thick tails") of surface heights, with many high peaks and low valleys, while a low kurtosis surface is relatively flat, with most of the surface heights close to the mean, as shown in Figure 6-3b. For a Gaussian surface, skewness = 0, and the kurtosis = 3. The effect of these parameters on friction was not considered in this study, as the focus was on larger scale patterns, but they have been considered extensively by others [15,50].

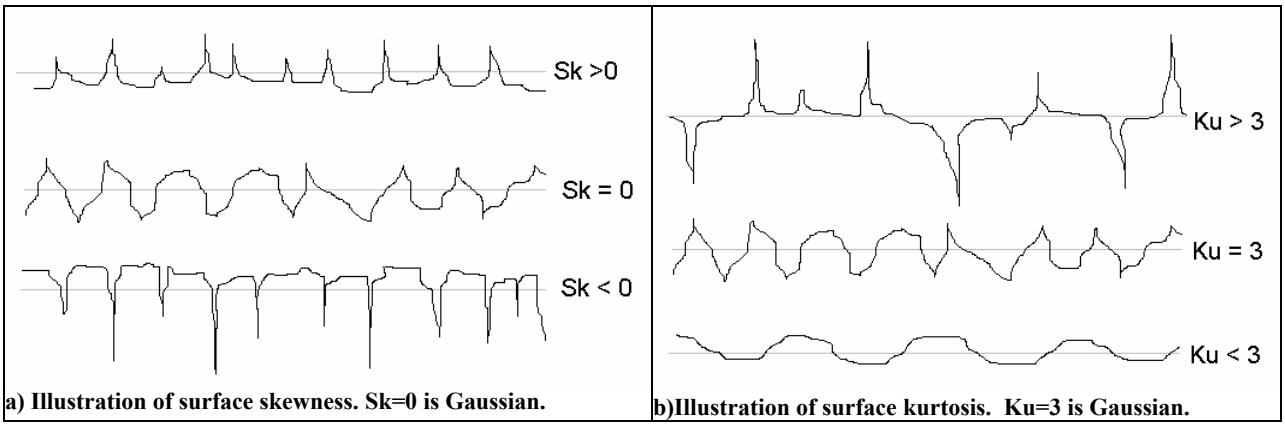

a) Illustration of surface skewness. Sk=0 is Gaussian.

b)Illustration of surface kurtosis. Ku=3 is Gaussian.

Figure 6-3: Illustrations of surface skewness and kurtosis

These parameters can be used, along with the Pearson system of frequency curves, to represent a rough surface in the calculation of contact pressure. The Pearson system is a curve-fitting method that derives the probability distribution function of a surface from its roughness, skewness and kurtosis. This distribution is then used to determine the amount of contact expected to occur, statistically, at a given separation between surfaces, and to then determine the contact force.

6.3. Averaged flow-factor Reynolds analysis

An averaged flow-factor Reynolds analysis was used in this study to evaluate the effects of grooved and dimpled surfaces. This method, and its limitations, are described in detail in Section 2. Because this method was used, the surface features studied were limited to a relatively small size, compared to many that have been studied in the literature. Also, the method does not allow the detailed analysis of flows and stresses that would be possible using a deterministic method. Still, the averaged method can provide information about the effects of various surface finishes, and reveal the trends in film thickness and ring/liner friction whose discovery was the object of this parametric study.

The averaged flow factor method can also shed some light on the physical effects of rough surfaces, in the interpretation of the flow and stress factors themselves. While a physical explanation of the factors' meanings is not agreed upon, understanding the various interpretations can give some intuition into the effects of rough surfaces. Also, looking at the relative importance of each factor in affecting fluid flow and stresses can aid in understanding the relative importance of the various physical parameters in the ring/liner system.

6.3.1. Physical interpretation of factors

The flow and stress factors represent the difference between the sliding of two smooth surfaces and the sliding of rough, textured surfaces. The physical effect of surface roughness on fluid flow is complex and depends on the nature of the actual surfaces under study. However, it

is possible to give a general physical interpretation of what the factors represent, to partly describe what occurs in the lubricant between rough surfaces.

Figure 6-4 illustrates one possible interpretation. For two smooth surfaces, there is a clear definition of the distance between them, which is also the thickness of the oil film if it is entirely filling the gap. For rough surfaces, the definition of gap height becomes complicated – its actual value depends on the surface features – and so an average value is used. Generally, this average value is taken as the difference between the mean surface heights of the rough surfaces, h_{mean} as shown in Figure 6-4b. In determining flow and stress factors, a comparison is made of smooth surface conditions vs. rough surface conditions at the same film thickness, where for the rough surface h_{mean} is used, and for the smooth surfaces h is used.

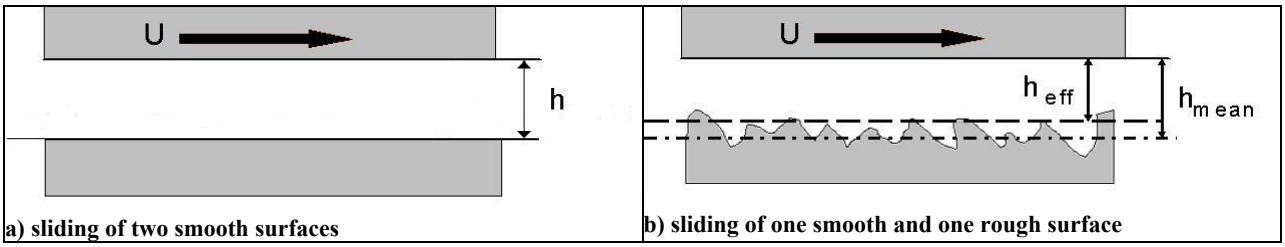

Figure 6-4: Flow and stress factors can be interpreted in relation to an effective film thickness

The effect of the roughness, however, is to make the effective region in which flow occurs even smaller than h_{mean}. If fluid remains trapped and stagnant in the roughness valleys, an effective flow thickness will be smaller than h_{mean}, and be closer to h_{eff}, in Figure 6-4b. In this interpretation, the roughness impedes flow simply by making the effective flow area smaller. For a pressure-driven case, the roughness will impede flow and increase pressure in the fluid for any rough surface. For shear-driven flow, fluid transport will be impeded if the stationary surface has a higher roughness, while it will be increased (due to transport of the stagnant fluid trapped in the valleys) if the moving surface is rougher.

The reduced effective film thickness also has an effect on shear stress. For a thinner oil film the shear rate within the fluid is higher, so shear stress is also higher. These effects can be observed in Section 6.3.2 below, which shows the effects of the different flow and stress factors on oil film thickness and ring/liner friction.

A second interpretation of the flow factors is based on their locations in the equation for oil flow rate:

$$Q = -\phi_p \frac{h^3}{12\mu}\frac{dP}{dx} + \frac{U}{2}\left(h\phi_g + R_q\phi_s\right) \tag{6.4}$$

In this equation, the pressure flow factor appears with the viscosity, μ, while the shear flow factor is coupled with the film thickness. Then, the effect of the pressure flow factor can be considered to modify the viscosity, and an "equivalent viscosity" can be defined:

$$\mu_{eq} \equiv \frac{\mu}{\phi_p} \tag{6.5}$$

An increase in ϕ_p can be thought of as a decrease in equivalent viscosity, and vice versa. Then, a low pressure flow factor indicates increased flow resistance, (high equivalent viscosity) as expected. Similarly, an equivalent film thickness:

$$h_{eq} \equiv h \cdot \phi_g + R_q \phi_s \tag{6.6}$$

is defined, with the shear and geometric flow factors. A decreased shear flow factor reduces the equivalent film thickness, decreasing shear-driven flow. The shear flow factor is related to the relative velocities of the sliding surfaces, so that when the rougher surface is stationary the shear flow factor will be negative, thus causing a decrease in equivalent film thickness.

6.3.2. Relative contributions of flow and stress factors

Each of the flow and stress factors has some effect on predictions of flow and stress within the lubricant. The pressure flow factor, however, has by far the dominant effect on flow, stress, and overall friction losses for the ring and liner. This suggests that the main effect of adding roughness to a sliding surface is on pressure-driven flow, and specifically in increasing the resistance to pressure-driven flow, and thus increasing hydrodynamic pressure within the fluid. Thus, the main effect of adding roughness appears to be increasing load support, or, for a given load, increasing film thickness. This has the simultaneous friction-reducing effects of reducing asperity contact, if there was any to begin with, and decreasing shear rate, and thus shear stress, in the fluid.

Figure 6-5 and Figure 6-6 show the effects of changing each of the flow and stress factors. A "smooth" case, in which flow factors were kept at their smooth surface values, is compared to cases in which a single factor is changed to its value for a surface with horizontal grooves, a surface with very different flow and stress factors than the smooth case. Then, each curve shows the effect of changing a single factor. As the figures show, changing the pressure flow factor has the dominant effect, with a smaller contribution from the shear stress factor. The shear flow and pressure stress factors have negligible effects, and cannot be distinguished from the "smooth" baseline in the figures.

Figure 6-6, which shows the total friction force between the ring and liner, also illustrates that the effects of the different factors are approximately additive. The change in pressure flow factor causes a large decrease in friction force, while changing shear stress factor causes a small increase. When all factors are changed to their rough surface values, the resulting friction force is the summation of those resulting the individual factor changes.

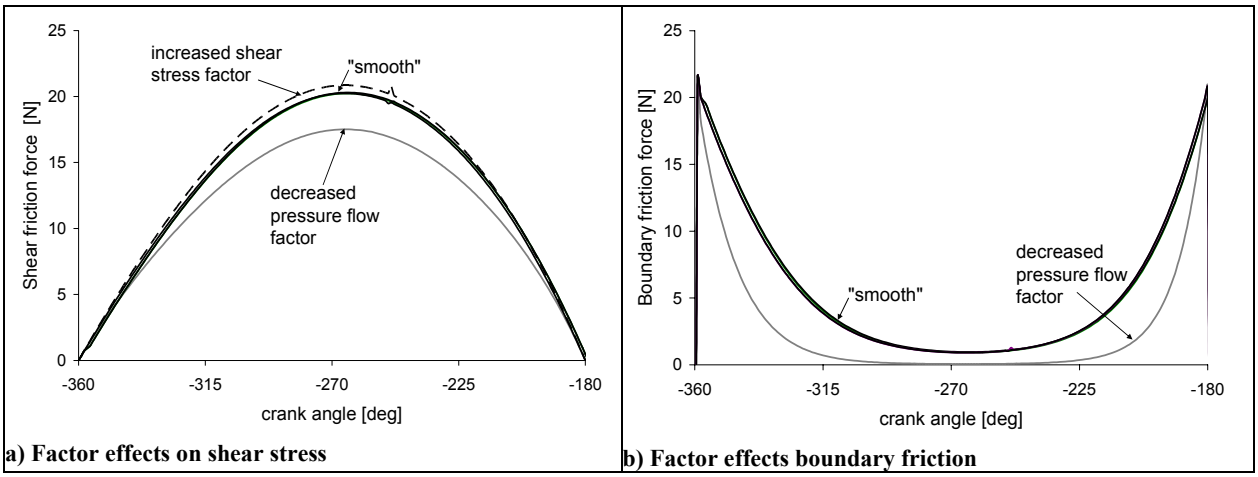

Figure 6-5: Flow and stress factor effects on hydrodynamic and boundary friction

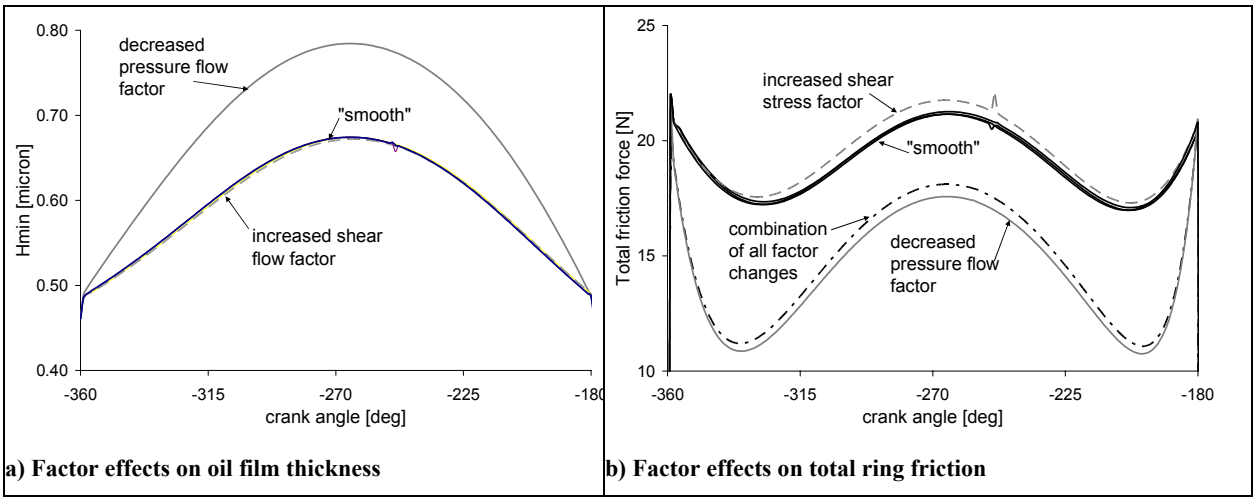

Figure 6-6: Flow and stress factor effects on oil film thickness and total ring/liner friction

6.4. Parametric study: grooves and round dimples

The averaged Reynolds equation method, summarized above and in Section 2, was used to study the effects of dimpled and grooved surface features on ring/liner friction. Surfaces with dimpled and grooved surface textures were first generated using a MATLAB program written for this purpose. Several programs written to facilitate the calculation and curve-fitting of flow factor relationships were used to obtain flow and stress factors. These factors were then used in the MIT ring-pack simulation program to predict ring/liner friction for different cylinder liner surface textures. Although not able to predict complexities of lubricant flow and surface contact that require a deterministic approach, this study was able to demonstrate trends in frictional losses with changing surface parameters.

This study did not consider the effects of stochastic surface properties such as roughness and skewness. Rather, the effects of patterns of discrete features, specifically dimples and grooves, were studied. Parameters considered include: for the dimples, diameter, depth, area ratio, and arrangement (hexagonal or rectangular); and for the grooves, width, depth, area ratio, angle, and arrangement (cross-hatch or parallel grooves). Area ratio is the percentage of the surface occupied by the surface features. The range of parameter values studied is given in Table 6-1.

As for the lubricant study, this study of surface texturing focused on the oil control ring, and all friction results presented below are for the oil control ring/liner interface only. This is because, as noted previously, the oil control ring contributes the majority of ring-pack friction, and most of the remaining losses stem from the top ring in the "dry region" where hydrodynamic effects are not expected to make any impact on friction (since there is little to no oil present). Thus, all predicted FMEP trends are for the oil control ring only, although they can be expected to also be representative of trends for the entire ring-pack, as surface texturing of the type studied should have little effect on the other major sources of ring-pack friction.

Table 6-1: Range of surface texture parameters studied

Parameter	**Range**
Dimples:	
Diameter	5-25 μ
Depth	3-8 μ
Area Ratio	10-22%
Arrangement	hexagonal or rectangular pattern
Grooves:	
Width	11-30 μ
Depth	3-8 μ
Area Ratio	15-35%
Angle	0-90^{o}
Arrangement	parallel or cross-hatch pattern

6.4.1. Method of surface construction

The textured surfaces used in this parametric study were simplified so that the effects of the surface features under consideration could be considered alone, rather than being coupled with the effects of a realistic surface roughness. Instead of using a rough texture, then, the "flat" part of the surface was assumed to be smooth, with either grooves or round dimples the only features present. Two examples of these surfaces are shown in Figure 6-7. In both Figure 6-7a and Figure 6-7b the vertical scale is exaggerated, so that the feature depth seems very large and the profile very sharp. In fact, the grooves and dimples studied were quite shallow.

The surfaces were generated using a two-stage process. In the first stage, the desired feature parameters were used as inputs to generate a matrix that indicated where the given features were to be placed on the surface. Then, this matrix was convolved with a second matrix that was built based on the desired feature profile. In all of the cases presented below, the features were given a Gaussian profile, because of its ease of construction and smooth shape. Because of the modular structure of the surface-generating program, however, it is easy to accommodate different profiles as well as different patterns and shapes.

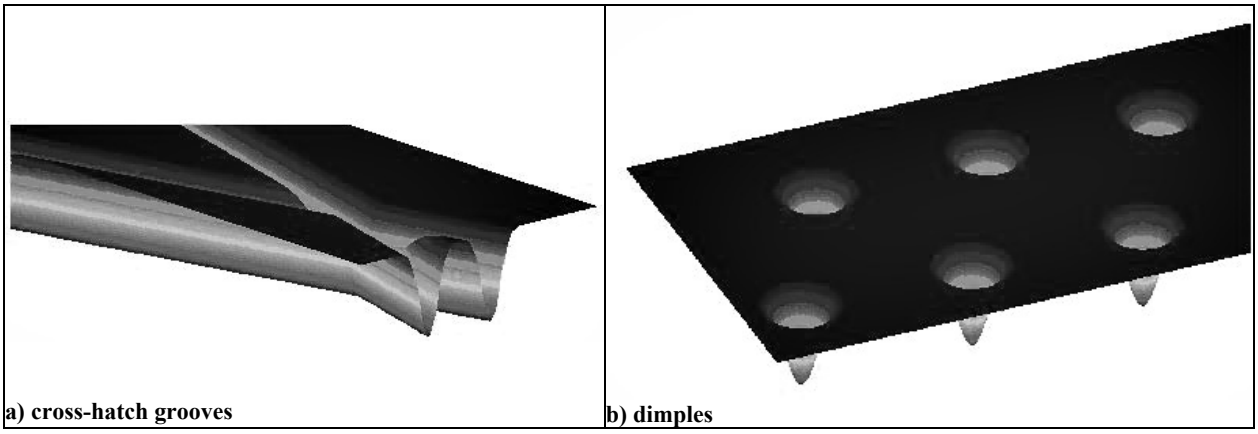

Figure 6-7: Examples of generated surfaces

It should be noted that the definition of groove angle was based on a cross-hatch groove pattern, as shown in Figure 6-8. The stated groove angle, in all results presented below, is twice the angle between the groove and a line perpendicular to the flow direction. This standard was adopted because optimization of a cross-hatch pattern, which is commonly found on honed cylinder liners, was thought to be the most likely application of the groove analysis. The same definition of angle was used for both cross-hatch and parallel groove patterns.

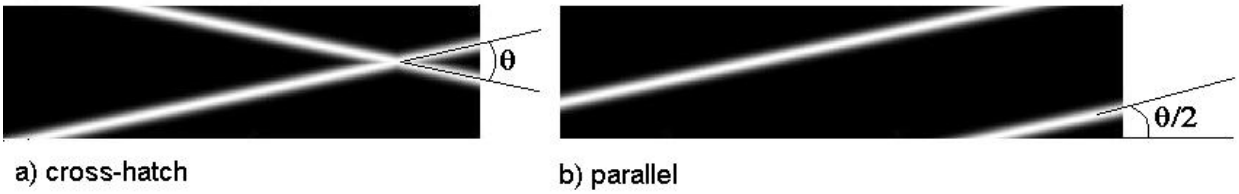

Figure 6-8: Definition of groove angle for cross-hatch and parallel patterns

6.4.2. Grooves: effect of linear surface features on sliding friction

Surfaces with various grooved patterns were studied, to find the effects of the groove parameters on ring/liner friction. Groove angle had the largest effect. Within the range studied, very small angles (grooves more perpendicular to flow direction) caused a reduction in friction, while grooves more parallel to the flow caused a friction increase. Depth also had a large effect,

with deeper textures generally showing reduced friction. In some cases, an ideal depth at which friction was minimized was found. Friction also decreased with increasing area ratio, and with groove width to a point, after which increasing width had no effect.

Both flow factor and FMEP results are presented below. Pressure flow factor, which has the largest effect on ring/liner friction, is shown, as are friction results. It should be noted that, for very deep textures in particular, the surfaces studied may be on the edge of the range of applicability for the averaged-flow-factor model. Also, this model is known to have inaccuracies at very small film thicknesses.

6.4.2.1. Flow factor results

Only pressure flow factor results are presented below, because this factor has the main effect on ring/liner friction, as demonstrated in Section 6.3.2. In general, a lower pressure flow factor indicates a decrease in ring/liner friction, because of the implied increase in hydrodynamic pressure generation.

Groove pattern had almost no effect on flow factor or ring/liner friction calculations. Figure 6-9 shows an example comparison of pressure flow factor calculations for cross-hatch and parallel ("single") groove patterns. In general, very little difference was found between cross-hatch and parallel groove results, as is indicated in the figure. Because of this, only parallel-groove results are presented in the remainder of this report.

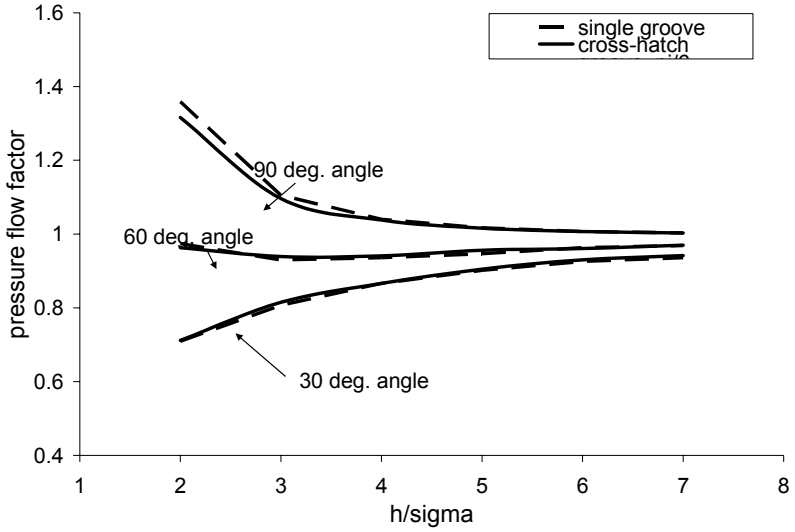

Figure 6-9: Flow factor results for parallel and cross-hatch groove patterns are very similar

Figure 6-10 shows the effects of groove angle on pressure flow factor. As Figure 6-10a shows, pressure flow factor decreases with decreasing groove angle – as the grooves become more perpendicular to the flow direction. For large angles, $\theta > 60^{o}$, pressure flow factor

increases beyond 1, the smooth surface value, and increases for larger angles. This means that for large groove angles, the presence of the grooves causes fluid to flow more easily, reducing load support and, as is shown in Section 6.4.2.2, also increasing friction.

For more perpendicular grooves, the diverging/converging nature of the texturing creates a "micro-hydrodynamic" pressure peak in the fluid, where oil that enters the groove is pushed against the opposite wall, which creates flow resistance and a pressure increase. This flow impedance causes a reduction in flow and thus pressure flow factor. For grooves with larger groove angles, which run more parallel to the flow direction (the largest angle considered is 90^o, in which the grooves run at 45^o to the flow direction) oil that enters the groove is partially pressed against the opposite wall, but is also able to flow along the groove relatively easily. For high groove angles, then, the effect of the addition of the grooves is to increase the effective flow area for the fluid, by adding the area within the grooves. This increases fluid flow, thus increasing the pressure flow factor.

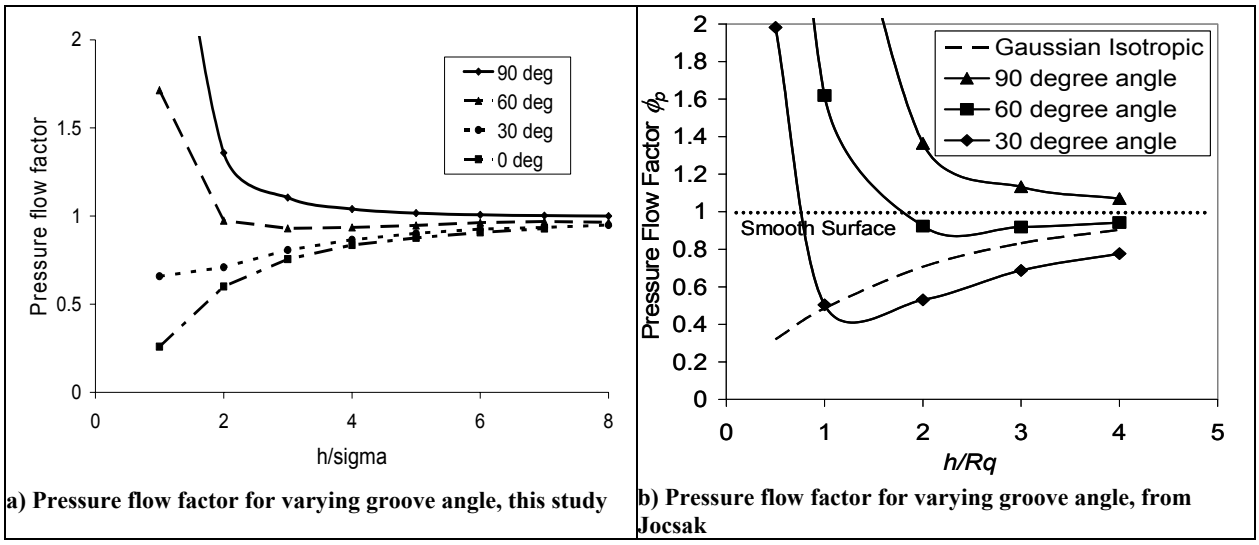

a) Pressure flow factor for varying groove angle, this study

b) Pressure flow factor for varying groove angle, from Jocsak

Figure 6-10: Groove angle effects, with comparison to previous calculations by Jocsak [15]

Figure 6-10b shows results from Jocsak [4], looking at the same groove angles as were considered in the present study. The same flow factor calculation methods were used in both studies, however Jocsak's results consider more realistic surfaces, with realistic roughness and groove profiles. Because the surface roughness is included, Jocsak's pressure flow factors are lower than those obtained in the current study. Also, groove spacing, rather than area ratio, is kept constant in Jocsak's study. Despite these discrepancies, the two sets of results show a good match in trends.

Figure 6-11 shows the effects of varying groove depth on pressure flow factor. As Figure 6-11a shows, there is no change in the pressure flow factor with groove depth, when ϕ_p is presented as a function of h/σ (σ is the RMS surface roughness). This is because the effects of groove depth on pressure flow factor are the same as the effects of groove depth on surface roughness, so that the flow factor as a function of h/σ does not change. This suggests that there

is a fundamental relationship between ϕ_p and groove depth, that mirrors the relationship between depth and the standard deviation of the surface heights, σ.

When studying a specific case in which the approximate value of the oil film thickness is known, it is useful to consider changes in ϕ_p at film thicknesses close to the expected values. Figure 6-11b shows the pressure flow factor as a function of h alone, for different groove depths. As the figure shows, at a given film thickness, ϕ_p decreases with groove depth. The depth of the grooves influences the micro-hydrodynamic effect, just as, in the macro-hydrodynamic case, the size of a step in surface height influences the amount of hydrodynamic pressure generated. (In the case of a macro-sized step bearing, the pressure generation is expected to be related to film thickness, depth, groove width and the distance between grooves [51]). For the surfaces studied, the flow impedance increases with groove depth, suggesting that hydrodynamic action and thus oil pressure also increases with depth.

It should be noted that Figure 6-11 shows flow factor results for grooves at an angle of 30^o, so that the effect of increasing depth is to decrease ϕ_p. For larger groove angles, ($\theta > 60^o$) the effect of increasing depth is actually to increase the pressure flow factor, because in this case the effect of the grooves is to reduce flow impedance and thus increase ϕ_p. The effect of increasing groove depth is to amplify the effect of the grooves, whether that be to block flow, for low groove angles, or increase it, for high groove angles. Because the purpose of this study was to identify surface textures that may be used to reduce friction, the flow factor results shown below are for a low groove angle ($\theta = 30^o$).

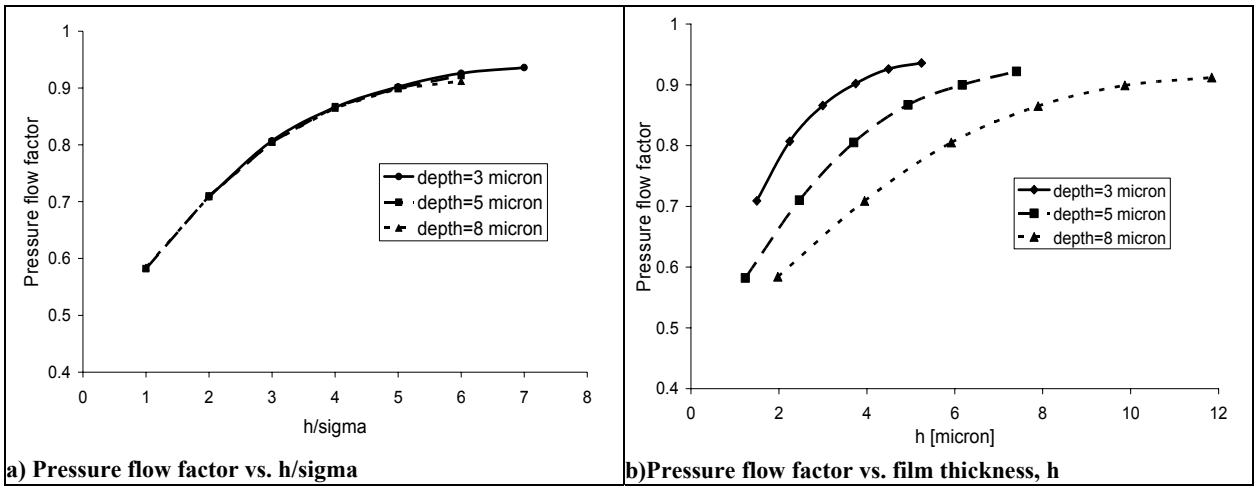

a) Pressure flow factor vs. h/sigma

b)Pressure flow factor vs. film thickness, h

Figure 6-11: Effect of groove depth on pressure flow factor, 30^o angle, width=20μ, area ratio=0.24

Plotting the pressure flow factor as a function of h/σ can show fundamental effects of surface texturing on pressure-driven fluid flow, including its relationship to surface roughness. It is also useful to show the relationship of ϕ_p to film thickness itself, however, when the effects of a given surface texture in a specific case are of interest. Thus, flow factor results in both this section and section 6.4.3.1, which presents the flow factor analysis for dimpled surfaces, are plotted vs. both h/σ and h, in order to illustrate both general and specific effects.

Figure 6-12 shows the effects of area ratio on the pressure flow factor. On the physical surface, the effect of increasing area ratio is to decrease the distance between grooves, so that the effect of increasing area ratio can be also interpreted as the effect of a reduced groove spacing. The decrease in ϕ_p with increasing are ratio may then be due to the effect of groove spacing on hydrodynamic action within the grooves. When grooves are very far apart, they can be considered to be independent in their effects on the lubricant flow and pressure. When they are closer together, there may be a cross-influence between grooves, where the presence of each groove affects the flow within the others. For the textures studied, the spacing between the grooves is relatively small (on the order of a few groove widths) so that some cross-influence is expected. More closely spaced grooves (higher area ratio) will have more influence on each other, and may work together to increase flow resistance.

The effect of area ratio may also be due to the simple fact that, when more of the surface is occupied by converging and diverging regions, there is a larger hydrodynamic effect. More "microhydrodynamic" bearings are present, so their net effect is greater. A combination of this and the cross-influence of more closely spaced grooves is likely the main contributor to the effect of area ratio on ϕ_p.

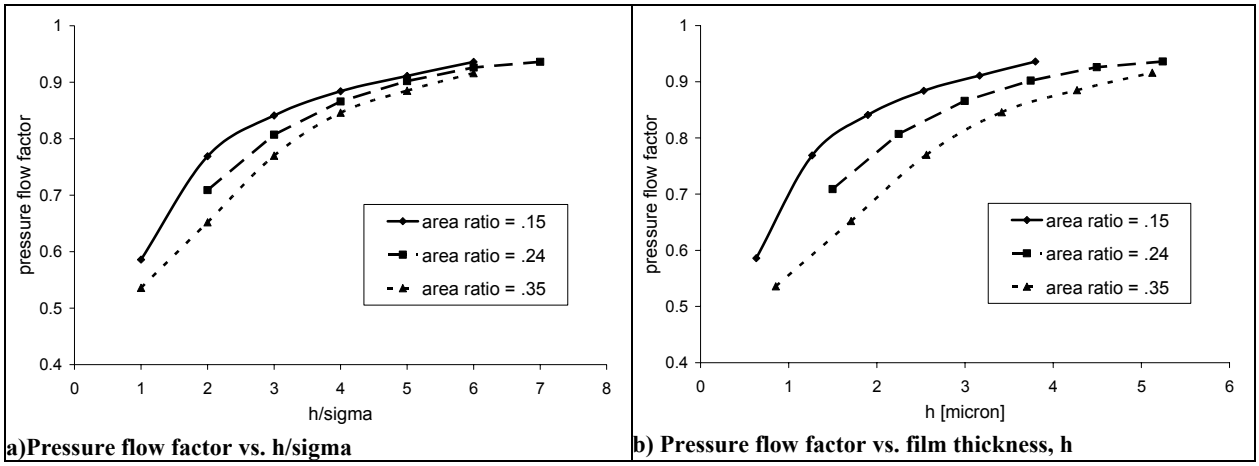

a)Pressure flow factor vs. h/sigma **b) Pressure flow factor vs. film thickness, h**

Figure 6-12: Effect of groove area ratio on pressure flow factor, 30° angle, width=20μ, depth=3μ

Figure 6-13 presents the changes in pressure flow factor with changing groove width. As the figure shows, the groove width has almost no effect on the pressure flow factor except at very small film thicknesses. This may indicate that the width has only a small effect on micro-hydrodynamic action within the groove – the pressure build-up due to the converging geometry of the groove exit is not strongly influenced by the width. There is no clear explanation for the change in trend at small film thickness, where groove width suddenly becomes important. It should be noted, however, that flow factor analysis becomes inaccurate at very small h/σ values, where the film thickness is close to the surface roughness, because the roughness asperities and flow blockages make the flow situation too far removed from a smooth, Reynolds case. Then, these thin-film effects may not be realistic, and should be studied further with a deterministic analysis.

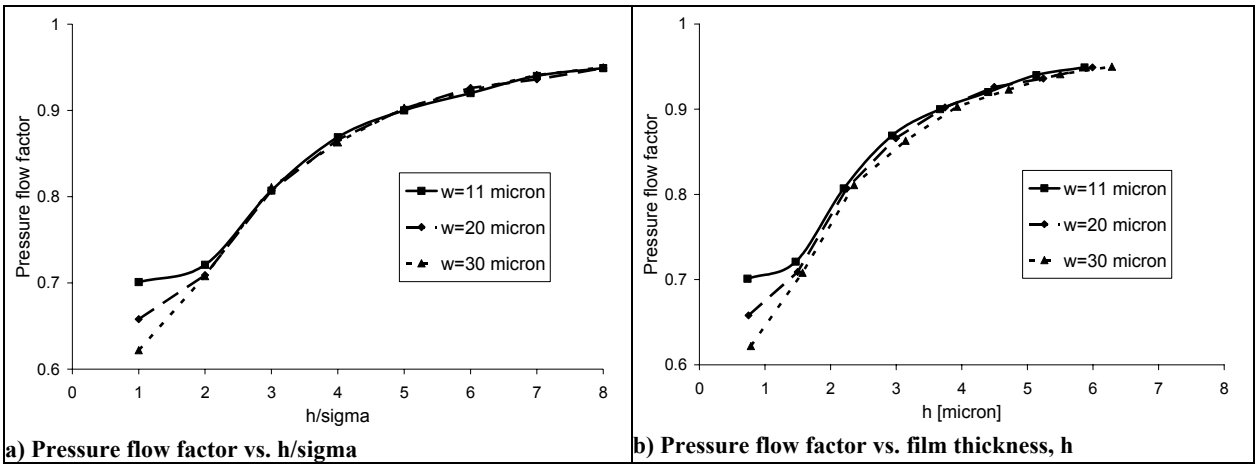

a) Pressure flow factor vs. h/sigma **b) Pressure flow factor vs. film thickness, h**

Figure 6-13: Effect of groove width on pressure flow factor, 30° angle, Area ratio = 0.24, depth=3μ

6.4.2.2. Ring/liner friction results

Friction results were consistent with expectation given the flow factor results presented above. Friction tends to decrease with increasing depth and decreasing groove angle, and also shows some reduction with increasing area ratio and width. The change in FMEP between best and worse cases is relatively large, up to ~30% between the highest and lowest friction examples (not including large groove angles, which cause friction to increase). While this result cannot be used to predict actual friction reductions in realistic situations, it indicates that liner surface texturing may have a major effect on ring/liner friction, and is worth studying further.

Ring/liner friction depends on the surface texture in two ways: oil film thickness, which influences both hydrodynamic friction and asperity contact, depends on the influence of the texturing on the oil flow (represented by flow and stress factors in this study); and asperity contact friction depends on the surface roughness and other features of the surface texture. For this parametric study, as described in Section 6.4.1, the surfaces are smooth except for the added grooved or dimpled patterns. This allows the hydrodynamic effects of the patterns to be studied more easily, but makes the asperity contact mechanics very unrealistic.

To account for this issue, the ring-pack friction program was modified slightly so that the surface properties related to contact mechanics were separated from those related to oil flows. Then, for each friction case studied the contact mechanics were to be kept the same, even as flow parameters were allowed to vary. For the sake of simplicity, the surface used to calculate contact pressures was kept constant as a Gaussian surface with a roughness of $\sigma = 0.21\mu$. This roughness is typical of the "truncated" roughness of a cylinder liner, where the surface is negatively skewed and the effects of the deep valleys are ignored. The presence of the surface features should have little to no effect on the contact mechanics, since the features are negative – that is, they are formed by the removal of material, rather than the addition – and so no extra asperities are added when the texturing is added. Changing area ratio of the texturing will affect the amount of surface area available for contact, but this should have only a small effect as the

contact force should be proportional to the material properties (hardness) and the load, and not to the apparent area of contact [39].

While contact surface features were kept constant, the surface properties controlling oil flows and stresses were varied. These surface properties were defined by the curve-fitted flow factor equations, which are functions of h/σ and derived from the values calculated deterministically using Li's program, and the surface roughness, σ, which together determine the value of a given flow or stress factor at a given film thickness, h. The value input as σ effectively defines the depth of the texture under study, since the flow and stress factor equations contain no information relating to the surface roughness itself, but only to its effects relative to h/σ. Then, friction results are presented as FMEP (friction mean effective pressure) vs. σ, as this roughness was used as the input in this study. As the value of σ approximately corresponds with the depth of the surface features, the trends of FMEP with σ shown should be considered to correspond to the same trend of FMEP with respect to depth. A value of $\sigma = 0.7\ \mu$ is roughly equivalent to a groove depth of 3μ, indicating that the feature depths studied were relatively shallow. This is in agreement with the literature, which predicts maximum friction reductions for shallow features [44].

Figure 6-14 shows the change in ring/liner FMEP with groove angle as well as depth. As expected from the flow factor results, FMEP decreases with groove angle. Friction also decreases with groove depth for low groove angles, while increasing with depth for a large angle (the $\theta = 90^o$ case, not shown in the figure, demonstrated even higher friction than $\theta = 60^o$), as expected – the effects of the texture increases as depth is increased. As shown in Figure 6-15, these reductions in total FMEP are the result of decreases in both the hydrodynamic and boundary contributions to friction, as the presence of the texturing causes the oil film thickness to increase.

For the $\theta = 0^o$ grooves, the surface texturing is able to almost entirely eliminate boundary contact, as well as cause a large decrease in hydrodynamic friction. At the maximum groove depth studied FMEP is continuing to decrease, indicating that the maximum effect of these grooves may occur at a greater depth. For the $\theta = 30^o$ grooves however, a minimum FMEP is found at a roughness of $\sigma \sim 0.55\ \mu$, or a depth of slightly more than 2μ. It is expected that the hydrodynamic effect of the grooves will not increase indefinitely with depth – as the grooves become too deep, fluid at the bottom will become stagnant and no longer contribute to the hydrodynamic system. At this point, the averaged flow-factor method also becomes inadequate to describe the fluid flow, and more detailed model must be used. For grooves that are not entirely perpendicular to the flow ($\theta > 0^o$), there may also be a trade-off between the hydrodynamic effect and the increased flow area. As groove depth increases hydrodynamic effects will increase (to a point), but the extra area available for fluid transport also grows. The minimum FMEP point predicted for the $\theta = 30^o$ groove case may also reflect this trade-off.

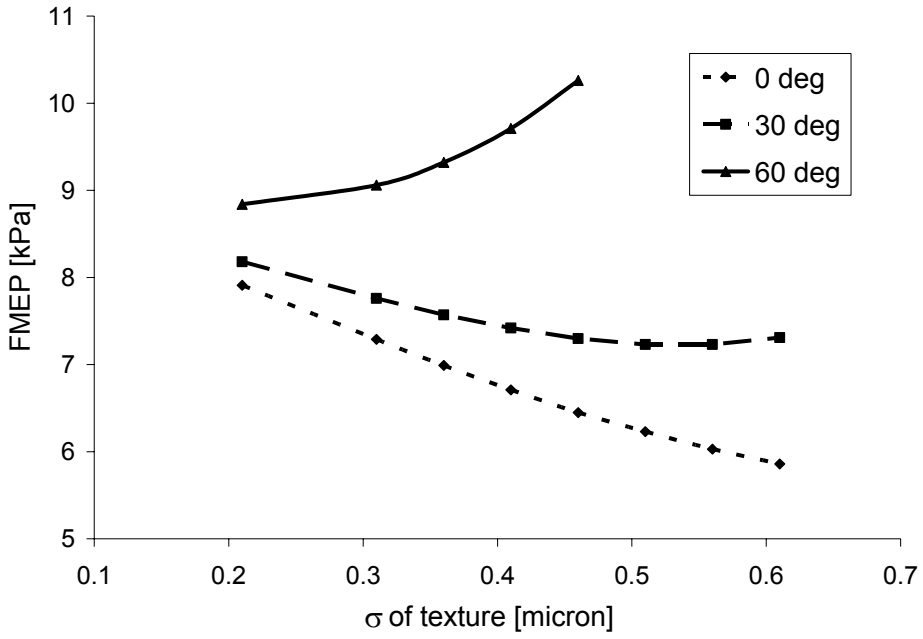

Figure 6-14: Effect of groove angle on ring/liner friction, width = 20μ, area ratio = 0.24

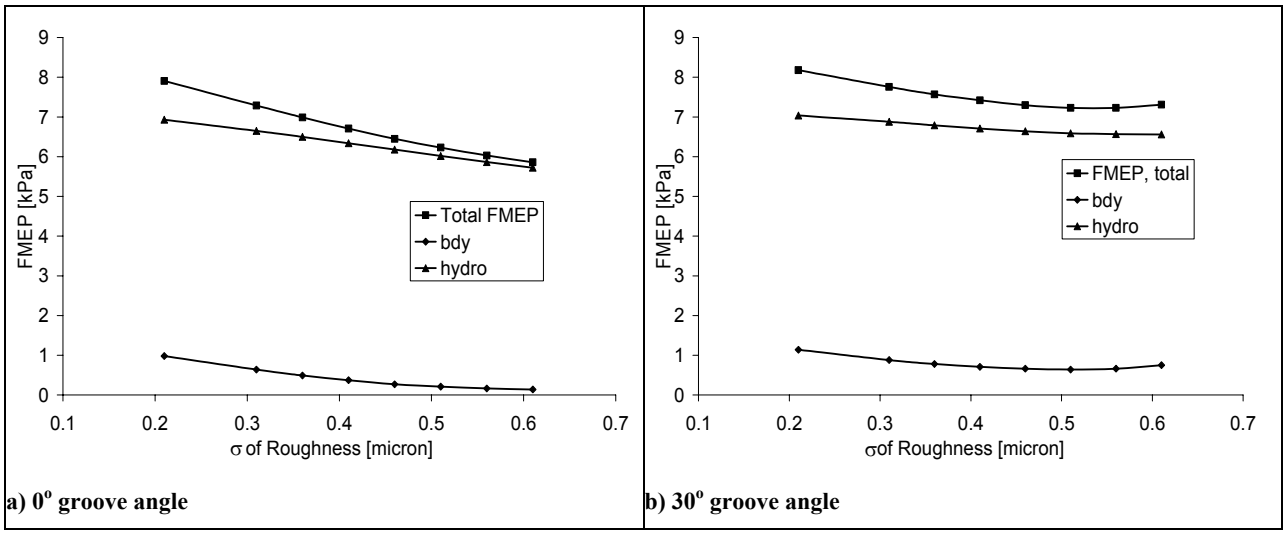

Figure 6-15: Hydrodynamic and boundary contributions to frictional losses, 0° and 30° groove angles

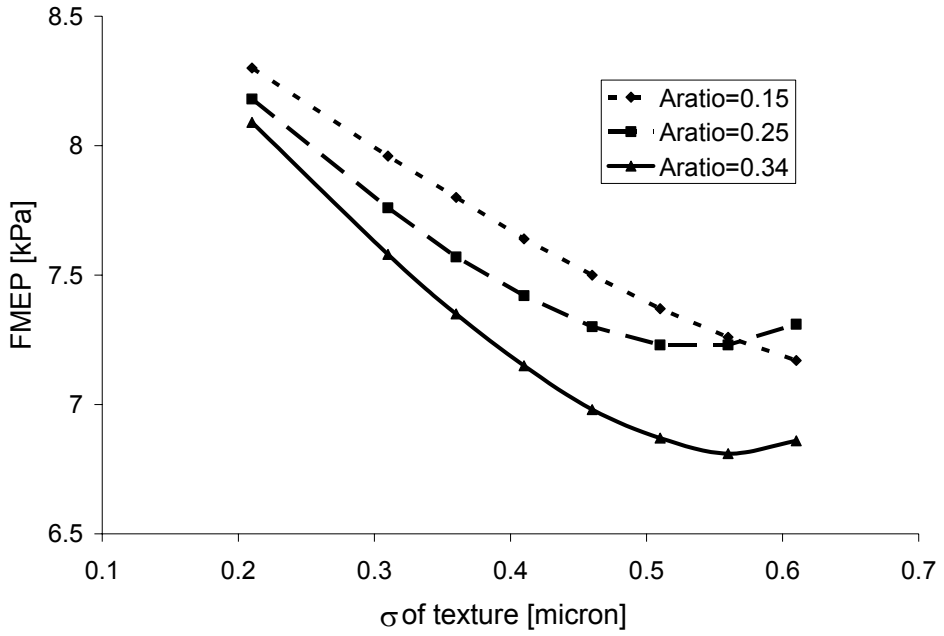

Figure 6-16: Effect of groove area ratio on ring/liner friction, angle = 30°, width = 20μ

Figure 6-16 and Figure 6-17 illustrate the effects of the area ratio and width, respectively, of the grooves on ring/liner FMEP. Again, friction decreases as depth increases, until an optimum point is reached at $\sigma \sim 0.55$ μ for most of the cases. This may reflect the trade-off between hydrodynamic effect and flow area discussed above (the results shown are for $\theta = 30^{o}$). FMEP also decreases as area ratio increases, as expected from the flow factor results, and also increases with groove width but only to a point. As Figure 6-17 shows, friction decreases as the groove width increases from 11μ to 20μ, but the further increase to w=30μ has no effect.

This results from the relation of the flow factors to oil film thickness, shown in Figure 6-17. For large film thicknesses, groove width does not affect the pressure flow factor - a width effect is only shown for thin films. Because the presence of the grooves increases oil film thickness, there is a feedback effect that removes the dependence of friction on groove width as width grows. When the grooves are narrow, the hydrodynamic effect is small as is the oil film thickness, which is small enough to be in the range where groove width matters. The increase in width from 11μ to 20μ increases the hydrodynamic pressure in the oil and also the value of h, into the regime in which groove width becomes unimportant. Then, for any further increase in width the oil film thickness is in a regime where the width has no effect on the pressure flow factor, and there is thus no effect on friction.

6.4.3. Round dimples: effect of discrete surface features on sliding friction

In addition to the grooved patterns, surfaces with patterns of round dimples were also studied, as such discrete surface features are also thought to hold promise for the reduction of ring/liner friction. FMEP was found to decrease as dimple area ratio and depth were increased,

as was the case with the grooves, and to be minimized at an optimum dimple diameter. In general, the effects of the various dimple parameters on friction was smaller than the effects of comparable parameters for the grooved surfaces. This suggests that dimpled surfaces may allow more freedom in selecting feature parameters, and may be useful over a larger range of running conditions than grooved patterns.

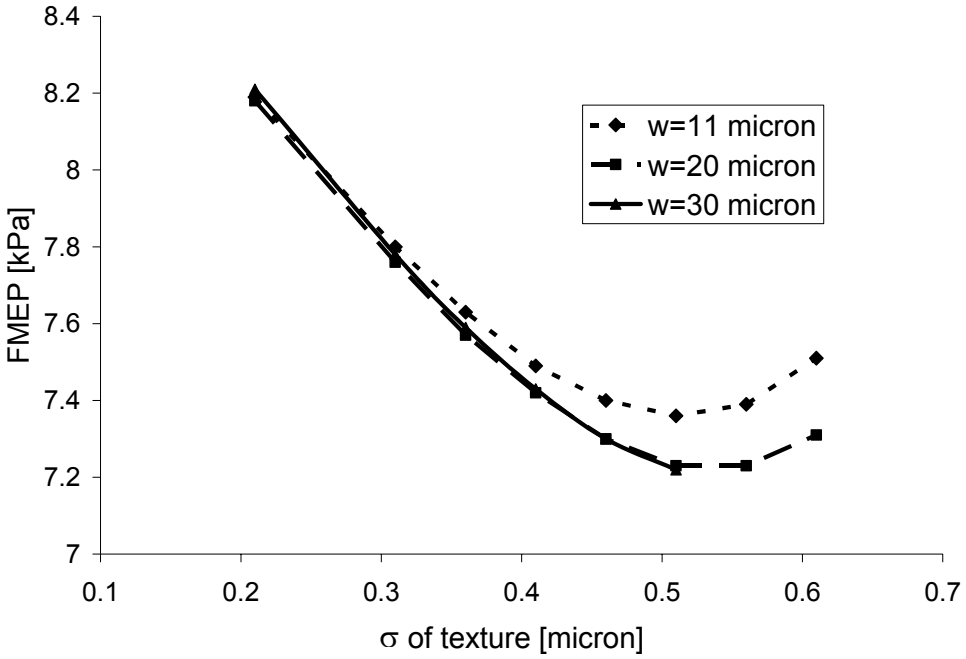

Figure 6-17: Effect of groove width on ring/liner friction, angle = 30°, area ratio = 0.24

Both pressure flow factor and FMEP results are presented. As for the groove analysis, it should be noted that the averaged flow factor model is limited in its applicability, and results at very small film thicknesses and for very deep textures may be pushing this limit. The results presented below are intended to illustrate the friction-reduction possibilities of dimpled surface textures, and the effects of some dimple parameters. Further analysis is required before recommendations can be made for friction-reducing surface textures in specific applications.

6.4.3.1. Flow factor results

Only pressure flow factor results are presented below, because this factor has the main effect on ring/liner friction, as demonstrated in Section 6.3.2. In general, a lower pressure flow factor indicates a decrease in ring/liner friction, because of the implied increase in hydrodynamic pressure generation.

Flow factor results for the dimpled cases showed several of the same trends that were observed for the grooved surfaces. For example, the dimple pattern had almost no effect on flow factor or ring/liner friction calculations, similar to the lack of influence of a cross-hatch vs.

parallel groove arrangement on friction. Figure 6-18 shows an example comparison of pressure flow factor calculations for square and hexagonal dimple arrangements. Because the pattern appears to have no effect, all results presented below are for the hexagonal pattern only.

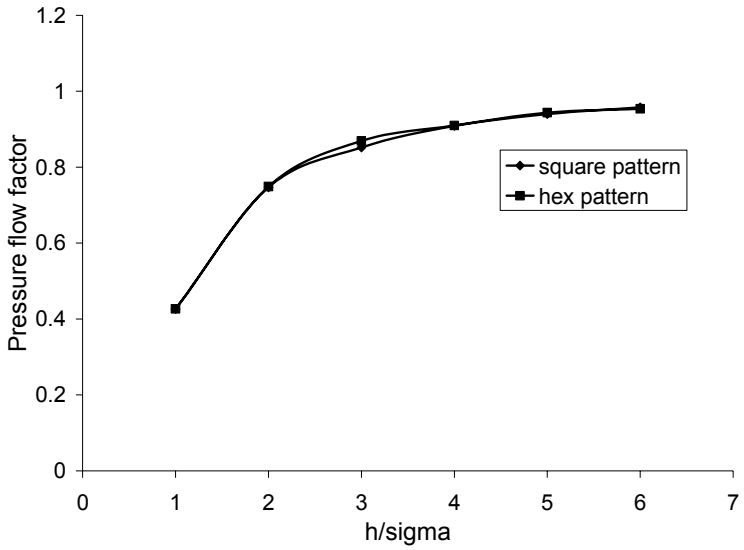

Figure 6-18: Flow factor results for square and hexagonal dimple patterns are very similar

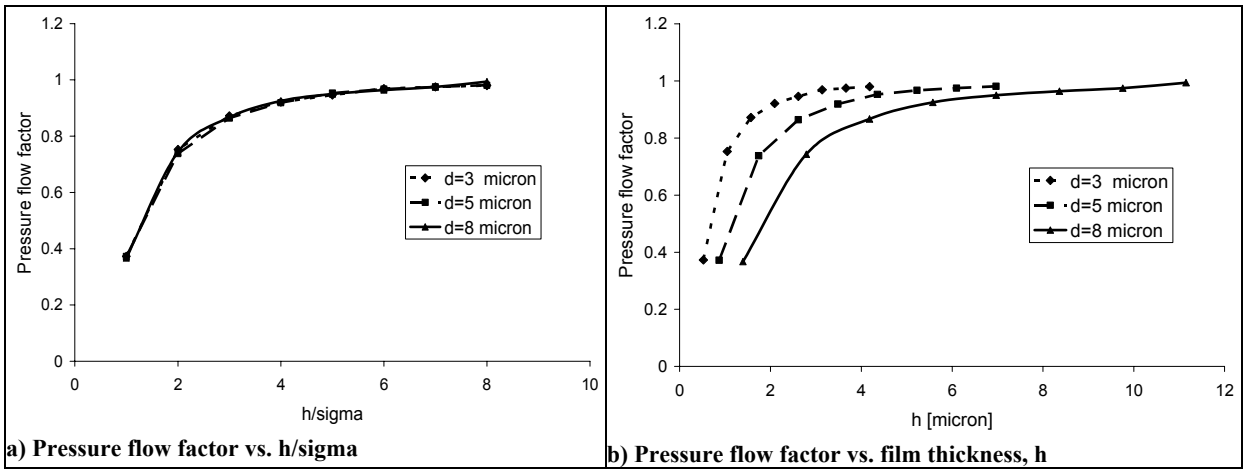

a) Pressure flow factor vs. h/sigma

b) Pressure flow factor vs. film thickness, h

Figure 6-19: Effect of dimple depth on pressure flow factor, diameter = 19μ, area ratio = 0.25

The dimpled patterns were also similar to the grooved cases in that the change in pressure flow factor with the depth of the features mirrored the changing surface roughness, so that plotting pressure flow factor as a function of h/σ shows no effect from depth changes. Figure 6-19 shows this, along with the pressure flow factor plotted vs. h only, which illustrates the effect of dimple depth at a given film thickness. Further discussion of this phenomenon is given in Section 6.4.2.1. Because it is useful to observe both the non-dimensionalized effects of various parameters and to evaluate the pressure flow factor at an expected film thickness for a specific case, ϕ_p is shown as a function of both h/σ and h alone in the examples below.

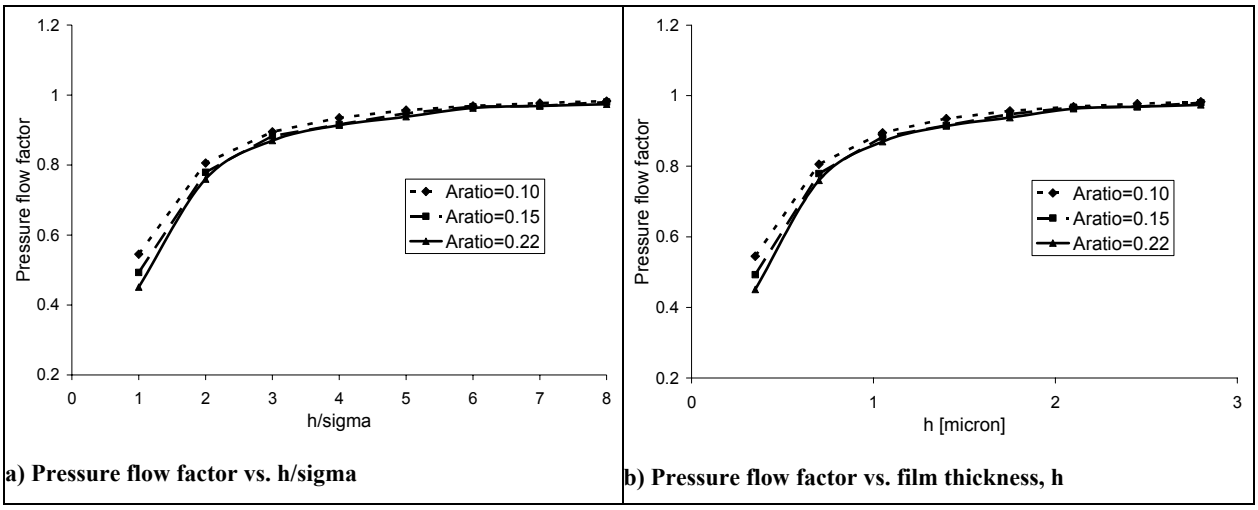

a) Pressure flow factor vs. h/sigma **b) Pressure flow factor vs. film thickness, h**

Figure 6-20: Effect of dimple area ratio on pressure flow factor, diameter = 19μ, depth = 3μ

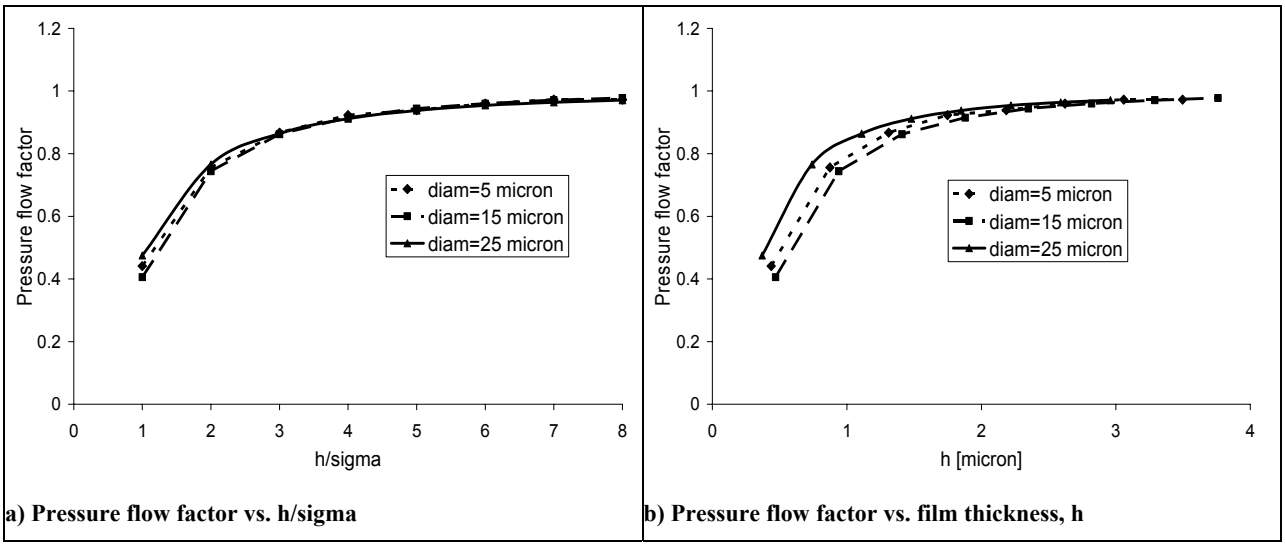

a) Pressure flow factor vs. h/sigma **b) Pressure flow factor vs. film thickness, h**

Figure 6-21: Effect of dimple diameter on pressure flow factor, depth = 3μ, area ratio = 0.25

Figure 6-20 shows the effect of dimple area ratio on the pressure flow factor. As the figure shows, pressure flow factor decreases slightly with area ratio, but the effect is weak. As for the grooves, it is expected that the effect of increasing area ratio will be to increase both the amount of interaction that occurs between dimples and the number of "micro-hydrodynamic" bearings that are present on the surface, and is expected to cause a decrease in pressure flow factor. It is unclear why this effect is so weak for the dimpled cases, although several studies have also shown this for dimpled surfaces, including Etsion et. al [44] and Ronen, et. al [45].

Figure 6-21 also shows a relatively weak effect, of the dimple diameter on pressure flow factor. In this case, there is an optimum diameter at which pressure flow factor is minimized –

the mid-range diameter, d = 15μ, shows the lowest ϕ_p. The optimal dimple diameter occurs at a value where the diameter and depth combine to define a dimple shape that provides the maximum hydrodynamic pressure generation, and is also similar to an effect observed by Etsion [44] in which an optimal ratio of dimple depth:diameter was found.

6.4.3.2. Friction Results

Ring/liner friction predictions for the dimpled surfaces were consistent with those expected given the flow factor results presented above. As the effects of the surface parameters on the pressure flow factor were small, changes in FMEP for different surfaces considered were also small relative to those predicted for different grooved patterns. It appears that dimpled surfaces are less sensitive to changes in feature geometry – except for dimple depth – than grooved surfaces, and may thus be easier to design for given slider geometry and running conditions. As for the friction analysis for the grooved surfaces presented above, the following results are based on an approximate analytical method and cannot be used to predict actual friction reductions in realistic situations, but they do indicate that liner surface texturing can reduce ring/liner friction, and should be studied further.

Some modifications were made to the ring-pack simulation program in order to obtain the results presented below. Details of these modifications are given in Section 6.4.2.2. In the model, the depth of the dimples was represented by the overall textured surface roughness, σ, which has therefore been used to represent dimple depth in the figures shown below. In both figures, FMEP is plotted as a function of σ, which is the RMS roughness of the surface under study. This should be understood to correspond to dimple depth, where a roughness of σ=0.5μ corresponds approximately to a depth of d=3μ.

Figure 6-22 shows the effects of both dimple depth and area ratio on ring/liner FMEP. As the figure shows, the effects of depth are much greater than those of area ratio, which has only a small influence on friction. FMEP decreases strongly with depth, and shows no sign of leveling off at large depths, as the grooved cases did. It is expected that the effect of dimples on FMEP with increasing depth will eventually disappear, as for very deep dimples the fluid in the bottom will simply be stagnant and not contribute to the hydrodynamic action of the texturing. However, this limit appears to be beyond the level of dimple depth that has been investigated here. The effect of area ratio is much smaller than that of dimple depth, so that it may not be necessary to optimize for this parameter in designing a friction-reduction surface.

Figure 6-23 shows the effects of dimple diameter on ring/liner friction. The effect of diameter is also small, with the minimum FMEP found at a mid-range value. This optimal diameter phenomenon has also been observed in the literature (see Section 6.4.2.1) and is the result of the effect of the dimple geometry on the amount of hydrodynamic pressure generation that occurs as lubricant flows through the dimple. The effect of diameter on both the converging/diverging length and the dimple profile contribute to this effect.

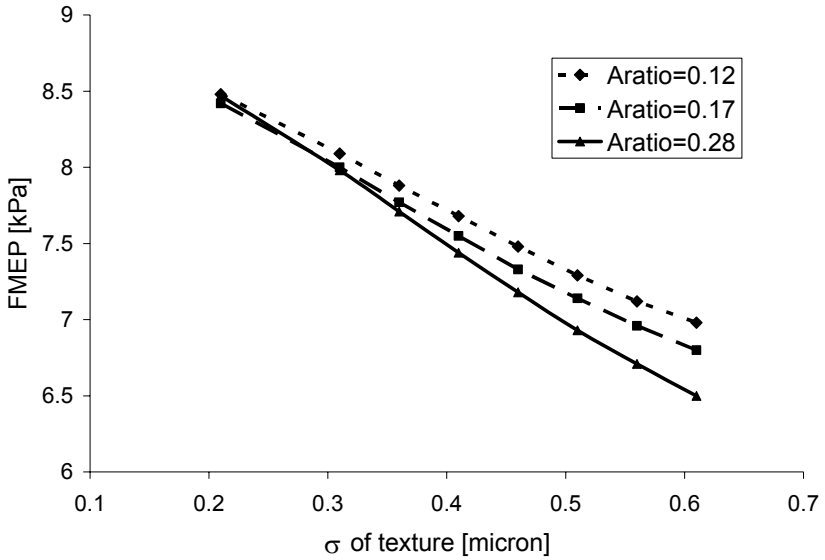

Figure 6-22: Effect of dimple area ratio on ring/liner friction, diameter = 19μ

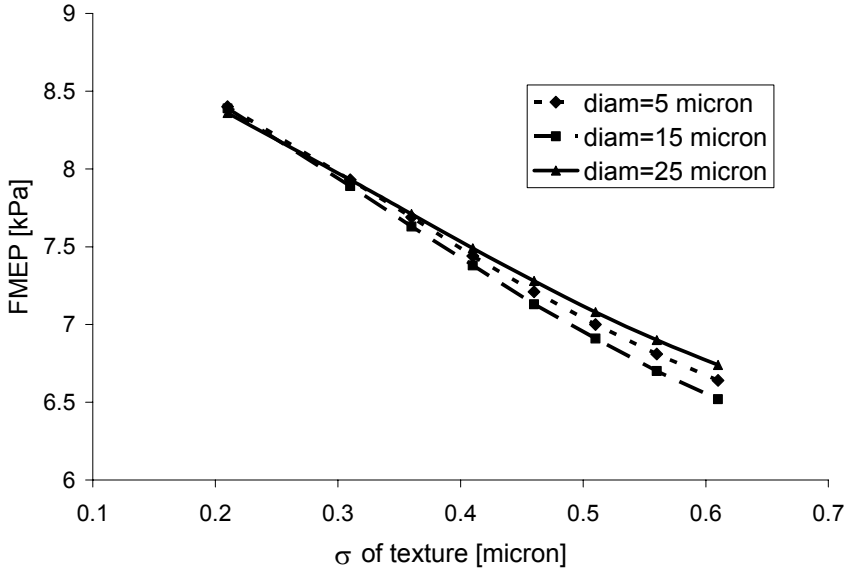

Figure 6-23: Effect of dimple diameter on ring/liner friction, area ratio = 0.25

6.5. Summary and conclusions of surface texturing parametric study

Surface features can affect sliding friction in many ways, including removing wear particles from the sliding interface and acting as fluid reservoirs to provide adequate lubrication where it is needed. This study considered the role played by surface texturing in the hydrodynamic regime, and its potential to reduce piston-ring/liner friction under this condition. An averaged flow-factor Reynolds analysis was used to evaluate the effects of patterns of either grooves or dimples on the cylinder liner. Because this averaged technique was used, a detailed study of the lubricant pressures and flows could not be made. Still, the results of this parametric

study can be used to estimate the potential of surface texturing for, and the effects of various texture parameters on, friction reduction.

In a well-lubricated regime, surface texturing affects both hydrodynamic and boundary friction between the ring and liner by influencing the hydrodynamic pressure generation within the lubricant, and thus the oil film thickness. Textures that impede lubricant flow increase oil pressure and thus increase film thickness, at a given load. This increase in h can cause a reduction in asperity contact, if any was present in the baseline case, and also reduces shear stress by reducing the shear rate in the oil. Thus, an appropriate surface texture can decrease both hydrodynamic and boundary friction between ring and liner. An inappropriate texture, however, can cause an increase in friction by allowing oil to flow more easily and thus reducing oil film thickness. It is necessary to understand the effects of different textures, and their relation to slider parameters and running conditions, in order to design surfaces for friction reduction in actual applications.

Both stochastic parameters, such as roughness and skewness, and deterministically defined features such as dimples influence the way in which a surface affects sliding lubrication and friction. This study focused on two texture categories: patterns of round dimples and patterns of grooves. For the dimpled cases, the effects of dimple diameter, depth and area ratio were studied, while for the grooved surfaces groove angle, depth, width, and area ratio effects were assessed. The results of a parametric study of both the flow factors, which give an indication of the physical effects of the surface texturing, and predicted friction losses, for Waukesha engine geometry and running conditions, were presented.

The effects of many of the surface parameters studied were similar for the dimpled and grooved surfaces. Friction was found to decrease as the depths of both dimples and grooves were increased, as well as with increasing area ratio for both pattern types. The effects of groove width and dimple diameter were both relatively small. In the case of the dimples, an optimum effect was observed in which the minimum friction was found at a mid-range diameter, because of the dependence of hydrodynamic pressure generation on the shape and size of the dimples. There may also be an optimum effect in relation to groove depth, stemming from a trade-off between hydrodynamic effects and lubricant flow area. Friction was also found to decrease strongly with groove angle, (where a groove with a lower angle is more perpendicular to the lubricant flow direction) in agreement with previous studies [15].

The analytical method used in this study is subject to several limitations and approximations, and therefore the results are not intended to be used directly in the design of friction-reducing surface textures. Rather, the trends presented here are used to illustrate the potential of appropriately designed surface textures to reduce friction both in the engine and other sliding friction applications, and to indicate the relative importance of the various texture parameters that define two common surface patterns. The study has showed that even relatively small-scale textures (compared to others that have been studied in the literature) can have a large effect on ring/liner friction, in some cases reducing FMEP by as much as 30% from a smooth surface case. Also, it may be possible to combine the effects of lubricant viscosity and surface texturing to reduce friction even further, while mitigating unwanted side-effects such as wear and oil consumption. This possibility is discussed in Section 7.5.

7. Application of Lubricant and Surface Texture Studies to Waukesha Engine

The lubricant and surface texture studies presented in Sections 2 and 3 were applied to an analysis of the piston ring-pack in the Waukesha VGF 18GL engine. These studies were part of an on-going program whose intention is to increase the efficiency of this engine from ~42% to 50%, over a ten year period. While reducing mechanical losses is only one of several efficiency-increasing measures to be developed in this time, it is an essential part of reaching the stated goal. Application of optimized lubricant and surface features to the piston ring-pack and cylinder liner is one of many measures that will help the goal efficiency to be achieved.

7.1. The standard engine parameters

The engine under study is the Waukesha VGF 18GL, a large natural gas engine used for stationary power generation, shown in Figure 7-1. Some engine specifications and operating conditions are given in Table 7-1.

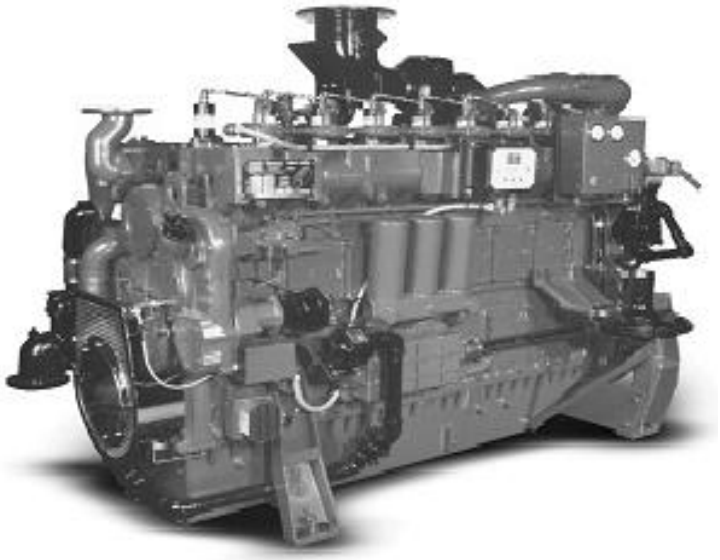

Figure 7-1: The Waukesha VGF 18GL engine

For baseline mechanical and surface roughness parameters, frictional losses in the Waukesha engine ring-pack are dominated by the oil control and top rings. The OCR is the largest contributor to friction because of its high ring tension. It is required to conform very well to the cylinder liner, while maintaining enough stiffness to resist warping and breakage, so a high tension is necessary. This results in a high ring-liner load throughout the cycle, leading to high friction.

The top ring contribution to friction is also significant, because of the large friction forces associated with boundary friction near the top dead center (TDC) of the combustion stroke. In this region, two factors combine to create high friction: first, the oil supply to the top ring at TDC is very limited, because the oil control ring doesn't reach this high on the liner; second, combustion chamber gas pressure, following compression and combustion, is very high. The combination of high ring load and poor lubrication results in very high asperity contact pressures, and thus high friction (and also high wear). Even though piston speed is very low here, the total frictional power loss from this region is still significant. Figure 7-2 shows this high-friction "spike" for the top ring, compared to the more evenly distributed frictional losses for the OCR.

Table 7-1: Waukesha Engine baseline parameters and operating conditions

Parameter	Value	Unit
Engine type	Natural gas, SI	-
Bore x Stroke	0.152 x 0.165	m x m
Number of cylinders	6	-
Displacement	18	liter
Engine Speed	1800	rev/min
BMEP @ 1800 RPM	1380	kPa
Lubricant grade	SAE 40W	-
Top Ring Type	Skewed barrel	-
Second Ring Type	Napier	-
OCR Type	Twin land	-

Because the majority of top ring friction comes from this dry-region friction spike, however, this ring has not been considered in detail in either of the studies presented here. Top ring friction it is not expected to be strongly affected by lubricant viscosity, because most of the friction is generated in a poorly lubricated regime – if no lubricant is present, its properties cannot matter. A brief study of the effect of lubricant viscosity on oil transport into the dry region was conducted, with results presented in previous reports, but the model used to obtain these results had a relatively simple oil transport model, and more research is needed to validate the conclusions.

Also, while top ring friction may be greatly reduced by the addition of surface texturing to the cylinder liner, the mechanism by which this would occur has not been investigated here. The focus of the surface texture study was on the hydrodynamic effects of the surface features, and their ability to reduce friction in a well-lubricated regime. It may be possible to reduce top-ring friction by adding dimples near TDC to act as lubricant reservoirs, and thus increase the lubrication in this area. However, this mechanism has not been studied in the current project.

Because of these considerations, the oil control ring (OCR) was the main focus of both the lubricant and surface texturing studies. The OCR contributes most of the ring-pack friction and is strongly affected by lubricant viscosity and surface texturing. Top ring friction is significant,

but stems mainly from a poorly-lubricated regime in which viscosity and surface effects are expected to be small. The trends observed for the OCR are expected to correspond to viscosity/friction trends for the entire ring-pack.

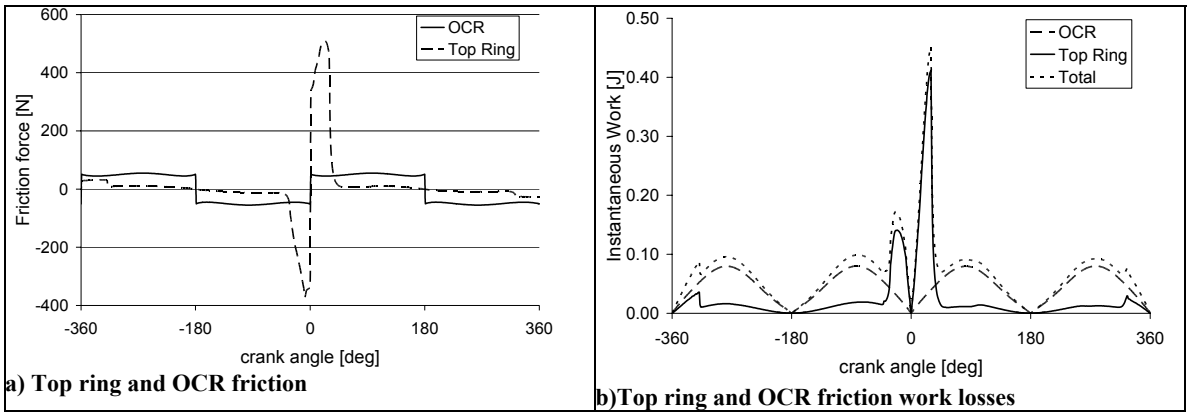

Figure 7-2: Top ring and OCR contributions to ring-pack friction losses

7.2. Lubricant viscosity and liner surface finish studies

Changes in both lubricant viscosity and surface finish can lead to reduced friction in the Waukesha engine ring-pack. Reductions in lubricant viscosity reduce hydrodynamic friction between ring and liner, and if viscosity can be maintained at a higher value near dead-centers, wear in that region can be reduced. Adding an appropriate texture to the cylinder liner may also reduce friction, both hydrodynamic and boundary, by increasing hydrodynamic pressure generation and thus oil film thickness.

In addition to the individual effects of these two parameters, an even greater friction reduction is possible when these two changes are combined. Friction reduction via lubricant viscosity reduction is possible, but not without a concurrent increase in wear. Surface texturing can also be used to reduce friction, but does so by increasing oil film thicknesses, which may cause increased oil consumption. A reduced viscosity lubricant can be combined with a textured liner surface to reduce friction while minimizing these adverse effects.

Fortunately, the side-effects of viscosity reduction and addition of surface texturing are complimentary, so that when these techniques are used concurrently the negative aspects can be minimized. Reducing lubricant viscosity causes a reduction in oil film thickness, which may lead to increased asperity contact, and thus, wear. Adding surface texturing, however, causes an increase in oil film thickness, by increasing hydrodynamic pressure generation. If lubricant and surface texturing parameters can be changed so that oil film thickness remains approximately equal to the baseline case, there should be little effect on wear and oil consumption. Friction will still be reduced, however, because of the reduced lubricant viscosity.

Application of both lubricant viscosity changes and surface texturing to the Waukesha engine power cylinder are discussed below, followed by consideration of the possibility of optimizing lubricant viscosity and surface texturing concurrently. Because the surface texturing study was a parametric exercise, no specific recommendations or friction reduction estimates can be made for the Waukesha engine, but possible benefits are estimated. Similarly, several examples are given to illustrate the effects of optimizing the lubricant and surface texturing together, but specific recommendations cannot be given. It is hoped that future analysis and testing will take a more in-depth look at the effects of surface texturing, and that an optimized, low-friction surface pattern for the Waukesha engine will be developed.

7.3. Optimization of lubricant viscosity

Friction power losses between the piston-rings and liner stem primarily from the mid-stroke region, while wear of the rings and liner is generally concentrated at the end-strokes. Reductions in both friction and end-stroke wear may be possible if lubricant viscosity can be reduced in the mid-stroke region and increased near dead-centers. Such a strategy was applied to the Waukesha engine, described above, and predictions of friction and wear made for an optimized lubricant.

As shown in Figure 7-3, a maximum friction reduction of ~10% is predicted for the OCR, from the baseline case, when viscosity in the mid-stroke region is reduced. An additional reduction of ~1% is possible when dead-center viscosity is held high to reduce boundary friction. For the Waukesha engine, the oil control ring accounts for ~65% of the total ring-pack losses. Then, an OCR friction reduction of 11% leads to a total ring-pack friction reduction of approximately 7%. Cross and Vogel equation parameters for the minimum-friction lubricant are given in Table 7-2 (those that are not given in the table are kept equal to baseline values, for SAE40 weight oil).

The top ring contributes most of the remainder of the ring-pack friction, but experiences most of its losses (~70%) as boundary friction in the poorly-lubricated TDC region of the stroke. Then, viscosity does not have a large direct affect on top ring friction. However, simulations show an indirect effect, where oil transport into the dry region may increase as viscosity decreases. This leads to a decrease in friction of up to 30%, leading to a ring-pack friction reduction of ~9%. However, the mechanism for this reduction is not clear, and a simplified oil-transport model was used which does not include all recognized oil transport mechanisms. Further research is required to investigate this top ring effect.

Ring/liner wear was also briefly considered, in a simple analysis of a wear coefficient related to boundary contact force and ring/liner sliding distance. Wear was found to increase strongly with decreasing viscosity, even as friction remains low. In the interest of keeping wear low, then, it may be necessary to accept a higher-than-minimum level of ring/liner friction. Controlling viscosity variation was shown to have some potential benefit in reducing wear near the end-strokes, because of the reduction in asperity contact forces in these regions, with an integrated wear coefficient reduction of ~25% for an engine cycle.

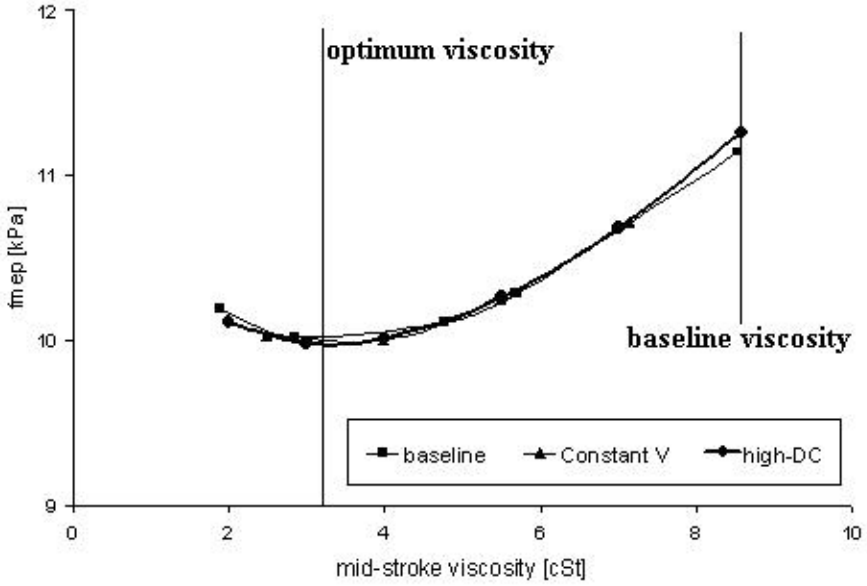

Figure 7-3: Reduction of oil control ring friction with mid-stroke viscosity. Three viscosity variation cases.

Table 7-2: Vogel and Cross equation parameters for low-friction lubricant

Parameter	Physical meaning	Current Value	Proposed Value	Ring-pack Friction Reduction
z	viscosity "thickness"	.09	.06	7%
c_1,c2	control critical shear rate	2.3, 0.0225	4.3, 0.0225	
m	controls width of transition region	1 (more gradual transition)	5 (sharper transition)	
μ/μ_0	ratio of high shear to low shear viscosities	1	0.5	

While it may be possible to develop a lubricant with the shear-dependence properties described here, or develop a liner temperature-control system to produce the same viscosity variation with location, the costs of these systems must be balanced against the potential benefits described above. Also, it should be emphasized that the study presented here considered the effects of lubricant viscosity on the piston ring-pack only. The effects of the considered viscosity changes on the other engine components must also be considered before any change in engine lubricant is made.

7.4. Optimization of liner surface finish

Surface texturing can be used in many different ways to reduce friction between a piston-ring and the cylinder liner. In this study, the ability of small-scale surface features to act as "micro-hydrodynamic" bearings, and thus increase the hydrodynamic pressure within the lubricant, was evaluated. The action of the micro-features causes an increase in oil film thickness between the ring and liner, both decreasing asperity contact (if any is present to begin with) and decreasing oil shear rate, which reduces hydrodynamic friction.

The averaged-flow-factor Reynolds analysis method that was used in this study is limited in its ability to model details of the flows and stresses between textured surfaces, and thus the results cannot be used to recommend a specific liner texture for the Waukesha engine, or predict actual reductions in friction resulting from a textured surface. Rather, the trends in friction with changing surface parameters may be used as a starting point for further investigation of the effects of liner texturing, and may be used to estimate the potential for friction reduction in the case of the Waukesha power cylinder.

It has been noted that the surface texture of the Waukesha engine cylinder liner is already well-optimized for low friction, with a low skewness of -2.15 (more plateau surface) and honing grooves with the relatively low honing angle of 45^o +/- 5^o [15]. Then, further friction reductions for this engine may be relatively small. Figure 7-4 shows the predicted decrease in friction with groove angle for the oil control ring, with a groove depth of ~2μ. The actual depth of the grooves in the existing Waukesha cylinder liner is not known, but known stochastic parameters including roughness and skewness indicate that this is a reasonable estimate.

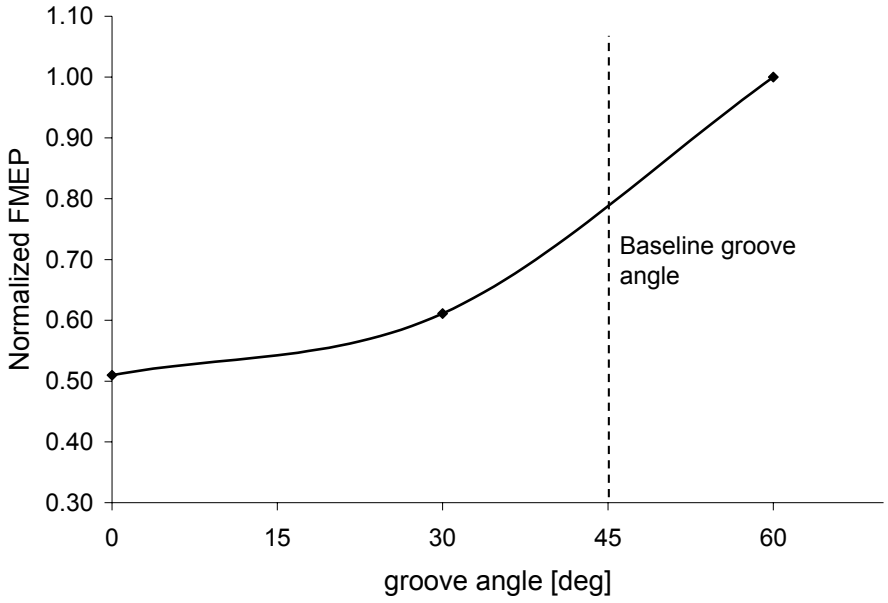

Figure 7-4: Estimate of OCR/liner friction reduction possible with reduced groove angle

Figure 7-4 indicates that, with a decrease in groove angle from 45° to 30°, a friction decrease of ~25% is expected. If the angle is further decreased down to a minimum value of 0°, the total reduction in FMEP is estimated at ~37%. These estimates are for the oil control ring alone. When frictional losses for the top and second rings are added, estimated friction reductions for the ring-pack become 15%, for 30° grooves, and 25% for 0° grooves. Although these numbers seem very promising, the simplifications made in both the surface modeling and the modeling of the ring/liner/lubricant interaction must be considered. Rather than being actual estimates for FMEP reduction with groove angle, these numbers should be taken as estimates of the magnitude of friction reduction that could be possible.

Although the largest friction reduction is predicted for a very low groove angle, it should be noted that issues of engine wear and scuffing may be associated with honing grooves that are very perpendicular to the cylinder axis (although there is some disagreement over whether this is the case). The reason for this is not well understood. One possibility is that honing grooves at a larger angle allow fluid to flow through them, and thus clean out wear particles that are deposited there, while more perpendicular grooves eventually fill up with particles which then cause increased wear and scuffing. Another possible explanation is that the effect of the textured surface in the high-load, low-speed conditions near TDC of combustion is much different than that in the well-lubricated mid-stroke region. In high-speed, low-load conditions, transverse textures may get "flattened" by contact pressures, while more longitudinal textures survive [52].

The existing Waukesha engine cylinder liner already has a grooved pattern due to the surface honing process. Comparing the relative effectiveness of grooved and dimpled surfaces, it is not recommended that the existing pattern be replaced by a dimpled arrangement, as this would add complications to the finishing process and most likely not incur greater friction-reduction benefits than a grooved surface. It may be useful to add a dimpled or other discrete pattern to the cylinder liner that is on a larger scale than those studied here. Many of the surface textures studied in the literature focus on much larger dimples (with diameters on the order of 100μ and larger, depths on the order of 10μ) that have been shown to reduce friction (see Section 7.1.2 for further detail). However, such large features cannot be studied using the current modeling system.

A parametric study of the effects of surface texturing on ring/liner friction indicates that there is potential for these surfaces to reduce friction by a significant amount. The method of analysis used for this study prevents detailed predictions of friction and oil flow effects from being evaluated, and also limits the size of the surface textures that can be considered. The results from this simple study, however, indicate that appropriate surface texturing may provide a substantial benefit in friction reduction, and that further study, encompassing both more detailed modeling and a larger range of parameters, is justified.

7.5. Combined optimization of lubricant and liner surface

Ring/liner friction can be reduced when lubricant viscosity is decreased in the mid-stroke region, but the resulting increase in asperity contact may result in an unacceptable level of wear. A friction reduction is also possible if appropriate surface texturing is added to the cylinder liner,

but the accompanying increase in oil film thickness may cause an increase in oil consumption. Alone, each of the friction-reduction techniques studied above can reduce losses but may also have an unwanted side effect. When used together, however, the side effects may be mitigated – the decrease in oil film thickness due to reduced viscosity may be offset by the increase due to the surface texturing – while still achieving a reduction in frictional losses.

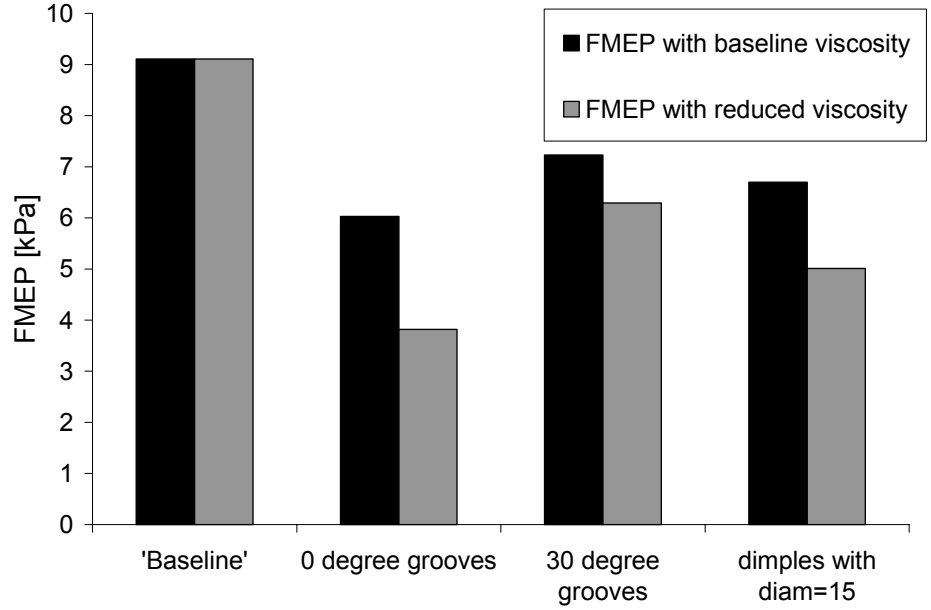

Figure 7-5: FMEP reduction due to combined lubricant and surface texturing effects, example cases

This possibility was studied using several promising surface textures. Because the surface texture study was parametric, and did not use realistic surface roughness in addition to the surface features under study, the results presented here should not be used to design an actual surface/lubricant combination. Rather, they are given as examples to illustrate the possibilities of optimizing the lubricant and surface texturing jointly, and to demonstrate the magnitudes of the possible friction-reduction benefits of doing so.

In each of the example cases, the given surface texturing was applied to the cylinder liner surface, and then the ring-pack simulation was run with varying lubricant viscosities. The viscosity at which oil film thickness and wear were closest to the original baseline case was selected as "ideal." At this viscosity, no net increase in asperity contact or oil film thickness should occur, so that changes in wear and oil consumption should be minimized.

Figure 7-5 shows the friction losses of three example surface textures, as compared to the baseline. For the baseline case the cylinder liner is untextured, and the lubricant is the baseline lubricant for the Waukesha engine (SAE 40). Surface and lubricant parameters for the example cases are given in Table 7-3. Only z, the oil "thickness" parameter from the Vogel equation (Eqn. 7.1) is varied for the lubricant, so that the viscosity temperature dependence remains the same as overall viscosity is changed.

Table 7-3: Surface and lubricant parameters for example cases

Surface texture properties		*Properties of reduced-viscosity lubricant*	
Baseline			
Type	none (smooth)	z	.09
0 degree grooves			
Type	parallel grooves	z	.025
depth, R_q	0.56 μ		
Width	19μ		
groove angle	0 deg.		
area ratio	0.24		
30 degree grooves			
Type	parallel grooves	z	.05
depth, R_q	0.56 μ		
Width	19μ		
groove angle	30 deg.		
area ratio	0.24		
dimples, diameter = 15			
Type	round dimples	z	.04
depth, R_q	0.56 μ		
Diameter	19μ		
area ratio	0.25		

As Figure 7-5 shows, adding the surface texturing alone causes friction reduction in all cases, and then additionally reducing the lubricant viscosity causes friction to decrease further. This additional decrease in friction is not as large as that due to texturing alone, but is still a sizable reduction. Also, the reduction due to reduced lubricant viscosity is approximately proportional to that due to the texturing alone. This is because the amount of viscosity decrease that is ideal – that reduces the film thickness back to the baseline value – is directly related to the increase in film thickness that is brought about by the addition of surface texturing. The friction reduction due to the surface texturing is also related to this film thickness, so that the two drops in friction – due to surface features and due to lubricant viscosity reduction – are closely related to each other.

Figure 7-6 and Figure 7-7 show the effects of the combined surface/lubricant optimization on oil film thickness and wear parameter. As was the intention of using a lubricant with reduced viscosity, in cases where the surface and lubricant were optimized together both the oil film thickness and wear parameter are very similar to the baseline case. When surface texturing is used alone, the resulting oil film thicknesses are much higher than in the baseline case, as shown in Figure 7-6. Similarly, as shown in Figure 7-7, if viscosity is reduced without any added surface texturing, a large increase in wear is predicted. Optimizing the liner surface texture and lubricant viscosity concurrently offers the opportunity to mitigate these negative side effects, while still substantially reducing ring/liner friction.

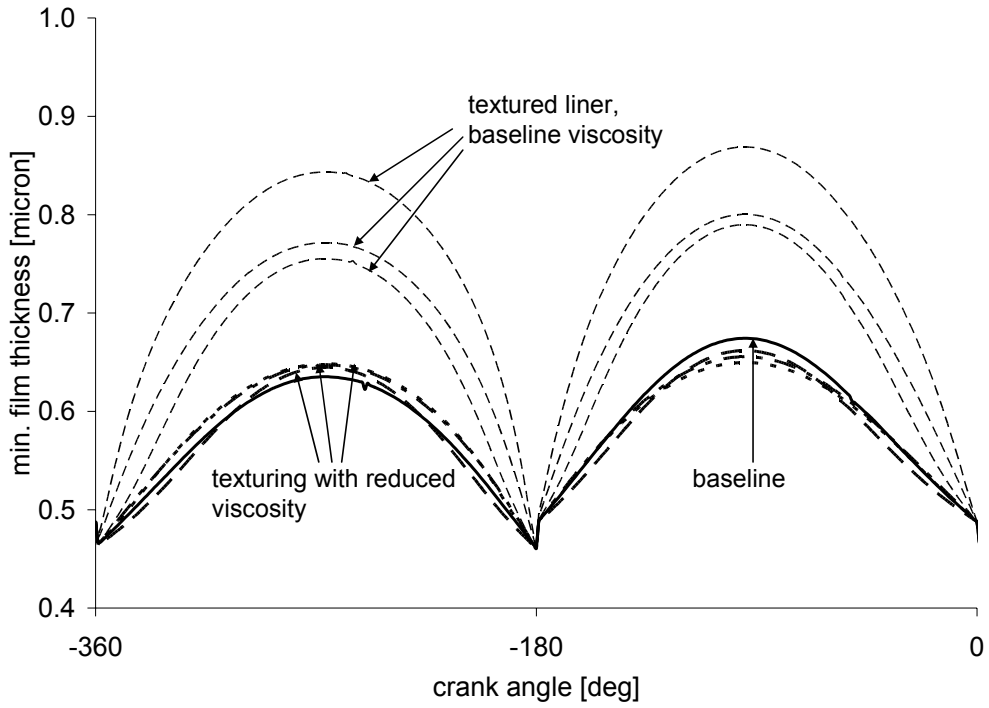

Figure 7-6: Minimum oil film thickness, for combined surface/lubricant effect example cases

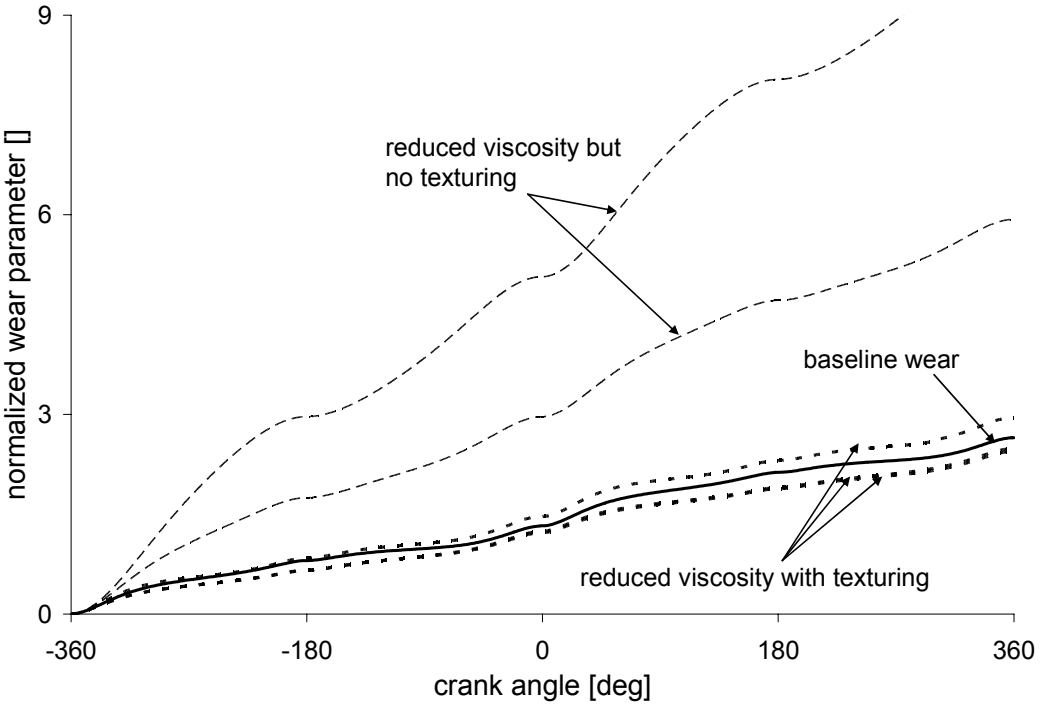

Figure 7-7: Normalized wear parameter, for combined surface/lubricant effect example cases

8. Summary of Lubricant and Surface Texture Effects on Ring-Pack Friction

The piston ring-pack is one of the largest contributors to mechanical losses in an internal combustion engine. In this study, the effects of lubricant viscosity and liner surface texturing on ring/liner friction were considered, with the intent of reducing these losses in the Waukesha VGF 18GL engine. An optimized low-friction lubricant was proposed, and a parametric study of surface texturing showed that adding appropriate surface features to the cylinder liner may also significantly reduce ring/liner friction. Also, if the lubricant and surface texturing can be optimized together, an even greater reduction in friction is possible, along with mitigation of undesired side-effects, such as oil consumption and wear, which may accompany changes made to the lubricant viscosity and surface texturing individually.

The ring-pack simulation model used for both the lubricant and surface texturing studies was based on averaged flow factor Reynolds analysis, and was developed at MIT. Inclusion of features such as ring dynamics, gas flows, and different lubrication modes makes this advanced model able to predict ring/liner friction accurately for a variety of conditions. While the lubricants studied in the first phase of this research were certainly unusual, they were not out of the realm of applicability for this model, and results of the lubricant study should be considered to be realistic. However, the textured surfaces considered in the second phase of this study may have been close to the limitations of surface roughness for which this model was intended. Also, the averaged flow-factor method takes into account less detail about fluid flows and asperity contact than is required for an in-depth study of surface texturing. Then, the results of the this study may be used to assess the effects of the various parameter considered, and evaluate the potential of texturing techniques for reducing ring/liner friction, but further, more detailed study is required to predict the effects of specific surface features with good accuracy.

The subject of the initial phase of this research was the potential of changes in the lubricant viscosity to bring about a reduction in ring/liner friction. Lubricant viscosity affects friction both directly, by having a direct affect on hydrodynamic friction, and indirectly, by influencing the oil film thickness and thus the amount of asperity contact that occurs. Increasing viscosity tends to increase oil film thickness, and thus reduce asperity contact, but causes hydrodynamic friction to increase. A viscosity that balances between the hydrodynamic and boundary lubrication modes is required for minimum friction.

Changes in ring speed and load cause the “ideal” viscosity for low friction to change during the engine cycle. The object of the lubricant study was to determine the optimum viscosity for all points in the engine cycle, and evaluate the potential for friction reduction with such an idealized lubricant. Also, the effects of viscosity change on wear were considered.

Because of changes in ring speed, boundary friction becomes large in the dead-center regions of the piston stroke, while hydrodynamic friction dominates in mid-stroke. Thus, for the reduction of ring/liner friction force, a high viscosity is desired near end-strokes and a low viscosity near mid-strokes. However, the purpose of this study was to reduce the power lost to friction, and, because of its dependence on speed, the power lost to friction is much higher near

the mid-strokes than at the end-strokes, where piston speed goes to zero. Because of this, the viscosity of the lubricant in the end-stroke regions was found to have only a small effect on ring/liner FMEP, with the major realm of influence of lubricant viscosity occurring in the mid-stroke region. For the Waukesha engine ring-pack, a friction reduction of ~7% is predicted from reduction of mid-stroke lubricant viscosity.

Although viscosity near the end-strokes has very little effect on friction losses, it does influence ring/liner wear. Slow piston speeds cause asperity contact to be high at the end-strokes, resulting in high wear rates. When viscosity is kept high in these regions asperity contact and thus wear is reduced. Advanced lubricants with appropriate shear-rate dependencies or liner cooling systems that take advantage of the temperature-dependence of the lubricant viscosity may be able to achieve this in practice. A wear parameter analysis predicts that a reduction in wear of ~25% over an engine cycle is possible.

Surface texturing, also, can be used to reduce friction between the ring and liner. Numerous studies have predicted friction reductions with the addition of grooves, dimples, or other features to sliding surfaces. In the second phase of this research, the effect of surface patterns on friction in the hydrodynamic regime was evaluated. Friction reduction was observed when the surface texturing caused an increase in flow resistance, increasing oil film thickness and thus causing a reduction in both asperity contact and hydrodynamic friction. (In the latter case, the increased film thickness causes a reduction in oil shear rate). A parametric analysis of both grooved and dimpled patterns was performed, with the two purposes of studying the effects of various geometrical parameters on this friction reduction, and evaluating the potential of textured surfaces to reduce ring/liner friction and possibly justify further research in this area.

Groove parameters studied included the groove angle, width, depth, and area ratio, while parameters for the round dimples were the dimple depth, diameter, and area ratio. For both types of texturing, friction was found to decrease strongly with the depth of the features, and for grooved surfaces friction dropped substantially as groove angle was reduced (a groove with a lower angle is more perpendicular to the direction of piston travel). Also, for both types of texture, friction decreased with increasing area ratio, although not as strongly as with depth or groove angle. Groove width and dimple diameter had only a minor effect on ring/liner friction, with the dimpled surfaces showing a slight optimum effect (the lowest FMEP was predicted for a mid-range dimple diameter).

The analytical method used in this study did not allow for accurate predictions of ring/liner friction for specific cases, but the trends and orders of magnitude of the friction results can be used to illustrate the effects of textured surfaces and their potential for friction reduction. The study has indicated that even the relatively small-scale (compared to many evaluated in the literature) surface features considered may have a substantial effect on friction power losses. A reduction in oil control ring FMEP of as much as 30%, from a smooth surface case, is predicted for the best case studied. If the results of the parametric study are applied to the Waukesha engine ring-pack, a possible friction reduction of 15-25% is estimated through control of groove angle. While these predictions are approximate and should not be used to design actual friction-reducing surfaces, they indicate that a substantial friction reduction may be possible with the addition of appropriate textures to the cylinder liner.

In addition to studying the lubricant viscosity and liner surface texture independently, the possibility of optimizing these two parameters together was also considered. Not only can concurrent optimization of lubricant viscosity and surface texture cause a greater friction reduction than each individual parameter, the occurrence of unwanted side-effects can also be reduced. A reduction in lubricant viscosity, while reducing friction, also causes an increase in wear because of the reduced oil film thickness. Adding a surface texture to the liner may also reduce friction, but does so by causing an increase in oil film thickness which may in turn cause an increase in oil consumption. Fortunately, the effects of the two changes are opposed: reducing viscosity reduces oil film thickness, whereas adding surface texturing increases it. If the viscosity and texturing effects are considered together, the lubricant and liner surface can be designed so that oil film thickness remains constant, thus eliminating the wear and oil consumption increases, while still reducing friction.

The nature of the combined optimization of lubricant viscosity and surface texturing is essentially to use the increase in hydrodynamic pressure brought about by the texture to allow lubricant viscosity to be reduced. Then, the source of the friction reduction is purely hydrodynamic, and stems from the reduced viscosity. This study has indicated that the amount of friction reduction possible using a combined method is proportional to that possible from surface texturing alone. For the best combination of surface and lubricant studied, compared to a smooth surface with the lubricant currently used in the Waukesha engine, a reduction in FMEP of greater than 50% is predicted for the oil control ring, translating into a reduction of ~30% for the ring-pack. While friction reduction will likely be less than this when applied in real situations (particularly as many surfaces and lubricants are already well-optimized compared to the smooth surface case used as the baseline in this comparison,) this prediction indicates that there is significant potential for friction reduction via concurrent optimization of lubricant and surface properties.

The results presented above are believed to be as realistic as possible given the scope and constraints of this study. However, several approximations and simplifications have been made, and some factors not considered. Several recommendations for further study, both analytical and experimental, can be made, to both advance the state of knowledge on the topics studied here and to move towards an integrated, low-friction system for the Waukesha engine.

(B) FRICTION REDUCTION VIA PISTON DESIGN – A CUMULATIVE REPORT

9. Friction Reduction Strategies - Piston Design

The piston skirt contributes as much friction as the ring-pack to the engine mechanical losses. Like the ring-pack, its friction can be reduced if asperity contact is reduced. The piston experiences both hydrodynamic and boundary lubrication, with the dominant lubrication regime changing during the engine cycle. While the hydrodynamic frictional losses from the two sides are approximately equal and occur throughout the stroke, boundary contact is only observed on the major thrust side, during the expansion stroke. This results from the high gas pressures present after combustion, as well as the piston "slap" as it moves from the minor to the major thrust side. The boundary friction generated in this region of the stroke contributes a significant amount of total piston skirt friction.

Several piston parameters have been studied earlier in the program, including design parameters such as the skirt profile and waviness, and other factors including lubricant viscosity and skirt-liner clearance, with the goal of reducing friction. The most important parameters identified thus were oil film thickness and skirt waviness, which can both be manipulated to reduce friction by reducing skirt/liner asperity contact.

In this reporting period, emphasis has been placed in the practical design parameters which offer the greatest potential for near term implementation, viz. mechanical design of the piston itself such as piston skirt ovality, the physical dimensions of the piston skirt, and optimizing the lubricant parameters for pistons of certain geometrical and material designs. These issues have not been addressed earlier. Rather than presenting only results of these incremental developments, this report includes results of all major piston design consideration to place the effects of each parameter in the proper context. A brief review of the model formulation and approach is also included for completeness.

9.1. Typical piston designs

In general, the piston consists of an upper region, containing grooves for the piston rings, and a lower region known as the "skirt". The skirt supports the piston/liner contact pressures, and is the site of friction generation and wear. Thus, this is the main region of interest in this study. Skirt friction and wear are affected by three design characteristics, the skirt profile, the waviness, and the surface roughness. The skirt profile is of the largest scale, and describes the large-scale variation in piston radius in the axial direction. The waviness results from the piston machining process and results in circumferential surface grooves on the scale of 10μ. The roughness is on yet a smaller scale, on the order of 1μ or less, and is controlled by the skirt material and the surface finishing techniques used. All of these piston characteristics affect friction, although the amount and the manner in which they affect friction depend on several other factors, including lubricant formulation and the extent of piston wear.

Pistons are produced with many different profiles, including tapered, barrel, and others, each offering advantages and disadvantages. This study focuses on barrel-profile pistons, such as the one shown schematically in Figure 9-1. The barrel shape of the skirt maintains a small piston diameter near the upper land, which allows for thermal expansion, while maintaining a relatively large wetted skirt area, which helps to reduce wear. The barrel shape also assists in creating a hydrodynamic oil film, and improves stability and reduces clearances by allowing for the natural secondary motion of the piston. The proportions of the barrel shape – i.e., the curvature of the bulge – have a large effect on piston/liner surface generation.

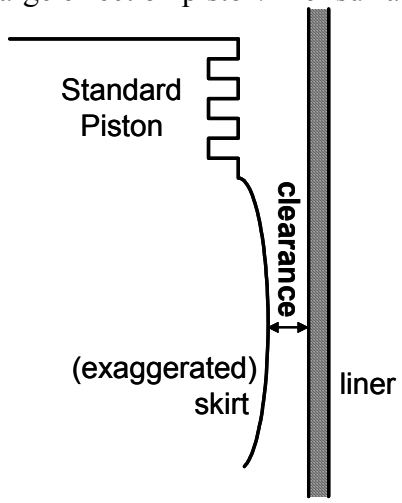

Figure 9-1: Piston with a barrel-shaped skirt

The waviness and roughness of the skirt also affect friction. Figure 9-2 shows a schematic of worn and unworn piston surfaces. For an unworn piston, the affect of the waviness dominates any roughness affects, because the waviness is on a larger scale. In this case, friction is dominated by the contact of the peaks of the waviness with the cylinder liner, causing boundary friction to occur. Contact occurs only at the high points of the machining grooves, with the height of those points determining when and how much contact occurs. As this type of contact continues, however, the peaks are worn down, as shown in the figure. In the worn case, the texture of the flat "plateaus" that has replaced the waviness peaks may become dominant. In this case, the height of flat surface roughness determines the extent of any asperity contact.

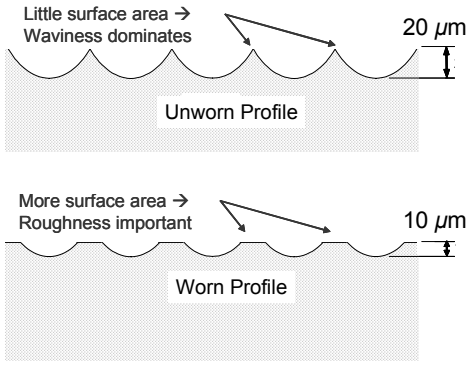

Figure 9-2: A side view of skirt waviness, worn and unworn cases

9.2. Analytical methods

A previously developed and experimentally validated model of piston secondary motion, developed by Wong et al., was modified and used in this study [1]. The modifications to the model consisted of including the influence of temperature on lubricant viscosity and variation of oil availability to the piston during the engine cycle [53]. When the piston moves up and down in the cylinder, it experiences substantial changes in temperature, which affect the local viscosity of the oil on the piston-skirt/liner interface. While the original model did not include this effect, and assumed a constant viscosity, a Vogel equation relationship was subsequently added in order to obtain a more accurate model of oil viscosity. For simplicity, only straight-weight oils (SAE-20, SAE-30, SAE-40, and SAE-50) were included in the analysis (shear rate dependence was not considered.

9.2.1. Modeling and governing equations for piston friction and lubrication

Several aspects of the piston/liner system make its analysis more complicated than the ring analysis. First, the piston is assumed to be always starved – that is, a fully-flooded condition does not exist, the piston is always only wetted over a portion of its surface. Also, the piston must be treated as a 2-dimensional system, a 1-D approximation like that used for the rings cannot be used, because of the spreading of lubricant in the tangential as well as the axial direction during wetting. In the model, the entire surface of the piston is taken into account, so that the changes in the locations of applied forces and lubricant wetting during the cycle are accounted for.

The flexibility of the piston also makes its analysis complex. In addition to tilting and displacing, as a unit within the cylinder liner, the piston skirt also deforms, in response to various applied forces. This skirt deformation is due in large part to the pressures applied by the oil film, which are in turn highly influenced by the skirt geometry. This phenomenon adds yet another iteration step to the analysis of the piston lubrication and friction.

9.2.1.1. Force and momentum balances

Simple force and momentum balances are used to model the dynamics of the piston. Vertical and lateral force balances are applied, taking into account gas pressures, piston inertia, ring forces, friction forces and thrust forces, as indicated in Figure 9-3. In the figure, the y-axis is in the vertical direction (positive up) and the x-axis is in the horizontal direction (positive to the right). Balances of forces and moments about the wrist-pin yield [37]:

$$\Sigma F_y: \quad F_g + \hat{F}_{IP} + \hat{F}_{IC} + \tilde{F}\cos\phi + \sum F_{qj} + F_f = 0 \tag{9.1}$$

$$\Sigma F_y: \quad \sum F_s \delta_s + F_{IP} + F_{IC} - \tilde{F}\sin\phi + \sum F_{rj} = 0 \tag{9.2}$$

$$\Sigma M_p: \; -\sum F_s y_s \delta_s + M_{IP} + M_{IC} + M_{PP} + F_{IC}(a-b) - \hat{F}_{IC} C_g + F_g C_p + M_f + C_p \sum F_{qj} + \sum F_{rj} Ij = 0 \tag{9.3}$$

where the terms in the above equations are shown in Table 9-1:

Table 9-1: Definition of terms in piston equilibrium equations

Parameter	**Definition**
F_g	Combustion gas force acting on top of the piston
$\hat{F}_{IP}$,F_{IP}	inertia force due to wrist-pin mass, x and y-directions
$\hat{F}_{IC}$,F_{IC}	inertia force due to piston mass, x and y-directions
F_q	vertical/normal force between piston and rings
F_r	horizontal/shear forces between piston and rings
F_f	total friction acting on the skirt, thrust and anti-thrust sides
F_s	side force, either F_1 or F_2 in the figure, depending on where contact occurs
δ	1 if contact occurs, 0 if it does not
$\tilde{F}$	connecting rod force
ϕ	connecting rod angle
M_{IC}	inertia moment of piston
M_{IP}	inertia moment of wrist-pin
M_{pp}	moment about wrist-pin due to wrist-pin friction
a	vertical distance from top of skirt to wrist-pin axis
b	vertical distance from top of skirt to piston center of gravity
C_g	horizontal distance between piston center of mass and wrist-pin
C_p	horizontal distance of wrist-pin from vertical piston axis (pin offset)
M_f	moment about wrist-pin due to all friction forces, thrust and anti-thrust sides
l_r	vertical distance(s) between wrist-pin axis and rings

These relationships are used to solve for the piston position and tilt as a function of time (or crank angle). Some inputs must be calculated iteratively, as they depend on the hydrodynamic lubrication of the piston, including side forces and piston/liner friction forces.

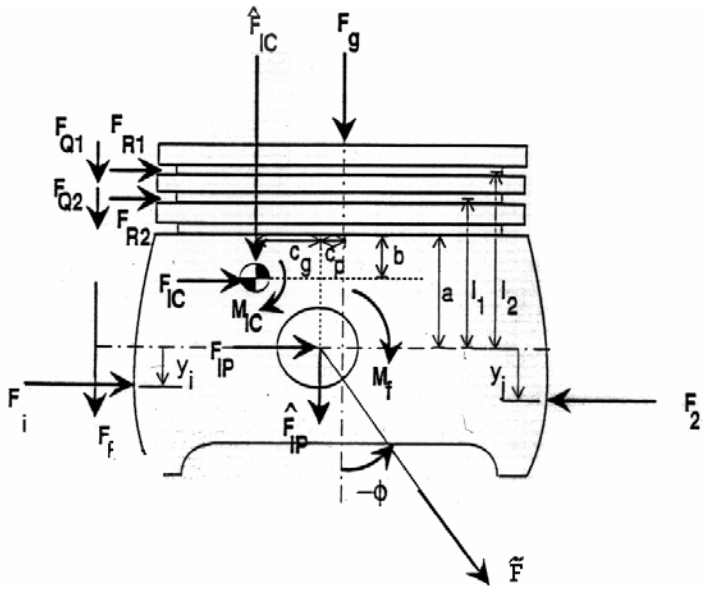

Figure 9-3: Forces and moments acting on the piston

Figure 9-4 shows the piston geometry, and definition of e_t and e_b, the eccentricities of the piston at the top and bottom of the skirt, respectively. These two terms and their time derivatives are used to define the piston tilt and displacement in the piston equations of motion:

$$\begin{bmatrix} m_{PP}(1-\frac{a}{L})+m_{Pis}(1-\frac{b}{L}) & m_{PP}\frac{a}{L}+m_{Pis}\frac{b}{L} \\ \frac{I_{Pis}}{L}+m_{Pis}(a-b)(1-\frac{b}{L}) & m_{Pis}(a-b)\frac{b}{L}-\frac{I_{Pis}}{L} \end{bmatrix} \begin{bmatrix} \ddot{e}_t \\ \ddot{e}_b \end{bmatrix} = \begin{bmatrix} F_\sigma + \sum F_s \delta_s + F_f \tan\phi \\ M_s + \sum F_s y_s \delta_s + M_f \end{bmatrix} \tag{9.4}$$

where m_{PP} is the wrist pin mass, m_{Pis} is the piston mass, L is the skirt height, F_σ and M_s, and all other terms are defined above in Table 9-1.

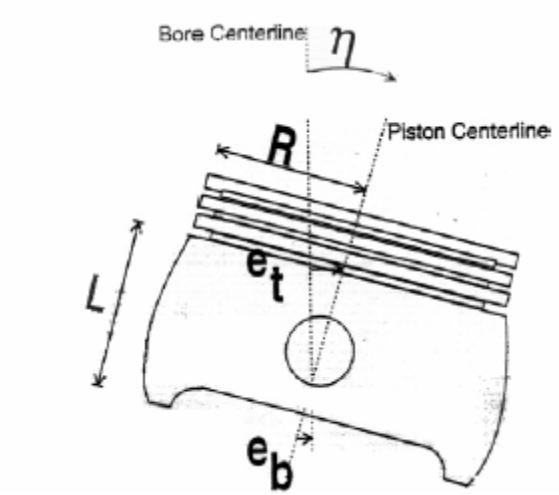

Figure 9-4: Piston geometry, showing definition of eccentricities

9.2.1.2. Reynolds equation: skirt hydrodynamic lubrication

The piston skirt experiences both hydrodynamic and boundary lubrication. In the hydrodynamic regime, the relationship between lubricant wetting and hydrodynamic pressure is defined by the two-dimensional Reynolds equation, which have been described in full in earlier annual report.

$$\frac{\partial}{\partial x}\left(\frac{h^3}{\mu}\frac{\partial p}{\partial x}\right)+\frac{\partial}{\partial z}\left(\frac{h^3}{\mu}\frac{\partial p}{\partial z}\right)=6U\frac{\partial h}{\partial x}+12\frac{\partial h}{\partial t} \qquad \textbf{(9.5)}$$

Flow factors are used in conjunction with the Reynolds equation, to account for piston roughness and waviness. The skirt/liner separation, h, consists of four components: the factory machined (cold) skirt profile, thermal distortion, deformation due to cylinder pressure force and deformation due to pressures on the skirt. Deformation at the waviness peaks is given by:

$$\left.\begin{array}{l}\delta=\Omega-h\\ \delta=0\end{array}\right\}\begin{array}{l}\Omega>h\\ otherwise\end{array} \qquad \textbf{(9.6)}$$

where δ is the deformation, and Ω is the amplitude of the surface waviness.

These lubrication and deformation equations must be solved iteratively with the equations of motion to define the piston motion and friction conditions.

9.2.1.3. Boundary conditions

Several boundary conditions are required to solve the piston/lubricant/liner system. At the edges of the wetted area, the oil pressure is assumed to be equal to the ambient gas pressure (external gas pressures are assumed to be known). Then:

$$p(wetted \quad edge) = P_{amb} \qquad \textbf{(9.7)}$$

where P_{amb} is the ambient gas pressure around the lubricant.

Also, if the skirt is symmetric, it is assumed that the pressure distribution is across a symmetry line is symmetric. For such a skirt, about thrust or anti-thrust lines:

$$\left.\frac{\partial p}{\partial x}\right|_{x=0}=0 \qquad \textbf{(9.8)}$$

There may be a significant amount of oil that does not contact the skirt, but must be accounted for in the analysis because of its effect on neighboring wetted areas. This oil is assumed to be at ambient pressure. Then, in the case of oil on the liner that does not contact the skirt, (is between peaks of the waviness, for example):

$$p = P_{amb} \qquad \textbf{(9.9)}$$

The wetted area of the piston is determined by geometry and conservation of mass for the lubricant. When the piston transitions from one side of the liner to the other, a given thickness of oil is present on the liner (the thickness is specified in the model, so that the effects of oil availability can be easily assessed). The extent of the wetting is then controlled by the amount of available oil and volume it occupies when squeezed between the piston and liner. The wetting condition must be solved iteratively along with the piston dynamics and deformation.

9.2.2. Iteration and solution algorithm

The piston tilt and displacement, as well as the deformed profile of the skirt must be known in order to solve for hydrodynamic and boundary friction forces, but these forces, in turn, must be known to calculate the piston dynamics. Using the boundary conditions described in the previous section, the pressure distribution and skirt profile are solved iteratively, using a finite-difference method in space and time, along with a relaxation scheme. The piston is assumed to be partially flooded, with wetting conditions defined by the boundary conditions given.

The numerical approach is to first determine piston-skirt side forces, using the hydrodynamic relationships, as functions of e_t, e_b and their time derivatives, and crank angle. These are then used to solve the piston dynamics equations in the time domain. The iteration is repeated until convergence is reached.

Like the ring-pack model, the piston model also takes surface roughnesses into account using averaged flow-factor techniques. The flow modeling equations used in the simulation are different than those shown above, which do not include flow factors for simplicity. Instead, averaged flow relationships are used, which account for surface texturing as explained further in [1].

9.3. Application to Waukesha engine

The project was conducted in collaboration with Waukesha Engine Dresser and Colorado State University, which operated a Waukesha VGF-18 in their laboratory. The Waukesha VGF in-line 6 engine configuration (155 mm bore x 165 mm stroke) is turbocharged, aftercooled, with modern combustion chamber design. The piston friction model was exercised with geometric and operating parameters from this engine; more details of the specifications are shown in Table 7-1 in an earlier Section 7.

10. Effects of Piston Parameters on Piston Friction

10.1. Skirt-liner clearance

As the piston travels up and down in the cylinder, it also rotates and moves transversally in a secondary motion, due to changing gas pressures and inertias. Instead of traveling along the axis of the cylinder, the piston presses against on side of the liner as it moves towards the combustion chamber, then moves to the other side as it travels down. When the piston transitions from one side to the other a "slap" occurs, when the piston hits the liner and oscillates briefly before remaining pressed against it, see Figure 10.1. The impact velocity of this slap affects the amount of noise produced by the engine as well as the piston frictional losses.

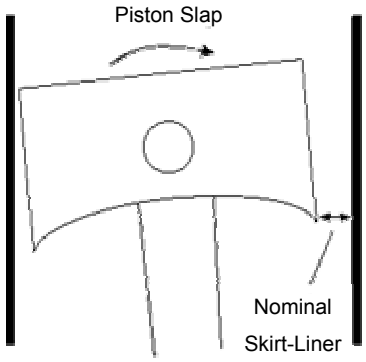

Figure 10-1: Schematic of piston and liner, showing skirt-liner clearance and piston slap

The skirt/liner clearance directly affects the impact speed of the piston slap. Figure 10-2 shows how the skirt impact velocity changes with cold clearance. A larger clearance allows the piston to accelerate over a larger distance, resulting in a faster impact speed at the slap. Large impact velocities lead to large impact forces, which lead in turn to large contact friction losses. Then, skirt/liner friction should be reduced as clearance is reduced. This was found to be the case for larger oil thicknesses, but for thinner oil films, as shown in Figure 10-3, a minimum point observed, where friction begins to increase again when clearance is decreased.

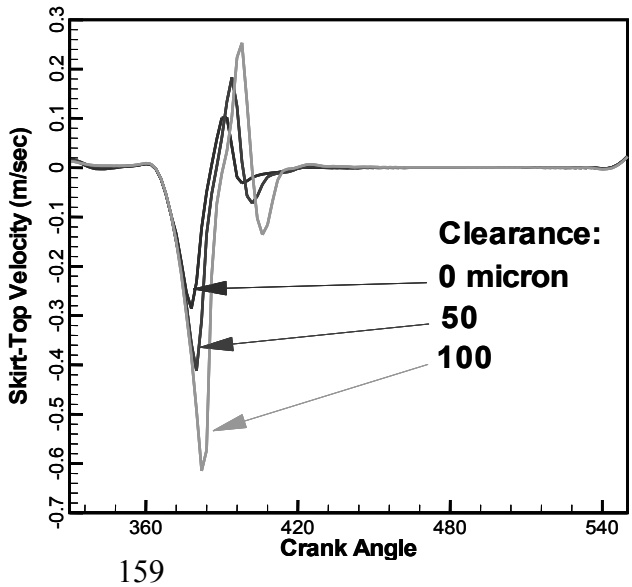

Figure 10-2: Skirt impact velocity increases as cold clearance increases

This minimum point results from asperity contact occurring at tight clearances, which increases friction, by bringing the skirt and liner surfaces closer together for low oil film thicknesses. In Figure 10-3, for large clearances the slapping velocity dominates and friction decreases as clearance decreases, while for very small clearances asperity contact becomes important and friction begins to rise while clearance is decreased. The figure also shows almost no change in hydrodynamic friction with clearance, showing that the cause for the friction change is largely due to changes in asperity contact.

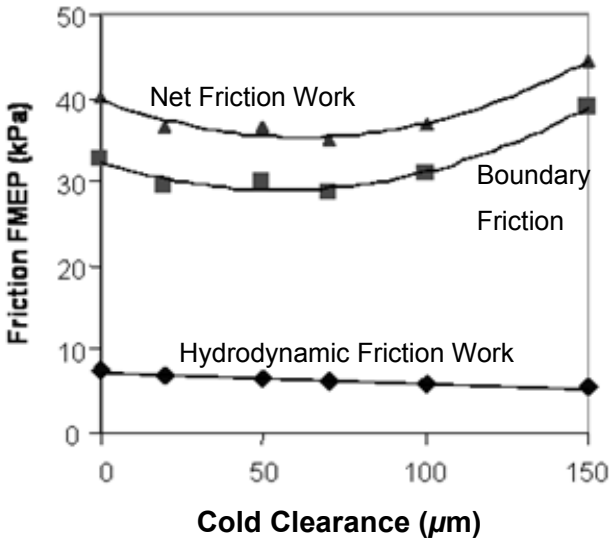

Figure 10-3: Effect of skirt/liner clearance on friction

The ideal skirt-liner clearance provides sufficient space for the oil but is not large enough to produce significant impact (Figure 10-4). For the Waukesha F18GL engine under the conditions of this study, the ideal clearance was 50 μm.

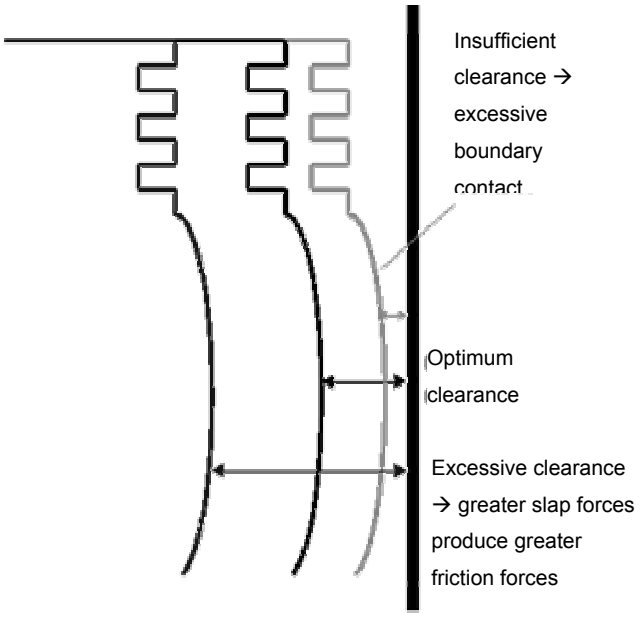

Figure 10-4: Illustration of optimal clearance on friction

(Interpretation of results: insufficient clearance produces excessive contact friction, while excessive clearance produces excessive impact)

10.2. Oil supply/oil film thickness

The mechanisms of oil distribution between the piston and liner are not fully understood. For the purposes of a parametric study, a simplified model was used that allowed oil availability to be set as a model input. The current model does allow the film thickness ahead of piston skirt motion to be specified as a function of time during the cycle. It is assumed that, prior to piston impact, an oil layer of a given thickness is available on the liner. The wetting locations are determined by the boundary condition that the oil film pressure is equal to the gas pressure around the skirt at the wetted edges, as well as piston and liner geometry. This served to specify the oil supply to the skirt and the oil film thickness between skirt and liner.

Oil film thickness, which is controlled by oil supply, has a direct impact on friction. A very thin oil film enables the skirt to easily push the oil aside and contact the liner, leading to boundary friction. On the other hand, a thick oil film tends to encourage hydrodynamic lubrication by providing more contact between the film and the piston surface, thereby enabling the lateral force to be spread over a larger area. Figure 10-5 provides a schematic comparison. As the film thickness is increased to a certain point, it reduces boundary contact friction to a very small value, which minimizes net friction work loss. If film thickness is increased beyond this critical point, however, no further reductions in boundary friction are available, and hydrodynamic friction increases due to an increase in wetted area. Thus, increasing film thickness beyond the critical point can actually increase net friction.

	
Large oil film thickness	**Small oil film thickness**
Large wetted area	Small wetted area
Negligible direct surface contact	Significant direct surface contact
Primarily hydrodynamic lubrication	Primarily boundary lubrication

Figure 10-5: Schematic of large and small oil film thicknesses, showing operational characteristics of each

The oil film thickness has a much greater impact on boundary friction than hydrodynamic. Figure 7-6 shows a rapid increase in boundary friction as film thickness is decreased, due to an increase in the amount of boundary contact that occurs as the piston and liner surfaces are brought closer together. In this example, the boundary contact friction dominates, so the total friction curve follows the same trend. When the film thickness has reached about 80 μm, the boundary contact friction component is negligible, and further increases in film thickness increase hydrodynamic, and therefore net, friction loss. (The minimum point shown in the figure stems from the fitting technique used to fit the simulation data points, and probably does not

have any physical basis). Only a small change in hydrodynamic friction is observed throughout the range of film thicknesses considered.

Comparing Figure 10-6 to Figure 10-3 also shows that the oil film thickness has a much larger effect on piston friction than skirt/liner clearance. The main effect of the clearance is to control friction at the "slap" period of the piston transition, while the film thickness affects skirt/liner contact throughout the cycle.

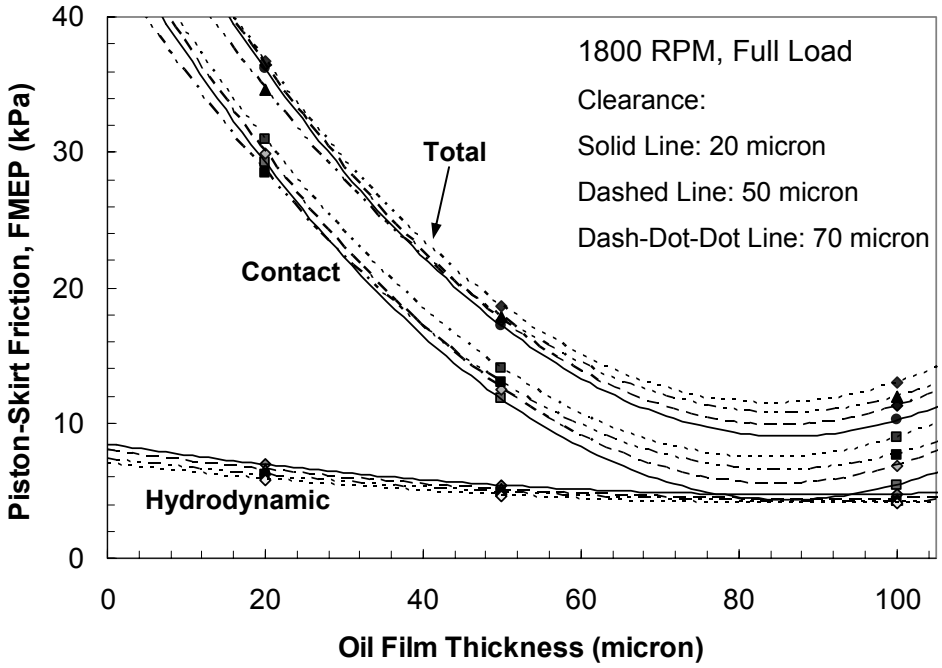

Figure 10-6: Effect of oil film thickness on skirt/liner friction
("Clearance" refers to cold skirt-to-liner clearances)

While its effect on friction is clear, the lubricant film thickness may also affect other engine parameters. For example, a thicker oil film can serve to cushion engine slap, reducing engine noise and vibration as well as friction. However, if the film is too thick, oil consumption may become a problem.

10.3. Surface finish/waviness

The piston skirt is typically machined so that it is covered by circumferential grooves, with depths on the order of 10μ, as well as smaller scale "roughness" asperities, of 1-2 orders of magnitude smaller in size. The grooves behave as oil reservoirs, supplying oil for hydrodynamic lubrication. The customary measure of groove size is waviness, which is the "amplitude" (*i.e.*, half of the peak-to-valley depth) of the groove. A schematic is shown in Figure 10-7.

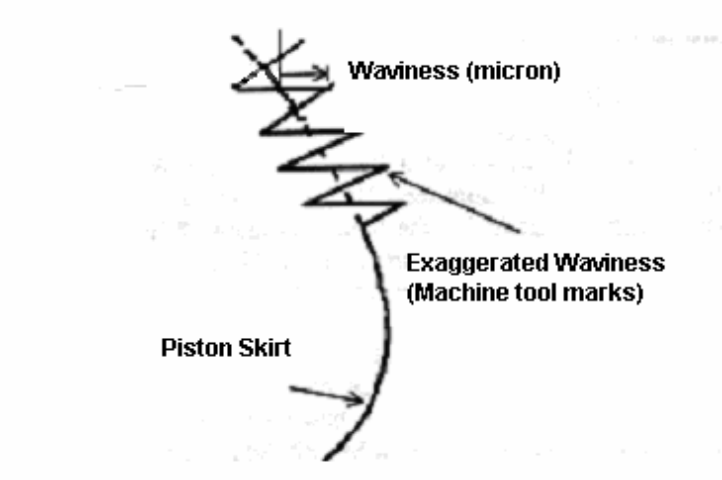

Figure 10-7: Piston skirt waviness, measured peak-to-peak values

The liner also affects oil flow and retention. In typical large natural-gas engines, liners have a honing pattern that serves much the same purpose as the waviness pattern on the piston: the grooves retain oil by surface tension and serve as an alternate supply, and they also provide flow paths for oil. Unlike the piston, in which grooves are machined circumferentially, the grooves in the liner are often oriented at an angle relative to the horizontal. The honing angle, as it is called, has a modest impact on friction. Shallow honing angles (relative to the horizontal) encourage oil to flow laterally rather than move up or down the liner, which would be undesirable.

10.3.1. Waviness vs. roughness

Surface roughness refers to the natural deviations of an actual surface from a geometrically smooth shape. Any metal shape has natural surface roughness that is related to the method of manufacture, degree of polishing, and other factors. In a ring surface, surface roughness plays an important role because it serves much the same purpose as waviness on a piston surface: the valleys serves as oil reservoirs, and the gaps between the peaks provide flow paths for oil. In a piston, however, the waviness amplitude is greater than the roughness amplitude, often by an order of magnitude. The difference between roughness and waviness in the model is illustrated in Figure 10-8. Thus, although roughness would be expected to play an important role in a piston with a nominally smooth (un-honed) surface, roughness only slightly modifies the effective amplitude of the waviness peaks in typical pistons. Therefore, roughness amplitude is expected to have a negligible effect on friction.

Tests were conducted to evaluate the effect of roughness on friction, but they showed a negligible effect, as expected. In the model, surface waviness was on the order of 10 microns, while surface roughness was on the order of only one micron, which are typical values for large natural-gas engines. The model, which assumed a sawtooth pattern for waviness, confirmed that changes in roughness had little impact on net friction.

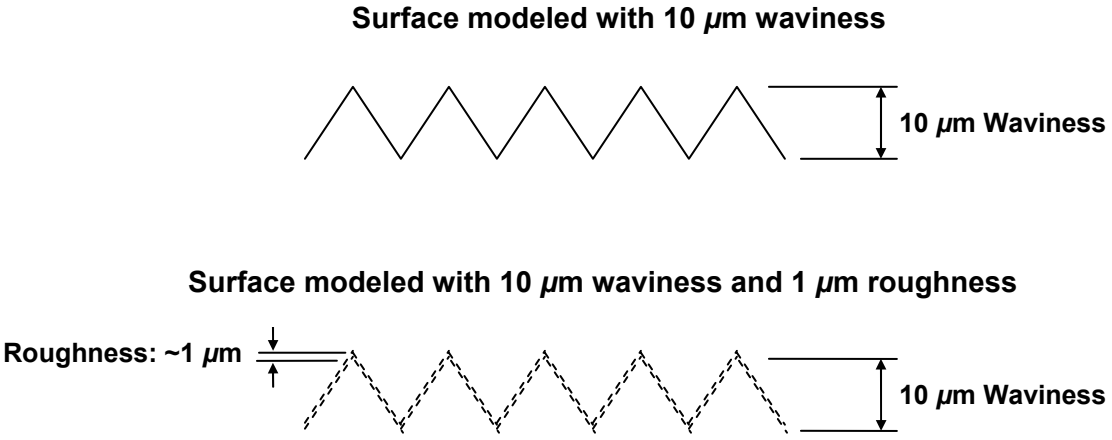

Figure 10-8: Schematic of surface waviness with and without roughness

10.3.2. Parametric study results (surface waviness)

Figure 10-9 and Figure 10-10 show that friction losses decrease as surface waviness decreases, largely due to a decrease in boundary friction. For a given availability of oil, a piston with deeper machining grooves has more volume to contain the oil – that is, the lubricant can be trapped within the machining grooves instead of staying between the piston and liner. When it is contained within the grooves, the oil is not useful as a lubricant or to support hydrodynamic pressure, and asperity contact occurs. Conversely, when the oil cannot escape into deep machining grooves and is compressed between the piston and liner, hydrodynamic pressure is generated and the piston load can be fully supported on the oil film.

The relation of friction to surface waviness suggests a dependence not only on waviness height, but on the relation of the waviness to oil availability. A smoother piston should require less oil to support hydrodynamic lubrication, while a very wavy piston should require more. Figure 10-11 indicates that this is indeed the case, and that there is a nearly linear relationship between waviness: film-thickness ratio and piston friction. Thus, in cases where very little lubricant is available to the piston a low waviness is preferred, whereas in cases where a large film thickness is possible, a smooth piston is still preferred but a wavier surface is allowable. However, in all cases, a very smooth piston is undesirable, due to factors not included in the present model.

Although skirts with low waviness values appear to produce the lowest friction, extremely smooth surfaces can lead to high friction, wear and sometimes seizure. Extremely smooth surfaces do not retain oil well, so that direct solid-solid contact, if and when it occurs, can be very poorly lubricated and quite severe. Also, the contact surface area may be larger in cases of very smooth surfaces, further contributing to friction and wear. Therefore, friction can be minimized by selecting small but nonzero waviness values, to prevent scuffing. For all other tests in this analysis, a constant waviness of 10 μm was used.

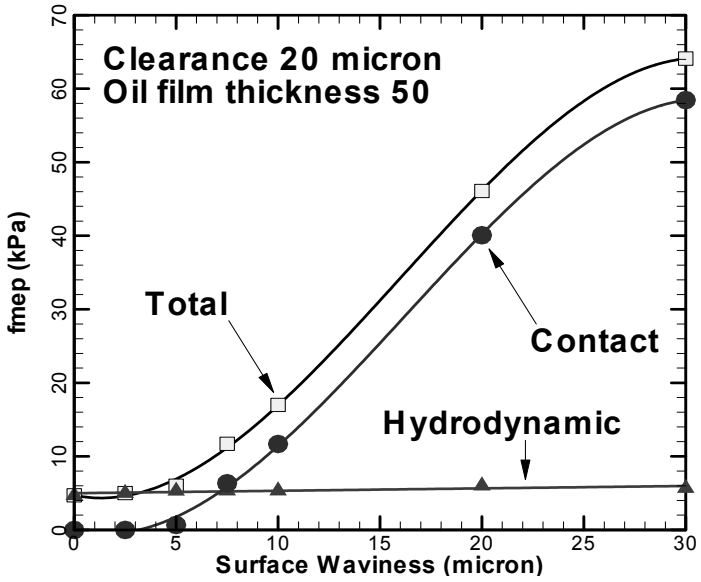

Figure 10-9: Dependence of friction on skirt waviness

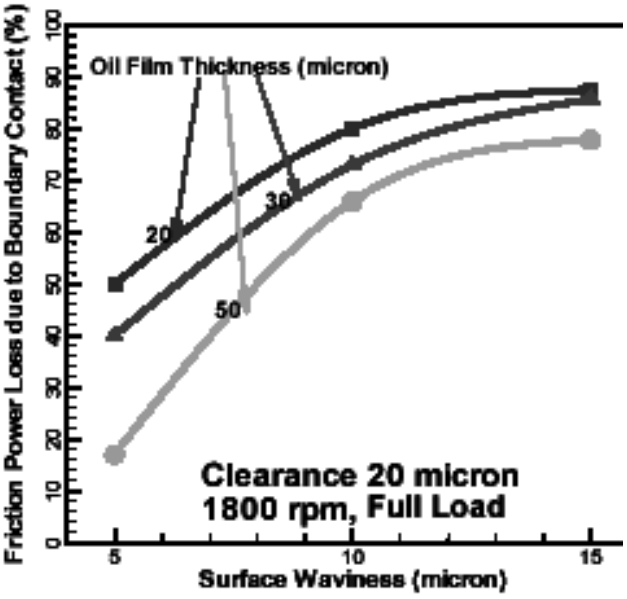

Figure 10-10: Dependence of friction power loss on skirt waviness

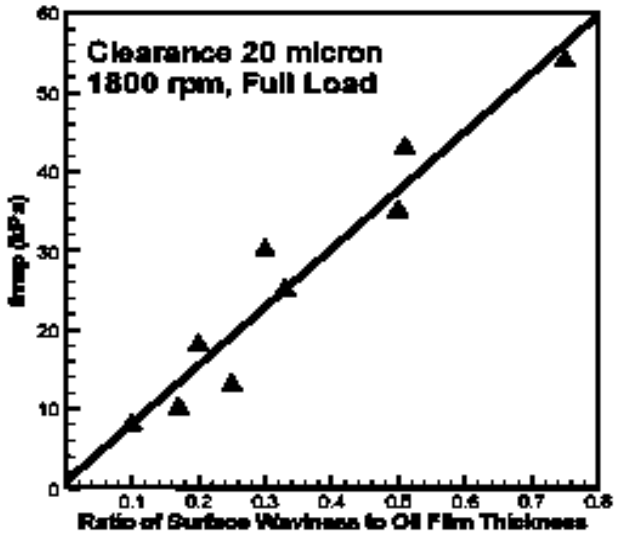

Figure 10-11: Dependence of friction loss on the ratio of waviness to film thickness

In addition to the waviness, the piston surface has a smaller scale roughness, of asperities on the scale of 1μ or less. An analysis of the effect of changing this roughness revealed almost no change in piston fmep with this variable, indicating that the effect of the roughness is dominated by the macroscopic waviness. Since the characteristic length of waviness (*i.e.*, the depth of the machined grooves) is typically an order of magnitude greater than roughness, the effect of waviness on friction loss dominates.

10.4. Piston-skirt profile/shape

A sensitivity analysis of the effects of piston curvature on skirt-friction was performed by evaluating a variety of polynomial piston-skirt axial profile shapes, shown in Figure 10-12. Each profile was defined by a simple $f(x) = x^n$ polynomial, where x was the vertical distance on the skirt (measured from the mid-point), n was the order of the polynomial, and $f(x)$ was the deviation of the profile from a perfect cylinder (which would be represented on the figure by a vertical face at 200μ). Higher-order polynomials were flatter in the midsection and dropped off dramatically at the extreme points, so that higher-order profiles were flatter overall. When cold, the maximum bulge of each profile was 200 μm, which is the same depth as the actual stock profile. For each profile, the cold skirt-to-liner clearance (measured at the point of maximum bulge to the liner) was kept constant at 20 microns.

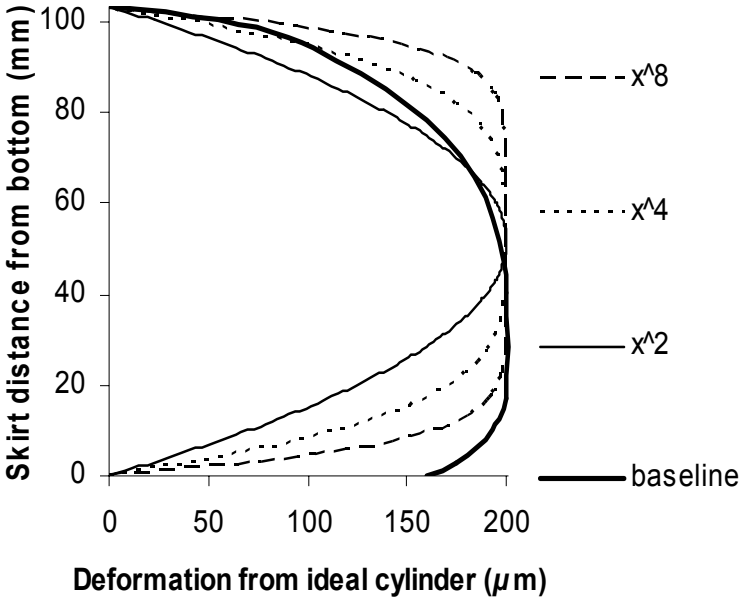

Figure 10-12: Piston profile shapes

As shown in the following figures, changing the "flatness" of the skirt changes both the hydrodynamic and boundary friction of the piston. All results shown are for the major thrust side of the piston, which is of primary interest because a large portion of total cycle friction (including almost all of the boundary friction) is generated there. Several are also shown at 50° after TDC combustion, because hydrodynamic forces are highest at this crank angle. Also, all simulations were run using SAE 40 grade oil. There is an interaction between piston profile and oil viscosity, which is discussed in a subsequent section.

Figure 10-13 shows the effect of a changing skirt profile on the piston wetting. A flatter skirt shows both a larger wetted area and a thicker oil film. The thicker oil film indicates that separation between the piston and liner is increased, decreasing boundary contact or possibly eliminating it entirely. An increase in wetted area size and film thickness tends to lead to an increase in hydrodynamic friction losses, but this also results in a lower average and peak oil

pressures, as is shown in Figure 10-14, which could help reduce hydrodynamic friction. The increase in wetted area and oil film thickness (skirt/liner clearance) is sustained throughout the stroke, as shown in Figure 10-15.

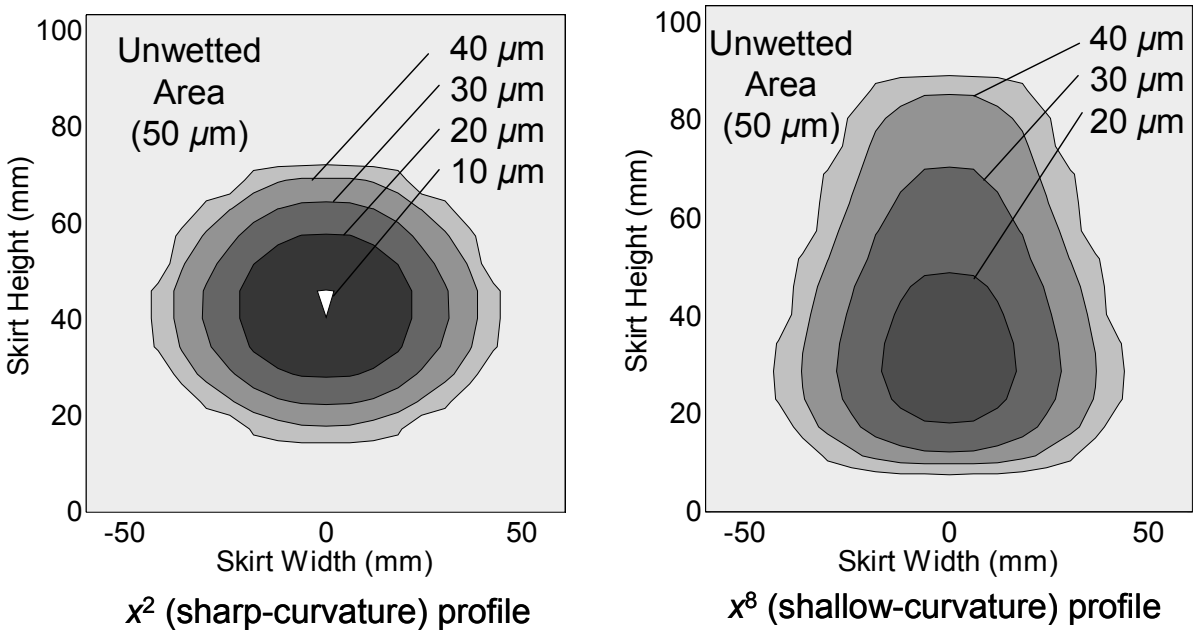

a. sharp-curvature skirt **b. shallow-curvature (flatter) skirt**

Figure 10-13: Oil film thickness in wetted areas for sharp and flat skirts, at 50° ATDC, during expansion

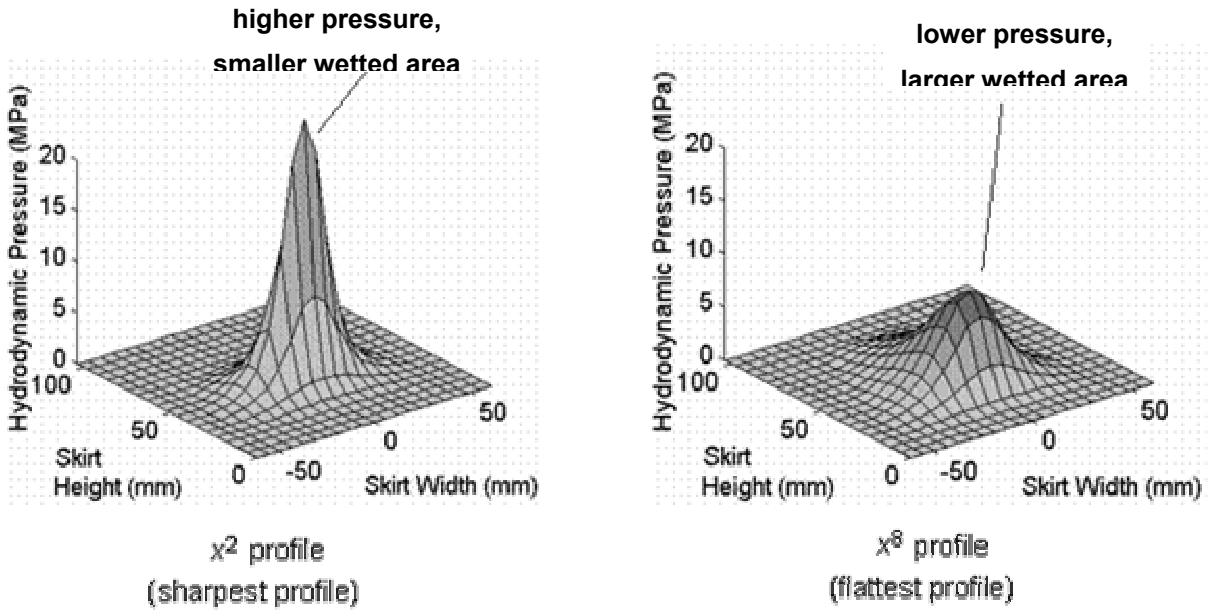

a. sharp-curvature skirt b. shallow-curvature (flatter) skirt

Figure 10-14: Pressure maps for sharp and flat skirts, at 50° ATDC, during expansion

In Figure 10-15a, the skirt-liner clearance for sharper profiles drops significantly below the waviness height, for a large portion of the cycle, meaning that substantial boundary contact is occurring and high friction forces created. For flatter profiles, skirt/liner clearance drops below the waviness height briefly, and only by a small amount, indicating that much less metal-metal contact is taking place. Figure 10-15b shows that a piston with a flatter profile experiences more wetting during the entire engine cycle, so that the change in hydrodynamic lubrication is the same throughout.

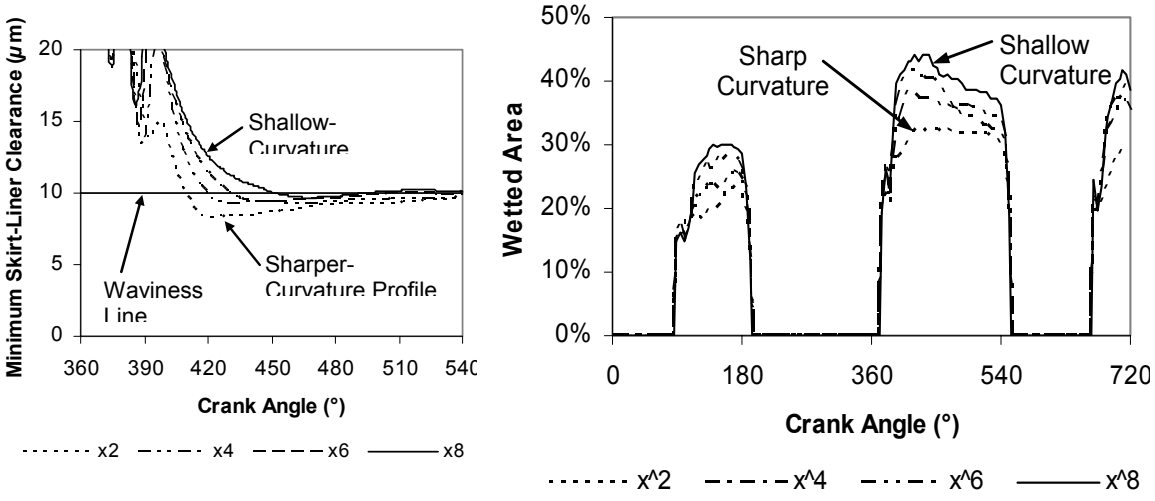

a. Details of profile effect on skirt-liner contact during 360-450° range

b. Percent wetted area for piston on thrust side

Figure 10-15: Effect of skirt-profile on skirt/liner wetting and contact

The change in skirt/liner clearance with piston profile suggests that a sharper profile experiences much more boundary friction than a flatter one. The simulation confirmed that a flatter piston profile causes a large reduction in boundary friction, along with a slight increase in hydrodynamic friction, as shown in Figure 10-16. Figure 10-16a shows that changing the piston profile has a substantial effect on the amount of boundary friction generated, with metal-metal contact almost entirely eliminated for the flattest case. In Figure 10-16b, a small increase in hydrodynamic friction is shown for flatter profiles, but the change is much smaller than the corresponding change in boundary friction. Figure 10-17 shows the cumulative cycle friction loss with profile, for two different viscosity oils. In both cases, the piston fmep decreases for flatter profiles, with boundary contact decreasing substantially along with smaller increases in hydrodynamic friction. This is the case for both oil viscosities, although the proportion of the changes in hydrodynamic and boundary friction is different for the two cases. The relationship between piston profile and lubricant viscosity is discussed further in the following section.

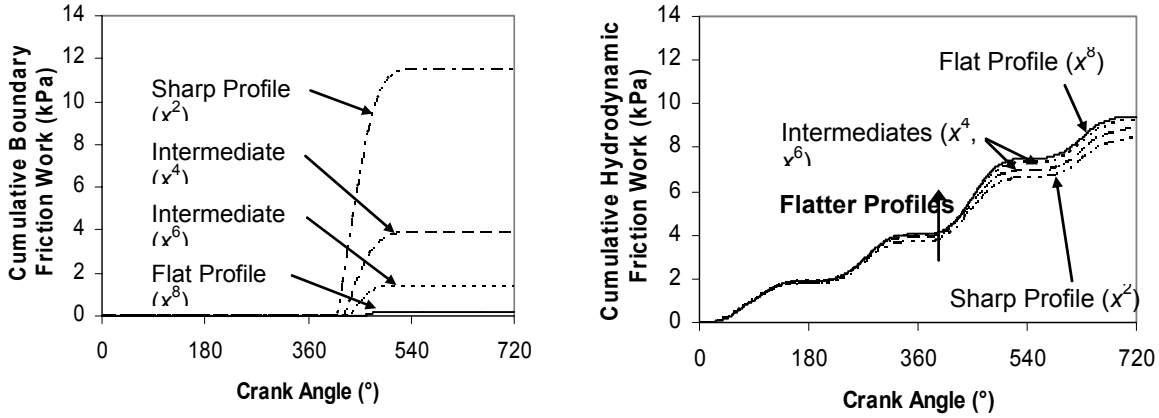

a. boundary friction work

b. hydrodynamic friction work

Figure 10-16: Comparison of cumulative friction work during the cycle, various piston skirt-profiles

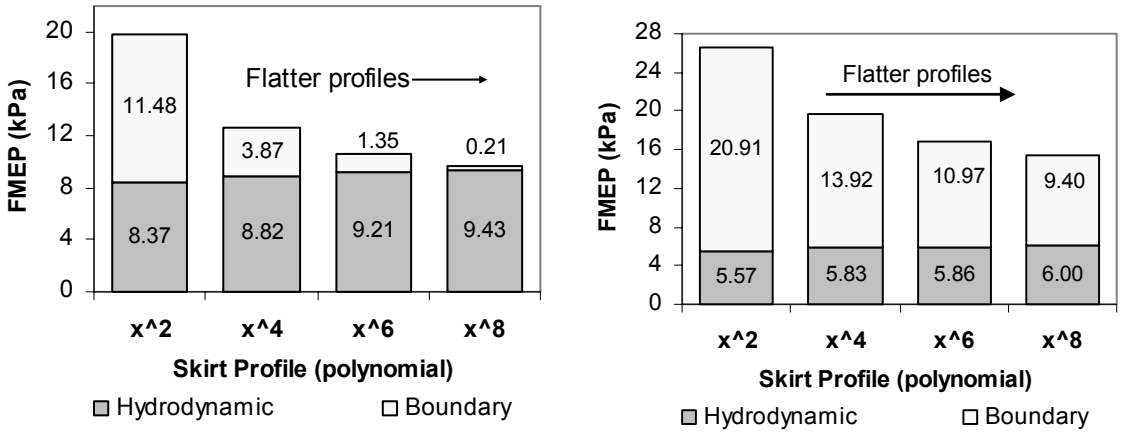

a. high viscosity (SAE-40) oil

b. low viscosity (SAE-20) oil

Figure 10-17: Effect of profile shape on hydrodynamic and boundary friction losses

10.5. Piston-skirt size

The size of the piston skirt is an important parameter in piston design. For example, a steel piston requires a dramatically different design than an aluminum piston because steel is a much denser material. Steel offers a stiffer structure that can handle much higher in-cylinder pressures, but if it is not designed carefully to reduce weight, it will require much larger connecting rods and other supporting structure, which could nullify any potential advantages. In a typical steel piston design, much of the material is removed, especially in low-stress areas like the periphery of the piston skirt. Figure 10-18 illustrates the difference in skirt size by comparing aluminum and steel pistons from MAHLE that were both designed for heavy-duty engines.

In order to gain a sense of the effect of skirt size on the friction, the baseline Waukesha F18GL piston skirt was scaled by various factors, down to 76% of the original, as shown in

Figure 10-19. (Obviously, it is simplistic to change the skirt size without modifying the profile, stiffness, or other characteristics, but this parametric study considered skirt size in isolation.) The effect of skirt size on friction can be understood by observing that smaller skirts must distribute the lateral load over a smaller area (i.e., have higher average and peak pressures), so they tend to have more boundary lubrication and less hydrodynamic lubrication. Indeed, Fig. 10-20 illustrates the dramatic increase in boundary friction as the skirt size is reduced. There is a slight decrease in hydrodynamic lubrication as the skirt gets smaller (Fig. 10-21). Figure 10-22 summarizes the results; for this specific design, it seems to be best to make this skirt as large as possible.

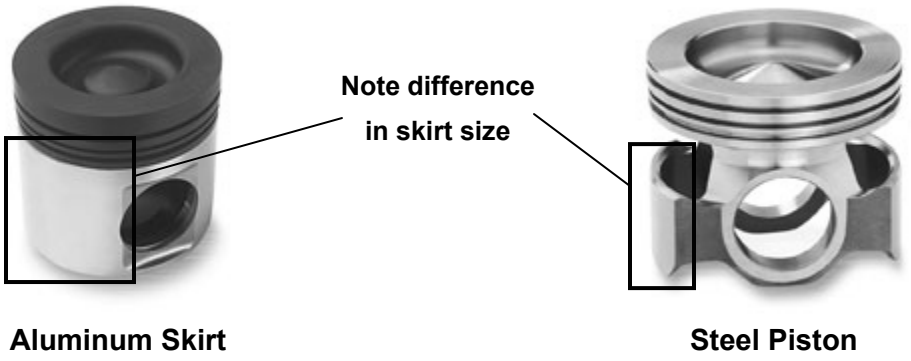

Figure 10-18: Comparison of aluminum and steel piston designs. MAHLE FERROTHERM® piston (aluminum skirt, steel crown) on left; MAHLE MONOTHERM® (all-steel) at right; both designed for heavy-duty engines.

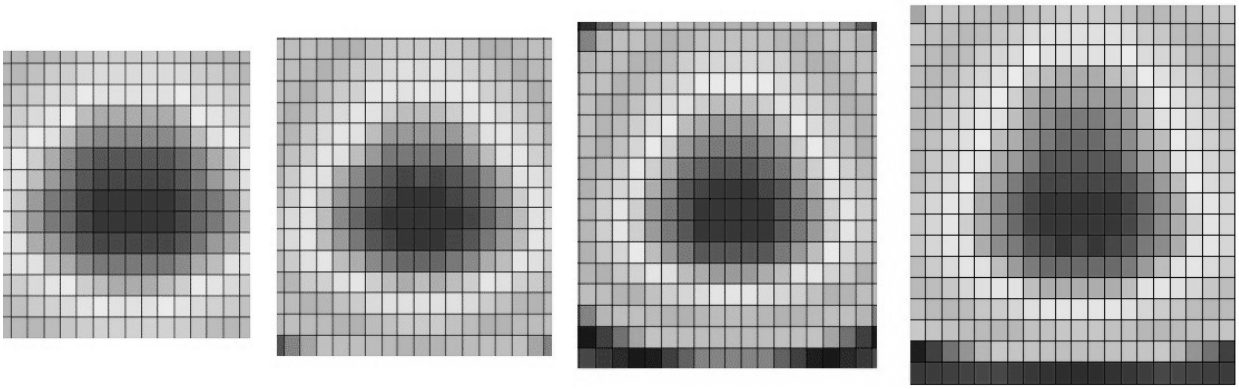

Figure 10-19: Schematic of skirts used in skirt size comparison

In actual piston designs, the tendency of smaller skirts to operate in the boundary lubrication regime can be offset by other design changes. For instance, the ovality can be adjusted to spread the load horizontally. Also, the profile can be adjusted to spread as much pressure in the center region as possible. As seen in Figure 10-14, most of the pressure is borne in the center of the skirt. Since the steel MONOTHERM® piston (shown in Figure 10-18) spreads the load horizontally across its width, it does not incur significant friction disadvantages by reducing skirt height.

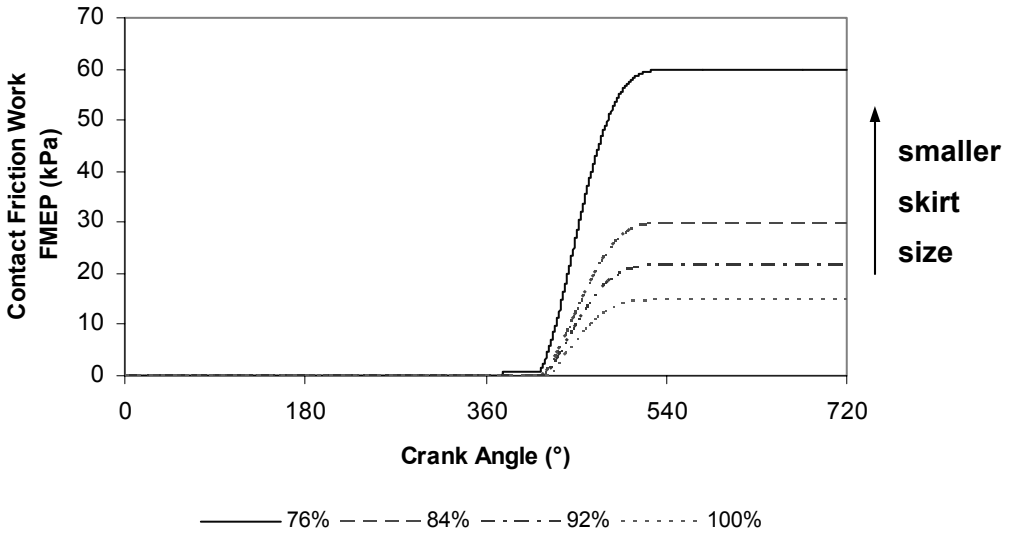

Figure 10-20: Cumulative contact friction work (thrust side, 100 μm oil film thickness, 20 μm waviness)

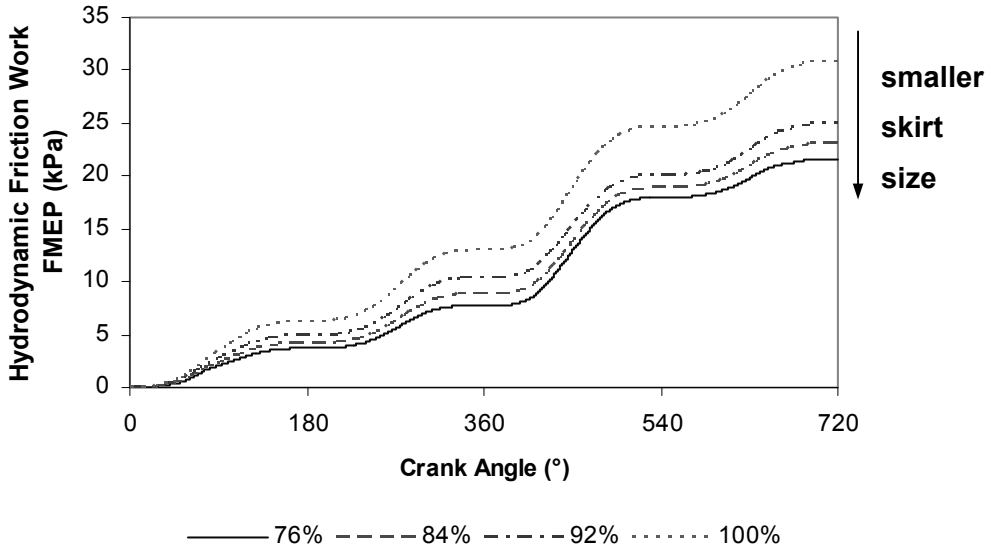

Figure 10-21: Cumulative hydrodynamic friction work (thrust side, 100 μm film thickness, 20 μm waviness)

Figure 10-22 (Right) : Skirt size vs. friction work (SAE-40 oil, thrust side, 100 μm oil film thickness, 20 μm waviness)

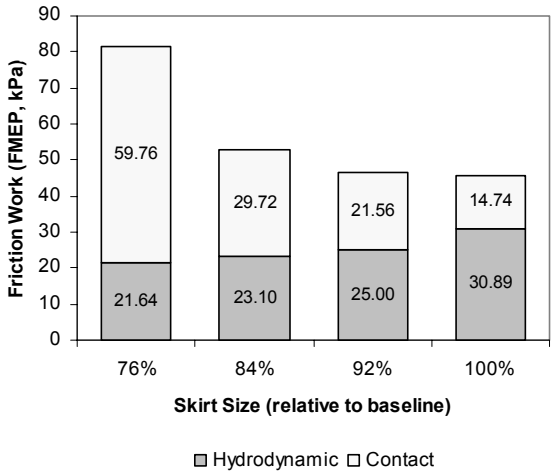

10.6. Piston ovality

The piston profile is designed not just to minimize friction, but also to minimize wear, reduce seizing, enhance guidance, etc. Piston ovality is essentially a piston profile oriented in the horizontal direction, and it fulfills several of the same purposes as the profile. As with the profile, this analysis of ovality focuses on its effect on friction. Figure 10-23 illustrates a cross-section of the piston/skirt system, emphasizing ovality.

When the engine is in operation, the piston skirt deforms in response to pressures stemming from lateral force on the connecting rod and inertial forces. Just as smooth, flattened profiles distribute pressure more evenly and thereby promote hydrodynamic friction, pistons with less ovality have the potential to reduce friction by conforming more closely to the liner. However, the same caveat regarding the profile applies to ovality: the system must be evaluated *after* the piston has been deformed by operational temperature and lateral pressure. The piston model used for this study included both thermal and pressure deformation effects.

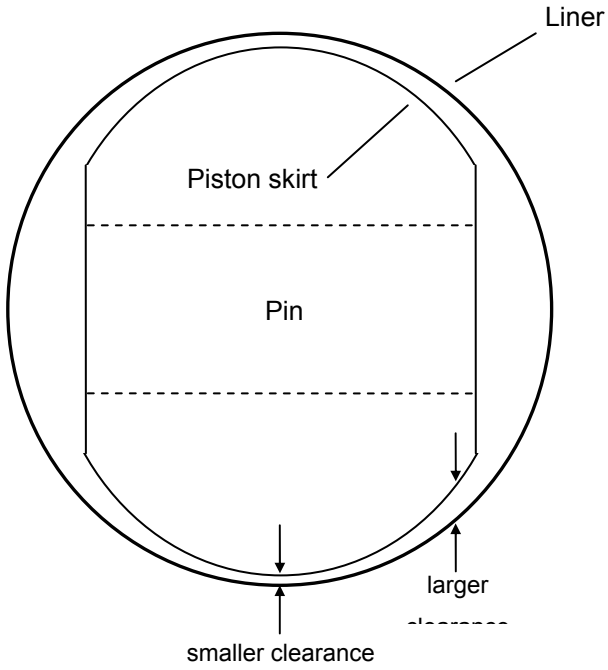

Figure 10-23: Diagram of piston skirt in the liner, showing ovality

Ovality is analogous to profile shape because both modify the effective clearance between the piston and liner. The objective of both is to facilitate a relatively flat oil film with gradual gradients in order distribute the lateral force over as large an area as possible. This promotes hydrodynamic lubrication and reduces wear. The ovality is to be adjusted so that it closely matches the shape of the liner, particularly at points in the cycle when the lateral force is high. (A comprehensive model of the engine would include deformation of each component in the power cylinder, including the liner, connecting rod, and pin, but such a model is extremely complex and requires intensive computation for even simple comparisons. The model exercised in this study included only deformation of the piston. However, the principle of piston-liner conformity applies in both types of models.)

Since reducing the ovality (i.e., making the piston more round) enables it to better conform to the liner surface, it is predicted that reducing ovality will also reduce friction. However, it is important to not completely eliminate ovality (i.e., make a perfectly circular piston). The lateral pressure is highest along the thrust and anti-thrust lines, so these areas will deform the most. A perfectly round piston will thus deform preferentially along the thrust and anti-thrust lines, leading to "negative ovality," or a concave shape that shifts pressure away from the thrust/anti-thrust lines. This could cause instabilities and produce undesirable high-pressure patches.

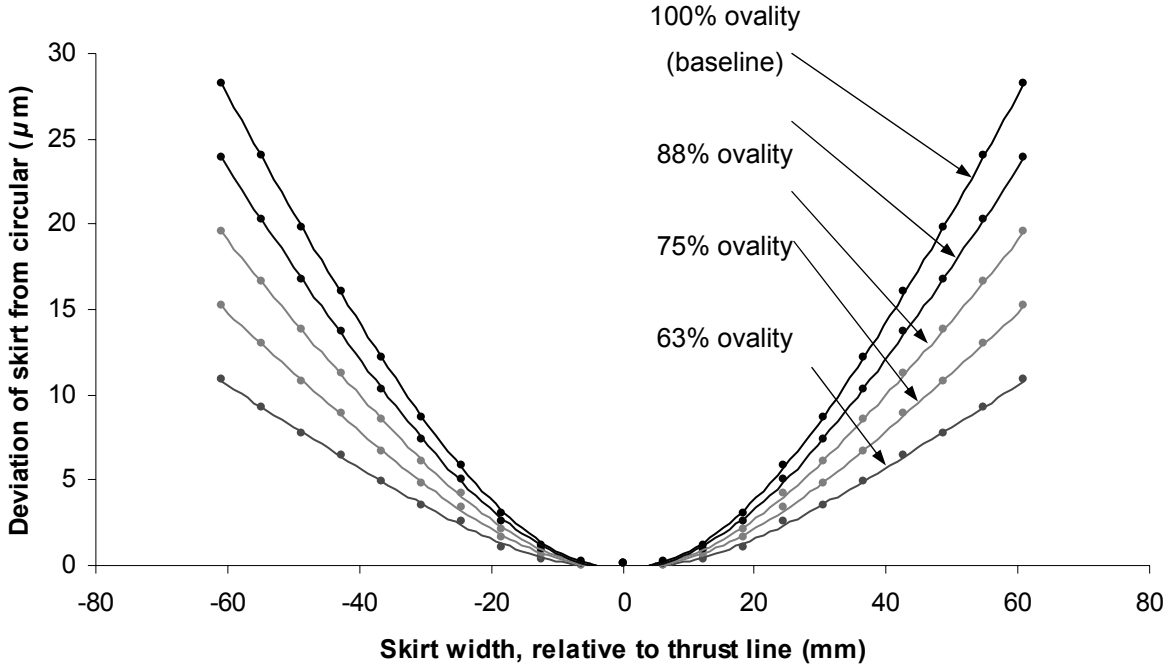

Figure 10-24: Cross-sectional view of piston, showing ovality. The baseline (100%) ovality was reduced to produce a more circular shape that conforms more closely to the liner surface (the *x*-axis in the figure).

In order to study the effect of ovality on friction, the baseline ovality was reduced by various proportions, as shown in Figure 10-24. Reducing ovality is equivalent to making the piston more circular, thereby causing it to conform more closely to the liner. Pistons with several relative ovality values were tested, and their effects on friction are shown in Figures 10-25 to 10-27. The model results confirm the prediction that reducing ovality dramatically reduces contact friction (it is eliminated entirely for 63% and 50% ovality pistons), thereby reducing net friction as well.

Since ovality can be adjusted independently of the piston profile, the two parameters can be jointly optimized to achieve ideal results. The profile is difficult to optimize because the piston rotates during the stroke—especially near the top-dead center—effectively changing the profile. The ovality does not change as much, however, since the piston does not rotate significantly about the thrust/anti-thrust axis. Therefore, in principle, the ovality can be optimized more precisely than the profile. Ideally, the two can be jointly optimized to minimize boundary contact friction while also achieving other objectives, such as smooth guidance throughout the stroke. Joint optimization requires specific, detailed information about the system in question.

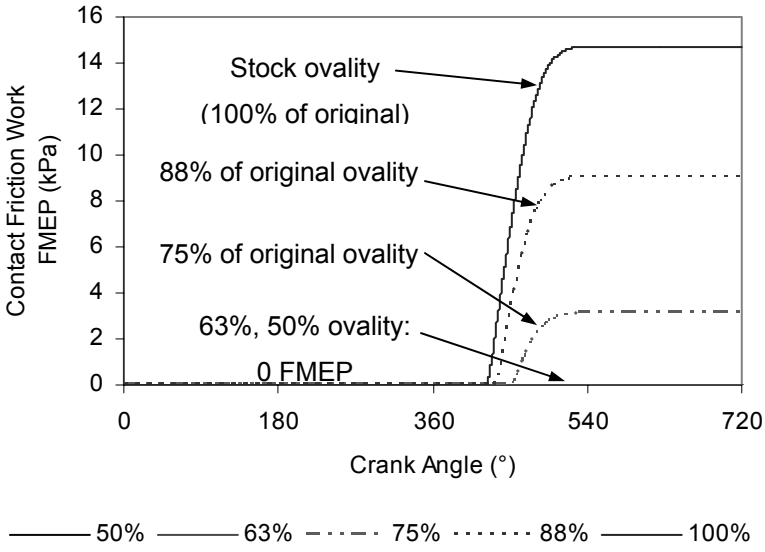

Figure 10-25: Cumulative contact friction work vs. ovality (thrust side, 100 μm oil film thickness, 20 μm waviness). Profiles that are more circular (i.e., have lower ovality) have lower contact friction work loss.

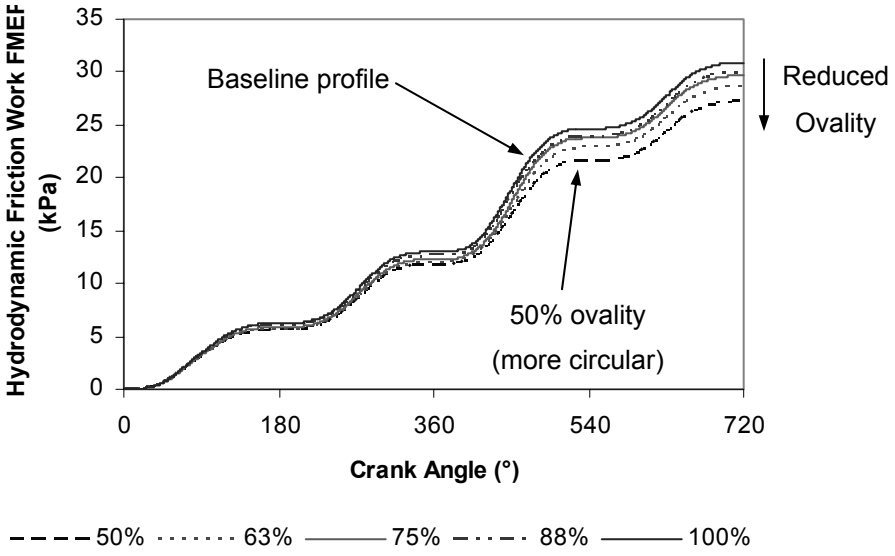

Figure 10-26: Cumulative hydrodynamic friction work vs. ovality (thrust side, 100 μm film thickness, 20 μm waviness). Reducing ovality slightly decreases hydrodynamic friction loss.

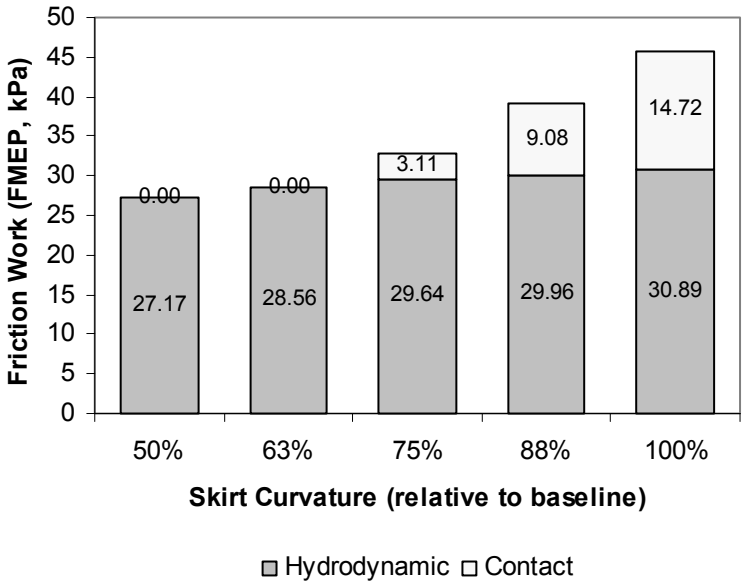

Figure 10-27: Ovality vs. net friction work (SAE-40 oil, thrust side, 100 μm oil film thickness, 20 μm waviness)

11. Effects of Lubricant Viscosity on Piston Friction

Reducing viscosity is an effective method to reduce friction, but reducing it beyond a critical point can promote both higher friction and substantially greater wear. Although high-viscosity oil produces greater friction work by increasing shear stresses, the greater shear stresses enable it to support a greater load (at a given sliding speed). The ability of viscous oils to sustain loads is essential for piston support, since this property helps avoid direct contact between the components. If the viscosity is reduced below the level required for hydrodynamic support, the piston surface will contact the liner surface and incur boundary contact friction. Typically, a design goal is to reduce boundary friction as much as possible, both because boundary friction involves significantly higher friction loss than hydrodynamic friction and because it promotes wear.

11.1. Engine oil temperatures and dependence of viscosity on temperature and shear rate (Vogel and Cross equations)

Hydrodynamic friction between the piston and liner is highly dependent on lubricant viscosity, and the viscosity is heavily dependent on temperature. As temperature increases, viscosity decreases dramatically. A robust model will treat viscosity as a function of temperature (instead of assuming a constant value) in order to predict friction accurately.

The temperature dependence of viscosity is specified by the Vogel equation (Eq. 11.1), where T is temperature (in °C), and the other variables are properties of the particular oil used. The θ_1 and θ_2 terms have units of °C, and k has units of cSt. Note that the Vogel equation is applicable only to single-grade oils, in which viscosity does not depend on shear rate. Since most large natural-gas engines use straight-weight oil (partially due to cost constraints), the Vogel equation is an accurate correlation between temperature and viscosity for these applications.

$\nu_0 = k \exp\left(\frac{\theta_1}{\theta_2 + T}\right)$	Eq. 11.1

The previous piston model assumed that viscosity was constant throughout the cycle, but this is not a very accurate approximation, since viscosity varies by a factor of 2 between top dead center and bottom dead center (Figure 11-1). Therefore, the model was modified such that viscosity was calculated from temperature and oil properties according to the Vogel equation, Eq. 11.1. At each crank angle increment, the current viscosity of the oil was determined, and Fig. 11-2 illustrates how the viscosity varied throughout the cycle.

Note the approximately sinusoidal nature of the viscosity as the piston moves up and down on the liner: the viscosity decreases toward the top of the stroke. The highest lateral pressure on the piston skirt occurs when the connecting rod force is highest, which happens when cylinder pressure is maximum. The pressure is maximum near TDC just after firing. The TDC position corresponds to the valleys on the curves in Figure 11-2, when viscosity is low. Since viscosity is

low and lateral pressure is high at TDC, this area is most vulnerable to boundary friction and its concomitant wear. In the field, the top of the liners exhibits the most wear, which is consistent with this prediction.

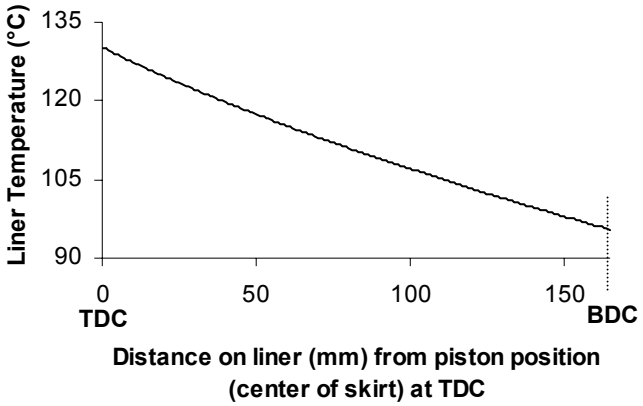

Figure 11-1: Liner temperature vs. position

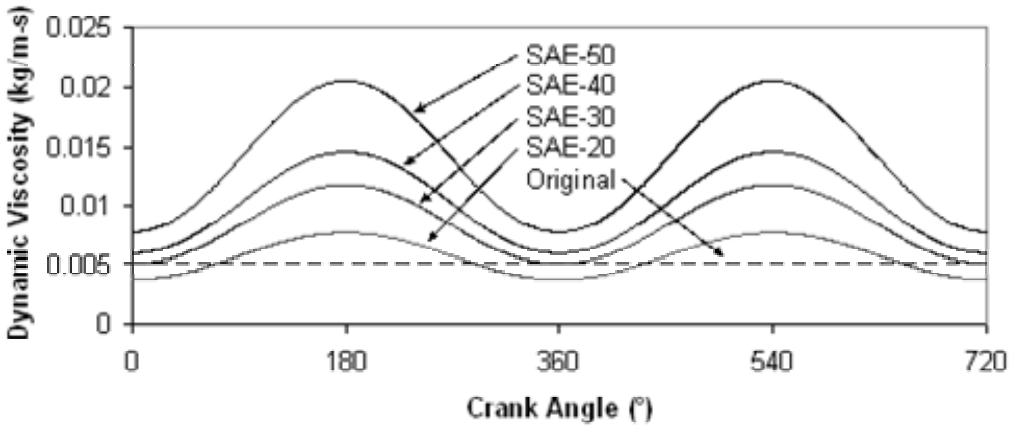

Figure 11-2: Viscosity vs. crank angle for straight-weight oils (original, constant viscosity shown for reference)

All lubricants display a strong dependence of viscosity on temperature. However, the viscosity of multi-grade oils also depends on shear rate—i.e., the ratio of sliding speed to film thickness. Multi-grade oils are formulated so that the viscosity is high when shear rate is low; hence, when piston speed is low near TDC and BDC, the shear rate is also low, and oil is more viscous. This increases hydrodynamic support. However, during mid-stroke when the piston is moving faster, it is already in the hydrodynamic regime, and the high shear rate causes the multi-grade oil to reduce its viscosity, decreasing friction work.

The viscosity characteristics of multi-grade oils are modeled by the Cross Equation (Eq. 11.2) , where γ is the absolute value of the shear rate (units of s^{-1}) and β is the critical shear rate (s^{-1}); β depends on temperature also. The μ_0 term is the low-shear oil viscosity and μ_∞ is the high-shear viscosity, m is a correlation constant controlling the width of the transition region, and

μ is the viscosity at shear rate γ (i.e., it is the viscosity to be calculated). Note that for single-grade oils, $\mu_\infty = \mu_0$.

$\mu = \mu_0 \dfrac{1 + \dfrac{\mu_\infty}{\mu_0}\left(\dfrac{\gamma}{\beta}\right)^m}{1 + \left(\dfrac{\gamma}{\beta}\right)^m}$	Eq. 11.2

The oil properties (specified by β, μ_0, & μ_∞) can be optimized to minimize friction. Hypothetically, the oil characteristics could be adjusted such that at high temperatures and low speeds (which are characteristic at TDC), the viscosity increases substantially. However, at high speeds during mid-stroke movement, the viscosity decreases to reduce hydrodynamic friction loss. Finally, at BDC where both speeds and temperatures are low, the viscosity would be increased again. Scenarios similar to this one have been explored for the ring pack, and while they cannot be readily implemented in practice, they provide valuable guidance for optimizing multi-grade oils for low-friction operation.

11.2. Dependence of piston-liner separation (clearance) on oil viscosity

Minimum clearance, or separation, between the piston and liner is a crucial lubrication parameter because it directly affects wear and boundary friction. If the minimum clearance is large, then the oil film is relatively thick, and the piston is supported hydrodynamically. However, if the minimum clearance is small for significant portions of the cycle, then boundary friction will likely be large as well. Oil viscosity has a direct impact on minimum clearance. As viscosity increases, both the shear stress and the supported load increase as well. Since the supported load is constant for a given engine, the shear stress can be reduced to maintain the same oil film thickness. Since shear stress is inversely proportional to separation distance (as an approximation), one would expect an increase in viscosity to lead to a corresponding increase in minimum separation.

Figures 11-3 and 11-4 depict the model predictions of skirt-liner separation for the entire cycle. To generate the plots, the minimum clearance value for the skirt at each crank angle was determined. A 10 μm waviness value was assumed in this scenario, so when oil film thickness dropped to about 10 μm, boundary contact began. Fig. 11-4 shows a close-up view of the minimum clearance around the 360° crank angle, which is top dead center at the beginning of the expansion stroke, and it clearly shows that an increase in viscosity promotes greater separation between skirt and liner. As stated earlier, this is the point in the cycle when most of the wear is generated, so the greater separation provided by more viscous lubricants can produce substantial reductions in wear. According to Figure 11-4, low-viscosity oils such as SAE-20 do not provide adequate hydrodynamic pressure to support the piston, and the deficiency must be balanced by increased boundary contact friction, which leads to increased wear.

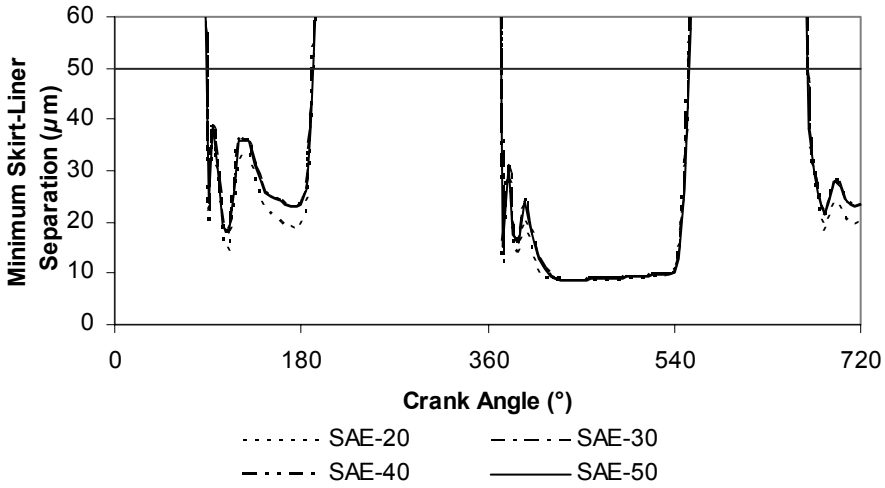

Figure 11-3: Minimum piston-liner separation vs. oil viscosity (thrust side, 50 μm oil film thickness, 10 μm waviness)

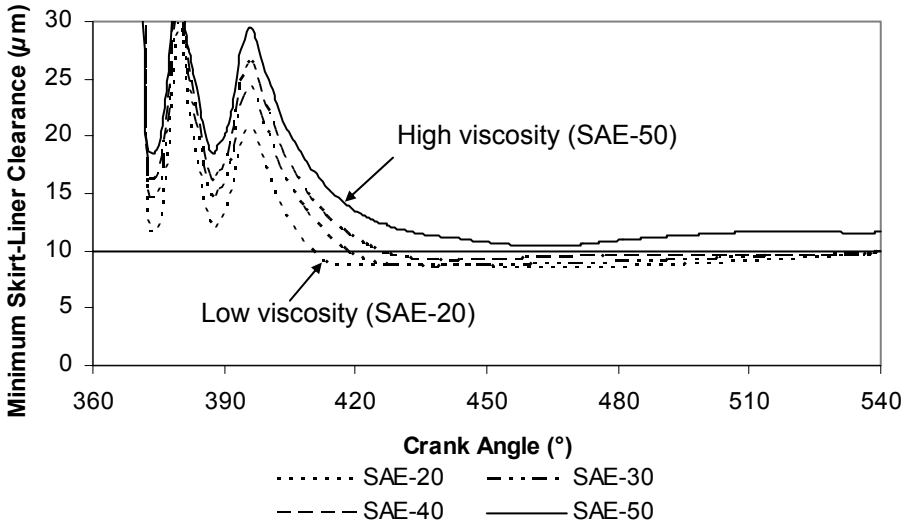

Figure 11-4: Close-up view of minimum separation vs. viscosity (thrust side, 50 μm oil film, 10 μm waviness)

A direct result of the greater separation that results from a more viscous lubricant is that the wetted area decreases. Since the piston "floats" higher in the oil film to produce greater separation, the wetted area decreases proportionally (in this model, a constant oil film thickness is assumed). Figure 11-5 illustrates this trend for the thrust side of the piston skirt; highly-viscous oils like SAE-50 have significantly less wetted area and significantly greater minimum skirt-liner clearance than low-viscosity oils like SAE-20.

Decreasing wetted area (assuming all else held constant) has the additional advantage of decreasing hydrodynamic friction. The off-center areas of the contact patch sustain only moderate pressure but they incur significant hydrodynamic drag. Thus, by decreasing the wetted area, viscous oils reduce hydrodynamic friction relative to what it would be with identical wetted areas. However, the reduction in hydrodynamic friction due to decreased wetted area is more than offset by the increase in friction due to increased shear stress, so increasing viscosity always increases hydrodynamic friction.

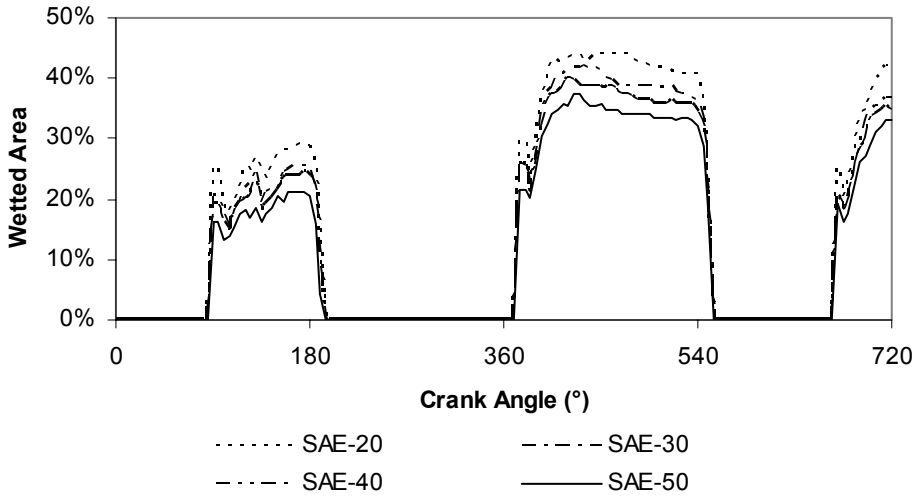

Figure 11-5: Percent wetted area vs. oil viscosity (thrust side, 50 μm oil film thickness, 10 μm waviness)

11.3. Effects of oil viscosity on piston-skirt friction

In general, more viscous oils tend to increase hydrodynamic friction, because of the increase in shear stress associated with higher viscosity, but decrease boundary contact, because the thicker oil films supported by highly viscous oils provide greater separation for two surfaces. This is the case for the piston. As oil grade is increased (where the grade is closely correlated to viscosity), the skirt/liner clearance increases, as shown in Figure 11-4. For the most viscous oil, SAE-50, boundary contact is completely eliminated, as indicated by the maintenance of a skirt/liner clearance greater than 10μ, the height of the skirt waviness.

As oil viscosity is increased, piston hydrodynamic friction increases, while boundary friction decreases. The effect of changing viscosity on the overall friction depends on the running conditions of the piston – if boundary contact contributes substantially to total piston friction, then increasing lubricant viscosity is likely to reduce overall friction. Conversely, if very little boundary contact is taking place, decreasing lubricant viscosity is more likely to lower total losses – even if asperity contact then increases, it will be outbalanced by the decrease in hydrodynamic friction. The value of the "ideal" oil viscosity, at which friction losses are minimized, is dependent on several factors, including the piston profile.

Figure 11-6 and Figure 11-7 show the dependence of piston friction on viscosity, for two different piston profiles. For a sharply curved profile, increasing viscosity causes a decrease in friction for all of the oil grades assessed. This is because the sharp profile of the piston causes substantial boundary contact to occur for all viscosities (as described in the preceding section). For the flatter profile, however, a minimum friction is found for SAE-40 oil, where hydrodynamic and boundary friction balance to provide the lowest overall friction.

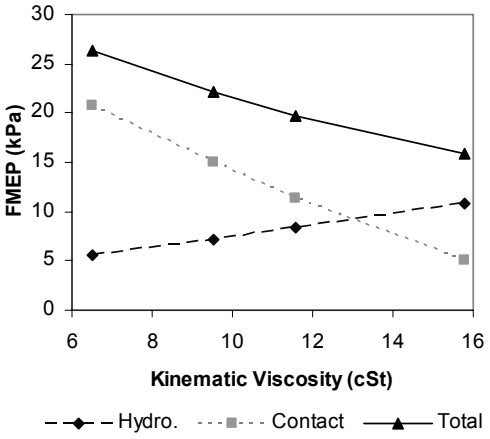

a. Friction change with oil viscosity

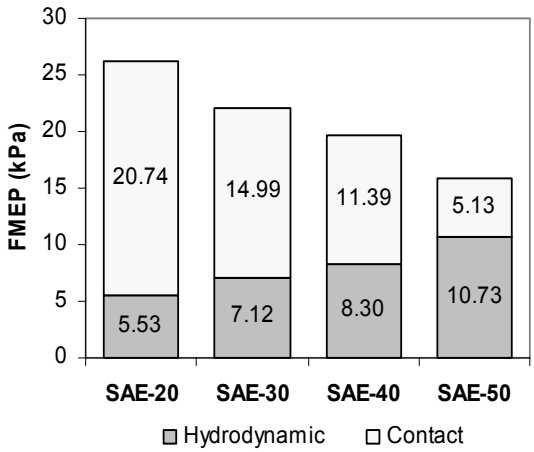

b. Friction change with oil weight

Figure 11-6: Friction change with oil viscosity, sharp curvature profile

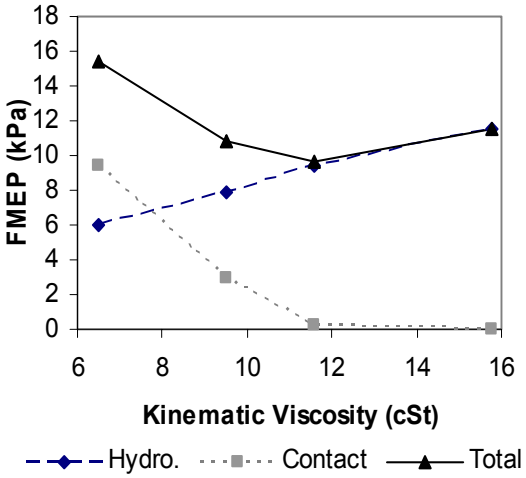

a. Friction change with oil viscosity

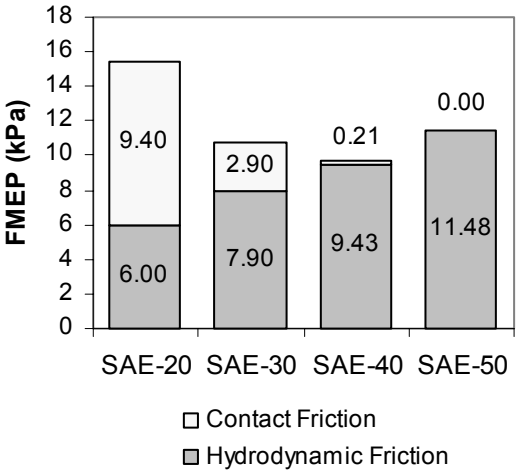

b. Friction change with oil weight

Figure 11-7: Friction change with oil viscosity, shallow curvature profile

12. Summary of Parametric Effects and Strategies on Piston-Friction Reduction

12.1. Parametric effects of piston friction

Each of the parameters studied above has the potential to affect friction, but they offer varying benefits. Figure 12-1 provides a rough comparison of each effect, assuming everything else remains constant. Obviously, the improvements are not additive; for example, if the waviness is excessive, profile curvature will no longer have much of an effect on friction. In order to reduce friction, the piston should be designed to provide a relatively even skirt-liner clearance in order to enhance hydrodynamic lubrication and avoid boundary lubrication. This can be achieved by using a relatively flat profile, adjusting piston ovality to match the liner shape, and reducing waviness peaks so they do not contact each other. Moreover, selecting the lubricant such that the viscosity is high enough to provide adequate hydrodynamic support, but not so high that is induces excessive drag, is also crucial to controlling friction. A key observation from this study is that the piston-liner system is highly-integrated, and changing one variable affects many other parameters.

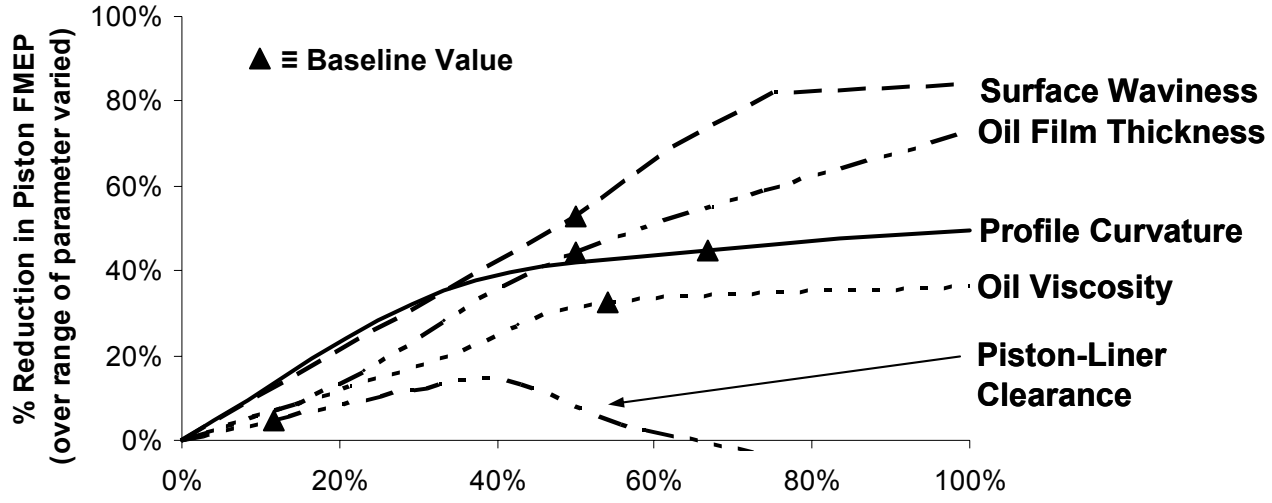

End of Range (0%)	% Change in Parameter	End of Range (100%)
20 μm	Surface Waviness	0.1 μm
0 μm	Oil Film Thickness	100 μm
x^2	Profile Curvature	Flattest (x^8)
0 μm	Piston-Liner Clearance	150 μm
8.1 cSt	Oil Viscosity (100° C)	20.4 cSt

Figure 12-1: Comparison of effects of various piston design parameters on friction; baseline values reflect parameters selected for the default engine

12.2. Piston friction reduction strategies

Piston friction arises from a complex combination of design characteristics, material and surface features, oil properties, and engine operating conditions. For the running conditions in the Waukesha engine, the most substantial reduction in friction arises from reducing boundary contact on the thrust side, which is the source of a large portion of the cycle total. The two most important design parameters identified thus far are oil film thickness and piston surface waviness. Increasing the oil film from 20 to 50 microns can reduce friction by 50%, primarily by providing more separation between the piston and liner, reducing contact friction. Similarly, reducing piston waviness from 10 to 5 microns can also reduce friction loss by 50%, by increasing piston/liner clearance at a given oil supply, as shown in Figure 12-6. While the result of changing both of these parameters clearly will not be 100% reduction in piston friction, substantial friction reduction should be possible.

Other parameters under consideration are the skirt-to-liner clearance, piston profile shape, and lubricant viscosity, all of which may entail friction reductions of 15-30%. Skirt-to-liner clearance can be optimized to reduce friction, either from piston slap, for large clearances, or metal-metal contact, for small clearances. Piston profile shape can also be optimized, primarily by flattening the profile to reduce boundary contact. Lubricant viscosity has a dual effect on piston friction: increasing viscosity decreases boundary friction, but also increases hydrodynamic friction. The viscosity can be optimized to minimize the total, taking into account the piston profile and other factors that contribute to the hydrodynamic/boundary balance.

Many other parameters contribute to piston friction which have not yet been considered. The most important of these is the skirt stiffness. Preliminary investigation indicates that a more flexible skirt can reduce friction, by increasing wetted area and decreasing contact friction. This possibility will be studied further. Also, analysis of the piston and liner surface textures will be carried out, to assess the possibilities for further friction reduction.

12.3. Summary of piston friction study

The parameters of the piston-liner system of a reciprocating engine are complex and highly interdependent, but numerical models have enabled significant progress to be made toward understanding them. In this project, which focused on reducing friction, the effects predicted by the model comport with physical intuition. Reducing viscosity reduces hydrodynamic friction while also reducing hydrodynamic pressure, but excessive reduction in viscosity makes the system vulnerable to boundary contact, which increases net friction. Thus, the strategy is to design the power cylinder system to operate primarily in the hydrodynamic lubrication regime while utilizing the lowest-viscosity oil practical.

The model confirmed that increasing oil film thickness (by increasing oil supply) tends to increase hydrodynamic support, which can supplant high-friction boundary contact. Thus, increasing oil film thickness can reduce friction losses. However, excessive oil supply can increase hydrodynamic drag needlessly and lead to heightened oil consumption, which can have

serious negative consequences for aftertreatment and exhaust. Therefore, methods other than simply increasing oil film thickness are preferred.

Changes to the design of the piston can promote hydrodynamic lubrication without increasing the supply or viscosity of the oil. The piston and liner geometry can be modified to maintain a smooth, even distribution of film thickness and hydrodynamic pressure. By avoiding pressure concentrations and the sharp film thickness gradients that cause them, the piston skirt is less likely to push the oil film aside and enter the boundary lubrication mode. The model confirmed that a relatively flat piston profile provides the best hydrodynamic support over the majority of the cycle because it conforms most closely to the liner. Likewise, a profile that contains minimal ovality (i.e., is nearly as circular as the liner) maintains an even distribution of film thickness and pressure, thereby maximizing hydrodynamic support and minimizing friction loss.

Some pistons are constructed of steel, which is significantly denser than the aluminum that is typically used. In order to reduce weight, much of the material is removed, including some around the piston skirt. Changing skirt size is expected to have a major impact on the distribution between hydrodynamic and boundary lubrication. The model predicted that smaller skirt sizes are at greater risk for boundary lubrication, with its concomitant increase in friction, since they concentrate the same lateral force over a smaller area. Therefore, if a smaller skirt surface is necessary, the other variables, such as piston profile and ovality, must be approached with great care to ensure adequate hydrodynamic support.

Finally, surface modifications can be selected to minimize friction. Although circumferential grooves (waviness) retain oil by surface tension and provide useful flow paths for oil, they can dramatically increase friction if their amplitude is excessive. The model predicts that if the amplitude is significantly greater than the average clearance between piston and liner, then the peaks of the grooves will penetrate through the oil film and scrape against each other, leading to boundary contact and its concomitant friction and wear. Therefore, waviness amplitude should be no larger than what is needed to provide adequate oil pathways and retain sufficient oil by surface tension. Moreover, the model indicated that the naturally-occurring asperities on the piston surface do not significantly affect friction, provided that they are substantially smaller than the machined grooves.

The contributions of each parameter to friction reduction are not additive, since each parameter affects the others. The most effective strategy is to combine a variety of techniques to achieve an overall decrease in friction while avoiding significant disadvantages. For example, the piston profile and piston ovality must be considered together because they both affect the separation between the skirt and liner. The waviness amplitude, skirt size, and cold skirt-liner clearance must be evaluated together with viscosity, since a low-viscosity lubricant tends to promote boundary lubrication and consequent high friction. By applying the computer model to a specific power cylinder arrangement, an optimized combination of design changes can be selected to minimize net friction loss and improve reliability.

(C) EXPERIMENTAL

13. Experimental Validation of Low-Friction Ring and Lubricant Designs

13.1. Background

The responsibility of Colorado State University within the friction reduction study was to procure install and conduct an experimental study on an ARES class engine. An ARES (Advanced Reciprocating Engine Systems) class engine is a high efficiency low emissions engine typically in the 1 MW range used for power generation. For this test a Waukesha VGF-F18GL inline 6 was fully instrumented for testing. This involved setting up and operating the engine in a dynamometer test cell with the normal engine performance measurements (rpm, torque, coolant, lubricant, operating temperatures, etc.). Specific measurements required included in-cylinder pressure from all cylinders from which the indicated effective pressure could be calculated. Brake torque measurement was required to determine the engine mechanical efficiency. Inter-ring pressure transducers were required in the engine to record inter-ring pressures for determination and validation of piston ring behavior. Blow-by and oil consumption measurements were recorded to check against model calculations and to monitor effects of friction variations on blow-by and oil consumption due to component changes.

Figure 13-1: Waukesha VGF-F18G Installed at the Large Bore Engine Test Bed at Colorado State University

The VGF-F18GL, donated by Waukesha Engine Dresser Inc., was installed within the industrial engine test bed at the Engines & Energy Conversion Lab (EECL). A wide variety of instrumentation was installed on the engine. A Midwest Dynamometer model 322 eddy-current dynamometer was used to control load on the engine. Rosemount 3051 pressure transmitters were employed for most of the system pressure measurement. Temperatures were measured using type Omega K type thermocouples. Control and monitoring of the system was accomplished using National Instruments Field Point DAQ and control in conjunction with LabVIEW software. For in cylinder pressure measurement Kistler 6067C water cooled pressure

transducers generously donated by Kistler Corporation were used due to the high level of accuracy needed in computing (NMEP).

13.1.1. Abbreviations and Symbols

ANGRE	Advanced Natural Gas Reciprocating Engine
ATDC	After Top Dead Center
BHP	Brake Horse Power
BMEP	Brake Mean Effective Pressure
BSFC	Brake Specific Fuel Consumption
BTDC	Before Top Dead Center
CO	Carbon Monoxide
CRO	Commercial Reference Oil
CSU	Colorado State University
DAQ	Data Acquisition
EECL	Engines and Energy Conversion Laboratory
IMEP	Indicated Mean Effective Pressure
NMEP	Net Mean Effective Pressure
MIT	Massachusetts Institute of Technology
NOx	Oxides of Nitrogen (NO, NO2, and N2O5)
RPM	Revolution per Minute
UHC	Unburned Hydrocarbon

13.2. Methods and Procedures

13.2.1. Friction Mean Effective Pressure

The key measurement of friction levels within and engine is friction mean effective pressure (FMEP). FMEP is calculated using two parameters derived from measurement: net mean effective pressure (NMEP) and brake mean effective pressure (BMEP)

$$FMEP = NMEP - BMEP$$

Equation 13.1

BMEP is the shaft output power measured as torque by the dynamometer which can be seen in Figure 13-2.

Figure 13-2: Eddy Current Dynamometer

In order to calculate FMEP, BMEP and NMEP must be calculated. BMEP is calculated from torque using the equation:

$$BMEP = \frac{4 * \pi * \tau}{V_d}$$

Equation 13.2

Where the Greek symbol, tau, is engine torque and V_d is the engine displacement. Engine torque is measured using an eddy current dynamometer. The dynamometer is accurate to .5% of scale. For this test series full scale was 1525 ft*lbs.

NMEP is the power created within the cylinder minus the pumping losses. NMEP was calculated from recordings of cylinder pressure traces using:

$$NMEP = \frac{\frac{2\pi}{360}\int_{-360}^{360}(P\frac{dV}{d\theta})d\theta}{V_d}$$

Equation 13.3

NMEP was calculated for each cycle and averaged over 1000 cycles. The data acquisition system used was a Hi-Techniques Win600 high speed DAQ that can be seen in Figure .

Calculations were made using combustion analysis software created at CSU's engine and energy conversion laboratory.

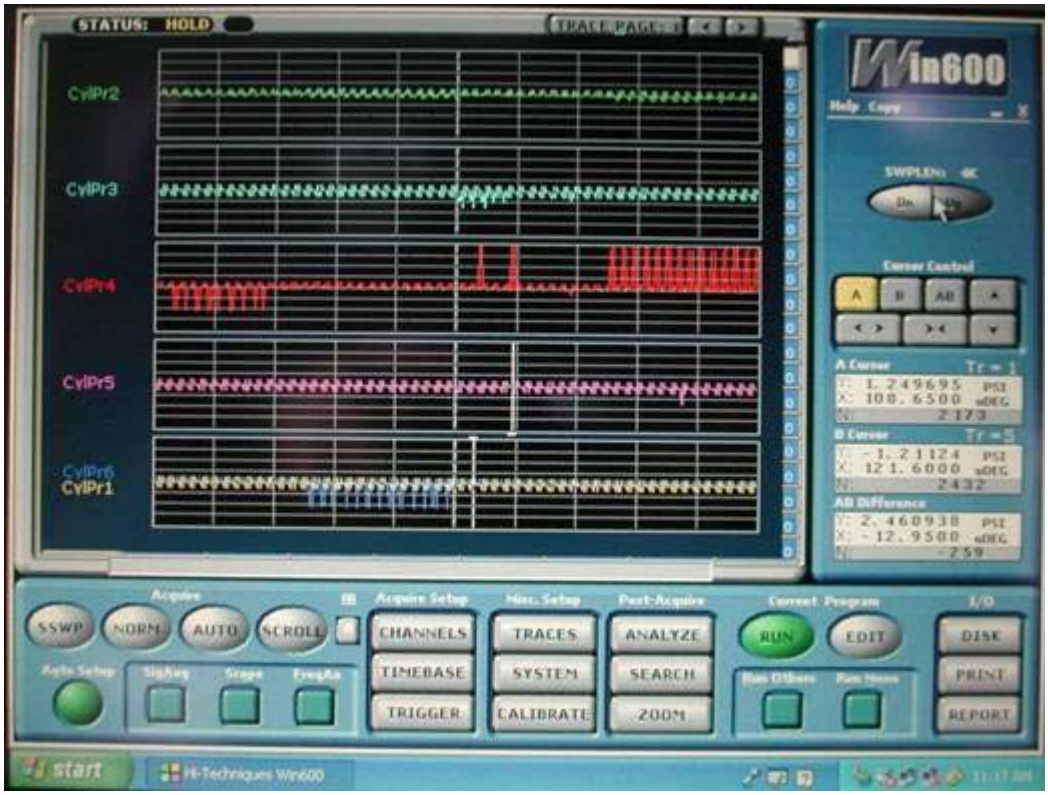

Figure 13-3: REVelation Interface Screen on Win600 High Speed DAQ

13.2.2. A/F Ratio Control

Early in the testing it was found that variations in combustion stability could affect the FMEP measurements with this technique. In essence, the day-to-day variation in natural gas composition from the pipeline was affecting the combustion stability at high load and biasing the NMEP measurements. In order to alleviate this condition, a closed loop air-fuel ratio controller was installed, and the engine was operated at a relatively "rich" condition.

An air-fuel ratio sweep was performed to identify the best operating air-fuel ratio for these tests. This desired operating air-fuel ratio was selected at a point where the Coefficient of Variation (COV) of IMEP all of the cylinders were not affected by fuel composition changes. The COV of IMEP for all of cylinder 6 and the engine average is plotted against exhaust O2 level in Figure 13-4. Cylinder 6 is displayed because it has a tendency to become more unstable at lower exhaust O2 levels than the other cylinders. All subsequent friction measurement tests were performed at 6% O2. An air/fuel ratio control was added to the system to maintain a constant A/F ratio during testing (Figure).

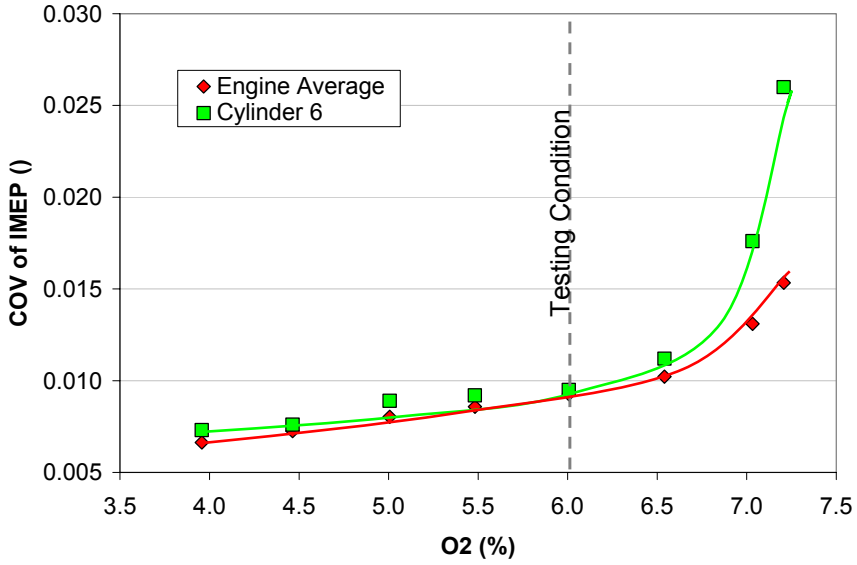

Figure 13-4: COV of IMEP of Cylinder 6 and the Engine Average

Figure 13-5: Closed Loop Air Fuel Ratio Controller

13.2.3. Oil Consumption

For measurement of oil consumption, a highly accurate oil consumption meter, AVL model 403S was used, see Figure 13-6. This oil consumption meter has a refill accuracy of ±1gram and a refill level accuracy of ±2 µm allowing for relatively short test points (~3 hours). The method used for testing was a constant level method. At the beginning of a test point the oil consumption meter records the initial level of the oil in the crankcase. It then meters in a precise amount of oil. This creates a rise in the oil level within the crankcase. The meter than measures

the time it takes for the oil level to return to its original level at which time the oil is considered consumed. The process is repeated, for ~3 hours and an average is taken over all of the fills.

Figure 13-6: AVL 403S Oil Consumption Meter

13.2.4. Blow-by Flow

For blow-by flow, a J-Tec Associates VF563B in line flow meter (Figure 13-7) specifically designed for blow-by flow measurement was used. Its accuracy is ± 2% of full scale, which is 16 ACFM for this meter.

Figure 13-7: J-Tech Associates VF563B In-Line Blow-by Meter

13.2.5. Inter-Ring Pressure Traces

The final and most technically challenging instrumentation requirement were the inter-ring pressure transducers. These sensors were required to mount through the crankcase, through a jacket water cavity and were attached to the cylinder liner (see Figure 13-8). Their location was set to measure piston land pressure at TDC and BDC. For this application, the Kistler 6052A pressure transducer was chosen due to its compact size and sleeve mounting capability. Installation of these sensors required precision machining to be done both on the engine and on the cylinder liner. Data taken with these sensors, was post processed at CSU into a usable form, and then sent to MIT for analysis. Due to this, inter-ring pressure trace will not be discussed in the results portion of this report.

Figure 13-8: Inter-ring Pressure Transducers Installed on Engine

13.2.6. Ring Changing Procedure

An important element in the procedure for testing different rings was the process of changing them. This process usually took between 2 and 3 full days to complete. The first step was to remove all of the wires, tubing and instrumentation that "gets in the way" or connects to parts that must to be removed (Figure).

Figure 13-9: Assembled Test Engine

All of the coolant systems were drained and sections of the exhaust and intake were removed. The valve covers, rocker arms, and push rods were then removed, followed by the fuel regulator and oil cooler. Jacket water connections were also disconnected. The head bolts were removed and the heads lifted off of the engine. The pistons were removed using the access openings in the side of the engine to remove the connecting rod cap screws. Finally, the pistons were removed from the engine from the top (Figure). The disassembled engine can be seen in Figure 13-9.

Figure 13-10: Piston Removal

Figure 13-11: Disassembled Test Engine

The rings were then changed one piston at a time, and the engine was then re-assembled in the reverse order. During this process, engine parts were cleaned and examined, and gaskets and seals were replaced as needed. The need to disassemble and rebuild the engine for every configuration of the rings tested had the potential to introduce additional variability in the measurements figure 13-11). Although it is unreasonable to expect that the engine condition was absolutely identical after every rebuild, extreme care was taken during this procedure. In addition, in order to ensure consistency in the ring exchange procedure, a single person was tasked with changing the rings every time.

The rings tests were performed in the following order:

1. LTOCR and NTSR
2. Baseline
3. LTOCR
4. Baseline
5. SBTR
6. LTOCR and NTSR
7. Baseline
8. Low-friction Configuration (LTOCR, NTSR, SBTR)

13.2.7. Oil Changing Procedure

The lubricant changing procedure was designed to replace as much oil as possible without needing to rebuild the engine. To start, oil was drained from the oil pan and oil consumption meter. The oil filters were replaced. The engine was then filled with new oil and run for nearly an hour. The engine was then shutdown and the oil pan and oil consumption meter were drained again. The oil filters were also replaced again. The engine and oil consumption meter were then filled for a final time. A sample of oil was taken at the beginning of testing after a break-in time and after the testing was complete. The oil samples were saved for future analysis.

Table 13-1: Engine Lubrication Oil Test Matrix

Oil	Viscosity Grade	Base Stock	Additive Package
Commercial Reference Oil	40W	X	A
LEF-F	40W	Y	B
LEF-G	30W	Y	B
LEF-H	20W	Y	B

The oil tests were preformed in the following order:

1. Commercial Reference Oil
2. LEF-F
3. LEF-G
4. LEF-H
5. Commercial Reference Oil

13.2.8. Testing Procedure

Complete emissions, DAQ and combustion data points were taken at each test point. The DAQ data was averaged over at least five minute test points, and the combustion data was averaged over at least 1000 cycles. Measurements were taken at 70% load through 100% load. Oil consumption data was only taken at the 100% load test points due to the time necessary to ensure accurate oil consumption data. During this ~3 hour data point, emissions, DAQ, and combustion data points were taken repeatedly. This repetition was used to ensure that a good average value of the measurements could be determined. For each of the ring packs discussed in this report, other than the baseline case which had already been broken in, initial break-in was done at Waukesha Engine Dresser Inc. Since piston ring pack friction was the basis of this study, only FMEP, piston ring blow-by, and oil consumption will be discussed in this report. The remainder of the data is included in the appendices.

13.3. Results and Discussion

13.3.1. Ring Pack Modification Test Data

When baseline testing was complete, the data showed an FMEP of approximately 21.9 (psi) at rated speed and load. The LTOCR, the LTOCR with NTSR, and the SBTR all showed a FMEP between 20.50 and 20.8 (psi). Finally, the complete low friction ring pack showed a 20.0 (psi). The total FMEP reduction was ~1.9 (psi). The results for all loads were plotted in Figure . The error bars on all of the following plots represented the 95% confidence interval.

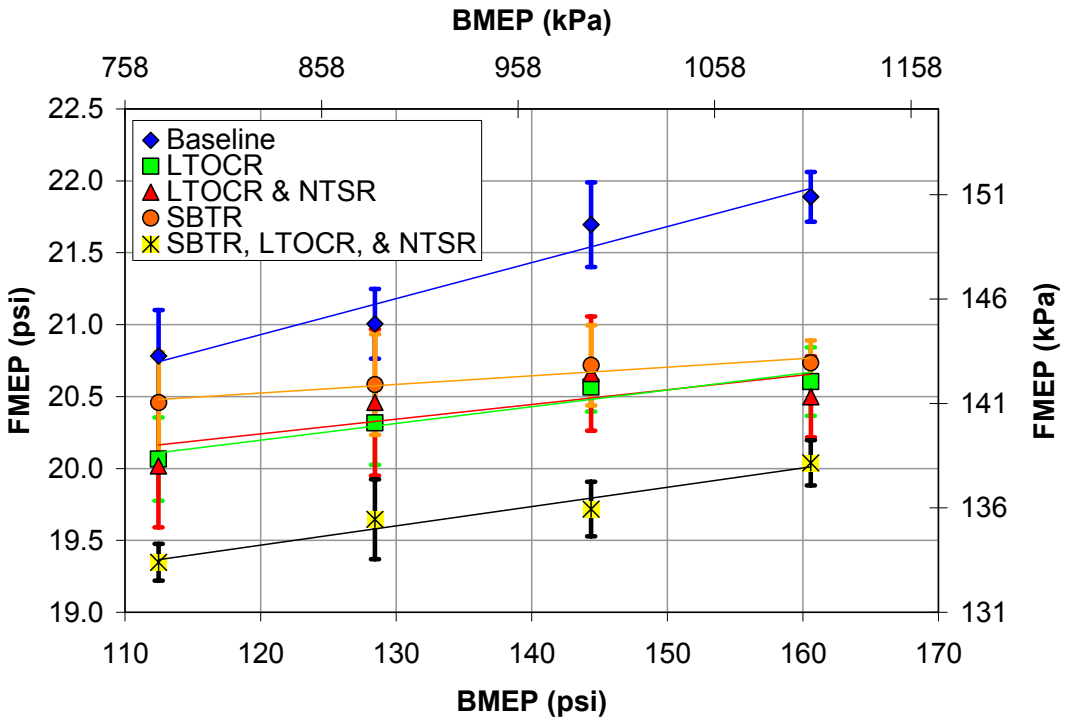

Figure 13-12: FMEP Measurements

The blow-by flow was approximately 3.2 (SCFM) for the baseline, LTOCR, SBTR, and low friction ring pack. The LTOCR with NTSR produced a slightly larger blow-by flow of approximately 3.9 (SCFM). The results of all the load conditions were plotted in Figure 13-13.

The baseline oil consumption was shown to be approximately 50 (g/hr). The oil consumption increased to approximately 130 (g/hr) with the LTOCR. The addition of the NTSR then reduced the oil consumption below 100 (g/hr). The SBTR alone only showed an increase of approximately 10 (g/hr) above the baseline condition. Finally, the low friction ring pack configuration produced an oil consumption rate of approximately 70 (g/hr). Due to the short test times, the results were thought to be only a general representation of actual oil consumption rates. All results were within the manufacturers expected ranges. The results of the oil consumption measurements were plotted in Figure 13-14.

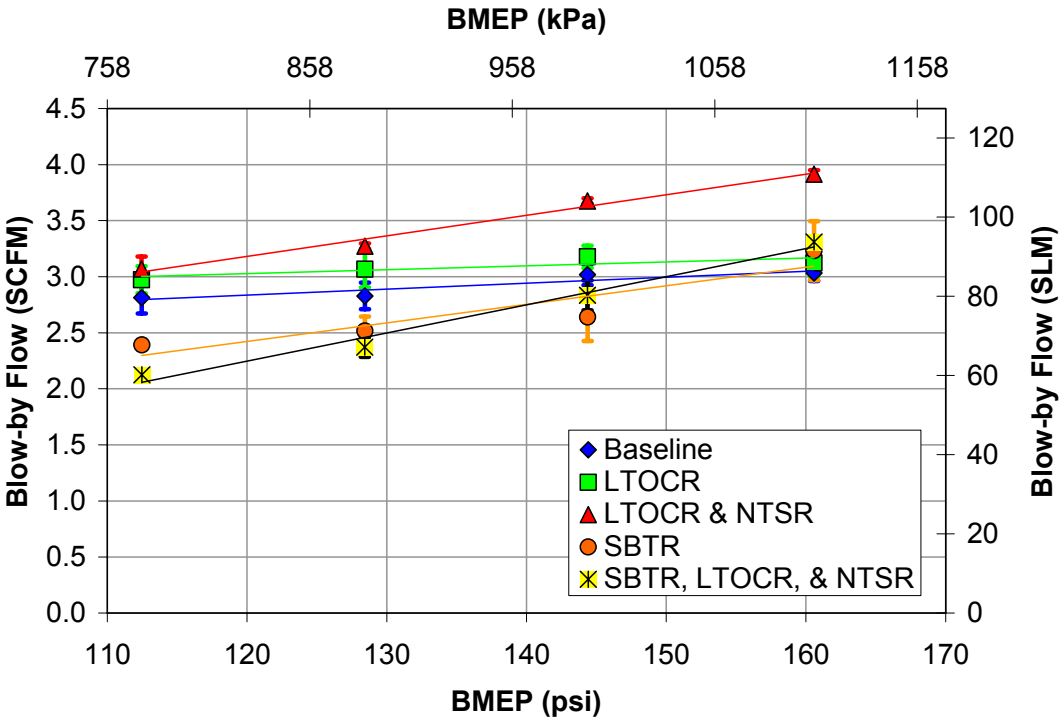

Figure 13-13: Blow-by Flow Measurements

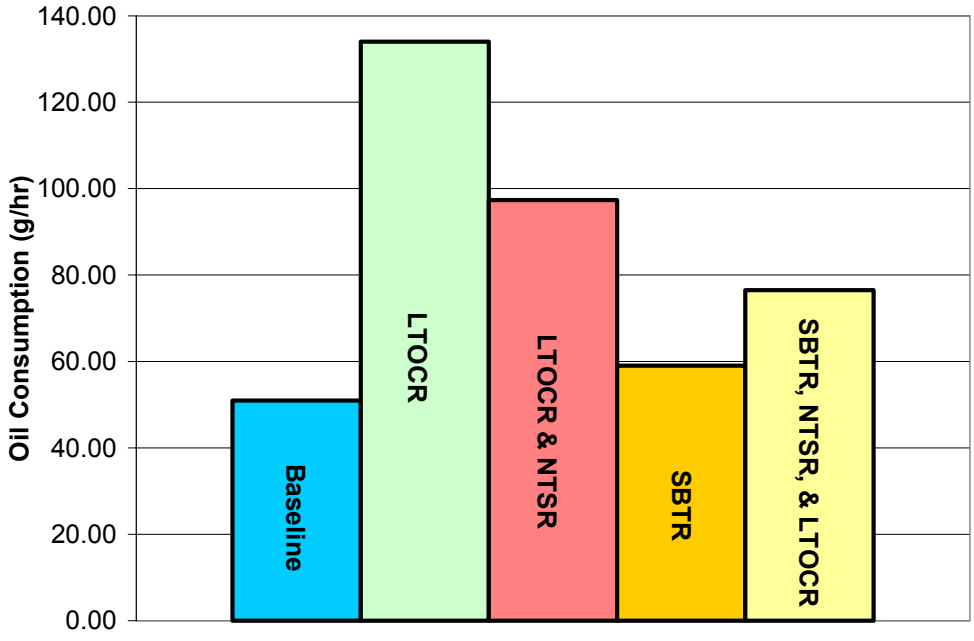

Figure 13-14 - Measured Oil Consumption @ 1800rpm and 400bhp (298kW)

13.3.2. Experimental Validation of Low-Friction Ring-Pack Predications

13.3.2.1. Summary of Low-Friction Designs

New designs for each of the three engine rings have been proposed. While the designs for the top and oil control rings directly reduce ring/liner friction, the proposed second ring design does not directly affect friction, but is intended to offset adverse effects from the altered oil control ring. Because most of the ring-pack friction comes from the top and oil control rings, these rings were the main focus of the friction-reduction strategies.

(a) Top Ring

As discussed in the analysis sections, most of the friction between the top ring and liner is generated near TDC of combustion, where high cylinder gas pressures push the ring into the liner with high force. To reduce friction during this period, a skewed barrel top ring is proposed. A schematic of the skewed barrel ring is shown in Figure 13-15.

In the figure, P_1 is the in-cylinder gas pressure, while P_2 is the gas pressure on the second land, which is much lower than P_1 near TDC combustion. The skewed barrel increases the area exposed to the high gas pressure on the front side (facing the liner) of the ring. This gas pressure results in a force pushing the ring away from the liner, which partially balances the high gas pressure on the back of the ring, reducing the net ring/liner force. Reducing the ring/liner force causes a reduction in friction as well as wear in this region.

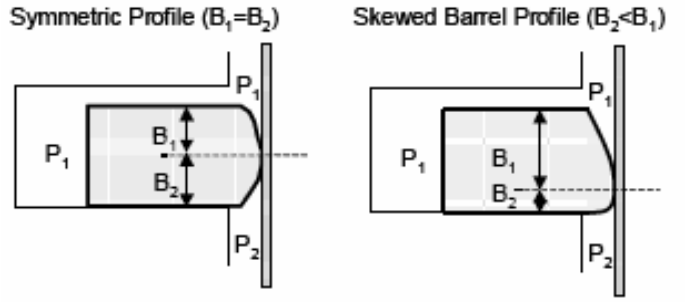

Figure 13-15: Low-friction top-ring design

Figure 13-16 shows the expected reductions in top ring friction as barrel skewness is increased. The x-axis shows "normalized B_2", which is a measure of the height of the ring below the centerline – a smaller B_2 indicates a greater amount of skewness. OS1 and OS2 are two oil supply conditions that have been studied in the ring analysis, and have relatively little effect on top ring friction. As the figure shows, top ring friction decreases approximately linearly with barrel skewness, with possible top ring friction reductions of 30-40% for very skewed barrels. This translates to a total ring-pack friction reduction of ~20%, as shown in Figure 13-17.

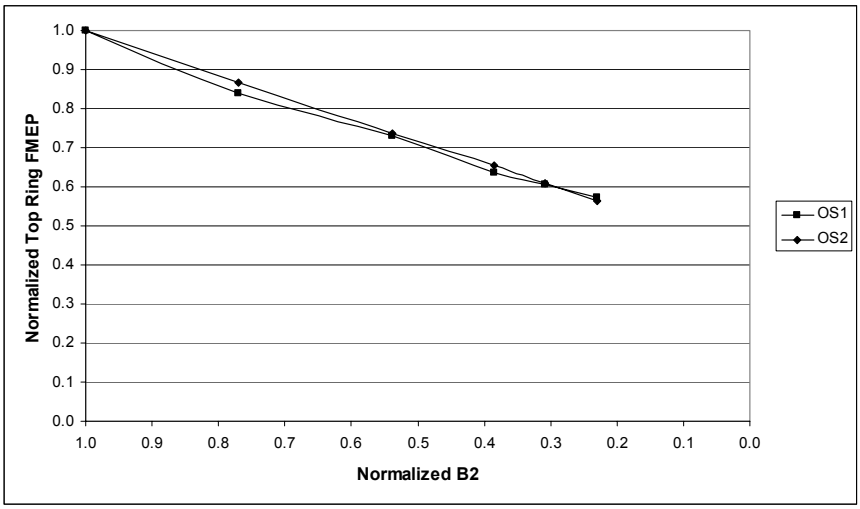

Figure 13-16: Effect of barrel skewness on top ring frictional losses

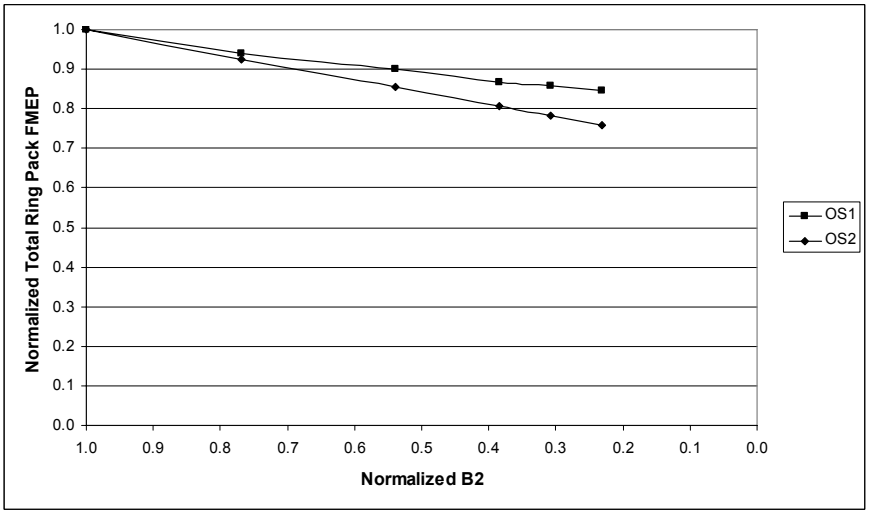

Figure 13-17: Effect of barrel skewness on total ring-pack frictional losses

(b) Oil-Control Ring

The main source of frictional losses between the OCR and liner is the high tension in the ring, which is required to ensure the good ring/liner conformability that is required for oil flow control. The high tension causing a high ring/liner force, which leads to high friction. A reduced tension oil control ring is proposed, to reduce the ring/liner normal force, and thus reduce friction as well. Figure 13-18 and Figure 13-19 show the effect of reducing oil control ring tension. There is a linear decrease of OCR friction as the ring's tension is reduced, with an OCR friction reduction of ~40% possible when the ring tension is reduced by half. This translates to an overall ring-pack friction reduction of ~25%. When the top and oil control ring designs are combined, a ring-pack friction reduction of up to 45% is predicted.

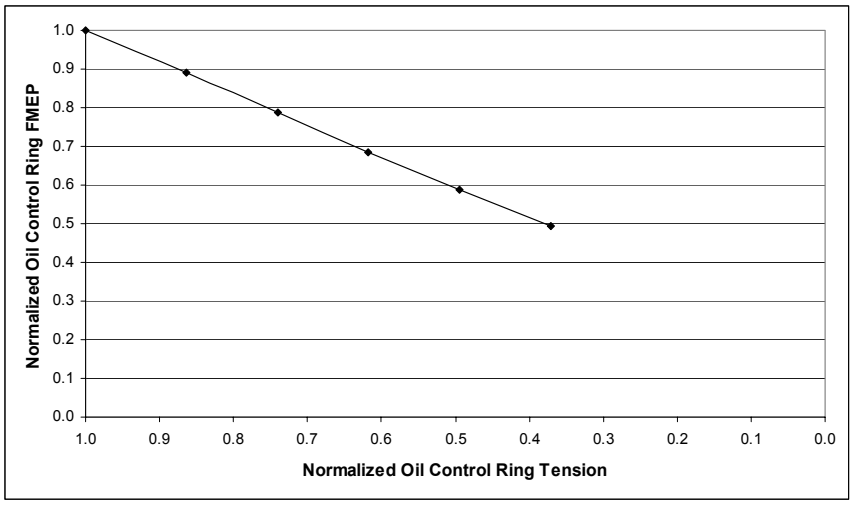

Figure 13-18: Effect of oil control ring tension on OCR frictional losses

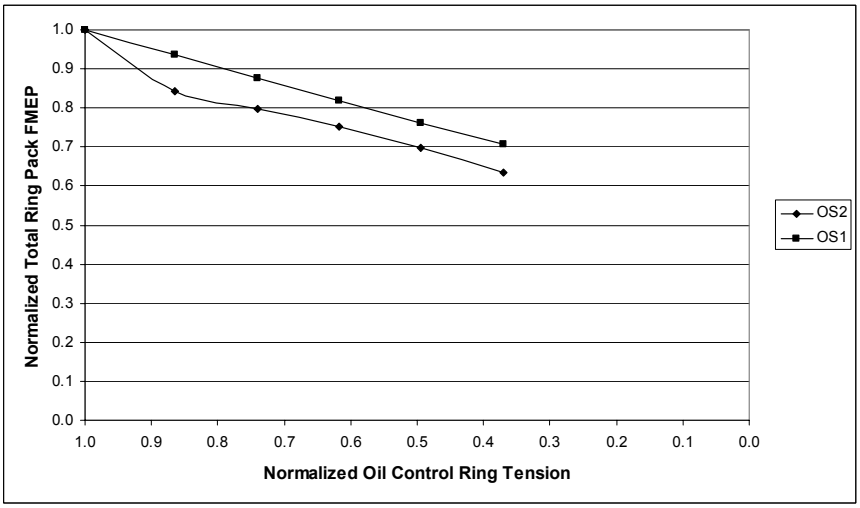

Figure 13-19: Effect of oil control ring tension on total ring-pack frictional losses

(c) Second Ring: Reducing Oil Consumption

Reducing the oil control ring tension can greatly reduce frictional losses, as shown, but this comes at the expense of an increase in oil consumption. The low tension ring is less able to conform to the cylinder liner, and is thus less able to control the film thickness that is allowed past the ring and into the combustion chamber. A negative twist second ring is proposed to offset this increase in oil consumption.

The benefit expected from the negative twist second ring lies in the ring dynamics, and in particular in the balance between the ring inertia and applied gas pressures near TDC of combustion. Near TDC, the inertia of the ring pulls it upwards – towards the top of the groove – because the piston acceleration is downwards (either the piston is slowing down approaching the TDC position, or it is increasing in speed in the downward direction, after TDC). Gas pressures, conversely, push the ring down, towards the bottom of the groove, because it is higher above the ring than below. The balance between these forces determines where the ring sits in the groove,

and whether it is stable. When the ring position is stable there is no effect on oil consumption. When the position is unstable, "ring flutter" can occur, in which the ring moves up and down in the groove for a portion of the stroke, allowing high-pressure gases to blow behind the ring. These high pressure gases can blow oil accumulated behind and below the second ring back down to the crank case, thus reducing oil consumption.

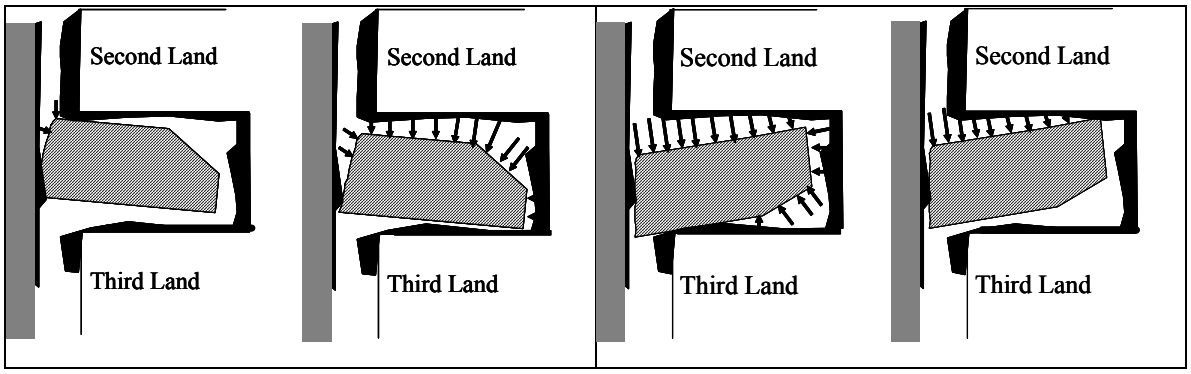

a) Positive Twist – stable. **b) Negative Twist - unstable, encourages 2nd ring flutter.**

Figure 13-20: Second-ring designs to reduce oil consumption

Figure 13-20 shows both positive twist and negative twist scraper rings, with the arrows showing net gas pressure. The positive twist case is stable – when the ring is at the top of the groove, the area exposed to the gas pressures is low, so the force pushing down is small. Inertia dominates the force balance and the ring remains at the top of the groove. When the ring is at the bottom, the area exposed to gas pressures is large, and the ring remains pressed to the groove bottom because of high gas forces.

The negative twist case is unstable. When the ring is at the top of the groove, a large area is exposed to the high gas pressure, so the force pushing the ring down is relatively high. If it is great enough to overcome the ring inertia, the ring will be pushed down to the groove bottom. When the ring is at the bottom of the groove, the high-pressure gas exerts a force not only on the top but also on the bottom of the ring, so that the net downward force is reduced. This may allow the ring inertia to bring it back up to the top of the groove, where the cycle begins again.

The ring movement caused by the negative twist allows gas to flow behind the second ring near TDC combustion, blowing accumulated oil back towards the crank case. It is hoped that this oil consumption reduction mechanism will offset any increases that occur when oil control ring tension is reduced.

13.3.2.2. Comparison between Experimental Data and Simulation Results

The FMEP results of the various rings were compared with the baseline configuration to determine the reduction in FMEP. The friction reductions measured tend to be conservatively predicted using the MIT model (Fig**. 13-21).** The error bars on the model predictions show the bounding oil supply conditions used by the model. The error bars on the experimental differences in Fig. **13-21** were calculated using Eq. 13.4 [54].

$$Error = z_{\alpha/2}\sqrt{\frac{\sigma_1^2}{n_1}+\frac{\sigma_2^2}{n_2}} \qquad \textbf{(Eq. 13.4)}$$

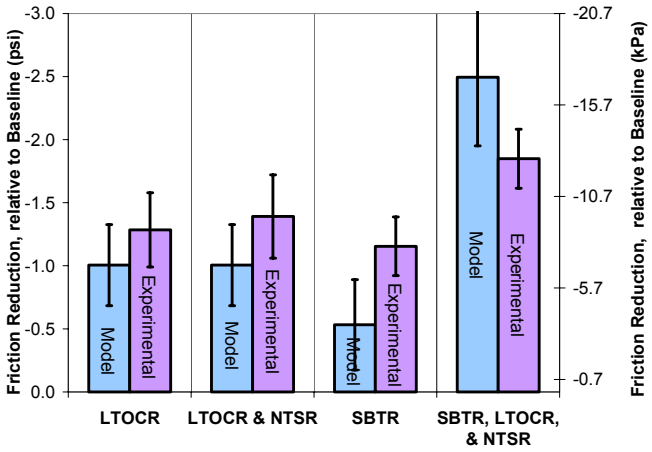

Figure 13-21 - Experimental and Modeled FMEP Results @ 1800rpm and 400bhp (298kW)

The mechanical efficiency (η_{mech}) was also calculated using Eq. 13.5

$$\eta_{mech} = \frac{BMEP}{NMEP} \qquad \text{(Eq. 13.5)}$$

These mechanical efficiency results are shown in Fig. 13-22 and Fig. 13-23.

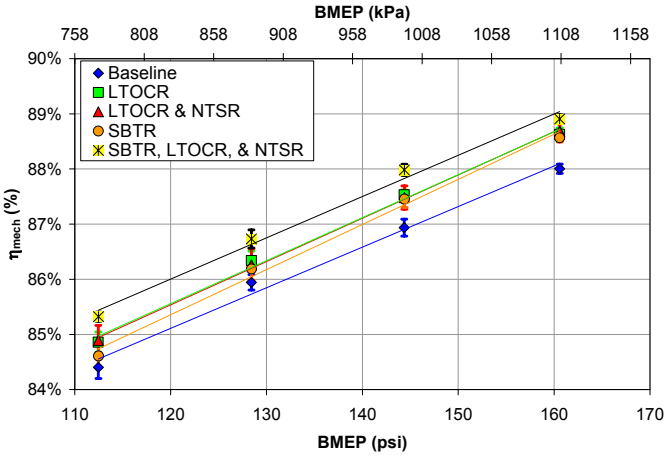

Figure 13-22 - η_{mech} vs. BMEP @ 1800rpm

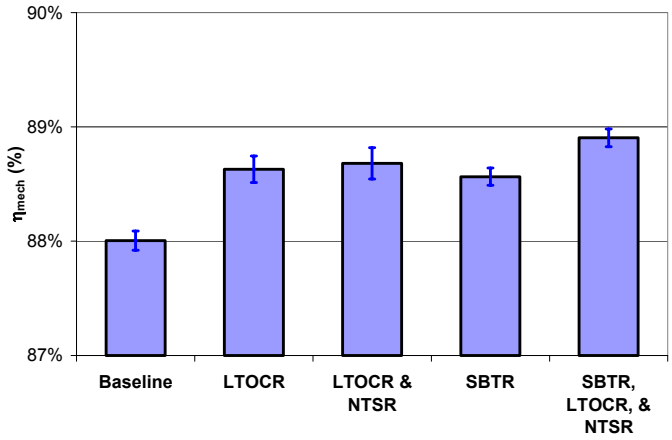

Figure 13-23 - η_{mech} vs. BMEP @ 1800rpm and 400bhp (298kW)

The blow-by flow was also compared to the values predicted by the model in Fig. 13-24. The blow-by differences among all configurations are relatively small.

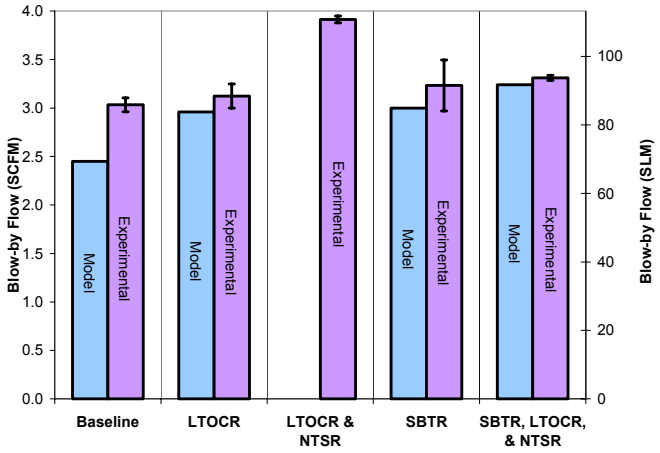

Figure 13-24 - Experimental and Modeled Blow-by Flow Results @ 1800rpm and 400bhp (298kW)

13.3.3. Low-Friction Lubricant Results

The lubrication oil tests were preformed only at 70% load and 100% load to allow more tests at each condition. The low friction ring pack was used for all lubrication tests. The commercial reference oil (CRO) was retested with new oil and found to match the test results from the ring pack testing. The testing showed the FMEP to be 138, 132, 125, and 115 (kPa) for CRO, LEF-F, LEF-G, and LEF-H respectively. The total FMEP reduction was 23 (kPa). The results were plotted in Figure 13-25.

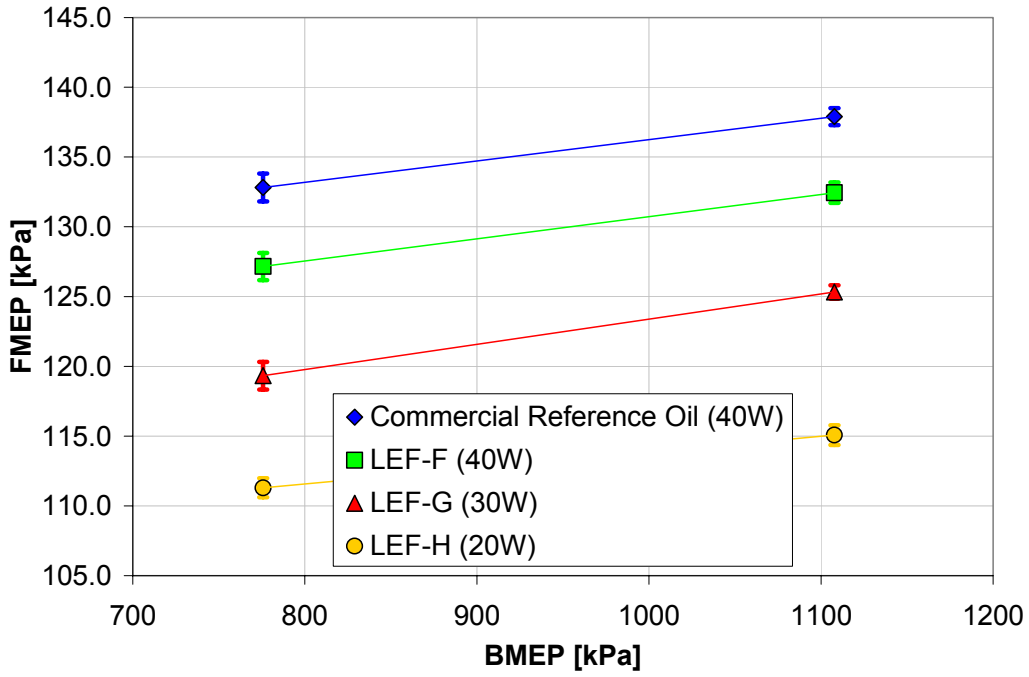

Figure 13-25: FMEP Measurements for Different Lubricants

The blow-by flow measurements did not show any significant change between the different lubrication oils. The blow-by flow measurements were approximately 130 (lpm). The results were plotted in Figure 13-26.

The oil consumption rates were approximately 130 (g/hr) for the commercial reference oil and LEF-F. The oil consumption dropped significantly to approximately 70 (g/hr) with LEF-G and increased to approximately 145 (g/hr) with LEF-H. The oil consumption results were within the manufacturers expected values. The results were plotted in Figure 13-27.

The model was used to predict the magnitude of friction reduction that could be obtained by using lubricants with 20W and 30W instead of 40W [55]. This model only predicts the power cylinder portion of the FMEP. The non-power-cylinder portion of the engine FMEP (other than rings/piston) should have more boundary lubrication and would be less sensitive to oil viscosity (but still comparable). Thus the slightly higher model predictions from the rings/piston are understandable. The experimental and modeled results were compared for the test oils in Fig. 13-28.

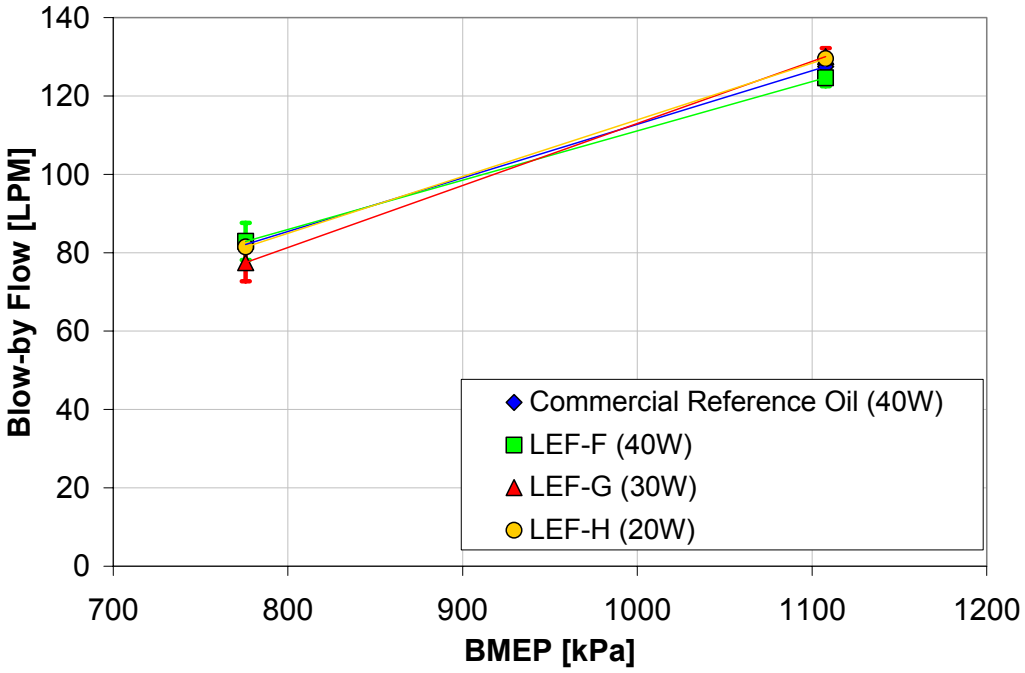

Figure 13-26: Blow-by flow measurements

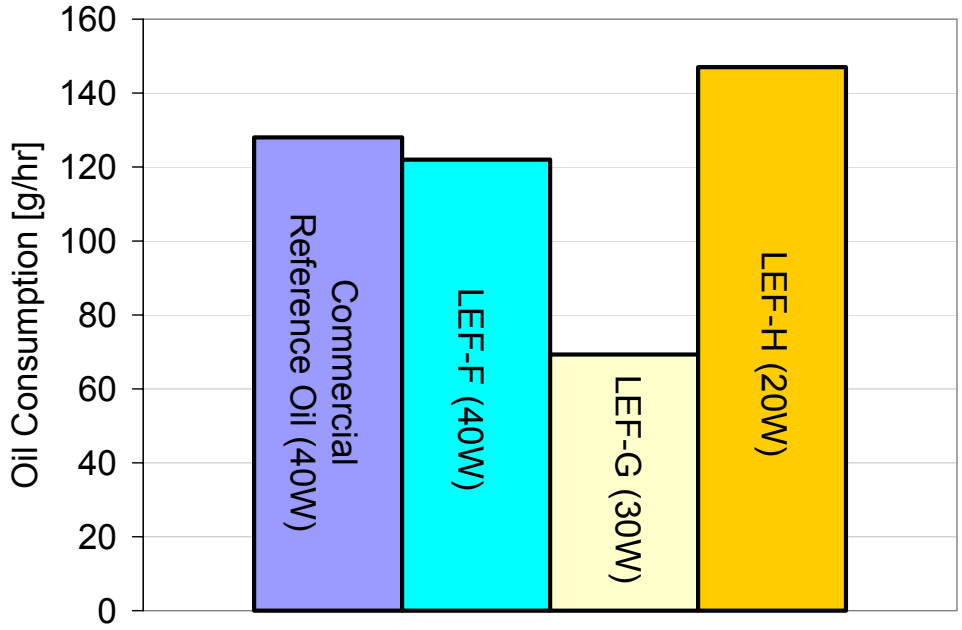

Figure 13-27: Oil consumption measurements

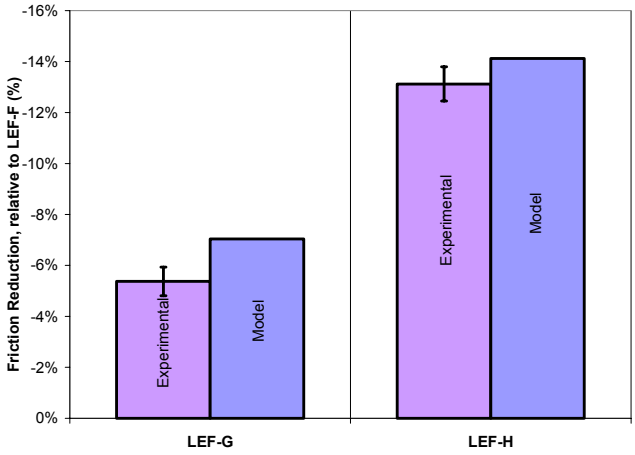

Figure 13-28 - Experimental and modeled results

The results of LEF-H showed a total engine FMEP reduction of ~16.5% from the commercial reference oil without significantly increasing oil consumption or blow-by flow. The measured FMEP reductions displayed good agreement with the model predictions.

These results show that gas engine oil formulation technology can be developed to provide reduced engine friction and fuel consumption. Lubricant viscosity is a major factor, while selection of base oil and additive composition may also influence these parameters.

13.4. Summary and conclusions of experimental validation

A ring pack model developed at MIT was used to design a low-friction ring pack configuration for a Waukesha VGF 18 liter engine. The low-friction ring pack features a skewed barrel top ring, a negative twist second ring, and a low-tension oil control ring. The MIT model predicted that the low-tension oil control ring has a potential to decrease ring pack friction by 20-30% and the skewed barrel top ring has the potential to reduce ring pack friction by 15-25%. Use of the negative twist second ring can help offset the adverse effects of the LTOCR on the rate of oil consumption.

Experiments related to reducing ring-pack friction were carried out at Colorado State University. Different ring-pack designs and lubricant oils were then tested to see their effect on friction, oil consumption and blow-by. The results showed that the SBTR and LTOCR rings can indeed reduce FMEP, and that the NTSR can help control the oil consumption rate. The results of combining all three ring designs showed a total engine FEMP reduction of 7-10% from the baseline configuration without significantly increasing oil consumption or blow-by flow. The measured FMEP reductions were in good correspondence with the model predictions.

III. SUMMARY AND CONCLUSIONS

The power cylinder is the main contributor to friction power losses in modern internal combustion engines. In this study, a combined analytical and experimental investigation on reducing friction in all power cylinder components was conducted, with particular emphasis on analysis on lubricant, surface finish, and piston design parameters in this reporting period. Results show that there is potential for friction reduction in all of the areas investigated. Experiments on recommended low-friction ring-pack designs as well as initial experiments on low-friction lubricants have been completed.

The focus of this study was on gas-fired reciprocating engines operating in high load, low speed conditions, with specific focus on the Waukesha VGF 18GL engine, which was used as the baseline engine in all studies. Results indicated that ring-pack friction reduction of ~35% was possible with optimized ring designs. This finding was demonstrated in the Waukesha engine tested at Colorado State University. The total engine FEMP (friction mean effective pressure) improved by 7-10% from the baseline configuration without significantly increasing oil consumption or blow-by flow. This represents a substantial (30-40%) reduction of the ring-pack friction alone. The measured FMEP reductions were in good agreement with the model predictions. Further improvements via piston, lubricant, and surface designs would offer additional opportunities.

In addition to component mechanical design, two other areas were also investigated; the effects of lubricant viscosity and liner surface texturing on ring/liner friction were considered. Three low-friction lubricants, having been formulated in collaboration with and by a lubricant supplier, were demonstrated on the Waukesha engine.

Effects of lubricant viscosity were studied as follows: (a) by changing the overall viscosity uniformly over the entire engine cycle, and (b) by preferentially changing, theoretically, the viscosity variations during the engine cycle, such as a higher viscosity near the end strokes and a lower viscosity near the mid-stroke. The rationale is that boundary lubrication is dominant near the end strokes which would benefit from a higher oil viscosity and higher oil film thickness, while near the mid-stroke of the engine cycle, hydrodynamic friction is dominant, which can be reduced by a lower viscosity. These variations could be achieved by lubricant formulation using viscosity dependency on shear rate, or by the temperature dependence of lubricant viscosity, or by proper thermal management of the engine. Results show that the strongest effect on friction reduction was by lowering the overall viscosity level of the lubricant everywhere in the engine cycle. While lowering viscosity near the mid-stroke region preferentially would also reduce friction in the same way, in that region, as lowering the viscosity everywhere, the effect on overall friction reduction by increasing oil viscosity near the end strokes was not as large as anticipated. The reason is that while boundary friction is reduced with higher oil viscosity near the end-strokes, hydrodynamic friction is also increased near the end strokes. The tradeoff obviously depends on the balance of asperity contact reduction versus hydrodynamic friction increase in the region near the end-strokes of piston travel.

Analysis of friction modifiers showed that asperity contact friction decreases in proportion to the reduction in friction coefficient. Hydrodynamic friction is not adversely affected. Thus friction modifiers are effective in friction reduction, but their practical implementation could be complex as they could affect engine deposits and/or other lubricant formulation issues. Further analysis and testing in this area are recommended.

A parametric study of surface texturing showed that adding appropriate surface features to the cylinder liner may also significantly reduce ring/liner friction. Also, if the lubricant and surface texturing can be optimized together, an even greater reduction in friction is possible, along with mitigation of undesired side-effects, such as oil consumption and wear, which may accompany changes made to the lubricant viscosity and surface texturing individually.

Friction reduction was observed when the surface texturing caused an increase in flow resistance, increasing oil film thickness and thus causing a reduction in both asperity contact and hydrodynamic friction. Parametric analyses of both grooved and dimpled patterns as well as liner finish and honing cross-hatch angle were performed. Specific recommendations from the liner finish study were reductions in both skewness and honing cross-hatch angle. Although the Waukesha engine is already well optimized in surface skewness and cross-hatch angle, further friction reduction of ~5% is expected. In the case of the piston, a friction reduction of up to 50% is predicted for reducing skirt waviness alone. Further reductions are expected when the skirt profile, skirt/liner clearance, and other parameters are optimized.

Surface groove parameters studied included the groove angle, width, depth, and area ratio, while parameters for the round dimples were the dimple depth, diameter, and area ratio. For both types of texturing, friction was found to decrease strongly with the depth of the features, and for grooved surfaces friction dropped substantially as groove angle was made more perpendicular to the direction of piston travel. Also, for both types of texture, friction decreased with increasing area ratio, although not as strongly as with depth or groove angle. Applied to the Waukesha engine ring-pack, a possible friction reduction of 15-25% is estimated through control of groove angle. Groove width and dimple diameter had only a minor effect on ring/liner friction, with the dimpled surfaces showing a slight optimum effect. The lowest FMEP was predicted for a mid-range dimple diameter.

For the best combination of surface and lubricant studied, compared to a smooth surface with the lubricant currently used in the Waukesha engine, a reduction in FMEP of greater than 50% is predicted for the oil control ring, translating into a reduction of ~30% for the ring-pack. This prediction indicates that there is significant potential for friction reduction via concurrent optimization of lubricant and surface properties.

Friction reductions of up to 50% are predicted for optimized piston design, resulting from reducing waviness alone. Pistons with large waviness experience asperity contact at larger film thicknesses, leading to high boundary friction losses. Reducing waviness reduces boundary contact, and thus friction. Other piston parameters were

studied and also show the potential to contribute to a reduced friction design, including piston/liner clearance, ovality and skirt profile. Lubricant effects were also considered.

The design strategies developed in this study have promising potential for application in all modern internal combustion engines as they represent simple, low-cost methods to extract significant fuel savings and to reduce harmful environmental damage, without compromising engine performance.

IV. RECOMMENDATONS FOR FUTURE RESEARCH

Results have shown that there is a synergistic benefit of using low-friction lubricant concurrently with implementing low-friction low-wear material/surface designs. Hence continued development should focus on the application of low-friction lubricants for various surface designs. It is recommended that a series of additional component and lubricant design and validation experiments continue in the future, to complement the current accomplishments in demonstrating friction reduction via ring-pack and lubricant designs. As reduction in engine parasitic losses will result in engine efficiency improvement and energy savings, a cooperative partnership among government, industry, university and national laboratories to continue to realize this benefit is strongly recommended.

Studies strongly indicate that piston friction is comparable to ring-pack friction and deserves as detailed a study and testing as low-friction ring-packs. Low-friction piston design should continue to be explored. Expanded studies of piston friction reduction beyond the current program may be appropriate and is recommended.

The current program has possible spinoffs in other applications such as in the transportation industry including automotive, marine, or in diesel power generation applications. Consortia or working groups involving various government agencies and University-Industry should be continued to ensure that the full potential for friction reduction in these areas will be fully explored and further areas for study identified. The progress made in this ARES program has far greater implications than applications in one focused industry.

Potential deployment of low-friction engine components or lubricants in the near term is not only possible, but quite probable, if future continued funding is made available in this area.

V. ACKNOWLEDGEMENT

This project is sponsored by the United States Department of Energy, Office of Distributed Energy, Advanced Reciprocating Engine Systems (ARES), as part of the Advanced University Reciprocating Engines Program (AUREP) under DOE Cooperative Agreement Number DE-FC26-02NT41339. We appreciate the participation of Colorado State University, Dr. Bryan Willson, Ted Bestor, Dr. Rudy Stanglmaier, Kirk Evans, Kris Quillen, and others, in performing the experiment and validation of the results. They are our important university partner in this project. The authors would also like to thank our industrial partner, Waukesha Engine Dresser, Inc., for their support and insight in this study. The authors would like to specifically acknowledge the technical contributions of

Ed Reinbold, Rick Donahue, Andy May and Jim Zurlo of Waukesha, who have worked closely with the MIT team and provided useful input and suggestions throughout the duration of the project. We also appreciate the individual contributions from Kathy Tellier, Martin Webster, and V. Carey for their support and collaboration in this program. We thank the DOE ARES project monitors, Tom George, Rob Martinez, William Cary Smith, and our technical project monitor Raj Sekar, and in particular the DOE manager and sponsor, Ronald Fiskum for their encouragement and support. Feedback from other industry participants such as Caterpillar and Cummins was very helpful. Prior work and the methodology used in the analyses were supported by related research in the MIT Industrial Consortium on Lubrication in I.C. Engines.

VI. REFERENCES

1. Wong, V., Tian, T., Lang, H., Ryan, J., Sekiya, Y., Kobayashi, Y. and Aoyama, S., "A Numerical Model of Piston Secondary Motion and Piston Slap in Partially Flooded Elastohydrodynamic Skirt Lubrication", International Congress and Exhibition, Detroit, MI, Paper 940696, (1994).

2. Tian, T., "Modeling the Performance of the Piston Ring Pack in Internal Combustion Engines", PhD Thesis, Department of Mechanical Engineering, Massachusetts Institute of Technology, June 1997

3. Tian, T., Wong, V.W. and Heywood, J.B., "A Piston Ring Pack Film Thickness and Friction Model for Multigrade Oils and Rough Surfaces", SAE Paper 962032, 1996; Also in SAE Trans., J. Fuels Lubricants, 1996, 105(4), pg. 1783-1795

4. Tian, T., Noordzij, L.B., Wong, V.W. and Heywood, J.B., "Modeling Piston-Ring Dynamics, Blowby, and Ring-Twist Effects", ICE - Vol. 27-2, 1996 ASME Fall Technical Conference, Vol. 2, pp. 67-80, Fairborn, Ohio, Oct. 1996

5. Smedley, G., Tian, T., and Wong, V.W., "Piston Ring Design for Friction Reduction in an Advanced Natural Gas Power Generation Engine," Paper No. 263, Proceedings of the Twenty-Fourth CIMAC World Congress on Combustion Engine Technology, Kyoto, Japan, June 7-11, 2004.

6. Smedley, G., Mansouri, S.H., Tian, T., and Wong, V.W., "Friction Reduction Via Piston Ring Design for an Advanced Natural-Gas Reciprocating Engine," ASME Paper ICEF2004-879, Proceedings of ASME-ICED Fall Technical Conference, Long Beach, CA, October 24-27, 2004

7. Richardson, D.E., ASME Paper 99-ICE-196, 1999 ASME-ICED Spring Conference.

8. Nakada, M., "Piston and Piston Ring Tribology and Fuel Economy", Proceedings of International Tribology Conference, Yokohama, 1995

9. Rohde, S.M., Whitaker, K.W. and McAllister, G.T., "A Study of the Effects of Piston Ring and Engine Design Variables on Piston Ring Friction", Energy Conservation through Fluid Film Lubrication Technology: Frontiers in Research

and Design, winter annual meeting of the ASME, New York, Dec. 2-7, 1979, Pg. 117-134

10. Hill, S.B. and Newman, B.A., "Piston Ring Designs for Reduced Friction", SAE Paper 841222, 1984

11. "Lubricant Additives – Chemistry and Applications" Edited by L. R. Rudnick, Marcel Dekker, Inc, 2003, ISBN: 0-8247-0857-1

12. Wakuda, M., et al. "Effect of surface texturing on friction reduction between ceramic and steel materials under lubricated sliding contact," Wear vol. 254, pp. 356-363, 2003.

13. Hegemier, T., Stewart, M., "Some Effects of Liner Finish on Diesel Engine Operating Characteristics," SAE paper 930716, 1996.

14. Jeng, Y., "Impact of Plateaued Surface on Tribological Performance," Tribology Transactions, vol . 29, pp. 354-361, 1996.

15. Jocsak, Jeffrey "The Effects of Surface Finish on Piston Ring-Pack Performance in Advanced Reciprocating Engine Systems," Master's Thesis, Massachusetts Institute of Technology, Cambridge, MA, June 2005

16. Water, F., Fundamentals of Manufacturing for Engineers, UCL Press, London, 1996.

17. Rohde, S.M., "A Mixed Friction Model for Dynamically Loaded Contacts with Application to Piston Ring Lubrication," Proc. of the 7th Leeds-Lyon Symposium on Tribology, Westbury House, pp. 19-50, 1980.

18. Liu, J.J., et. al., "Current and Future Approaches for Laser Texturing of Thin Film Media," IEEE Transactions on Magnetics, vol. 36, pp. 125-132, 2000.

19. Etsion, I., "State of the Art in Laser Surface Texturing," ASME Journal of Tribology, vol. 127, pp. 248-253, 2005.

20. Website: "The Future of the Surface: Optimum Tribosystems Through Functionally Optimized Surfaces," www.Gehring.de/enpdf/LaserHoning.pdf

21. Greenwood, J.A., Tripp, J., "The Contact of Two Nominally Flat Surfaces," Proc. Inst. Mech. Engrs., vol. 185, pp. 625-633, 1971.

22. Hu, Y., et. al., "Numerical Simulation of Piston Ring in Mixed Lubrication – A Non-Axisymmetrical Analysis," ASME Journal of Tribology, 1993.

23. Elderton, P.E. and Johnson, L.J., Systems of Frequency Curves, London: Cambridge University Press, 1969.

24. Patir, N. and Cheng, H.S., "Application of Average Flow Model to Lubrication Between Rough Sliding Surfaces," ASME Journal of Lubrication Technology, vol. 101, pp. 220-230, 1979.

25. Tian, T., et.al., "A Piston Ring-Pack Film Thickness and Friction Model for Multigrade Oils and Rough Surfaces," SAE paper 962032, 1996.

26. Arghir, et. al., "Theoretical Analysis of the Incompressible Laminar Flow in a Macro-Roughness Cell," ASME Journal of Tribology, vol. 125, pp. 309-318, 2003.

27. Heywood, J.B., "Internal Combustion Engine Fundamentals", McGraw-Hill Inc., © 1988

28. Tian, T., "Dynamic Behaviors of Piston Rings and their Practical Impact. Part 2: Oil Transport, Friction and Wear of Ring/Liner Interface and the Effects of Piston and Ring Dynamics", ImechE 2002, Pg. 229-247

29. Richardson, D.E., "Review of Power Cylinder Friction for Diesel Engines", Internal Report, Cummins Engine Company

30. Cullen, Joao A. and Frodsham, Gary M., "Reduced Cross Section Compression Rings for Diesel Engines", SAE Paper 971146, 1997

31. Tian, T., "Dynamic Behaviors of Piston Rings and their Practical Impact. Part 1: Ring Flutter and Ring Collapse and their Effects on Gas Flow and Oil Transport", ImechE 2002, Pg. 209-227

32. Thirouard, B., "Characterization and Modeling of the Fundamental Aspects of Oil Transport in the Piston Ring Pack of Internal Combustion Engines", PhD Thesis, Department of Mechanical Engineering, Massachusetts Institute of Technology, June 2001

33. Yilmaz, E., Thirouard, B., Tian, T., Wong, V., Heywood, J.B. and Lee, N., "Analysis of Oil Consumption Behavior During Ramp Transients in a Production SI Engine", SAE Paper 2001-01-3544, presented at the 2001 SAE Fall Fuel and Lubricant Meeting and Exposition, San Antonio, TX, Sept. 2001

34. Hamilton, D.B., Walowit, J.A. and Allen, C.M., "A Theory of Lubrication by Microasperities", ASME J. Basic Eng., vol. 88, pp. 177-185, 1966.

35. Anno, J.N., Walowit, J.A. and Allen, C.M., "Microasperity Lubrication", ASME Journal of Lubrication Technology, vol. 90, pp. 351-355, 1968.

36. Anno, J.N., Walowit, J.A., and Allen, C.M., "Load Support and leakage from Microasperity- Lubricated Face Seals", ASME Journal of Lubrication Technology, vol. 91, pp. 726-731, 1969.

37. Tian, H., Saka, N., Suh, N., "Boundary Lubrication Studies on Undulated Titanium Surfaces", Tribology Transactions, vol. 32, pp. 289-296, 1989.

38. Tonder, K., "Inlet Roughness Tribodevices: Dynamic Coefficients and Leakage", Tribology International, vol. 34, pp. 847-852, 2001.

39. Suh, N., Tribophysics, Englewood Cliffs, NJ: Prentice-Hall, Inc., 1986.

40. Petterson, U. and Jacobson, S., "Influence of Surface Texture on Boundary Lubricated Sliding Contacts", Tribology International, vol. 36, pp. 857-864, 2003.

41. Blatter, A., et. al., "Lubricated Sliding Performance of Laser-Patterned Sapphire," Wear, vol. 232, pp. 226-230, 1999.

42. Kovalchenko, A., Ajayi, O., Erdemir, A., Fenske, G., Etsion, I., "The Effect of Laser Surface Texturing on Transitions in Lubrication Regimes During Unidirectional

43. Sadeghi, F., et. al., "Advanced Natural Gas Reciprocating Engine: Parasitic Loss Control Through Surface Modification," presented at ARES/ARICE Low Engine Friction Alliance Workshop, Cambridge, MA, Dec. 1, 2005.

44. Etsion, I., et. al., "Analytical and Experimental Investigation of Laser-Textured Mechanical Seal Faces," Tribology Transactions, vol. 42, pp. 511-516, 1999.

45. Ronen, A., Etsion, I., Kligerman, Y., "Friction-Reducing Surface-Texturing in Reciprocating Automotive Components," Tribology Transactions, vol. 44, pp. 359-366, 2001.

46. Ryk, G., Kligerman, Y., Etsion, I., "Experimental Investigation of Laser Surface Texturing for Reciprocating Automotive Components," Tribology Transactions, vol. 45, pp. 444-449, 2002.

47. Siripuram, R. and Stephens, L., "Effect of Deterministic Asperity Geometry on Hydrodynamic Lubrication", ASME Journal of Tribology, vol. 126, pp. 527-534, 2004.

48. Hsu, S., "Integrated Surface Modification Technology Development," presented Sept. 15, 2005.

49. Michail, S.K. and Barber, G.C., "The Effects of Roughness on Piston Ring Lubrication Part I: Model Development," Tribology Transactions, vol. 38, pp. 19-26, 1995.

50. Kotwal, C. and Bhushan, B., "Contact Analysis of Non-Gaussian Surfaces for Minimum Static and Kinetic Friction and Wear," Tribology Transactions vol. 39, pp. 890-898, 1996.

51. Pinkus, O., Theory of Hydrodynamic Lubrication, New York:, McGraw-Hill Book Co., 1961.

52. Kweh, et. al., "Micro-Elastohydrodynamic Lubrication of an Elliptical Contact with Transverse and Three-Dimensional Sinusoidal Roughness," ASME Journal of Tribology, vol. 111, pp. 577-584, 1989.

53. Mufti, R. and Priest, M., "Experimental Evaluation of Piston-Assembly Friction Under Motored and Fired Conditions in a Gasoline Engine," ASME Journal of Tribology, Vol. 127, 2005, pp. 826-836.

54. Devore, Jay L., "Probability and Statistics for Engineering and The Sciences", Fifth Edition, Duxbury Thomson Learning, © 2000

55. Quillen K., Stanglmaier R.H., Wong V., Reinbold E., Donahue R.,Tellier K., Carey V. "Friction Reduction Due To Lubrication Oil Changes In A Lean-Burn 4-Stroke Natural Gas Engine: Experimental Results" by ASME Paper JRCICE2007-40128, submitted and presented at the Joint Rail Conference & Internal Combustion Engine Division Spring Technical Conference, March13-14, 2007, Pueblo, Colorado

APPENDIX A

DERIVATION OF FUNDAMENTAL EQUATIONS

A.1. Shear Stress Between the Ring and the Liner and Volumetric Flow Rate of Oil

The shear stress generated between the ring and the liner and the volumetric flow rate of oil can be determined by applying conservation of mass and momentum to a fluid element under the ring surface as follows.

Conservation of Mass:

$$\frac{d\rho}{dt} + \frac{\partial}{\partial x}(\rho u) + \frac{\partial}{\partial y}(\rho v) + \frac{\partial}{\partial z}(\rho w) = 0 \qquad \text{(A.1)}$$

Conservation of Momentum (Navier-Stokes Equations) [26,27]:

x-direction:

$$\rho\left(\frac{\partial u}{\partial t} + u\frac{\partial u}{\partial x} + v\frac{\partial u}{\partial y} + w\frac{\partial u}{\partial z}\right) = -\frac{\partial p}{\partial x} + \mu\left(\frac{\partial^2 u}{\partial x^2} + \frac{\partial^2 u}{\partial y^2} + \frac{\partial^2 u}{\partial z^2}\right) + \rho X$$

y-direction:

$$\rho\left(\frac{\partial v}{\partial t} + u\frac{\partial v}{\partial x} + v\frac{\partial v}{\partial y} + w\frac{\partial v}{\partial z}\right) = -\frac{\partial p}{\partial y} + \mu\left(\frac{\partial^2 v}{\partial x^2} + \frac{\partial^2 v}{\partial y^2} + \frac{\partial^2 v}{\partial z^2}\right) + \rho Y \qquad \text{(A.2)}$$

z-direction:

$$\rho\left(\frac{\partial w}{\partial t} + u\frac{\partial w}{\partial x} + v\frac{\partial w}{\partial y} + w\frac{\partial w}{\partial z}\right) = -\frac{\partial p}{\partial z} + \mu\left(\frac{\partial^2 w}{\partial x^2} + \frac{\partial^2 w}{\partial y^2} + \frac{\partial^2 w}{\partial z^2}\right) + \rho Z$$

For this particular case and in most bearing lubrication applications, the following assumptions are valid:

1. Height of fluid film y << x, z (film curvature can be ignored)
2. Negligible pressure variation across fluid film
   $\Rightarrow \frac{\partial p}{\partial y} = 0$
3. Laminar flow
4. No external forces act on fluid film $\Rightarrow X = Y = Z = 0$

5. Fluid inertia is small compared to viscous shear $\Rightarrow$ LHS terms in Eq. (A.2) neglected
6. All velocity gradients are negligible compared to.

$$\frac{\partial u}{\partial y}, \frac{\partial w}{\partial y}$$

With the above assumptions, Eq. (A.2) reduces to:

$$\frac{1}{\mu}\frac{\partial p}{\partial x} = \frac{\partial^2 u}{\partial y^2}$$
$$\frac{1}{\mu}\frac{\partial p}{\partial z} = \frac{\partial^2 w}{\partial y^2} \qquad \text{(A.3)}$$

An expression for shear stress can be obtained as follows. The following boundary conditions are needed:

$$u(y=0) = 0$$
$$u(y=h) = U$$

Integrating the x-direction component of Eq. (A.3) with respect to y and applying the above boundary conditions, an expression for u(y) can be obtained:

$$u(y) = \frac{1}{2\mu}\frac{dp}{dx}(y^2 - hy) + \frac{Uy}{h} \qquad \text{(A.4)}$$

It should be noted that performing the integration in this way assumes that the viscosity is not a function of the distance from the liner in the cross-flow direction. However, for a shear-thinning fluid, the viscosity is a function of the local shear rate, which is given by the rate of change of the velocity in the cross-flow direction. Although many oils are shear-thinning fluids, it has been shown in [11] that accurate results can be obtained for these oils by approximating the viscosity as the piston speed divided by the average distance between the nominal lines defining the ring and liner surfaces. Therefore, the above integration is still valid even in these cases.

Shear stress is given by:

$$\tau(x) = \mu \left.\frac{\partial u}{\partial y}\right|_{y=0}$$

Using Eq. (A.4):

$$\tau(x) = \frac{\mu U}{h} - \frac{h}{2}\frac{dp}{dx} \qquad \text{(A.5)}$$

The volumetric flow rate can also be derived using the above results:

$$Q(x) = \int_0^h u(y)dy$$

Using Eq. (A.4):

$$Q(x) = -\frac{h^3}{12\mu}\frac{dp}{dx} + \frac{Uh}{2} \tag{A.6}$$

A.2. Derivation of the Reynolds Equation

A relationship between the film height and width and the pressure distribution under the ring surface can be derived by applying conservation of mass and conservation of momentum to a fluid element under the ring surface.

Starting again with Eq. (A.3), the following boundary conditions can be applied, which assume that the motion of the ring surface occurs only in the x-direction:

$$u(y=0) = 0$$
$$u(y=h) = U$$
$$w(y=0) = 0$$
$$w(y=h) = 0$$

Integration of Eq. (A.3) and application of the above boundary conditions yields the following result:

$$u = \frac{1}{2\mu}\frac{\partial p}{\partial x}y(y-h) + \frac{h-y}{h}U$$
$$w = \frac{1}{2\mu}\frac{\partial p}{\partial z}y(y-h) \tag{A.7}$$

Substitution of Eq. (A.7) into the expression for conservation of mass given by Eq. (A.1) yields:

$$\frac{\partial}{\partial y}(\rho v) = -\frac{\partial}{\partial x}(\rho u) - \frac{\partial}{\partial z}(\rho w) \tag{A.8}$$

The following boundary conditions will be applied [26,27]:

$$v(y=0) = \frac{\partial h}{\partial t}$$
$$v(y=h) = 0$$

Now, integrating Eq. (A.8) with respect to y and applying the boundary conditions, assuming an incompressible lubricant, yields:

$$\frac{\partial}{\partial x}\left(\frac{h^3}{\mu}\frac{\partial p}{\partial x}\right) + \frac{\partial}{\partial z}\left(\frac{h^3}{\mu}\frac{\partial p}{\partial z}\right) = 6U\frac{\partial h}{\partial x} + 12\frac{\partial h}{\partial t} \tag{A.9}$$

This is the two-dimensional Reynolds Equation for incompressible lubricants. This equation relates the pressure distribution in the oil film with the film height and width between the ring and the liner.

APPENDIX B

METRICS FOR EVALUATING FRICTION REDUCTION

B.1. Determination of FMEP in the Friction Model

FMEP is a measure of the work done by friction normalized by the engine's displaced volume. It is thus a useful metric with which to compare the performance of different engines in a way that removes the effect of engine or component size. In this study, it is useful in that it provides a simple metric to use in order to evaluate and compare the performance of different piston ring designs.

The determination of the friction force was derived in Section 2 for pure hydrodynamic, mixed and pure boundary lubrication conditions. Friction power losses can be obtained from friction force by the following relationship:

$$P_f = UF_f \tag{B.1}$$

In other words, the friction power loss at a given crank angle in the engine cycle can be determined by the product of the friction force and the piston velocity. FMEP is defined as follows:

$$FMEP = \frac{W_f}{V_d} \tag{B.2}$$

To obtain the work done by friction from friction power losses, the following relationship is needed:

$$P_f = \frac{dW_f}{dt} \tag{B.3}$$

This can be rearranged to yield:

$$W_f = \int P_f dt \tag{B.4}$$

Substituting into Eq. (B.2) yields:

$$FMEP = \frac{\int P_f dt}{V_d} \tag{B.5}$$

The friction model discussed in Section 2.4 provides the friction power loss of the different piston rings at each crank angle throughout the engine cycle as output. To convert from time to crank angle, the following relation is needed:

$$\omega = \frac{d\theta}{dt} \tag{B.6}$$

where θ is the crank angle, and ω is the angular velocity of the crankshaft in radians per second. Rearranging and substituting this relationship into Eq. (B.5) yields:

$$FMEP = \frac{\int_{cycle} P_f d\theta}{\omega V_d} \tag{B.7}$$

This integration is carried out numerically in the friction model described in Section 2.4, since friction power loss can be determined at every crank angle from Eq. (B.1).

B.2. Determination of FMEP from the Experimental Results

Before the determination of the FMEP for a given ring design can be described, some introductory comments are required. In particular, the exact definitions of gross IMEP, net IMEP and their relationship to BMEP and FMEP must be clarified.

IMEP defines the work that is delivered to the piston by the cylinder gases. In this study, IMEP was determined from the cylinder pressure data as follows:

$$IMEP = \frac{\int pdV}{V_d} \tag{B.8}$$

The distance between the crank axis and the piston axis at any crank angle is given in:

$$s = a\cos\theta + (l^2 - a^2 \sin^2\theta)^{1/2} \tag{B.9}$$

where a is the crank radius and l is the connecting rod length. The volume change at any crank angle can be expressed as:

$$dV = -\frac{\pi B^2}{4}\frac{ds}{d\theta}d\theta$$

where B is the bore diameter of the engine, and the negative sign is added to reflect the positive volume change induced by a reduction of the distance between the crank axis and the piston axis. Differentiating Eq. (B.9) and substituting it into the above expression yields:

$$dV = \frac{\pi B^2}{4}\left\{a\sin\theta\left[1 + \frac{\cos\theta}{\left[l^2 - a^2\sin^2\theta\right]^{1/2}}\right]\right\}d\theta \tag{B.10}$$

The displaced volume can be expressed as:

$$V_d = \frac{\pi B^2}{4}L \tag{B.11}$$

where L is the stroke length of the engine. Substituting Eq. (B.10) and Eq. (B.11) into Eq. (B.8) yields the desired expression for IMEP:

$$IMEP = \frac{1}{L}\int p(\theta)\left\{a\sin\theta\left[1+\frac{\cos\theta}{\left[l^2 - a^2\sin^2\theta\right]^{1/2}}\right]\right\}d\theta \qquad \text{(B.12)}$$

The bounds of integration in Eq. (B.12) depend on whether or not the work done to flush out exhaust gases and bring in fresh charge, also called pumping work or PMEP, is to be included in the IMEP. If Eq. (B.12) is integrated over the compression and expansion strokes only, the result is referred to as gross IMEP, or IMEPg. If Eq. (B.12) is integrated over the intake and exhaust strokes only, and the result is subtracted from the gross IMEP, this yields the net IMEP. In other words, gross and net IMEP are related as follows:

$$IMEP_n = IMEP_g - PMEP \qquad \text{(B.13)}$$

BMEP defines the work that is available at the engine's crankshaft. Therefore, the relationship between gross IMEP, net IMEP, BMEP and FMEP can be summarized as follows:

$$\begin{aligned} IMEP_g &= BMEP + FMEP + PMEP \\ IMEP_n &= BMEP + FMEP \end{aligned} \qquad \text{(B.14)}$$

In principle, if the BMEP could be held exactly constant, the difference in FMEP between two designs could be determined by comparing the net IMEP of each of the designs. In reality, there is some variation in the BMEP as the load cannot be perfectly controlled by the dynamometer.

As a result, the following process was used to determine the FMEP of a given design. First, the gross IMEP was determined by integrating the expression in Eq. (B.12) using cylinder pressure data taken over 1000 engine cycles from each of the cylinders over three test runs. The integration was carried out over the compression and expansion strokes for each of the 1000 cycles, six cylinders and three test runs, and the mean value from this data set is the desired gross IMEP. This process was repeated over the entire cycle to determine the net IMEP. The average BMEP was obtained from a set of torque values that were measured from the dynamometer at a rate of 1 Hz for a 5 minute sampling period (or 1 measurement per second). BMEP was determined from torque by dividing by the engine's displaced volume. FMEP was then determined as the difference between the net IMEP and the BMEP. The change in FMEP between designs was evaluated by finding the difference between the FMEP for each of the individual designs. There was therefore a significant amount of error introduced while finding this value, since it is the result of two subtractions and two averaging processes. This error is discussed in detail and quantified in the section that follows.

B.3. Error Analysis of the Experimental Results

For each of the rings that were tested, a statistical analysis was conducted to determined whether or not a reduction in the mean FMEP was achieved. This section begins with a detailed description of this calculation, followed by a short description of the determination of the error in the experimentally measured oil consumption and blowby values.

BMEP data was first obtained for each of the three test runs. Since the data was taken at a rate of 1 sample per second, and this test was conducted over a period of 5 minutes, 300 values were obtained in total for each test. The mean and standard deviation of this data set was taken for each ring design that was tested.

Gross IMEP data was then obtained from the cylinder pressure data as described in the previous section. 1000 cycles of data were taken in each of the six cylinders for the three test runs, yielding a sample size of 18,000 of gross IMEP values. The mean and standard deviation for this data set was determined. A similar approach was also to determine the mean and standard deviation for the PMEP.

The procedure described in the previous section was then used to determine the change in FMEP between two designs once gross IMEP, PMEP and BMEP were determined. As mentioned previously, since each of these values has an average and a standard deviation, a significant amount of error was introduced in manipulating these values.

The following general equation was used to determine the error as a result of a calculation. For a function of two variables, f(x1,x2), if the errors in the independent variables were Δx1 and Δx2, the error as a result of an operation is determined by:

$$\Delta f(x_1, x_2) = \sqrt{\left(\frac{\partial f}{\partial x_1}\Delta x_1\right)^2 + \left(\frac{\partial f}{\partial x_2}\Delta x_2\right)^2} \qquad \text{(B.15)}$$

For example, since net IMEP is determined by the difference between the gross IMEP and PMEP, the associated error was determined as:

$$\Delta IMEP_n = \sqrt{(\Delta IMEP_g)^2 + (\Delta PMEP)^2}$$

This error propagation was carried out for each of the subtractions involved in the determination of the difference in the FMEP between two designs. However, using this method, the error in the result always ended up being larger than the value itself. As a result, a statistical approach was required to assess whether or not there was a difference in the mean FMEP values between different designs.

For this purpose, a hypothesis test was conducted. In this approach, a hypothesis is made about a quantity of interest, in this case, the difference in the FMEP values between two different ring designs. The initial hypothesis is that the difference between the FMEP values between two designs is actually zero. The idea is to use statistical evidence to reject this hypothesis within a certain level of confidence.

Specifically, the hypothesis that the difference in the mean FMEP values between two tests is zero can be rejected provided that:

$$z_0 = \frac{\overline{x_1} - \overline{x_2} - \Delta_0}{\sqrt{\frac{\sigma_1^{\,2}}{n_1} + \frac{\sigma_2^{\,2}}{n_2}}} > z_\alpha \qquad \text{(B.16)}$$

where $\overline{x_1}$ and $\overline{x_2}$ are the mean FMEP values for the ring designs being compared, $\Delta 0$ is the hypothesized value of the difference in the mean values (zero in this case), $\sigma 1$ and $\sigma 2$ are the standard deviations associated with the mean FMEP values, and n1 and n2 are the associated sample sizes. $z\alpha$ is a value obtained from the standard normal distribution for a given α, which is a measure of the confidence with which the conclusion can be reached. In this study, a 95% confidence interval was used, which corresponds to α=0.05.

An example is used to illustrate this approach as well as the process used to conduct the error analysis in this study. For this purpose, the low-tension oil control ring results will be used. The mean values and associated standard deviations from data obtained from the baseline test and the low-tension OCR test are summarized in Table B-1 below.

	Baseline	**Low-Tension OCR**
BMEP (psi)	200.848 ± 0.152	200.998 ± 0.141
$IMEP_n$ (psi)	221.610 ± 13.094	220.118 ± 8.251
FMEP (psi)	20.762 ± 13.095	19.120 ± 8.252

Table B-1: Data Summary

To determine the associated error in the FMEP, the statistical analysis described above was used with the following values:

$\overline{x_1}$ = 20.762

$\overline{x_2}$ = 19.120

$n_1 = n_2$ = 18,000

$\sigma_1 = 13.095$

$\sigma_2 = 8.252$

$\alpha=0.05$

With these values, the hypothesis that the mean FMEP was the same for the low-tension OCR design as for the baseline design could be rejected because the criteria defined in Eq. (B.16) was met. Specifically, by substituting the above values into Eq. (B.16), the following result is obtained: 14.237>1.645.

The error on the difference in FMEP within 95% confidence can be determined as follows:

$$Error = z_{\alpha/2}\sqrt{\frac{\sigma_1^{\,2}}{n_1}+\frac{\sigma_2^{\,2}}{n_2}} \qquad \text{(B.17)}$$

With $z\alpha/2 = 1.96$, the error on the FMEP within 95% confidence is 0.226 psi. In kPa, the mean value and error associated with the difference in FMEP for the case of the low-tension oil control ring is 11.17 ± 1.54. This is the result that appears in Table 6-4.

The error in the blowby data was determined by calculating the standard deviation based on the sample of 300 data points obtained from the blowby flow meter over the five minute averaging period for the three test runs that were considered. To determine the error in oil consumption measured experimentally, it was assumed to be possible to read the refill meter within an accuracy of 1%. Since this value was measured several times and averaged, the overall error was determined by applying the method in Eq. (B.15).

Oil consumption was not determined using the model and therefore no comparison could be made between the model and the experiment. Blowby was measured experimentally and was determined by the model, and a comparison could be therefore be made directly. The change in FMEP between designs was also compared directly. Some explanation should be given to justify this comparison. This is provided in the following section.

B.4. Comparison of FMEP between Model and Experiment

The model and the experiment use slightly different approaches to determine FMEP. In the model, the same cylinder pressure (and therefore IMEP) is used as input and the ring design parameters are varied. The FMEP contribution from the ring pack is provided as output from the model. In the experiment, the FMEP is determined by fixing the BMEP, and by measuring the change in cylinder pressure (and therefore IMEP) resulting from a change in the ring design. These two methods are entirely equivalent. The model's approach assumes that the changes in the ring design affect BMEP, whereas the experimental approach allows the changes in the ring design to affect IMEP. To ensure a consistent comparison between the experimental data and the results from the model, the experimentally measured cylinder pressure data from the baseline case was used as input into the model for all of the different cases considered. This is equivalent to fixing the IMEP. In the experimental approach, BMEP is fixed and the variation in net IMEP between the cases considered reflects the change in the FMEP of the ring pack.